

**NASA CONTRACTOR  
REPORT**



**NASA CR-2924**

**NASA CR-2924**

**COMPUTATIONAL TECHNIQUES  
FOR SOLAR WIND FLOWS  
PAST TERRESTRIAL PLANETS -  
THEORY AND COMPUTER PROGRAMS**

*Stephen S. Stahara, Denny S. Chaussee,  
Barbara C. Trudinger, and John R. Spreiter*

*Prepared by*  
**NIELSEN ENGINEERING & RESEARCH, INC.**  
Mountain View, Calif. 94043

*for*

**NATIONAL AERONAUTICS AND SPACE ADMINISTRATION • WASHINGTON, D. C. • NOVEMBER 1977**

1. Report No. NASA CR- 2924		2. Government Accession No.		3. Recipient's Catalog No.	
4. Title and Subtitle Computational Techniques for Solar Wind Flows Past Terrestrial Planets - Theory and Computer Programs				5. Report Date November 1977	
				6. Performing Organization Code	
7. Author(s) Stephen S. Stahara, Denny S. Chaussee, Barbara C. Trudinger, and John R. Spreiter				8. Performing Organization Report No. NEAR TR 140	
				10. Work Unit No.	
9. Performing Organization Name and Address Nielsen Engineering & Research, Inc. 510 Clyde Avenue Mountain View, California 94043				11. Contract or Grant No. NASW-2945	
				13. Type of Report and Period Covered Contractor Report June 1976-July 1977	
12. Sponsoring Agency Name and Address National Aeronautics and Space Administration Washington, D.C. 20546				14. Sponsoring Agency Code	
				15. Supplementary Notes	
16. Abstract <p>Theoretical analysis and the development of user-oriented computer programs were carried out for the purpose of developing computational techniques for predicting the interaction of the solar wind with terrestrial planets. The procedures are based on a single-fluid, steady, dissipationless, magnetohydrodynamic model and are appropriate for the calculation of axisymmetric, supersonic, super-Alfvénic solar wind flow past both magnetic and nonmagnetic planets. The actual calculations are implemented by an assemblage of computer codes organized into one program. These include finite-difference codes which determine the gas-dynamic solution, together with a variety of special-purpose output codes for determining and automatically plotting both flow field and magnetic field results.</p> <p>Theoretical results obtained using these procedures are reported for a variety of solar wind conditions and different obstacle shapes. Comparisons are made with previous results, and new results are presented for a number of solar wind flows. The computational programs developed under this work have been documented and are presented in a general user's manual included as part of this report.</p>					
17. Key Words (Suggested by Author(s)) Solar Wind Flows Finite-Difference Computations Steady Flow Magnetosphere Ionosphere			18. Distribution Statement  UNCLASSIFIED-UNLIMITED  Cat. 92		
19. Security Classif. (of this report) UNCLASSIFIED		20. Security Classif. (of this page) UNCLASSIFIED		21. No. of Pages 133	22. Price* \$6.00

## TABLE OF CONTENTS

<u>Section</u>	<u>Page No.</u>
LIST OF ILLUSTRATIONS	iv
LIST OF TABLES	v
SUMMARY	1
INTRODUCTION	1
LIST OF SYMBOLS	3
ANALYSIS	7
General Considerations	7
Mathematical Representation of Solar Wind-Magneto/Ionosphere Interaction	8
Magnetic Planet - Determination of the Magnetosphere Boundary	11
Nonmagnetic Planet - Determination of the Ionosphere Boundary	16
Calculation of the Gasdynamic Flow Properties	19
Calculation of the Magnetic Field	26
RESULTS AND DISCUSSION	29
CONCLUDING REMARKS	32
APPENDIX A - COMPUTER PROGRAM USER'S MANUAL	34
APPENDIX B - LISTING OF COMPUTER PROGRAM	73
REFERENCES	107
TABLE 1	110
FIGURES 1 THROUGH 15	113

## LIST OF ILLUSTRATIONS

### Figure

- 1 Comparison of the equatorial and principal meridian traces of the magnetosphere boundary as provided by the simplified theory of equation 16.
- 2 Illustration of ionopause shapes for various values of the ionosphere scale height to shock standoff distance ratio  $H/R_0$ .
- 3 Comparison of former and present computational procedures for determining the gasdynamic flow properties of solar wind-magneto/ionopause interactions.
- 4 Illustration of the components of the three-dimensional magnetic field.
- 5 Comparison of flow properties predicted by the present implicit method with other techniques and experiment for supersonic flow past a sphere;  $M_\infty = 4.926$ ,  $\gamma = 1.4$ .
- 6 Comparison of implicit and inverse methods for shock shape and sonic line location, and density distribution along bow shock and magnetosphere boundary for  $M_\infty = 8$ ,  $\gamma = 5/3$  flow past the rotated equatorial trace of the magnetopause.
- 7 Bow wave and sonic line locations for various supersonic flows past the rotated equatorial trace of the magnetopause with  $\gamma = 5/3$ .
- 8 Bow shock location for solar wind flow with  $M_\infty = 8$ ,  $\gamma = 5/3$  past various ionopause shapes.
- 9 Bow shock and embedded shock locations for solar wind flow with  $M_\infty = 5$ ,  $\gamma = 5/3$  past the rotated principal meridian of the magnetosphere.
- 10 Magnetopause pressure coefficients for the principal meridian magnetopause shapes shown in figure 9.
- 11 Variation of shock stand-off distance with oncoming Mach number and ratio of specific heats for various magneto/ionopause traces as determined by the present implicit procedure.
- 12 Shock shapes for various supersonic flows past the rotated equatorial trace of the magnetopause; combined near (blunt body) and far (marching) solutions.
- 13 Shock shapes for  $M_\infty = 8$ ,  $\gamma = 5/3$  flow past an ionopause shape with  $H/R_0 = 0.1$ ; combined near (blunt body) and far (marching) field solutions.

LIST OF ILLUSTRATIONS (CONTINUED)

Figure

- 14 Streamline, density, and velocity maps for  $M_\infty = 8.0$ ,  $\gamma = 5/3$  flow past the rotated equatorial trace of the magnetopause; combined blunt body and marching flow field.
- 15 Contours and field line locations of the in-plane magnetic field components  $(B/B_\infty)_\perp$  and  $(B/B_\infty)_\parallel$  for  $M_\infty = 8$  and  $\gamma = 5/3$  flow past the rotated equatorial trace of the magnetopause.
- A.1 Card input for sample case.
- A.2 Abbreviated output for sample case.
- A.3 Plot output for sample case.

LIST OF TABLES

Table

- 1 Ordinates of various magneto/ionopause shapes.

COMPUTATIONAL TECHNIQUES FOR SOLAR  
WIND FLOWS PAST TERRESTRIAL PLANETS  
- THEORY AND COMPUTER PROGRAMS

by Stephen S. Stahara, Denny S. Chaussee,  
Barbara C. Trudinger, and  
John R. Spreiter\*  
Nielsen Engineering & Research, Inc.

SUMMARY

Theoretical analysis and the development of user-oriented computer programs were carried out for the purpose of developing computational techniques for predicting the interaction of the solar wind with terrestrial planets. The procedures are based on a single-fluid, steady, dissipationless, magnetohydrodynamic model and are appropriate for the calculation of axisymmetric, supersonic, super-Alfvénic solar wind flow past both magnetic and nonmagnetic planets. The actual calculations are implemented by an assemblage of computer codes organized into one program. These include finite-difference codes which determine the gasdynamic solution, together with a variety of special-purpose output codes for determining and automatically plotting both flow field and magnetic field results.

Theoretical results obtained using these procedures are reported for a variety of solar wind conditions and different obstacle shapes. Comparisons are made with previous results, and new results are presented for a number of solar wind flows. The computational programs developed under this work have been documented and are presented in a general user's manual included as part of this report.

INTRODUCTION

The gasdynamic and magnetohydrodynamic calculations of solar wind flow around magnetic and nonmagnetic planets that Spreiter et al. (refs. 1-8) carried out some years ago have been and continue to be widely used in the interpretation of data measured in space around the Earth and other planets. The objective at the time those calculations were made, was to

---

\*Professor, Department of Applied Mechanics, Stanford University.  
Consultant, Nielsen Engineering & Research, Inc.

provide some theoretical results based on a fluid rather than particle description of the flow that might be compared with measurements in space to determine the applicability of such a description. During the intervening years, the usefulness and accuracy of those results have become so well established that they are currently being used, for instance, as one of the ways in which the magnetic field of a planet such as Mercury or Mars is estimated from measurements of fly-by or orbiting spacecraft.

In such applications, the previous calculations leave much to be desired. They have been carried out for only a limited set of conditions such as obstacle shape, oncoming Mach number, angle between free-stream flow and magnetic vectors, etc., and are presented in archival publications only in the form of plots from which results for other conditions must be determined by scaling and interpolation. The usefulness of the present theoretical model, therefore, would be considerably enhanced if similar but more detailed results for the specific conditions measured by a spacecraft would be provided by the application of a documented, user-oriented, economical computer code.

That objective has been successfully accomplished in the work reported here. Based upon the identical theoretical model employed previously (refs. 1-8), and discussed in more detail below, a new more versatile means of solution far superior in efficiency and generality to the former method is now available. Current advances in computational methods have been incorporated in these programs and, in fact, an entirely new blunt body code based on a recently published algorithm was developed to determine the flow field in the region surrounding the nose of the obstacle. The new methods confirm previous results and are readily applicable to additional cases involving different geometries and flow conditions. The entire procedure is fully automated and provides detailed flow field and magnetic field properties in a convenient output format. An automatic plotting capability for generating report-quality plots is also included.

LIST OF SYMBOLS

a	speed of sound, $(\gamma p/\rho)^{1/2}$
$a_e$	planetary radius of earth, $6.37 \times 10^8$ cm
A	Alfvén speed, $(B^2/4\pi\rho)^{1/2}$
$\bar{A}$	Jacobian matrix associated with IMP code, equal to $\partial \hat{E}/\partial \hat{U}$
$\vec{B}$	magnetic field vector
$B_{eq}$	strength of Earth's magnetic field at geomagnetic equator, equal to 0.312 gauss
$\bar{B}$	Jacobian matrix associated with IMP code, equal to $\partial \hat{F}/\partial \hat{U}$
$C_p$	specific heat at constant pressure
$C_v$	specific heat at constant volume
D	geometric distance to magnetosphere nose, equal to $a_e (f^2 B_{eq}^2 / 2\pi K \rho_\infty V_\infty)^{1/6}$
e	internal energy, eq. (5)
E	column matrix defined by eq. (29)
$\hat{E}$	column matrix associated with IMP code, equal to $(\xi_T U + \xi_X E + \xi_R F)/J$
f	constant associated with tangential component of Earth's magnetic dipole field at magnetopause location
F	column matrix defined by eq. (29)
$\hat{F}$	column matrix associated with IMP code, equal to $(\eta_T U + \eta_X E + \eta_R F)/J$
$\vec{F}$	column matrix defined by eq. (34)
g	acceleration due to gravity
G	column matrix defined by eq. (29)
$\vec{G}$	column matrix defined by eq. (34)
h	enthalpy, eq. (6)
H	local scale height of atmosphere, $\bar{R}T/\mu g$
$H_t$	total enthalpy, eq. (35)
$\vec{H}$	column matrix defined by eq. (34)
J	Jacobian matrix, eq. (30)



LIST OF SYMBOLS (Continued)

K	constant defined by eq. (14)
$\Delta \ell$	vector length of elemental magnetic flux tube
M	local Mach number, $ \underline{v} /a$
$M_A$	local Alfvén Mach number, $ \underline{v} /A$
p	pressure
q	magnitude of velocity vector, eq. (36)
Q	dummy parameter
r	spherical radial distance
R	cylindrical radial distance
$\bar{R}$	gas constant, $8.315 \times 10^7$ ergs/gm $^\circ$ K
$R_i$	spherical radius of ionopause, eq. (25)
$R_m$	spherical radius of magnetopause, eqs. (16-18)
$R_o$	spherical distance from center of planet to ionopause nose
S	entropy
$\Delta S$	incremental distance along streamline
T	time
(u,v,w)	velocity components associated with the (X,R, $\omega$ ) coordinate directions, respectively
U	column matrix defined by eq. (29)
$\hat{U}$	column matrix associated with IMP code, equal to U/J
$\tilde{U}$	column matrix defined by eq. (34)
$\underline{v}$	velocity vector
x	axial distance from center of planet measured positive upstream
X	axial distance from center of planet measured positive downstream
$\beta$	spherical polar angle, measured with respect to planet center, from subsolar point with respect to undisturbed solar wind direction; varies from 0 in upstream direction to $\pi$ in downstream direction; eq. (25)
$\gamma$	ratio of specific heats

LIST OF SYMBOLS (Continued)

$\delta_s$	local angle of bow shock wave
$(\delta_\xi, \delta_\eta)$	second-order difference operators in $(\xi, \eta)$ direction
$\eta$	transformation variable; eqs. (27), (37)
$\theta$	polar angle measured with respect to north geomagnetic pole, eq. (15)
$\Lambda$	quantity defined by eq. (26)
$\mu$	nondimensionalized mean molecular mass, equal to 1/2 for ionized atomic hydrogen
$\xi$	transformation variable, eqs. (27), (37)
$\rho$	density
$\tau$	transformed time, eq. (27)
$\phi$	geomagnetic longitude, eq. (16)
$\psi$	angle between outward normal to magneto/ionosphere boundary and oncoming undisturbed solar wind, eq. (12)
$\omega$	azimuthal angle in axis-normal plane, eq. (33)

Subscripts

n	normal direction
P	arbitrary point on streamline
R	reference quantity
t	tangential direction
o	reference quantity at subsolar point
1	conditions upstream of a discontinuity
2	conditions downstream of a discontinuity
$\infty$	upstream undisturbed quantity
(" , $\perp$ , n)	parallel, perpendicular, and normal magnetic field components as defined in eq. (42)

**Page  
Intentionally  
Left Blank**

## ANALYSIS

### General Considerations

An overall description of solar wind flow past terrestrial planets, including an account of the principal features of the interplanetary solar wind and a description of the physical basis of the continuum fluid model are provided in references 3 and 6. Although details of those accounts won't be repeated here, several specific points relevant to the present work will be reviewed.

The fundamental assumption underlying the theoretical analysis of large-scale features of the interaction of the solar wind with terrestrial planets is that the average bulk properties of the flow can be described adequately by the continuum equations of magnetohydrodynamics for a single-component, perfect, dissipationless (perfect electrically conducting, inviscid, nonheat-conducting) gas. Theoretical justification of this point has not yet been established, and proof remains essentially qualitative at present. The primary justification for use of the continuum fluid model is the outstanding agreement of the qualitative results predicted on this basis with those actually measured in space. It appears that the continuum model is capable of accounting both for many of the details as well as the broad features of the observations.

The primary emphasis on development of the continuum model has been on steady flow past the Earth (refs. 3, 4), a planet with a strong magnetic field. Initial applications to nonmagnetic planets have also been made (ref. 5). These particular applications are the ones toward which this study is directed.

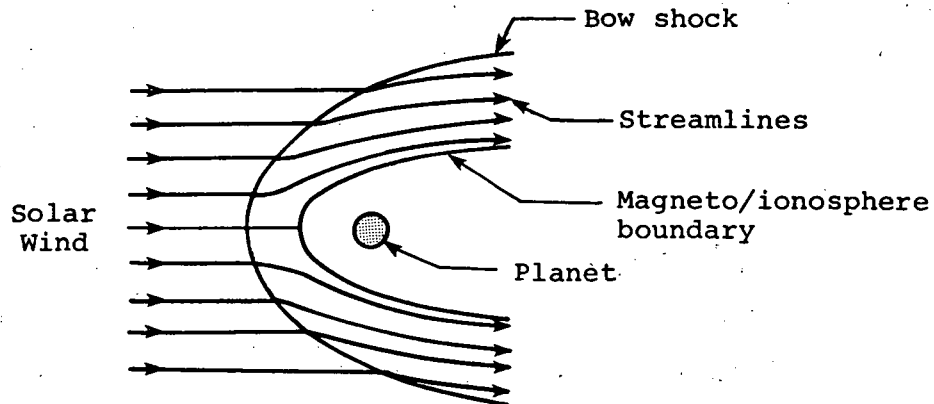
The following subsection provides the mathematical basis of the interaction of the solar wind with planetary magneto/ionospheres. The governing differential equations as well as relations for discontinuities present in the flow are discussed. The next two subsections provide the determination of the magnetosphere and ionosphere boundary shapes. The following two subsections discuss the calculation of the gasdynamic and magnetic field properties.

## Mathematical Representation of Solar Wind- Magneto/Ionosphere Interaction

The differential equations governing the motion of the solar wind are the magnetohydrodynamic equations for steady flow of a dissipationless perfect gas and can be written as follows

$$\left. \begin{aligned}
 \nabla \cdot \rho \vec{v} &= 0 \\
 \rho (\vec{v} \cdot \nabla) \vec{v} + \nabla p &= -(1/4\pi) \vec{B} \times \text{Curl } \vec{B} \\
 \text{Curl} (\vec{B} \times \vec{v}) &= 0 \\
 \text{div } \vec{B} &= 0 \\
 (\vec{v} \cdot \nabla) S &= 0 \\
 S - S_0 &= C_v \ln \frac{p/p_0}{(\rho/\rho_0)^\gamma}
 \end{aligned} \right\} \quad (1)$$

and apply in the region exterior to the magneto/ionosphere boundary, as shown in the sketch below.



In these equations,  $\rho$ ,  $p$ ,  $S$ , and  $\vec{v}$  refer to the density, pressure, entropy, and velocity of the gas,  $\vec{B}$  denotes the magnetic field, and  $\gamma = C_p/C_v$  is the ratio of specific heats, equal to 5/3 for a monatomic gas. The temperature  $T$  is related to the pressure and density by the equation of state for a perfect gas

$$p = \rho \bar{R} T / \mu \quad (2)$$

in which  $\bar{R} = (C_p - C_v)\mu = 8.315 \times 10^7$  ergs/gm $^\circ$ K is the universal gas constant, and  $\mu$  is the mean molecular mass nondimensionalized so that  $\mu = 16$  for atomic oxygen. For fully ionized hydrogen,  $\mu$  is thus 1/2. The magnetic field  $\vec{B}$  is expressed in terms of gaussian units.

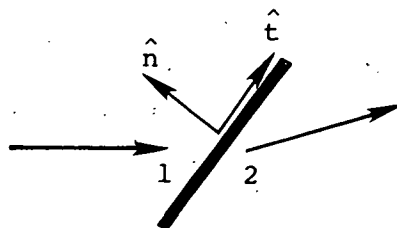
We note that it is fully equivalent and convenient for some purposes to replace the entropy equation  $(\vec{V} \cdot \vec{\nabla})S = 0$  in equation (1) by the following energy equation:

$$\text{div}[\rho \vec{V} (\frac{1}{2} V^2 + h) + \vec{V} B^2 / 4\pi - (\vec{B} \cdot \vec{V}) \vec{B} / 4\pi] = 0 \quad (3)$$

Because of the omission of dissipative terms in equation (1), surfaces of discontinuity, such as the bow shock and the magneto/ionosphere boundary indicated in the sketch above, may develop in the flow. Across these surfaces, continuous solutions of the dissipationless differential equations cease to exist. The flow is no longer governed solely by the differential equations (1), but must be supplemented by additional considerations. Mass, momentum, magnetic flux, and energy must be conserved across these surfaces, and these conditions lead to the following relations which relate quantities on the two sides of any such discontinuity:

$$\left. \begin{aligned} [\rho V_n] &= 0 \\ [\rho V_n V_t + (p + B^2/8\pi) \hat{n} - B_n B_t / 4\pi] &= 0 \\ [B_n V_t - B_t V_n] &= 0 \\ [B_n] &= 0 \\ [\rho V_n (h + V^2/2) + V_n B^2 / 4\pi - (\vec{B} \cdot \vec{V}) B_n / 4\pi] &= 0 \end{aligned} \right\} \quad (4)$$

Here,  $(\hat{n}, \hat{t})$  denote unit vectors normal and tangential to the discontinuity surface, as sketched below,



The basis for important simplifying approximations to the governing tangential discontinuity conditions

$$\begin{aligned} v_n = B_n = [p + B^2/8\pi] = 0 \\ [v_t] \neq 0; [B_t] \neq 0; [\rho] \neq 0 \end{aligned} \quad (9)$$

which apply at the Earth's magnetosphere boundary are that the gas pressure  $p$  is much less than the magnetic pressure  $B^2/8\pi$  in the confined region interior to the magnetopause, and that  $p$  is much greater than  $B^2/8\pi$  in the exterior flow region around the forward part of the magnetopause. Consequently, the boundary condition to be satisfied by the exterior flow at the magnetopause can be satisfactorily approximated by the limiting case of the tangential discontinuity conditions in equation (9) in which there is a vacuum ( $p = \rho = 0$ ) on one side, and no magnetic field on the other. Thus, the condition  $[p + B^2/8\pi] = 0$  becomes

$$(B^2/8\pi)_{\text{mag}} = (p)_{\text{flow}} \quad (10)$$

while the equations governing the magnetic field interior to the magnetopause are

$$\text{div } \vec{B} = 0, \text{ Curl } \vec{B} = 0 \quad (11)$$

Furthermore, it has been shown (refs. 3, 6) that the gas pressure of the flow on the forward portion of the magnetosphere boundary -  $(p)_{\text{flow}}$  in equation (10) - can be approximated adequately by the Newtonian formula

$$p = p_{\text{st}} \cos^2 \psi \quad (12)$$

Here,  $\psi$  is the angle between the outward normal to the magnetosphere boundary and the flow direction of the oncoming undisturbed solar wind, and  $p_{\text{st}}$  is the stagnation or ram pressure exerted on the nose of the magnetosphere and is given by

$$p_{\text{st}} = K \rho_{\infty} V_{\infty}^2 \quad (13)$$

In this relation,  $K$  is a constant usually taken as one, but whose actual value is

$$K = \frac{1}{\gamma} \left[ \frac{(\gamma + 1)(\gamma - 1)}{\gamma - (\gamma - 1)/2M_\infty^2} \right]^{\frac{1}{\gamma - 1}} \quad (14)$$

For the high Mach number flows typical of solar wind conditions,  $K$  approaches 0.844 for  $\gamma = 2$  and 0.881 for  $\gamma = 5/3$ . The important implication associated with the introduction of the Newtonian approximation is that the calculation of the shape of the magnetosphere boundary decouples from the calculation of the external flow.

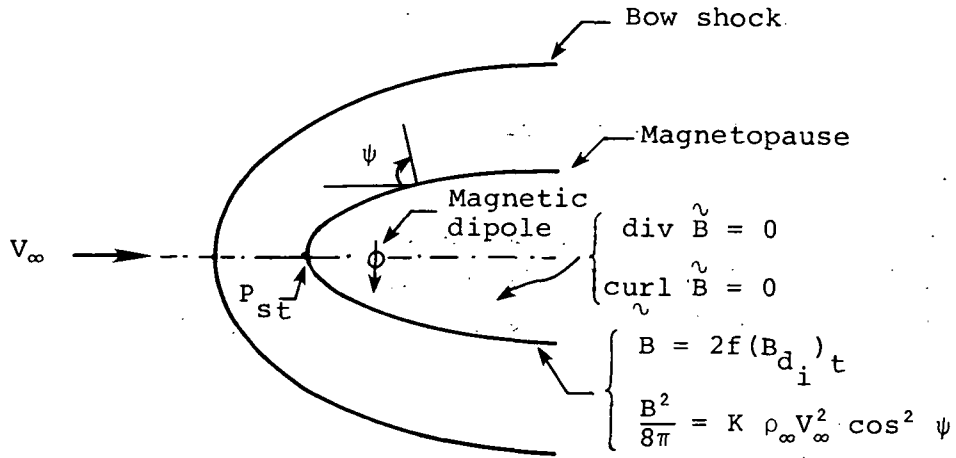
Implementation of the above analysis requires a representation of the Earth's magnetic field. This is provided with sufficient accuracy for the present application by a magnetic dipole located at the center of the Earth and given by

$$\vec{B} = -B_{eq} (a_e/r)^3 (\sin \theta \hat{e}_\theta + 2 \cos \theta \hat{e}_r) \quad (15)$$

where  $B_{eq} = 0.312$  gauss is the strength of the field at the geomagnetic equator,  $a_e = 6.37 \times 10^8$  cm is the radius of the Earth,  $r$  is the geocentric distance, and  $\theta$  is the polar angle measured with respect to the north geomagnetic pole which is at  $78.6^\circ$  north latitude and  $70.1^\circ$  west longitude. The problem for determining the magnetopause and the distortion of the confined geomagnetic field is then reduced to finding a solution of equations (11) which has the dipole singularity equation (15) at the origin, and which satisfies the tangential discontinuity conditions  $B_n = 0$  and  $B^2/8\pi = K\rho_\infty V_\infty^2 \cos^2 \psi$  at the unknown location of the magnetopause. This problem is identical to the classical steady-state Chapman-Ferraro problem (ref. 10) specified over four decades ago, and based on particle rather than continuum concepts. Even at this stage, however, the problem still remains sufficiently complex that only a few numerical solutions have been carried out (refs. 11-13) at the present time. An early approximation which has proven quite successful in providing accurate magnetopause shapes (refs. 9, 12, 14) is to replace the  $B_n = 0$  condition with the condition that the magnetic-field intensity at the magnetosphere boundary is equal to  $2f$  times the tangential component of the Earth's dipole field, where  $f$  is a constant usually taken as unity (refs. 15-17).



The final mathematical statement for the free-boundary problem for the shape of the magnetosphere boundary, then, is summarized in the sketch below:



This formulation leads to the following partial differential equation for the geocentric distance  $r$  to the magnetopause for the case in which the dipole axis is perpendicular to the solar-wind flow (ref. 18)

$$\left[ \frac{1 + 3 \cos^2 \theta}{R_m^6} \left( \frac{1}{R_m \sin \theta} \frac{\partial R_m}{\partial \phi} \right)^2 + \frac{1}{R_m^6} \left( \sin \theta + \frac{2 \cos \theta}{R} \frac{\partial R_m}{\partial \phi} \right)^2 \right] = \left[ \sin \phi \sin \theta - \frac{\sin \phi \cos \theta}{R_m} \frac{\partial R_m}{\partial \theta} - \frac{\cos \phi}{R_m \sin \theta} \frac{\partial R_m}{\partial \phi} \right]^2 \quad (16)$$

where  $R_m = r/D$ ,  $D = a_e (f^2 B_{eq}^2 / 2\pi K \rho_\infty V_\infty^2)^{1/6}$  is the geocentric distance to the magnetosphere nose,  $\phi$  is the geomagnetic longitude measured with respect to a line through the origin that is normal to both the dipole axis and the free-stream direction, and is equal to  $\pi/2$  when directed in the upstream direction, and  $3\pi/2$  when directed downstream.

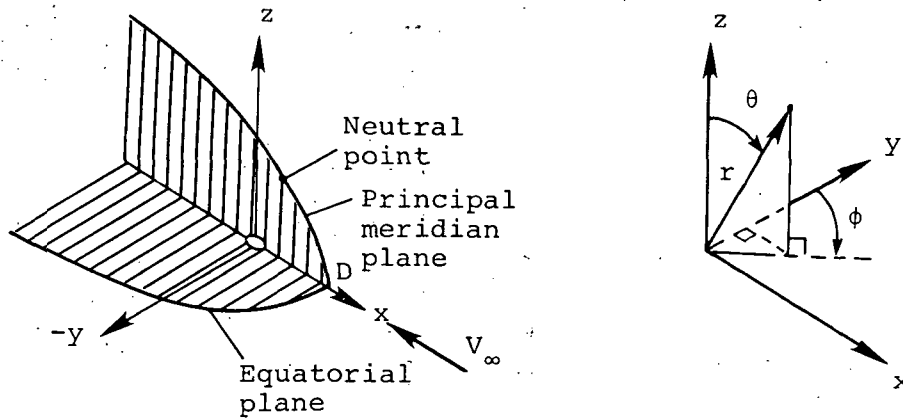
A considerable simplification occurs if attention is confined to either the geomagnetic equatorial plane or the principal meridian plane defined by the dipole axis and the direction of the incident solar wind. These equations are; in the equatorial plane ( $\theta = \pi/2$ ,  $\partial R_m / \partial \theta = 0$ )

$$\frac{dR_m}{d\phi} = R_m \left( \frac{R_m^6 \sin \phi \cos \phi + \sqrt{R_m^6 - 1}}{R_m^6 \cos^2 \phi - 1} \right) \quad \pi/2 \leq \phi \leq \frac{3\pi}{2} \quad (17)$$

and in the principal meridian plane ( $\phi = \pm \pi/2$ ,  $\frac{\partial R}{\partial \phi} = 0$ )

$$\frac{dR_m}{d\theta} = (R_m \tan \theta) \frac{R_m^3 \mp 1}{R_m^3 \pm 2} \quad -\pi/2 \leq \theta \leq \frac{\pi}{2} \quad (18)$$

A sketch of the traces of the magnetosphere boundary in the equatorial and principal meridian planes is provided below together with the spherical ( $r, \theta, \phi$ ) coordinate system. We note in particular that the



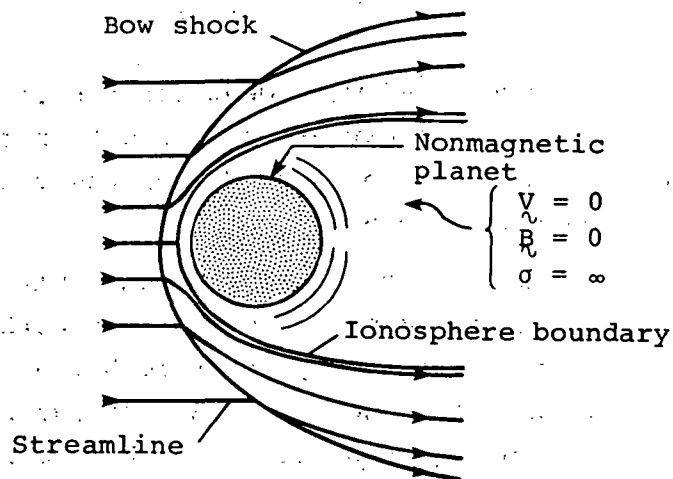
shape of the equatorial trace is a smooth curve, while that of the principal meridian contains a pronounced dent at the location of the neutral point where the magnetic field vanishes in the ideal theory. In all of the reported work to date (refs. 1-4, 6, 8) concerning flow fields past the magnetosphere, the magnetopause has been approximated by an axisymmetric shape obtained by rotating the equatorial trace of the boundary about the longitudinal axis. That this provides a very good approximation to the actual three-dimensional shape is shown in figure 1 which displays in more detail the comparison of the equatorial and principal meridian traces of the magnetopause as calculated by equations (17) and (18), respectively. Also shown on the principal meridian trace is a dashed line which forms a tangent surface across the cusped neutral point region, and which represents the free-streamline surface which will

most likely appear in nature (ref: 19). We note that all three of these shapes are quite close to one another so that the rotated equatorial trace provides a satisfactory approximation to the three-dimensional shape. Furthermore; it has been shown (ref. 3, 13) that higher-order approximations to the Chapman-Ferraro problem for the magnetosphere shape are in reasonable agreement with the approximate shape given by the solution to equation (16).

Consequently, the boundary shape of the magnetosphere for which the majority of results are presented here is the rotated equatorial trace given by equation (17). That shape has been incorporated in the associated computer codes developed herein as the default shape for magnetosphere calculations. Tabulated ordinates ( $Y_m/D$  - vs.  $-x/D$ ) for the equatorial trace are provided in Table 1 where  $Y_m$  is the cylindrical radial coordinate of the profile.

#### Nonmagnetic Planet - Determination of the Ionosphere Boundary

The determination of the ionosphere boundary initiates from the assumptions that the ionosphere, or at least the outer part of it that participates in the interaction with the solar wind, is idealized as a spherically symmetric and hydrostatically supported plasma having infinite electrical conductivity, effectively bound to the planet and incapable of mixing with the solar wind, as indicated in the sketch below:



This interior plasma is separated from the flowing solar plasma by a tangential discontinuity across which the same relations, given previously by equations (9) for the analogous problem for a magnetic planet, must hold. The assumption of hydrostatic support implies a quiescent ionosphere in which the bulk motions of the gas with respect to the planet are sufficiently small ( $v = 0$ ) that equilibrium exists between the pressure gradient and gravity, viz.

$$\frac{dp}{dr} = -\rho g \quad (19)$$

where  $p$  and  $\rho$  are the gas pressure and density,  $r$  is the radial distance measured from the center of the planet, and  $g$  is the acceleration due to gravity. The variation of  $g$  is inversely proportional to  $r^2$ , so that  $g = g_s (r_s/r)^2$  where the subscript  $s$  denotes values at the surface of the planet. Since the density  $\rho$  is related to the pressure according to the perfect gas law equation (2), equation (19) can be integrated to yield

$$p = p_R \exp\left(-\int_{R_R}^r \frac{dr}{H}\right) \quad (20)$$

where  $p_R$  is the pressure at some reference radius  $R_R$  and  $H$  is the local scale height of the atmosphere given by  $H = RT/g$ . If  $H$  is regarded as constant; that is, if variations of  $g$  and  $T$  with  $r$  are neglected, equation (20) can be integrated directly to yield

$$p = p_R \exp\left(-\frac{r - R_R}{H}\right) \quad (21)$$

In view of uncertainties associated with measurements of the atmospheric properties of Venus and Mars, the variation of  $p$  with  $r$  as given by equation (21) was adopted in previous solar wind/ionosphere applications (ref. 5) and has also been used herein.

In the present application, it is also evident that the gas pressure  $p$  is much larger than the magnetic pressure  $B^2/8\pi$  on both sides of the ionopause. Therefore, the discontinuity pressure balance relation  $[p + B^2/8\pi] = 0$  of equation (9) reduces to a simple equality between the ionospheric pressure given by equation (21) and the static pressure of the flowing solar plasma adjacent to the ionopause. Introducing as in the magnetosphere application the Newtonian approximation equation (12) for

the static pressure of the flowing plasma on the exterior boundary of the ionosphere, we arrive at the following equation for the pressure balance at the ionopause  $R_i$ :

$$p_{st} \cos^2 \psi = K \rho_{\infty} V_{\infty}^2 \cos^2 \psi = p_R \exp \left( - \frac{R_i - R_R}{H} \right) \quad (22)$$

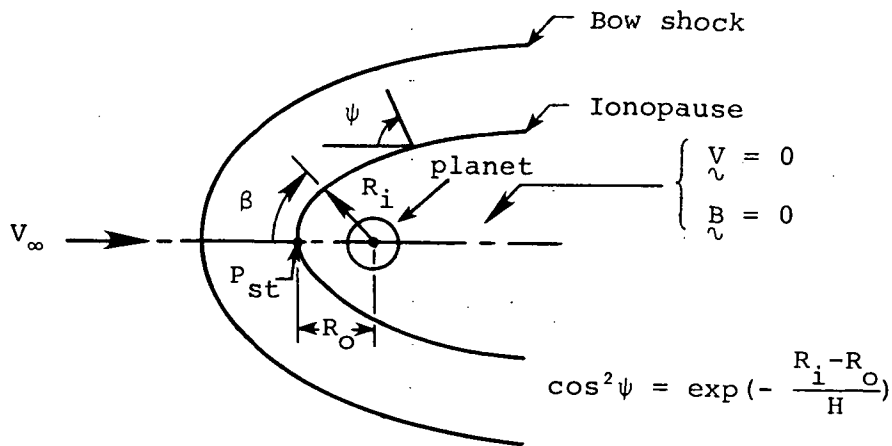
It is convenient to choose as the reference radius and location the stagnation point on the ionopause; that is,  $R_R = R_O$  where  $R_O$  is the distance from the center of the planet to the nose of the ionopause. This implies that

$$p_R = p_O = K \rho_{\infty} V_{\infty}^2 \quad (23)$$

and that at all points along the ionosphere boundary

$$\cos^2 \psi = \exp \left( - \frac{R_i - R_O}{H} \right) \quad (24)$$

The final mathematical statement of the free-boundary problem for determining the shape of the ionosphere boundary then is summarized in the sketch below:



By relating the local angle  $\psi$  to the slope of the ionopause, the following ordinary differential equation results for the ordinates of the ionosphere boundary

$$\frac{dR_i}{d\beta} = R_i \left[ \frac{\sin 2\beta - 2\sqrt{\Lambda - \Lambda^2}}{2(\Lambda - \sin^2 \beta)} \right] \quad 0 \leq \beta \leq \pi \quad (25)$$

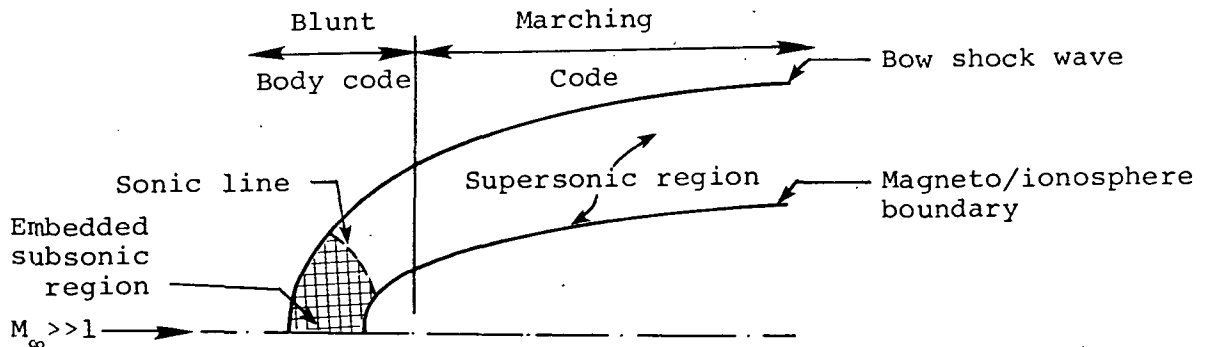
where

$$\Lambda = \exp[-(R_i - R_0)/H] \quad (26)$$

and  $\beta$  is the angle measured from the subsolar point as indicated above. Results for various ionopause shapes obtained by integrating equation (25) for different values  $H/R_0$  in the range  $0.001 \leq H/R_0 \leq 1.0$  are provided in figure 2. We note that the range of interest for planetary applications to Venus and Mars appears to be  $0.01 \lesssim H/R_0 \lesssim 0.30$  (ref. 5). Tabulated ordinates ( $Y_i/R_0$  vs.  $-X/R_0$ ) are provided in Table 1 for  $H/R_0 = 0.01, 0.1, 0.2,$  and  $0.5$ , where  $Y_i = R_i \sin \beta$  is the cylindrical radial coordinate of the ionopause profile.

### Calculation of the Gasdynamic Flow Properties

Computation of the gasdynamic flow properties consists of determining solutions to the differential equations and discontinuity conservation equations given by equations (7). Because both the downstream tail region (far field) as well as the region in the vicinity of the obstacle nose (near field) are generally of interest in solar wind-magneto/ionopause interactions, the computational methods selected must be capable of determining this entire flow field. In view of the need to carry the flow calculation to an arbitrary downstream distance, the most computationally efficient procedure to employ is to subdivide the flow field into two regions, as indicated in the sketch below:



Illustrated here are the essential features of the high supersonic Mach number flow typical of solar wind flows past terrestrial planets. Of special note is the embedded subsonic pocket, located at the nose of the magneto/ionopause. The presence of this pocket necessitates use of a computational technique capable of treating a mixed subsonic/supersonic flow. Downstream of this region, the flow becomes supersonic and remains so for the convex shapes typical of magneto/ionopause boundaries. In that far field region, a more economical procedure than that used near the nose can be employed.

We note that this subdivision of flow field and use of different solution procedures in each region is common practice for calculating hypersonic blunt-body flows, and was employed in the former solar wind method (ref. 3) as well as in a more recent application to space shuttle re-entry flows (ref. 20). Indicated in figure 3 is a comparison of the former and present computational procedures which illustrates the breakdown of the various solution domains. The previous method treated the nose region by the inverse iteration method, and the remainder of the flow field by the method of characteristics. In light of recent advances, both of those techniques, particularly the inverse method, are now considered dated and inferior to more current methods. In the present study, those two methods have been superseded by: (1) a new axisymmetric implicit unsteady Euler equation solver (IMP) specifically developed under this contract (ref. 21) and which determines the steady state solution in the nose region by a time-marching procedure, and (2) a shock-capturing marching solution (SCT) which spatially advances the solution downstream as far as required by solving the steady Euler equations. As indicated in figure 3, the implicit unsteady Euler equation (IMP) code is used to determine the flow in the region between the stagnation streamline on the symmetry axis and a body-axis normal plane ( $x = \text{constant}$ ) conveniently chosen at the  $\beta = 90^\circ$  ( $x = 0$ ) location. For the magneto/ionopause shapes considered here, purely supersonic flow exists on this plane and the conditions there provide the starting data for the SCT code. The SCT code then marches the solution downstream in axis normal planes to the final specified location.

Obstacle nose solution - implicit unsteady Euler equation (IMP) code.-  
The partial differential equations employed in the implicit (IMP) code are the unsteady axisymmetric versions of the gasdynamic Euler equations given

by equations (7). To implement the calculation, those equations are written in conservation-law form under the generalized independent variable transformation

$$\left. \begin{aligned} \tau &= T \\ \xi &= \xi(T, X, R) \\ \eta &= \eta(T, X, R) \end{aligned} \right\} \quad (27)$$

as follows:

$$\begin{aligned} (U/J)_{\tau} + [(\xi_T U + \xi_X E + \xi_R F)/J]_{\xi} \\ + [(\eta_T U + \eta_X E + \eta_R F)/J]_{\eta} + G = 0 \end{aligned} \quad (28)$$

where

$$U = \begin{pmatrix} \rho \\ \rho u \\ \rho v \\ e \end{pmatrix} \quad E = \begin{pmatrix} \rho u \\ p + \rho u^2 \\ \rho uv \\ (e + p)u \end{pmatrix} \quad (29)$$

$$F = \begin{pmatrix} \rho v \\ \rho uv \\ p + \rho v^2 \\ (e + p)v \end{pmatrix} \quad G = \frac{1}{RJ} \begin{pmatrix} \rho v \\ \rho uv \\ \rho v^2 \\ (e + p)v \end{pmatrix}$$

and the Jacobian

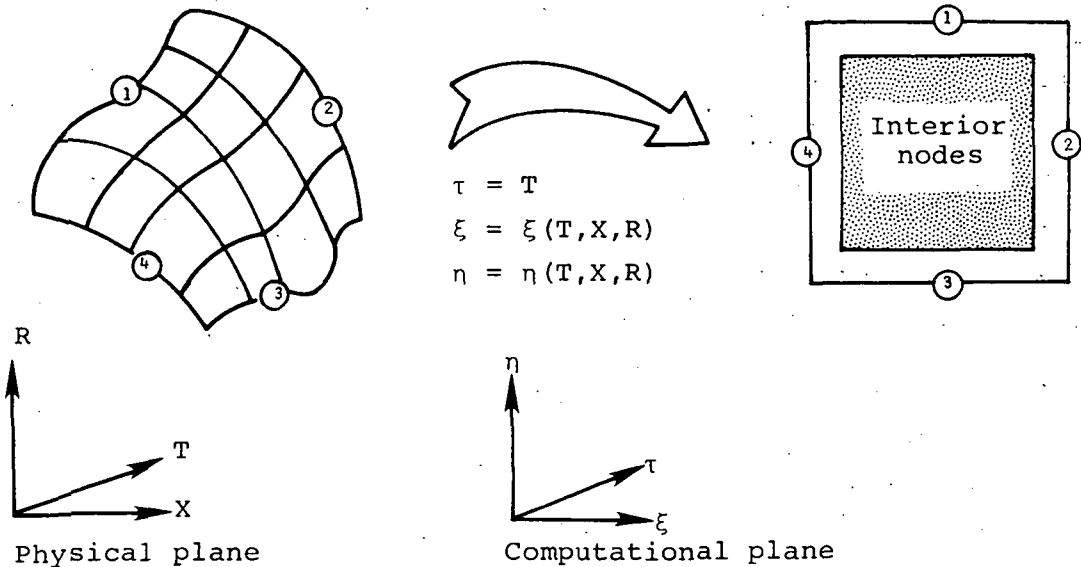
$$J = \xi_X \eta_R - \xi_R \eta_X \quad (30)$$

In equations (27) to (30),  $T$  denotes time,  $X$  is the axial downstream direction, and  $R$  is the cylindrical radial distance;  $p$  represents the pressure;  $\rho$  the density;  $u$  and  $v$  the velocity components in the  $X$  and  $R$  directions, respectively; and  $e$  the total energy per unit volume. The following equation relates the pressure, density, and velocity components to the energy for an ideal gas

$$e = p/(\gamma - 1) + \rho(u^2 + v^2)/2 \quad (31)$$



Using the independent variable transformation equation (27), the physical plane with boundaries 1-4 in  $X, Y, T$  space is mapped into the rectangular computational plane  $\xi, \eta$ , and  $\tau$  space as shown in the sketch below. Generally, at each time step the transformation metrics are not known beforehand and must be determined numerically. Integration step size is established by using the eigenvalues of the Jacobian matrices  $\bar{A}$  and  $\bar{B}$ , where  $\bar{A} = \partial \hat{E} / \partial \hat{U}$ ,  $\bar{B} = \partial \hat{F} / \partial \hat{U}$  and  $\hat{U} = U/J$ ,  $\hat{E} = (\xi_T U + \xi_X E + \xi_R F) / J$ , and  $\hat{F} = (\eta_T U + \eta_X E + \eta_R F) / J$ .



The boundaries, as indicated in the sketch, at which appropriate conditions are imposed on the present problem consist of: (1) the bow shock surface at which the Rankine-Hugoniot relations are satisfied, (2) the downstream outflow boundary where the flow is assumed to be entirely supersonic, (3) the obstacle surface at which a no flow condition in the normal direction is imposed, and (4) the stagnation streamline where symmetry conditions are implemented. Initial flow field conditions are determined by guessing a bow shock shape for the particular blunt obstacle at hand and by prescribing a Newtonian pressure distribution on the body. Since the maximum entropy streamline wets the body, that fact plus the known surface flow direction serve to determine the remainder of the flow properties on the obstacle surface. A linear variation for the flow properties between the bow shock and the obstacle is then prescribed.

This provides the initial flow field which is then integrated in a time-asymptotic fashion until the steady-state solution is obtained.

The basic numerical algorithm used in the IMP code was developed by Beam and Warming (ref. 22) and is second-order accurate, noniterative, and spatially factored. In particular, the "delta form" with Euler time differencing is employed. When applied to equation (28) the algorithm assumes the form

$$(I + \Delta\tau\delta_{\xi}\bar{A}^n)(I + \Delta\tau\delta_{\eta}\bar{B}^n)(\hat{U}^{n+1} - \hat{U}^n) = -\Delta\tau(\delta_{\xi}\hat{E}^n + \delta_{\eta}\hat{F}^n + G) \quad (32)$$

where  $\bar{A}$  and  $\bar{B}$  are the Jacobian matrices,  $I$  is the identity matrix,  $\delta_{\xi}$  and  $\delta_{\eta}$  are second-order, central difference operators,  $U^{n+1} = U(n\Delta\tau)$  and  $\Delta\tau$  is the integration step size.

Equation (32) is solved at the interior points only. It requires two  $4 \times 4$  block tridiagonal inversions at each time step of the integration. The solution procedure is as follows:

1. Define  $\Delta\hat{U} = U^{n+1} - \hat{U}^n$ .
2. Form the right-hand side of equation (32) and store results in the  $\hat{U}^{n+1}$  array.
3. Define  $\bar{U} = (I + \Delta\tau\delta_{\eta}\bar{B}^n)\Delta\hat{U}$  and solve the matrix equation  $(I + \Delta\tau\delta_{\xi}\bar{A}^n)\bar{U} = \hat{U}^{n+1}$  for  $\bar{U}$  storing the result in the  $\hat{U}^{n+1}$  array.
4. Solve the matrix equation  $(I + \Delta\tau\delta_{\eta}\bar{B}^n)\Delta\hat{U} = \hat{U}^{n+1}$  for  $\Delta\hat{U}$ .
5. Obtain the values of  $\hat{U}^{n+1}$  from the relation  $\hat{U}^{n+1} = \Delta\hat{U} + \hat{U}^n$ .
6. Obtain the final solution after applying the smoothing;  $\hat{U}^{n+1} = \hat{U}^{n+1} - (\epsilon/8)S/J$ .

A fourth-order smoothing term  $S$  is usually required to eliminate nonlinear instabilities which may arise since the use of central differences in the spatial directions results in a neutrally stable algorithm.

Downstream solution - shock capturing steady Euler equations (SCT) code. - Since the shock-capturing technique employed has been established previously (refs. 23, 24, 25) only a brief description will be provided here. The steady, full three-dimensional Euler equations are written in cylindrical coordinates in the form:

$$\frac{\partial \tilde{U}}{\partial X} + \frac{\partial \tilde{F}}{\partial R} + \frac{\partial \tilde{G}}{\partial \omega} + \tilde{H} = 0 \quad (33)$$

where

$$\left. \begin{aligned} \tilde{U} &= \begin{pmatrix} \rho u \\ p + \rho u^2 \\ \rho uv \\ \rho uw \end{pmatrix} & \tilde{G} &= \frac{1}{R} \begin{pmatrix} \rho w \\ \rho uw \\ \rho vw \\ p + \rho w^2 \end{pmatrix} \\ \tilde{F} &= \begin{pmatrix} \rho v \\ \rho uv \\ p + \rho v^2 \\ \rho vw \end{pmatrix} & \tilde{H} &= \frac{1}{R} \begin{pmatrix} \rho v \\ \rho uv \\ \rho(v^2 - w^2) \\ 2\rho vw \end{pmatrix} \end{aligned} \right\} \quad (34)$$

Here  $p$  and  $\rho$  represent dimensional pressure and density and  $(u, v, w)$  denote velocity components in the cylindrical coordinate directions  $(X, R, \omega)$ , respectively, where  $X$  is the axial downstream direction,  $R$  is the cylindrical radius in an axis-normal plane, and  $\omega$  is the azimuthal angle measured in the axis-normal plane. This set of equations is closed by the use of energy conservation as provided by the equation for total enthalpy

$$H_t = h(p, \rho) + \frac{q^2}{2} = \text{constant} \quad (35)$$

where

$$q = \sqrt{u^2 + v^2 + w^2} \quad (36)$$

is the magnitude of the velocity vector and  $h(p, \rho)$  is the caloric equation of state.

The equations are then transformed to a computational plane by using the independent variable transformation

$$\begin{aligned} X &= X \\ \xi(X, R, \omega) &= \frac{(R - R_b)}{(R_s - R_b)} \end{aligned} \quad (37)$$

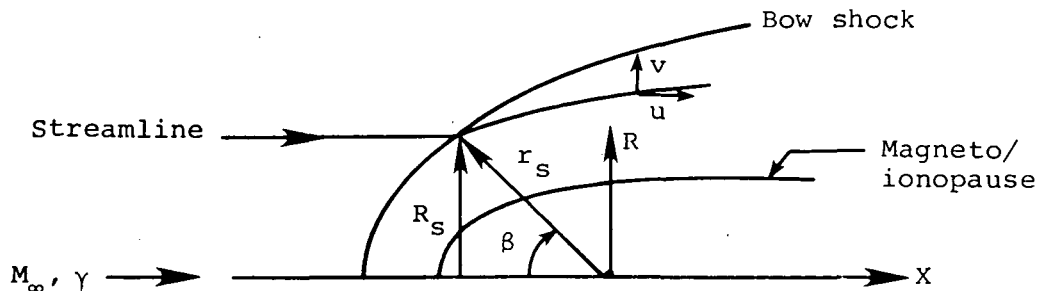
$$\xi(\omega) = f(\omega)$$

where the subscripts (b,s) denote body and shock surfaces, respectively. This change of variable is employed in equation (33) and the result then rearranged into the following conservation law form (refs. 23,24,25).

$$\frac{\partial U}{\partial X} + \frac{\partial F}{\partial \xi} + \frac{\partial G}{\partial \eta} + H = 0 \quad (38)$$

The finite-difference formulation of MacCormack (ref. 26) is used to integrate equation (38) with respect to the hyperbolic coordinate X to yield values of the conservative variable U. This procedure is calculable as long as the flow velocity in the axial (X) direction is greater than the local speed of sound. We note that for the axisymmetric obstacle shapes considered here,  $\partial/\partial\omega = 0$ ; however, the version of the SCT code employed has the capability for treating full three-dimensional geometries.

Streamline and contour calculations.- A number of special purpose subroutines were written to calculate streamlines and contour maps of various flow field properties, and also to provide automated plots of these quantities. The streamlines are determined by integrating trajectories through the known velocity field as this procedure was found to be more accurate than a mass flow calculation. The calculation of a particular streamline is initiated at the point where the streamline crosses the bow shock, as shown below:



At that point, exact values of the streamline slope  $dR_s/dX$  are known in terms of the local shock angle  $\delta_s$  and free-stream quantities according to the relation

$$\frac{dR_s}{dX} = \frac{2 \cdot \cot \delta_s \cdot (M_\infty^2 \sin^2 \delta_s - 1)}{2 + M_\infty^2 (\gamma + 1 - 2 \sin^2 \delta_s)} \quad (39)$$

which is implicit in the blunt-body (IMP) and marching (SCT) code solutions. At other points in the flow field, the local streamline slope is given by the ratio of radial to downstream velocity, i.e.

$$\frac{dR_s}{dX} = \frac{v}{u} \quad (40)$$

and the streamline determination is made by stepwise integration in X of equation (40) according to a modified third-order Euler predictor/corrector method. Two-dimensional linear interpolation from the flow field grid points is employed to obtain the velocity components (u,v) required at the stepwise points along the streamline trajectory. Separate streamline calculations are made for the near field (IMP results) and far field (SCT results) because of the different coordinate systems employed in those two regions.

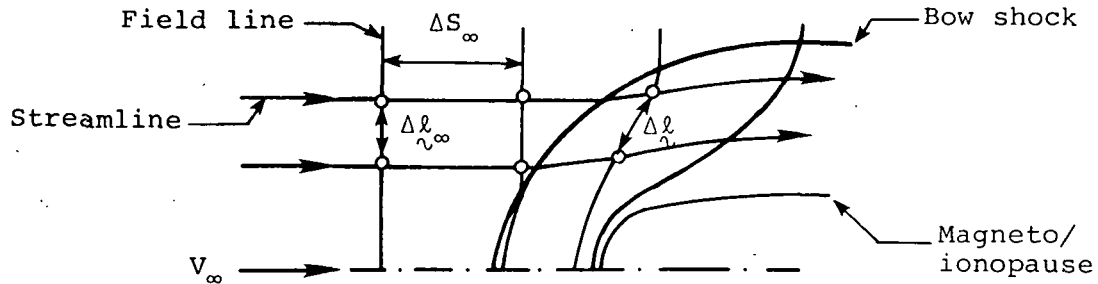
Contours of various flow field quantities are determined for the entire flow field (near field plus far field) by using a modified version of the contour package developed by R. Sorensen at NASA/Ames Research Center. Pertinent details of that package are provided in the user's manual section of this report.

#### Calculation of the Magnetic Field

With the flow properties known from the gasdynamic calculations, determination of the magnetic field  $\vec{B}$  proceeds by integrating equations (8). Those equations are commonly interpreted as indicating the field lines move with the fluid. This leads to a straightforward, although tedious, calculation in which the vector distance from each point on an arbitrarily selected fluid line to its corresponding point on an adjacent field line in the downstream direction is determined by numerically integrating  $\int \vec{v} dt$  over a fixed time interval  $\delta t$ . While that calculation determines the location of the field lines, the intensity of the magnetic field at any point may then be calculated from the relation

$$\frac{|\underline{B}|}{|\underline{B}_\infty|} = \frac{\rho |\Delta \underline{\ell}|}{\rho_\infty |\Delta \underline{\ell}_\infty|} \quad (41)$$

where  $\Delta \underline{\ell}$  is the vector length of a small element of a flux tube. The sketch below clarifies these quantities for the case when the oncoming  $\underline{B}_\infty$  field is perpendicular to the flow:



where the open symbol  $\odot$  denotes locations of points on the streamlines corresponding to a fixed time interval  $\Delta t = \Delta S_\infty / V_\infty$ .

Because of the axisymmetry of the gasdynamic quantities and the linearity of the equations for  $\underline{B}$ , Alksne and Webster (ref. 27) have shown that the magnetic field at any point in the flow field can be calculated by vectorially summing the contributions of the three component fields indicated in figure 4. At any point P, the magnetic field  $\underline{B}_P$  is given by

$$\underline{B}_P = \left( \frac{B_P}{B_\infty} \right)_{\parallel} B_{\infty \parallel} + \left( \frac{B_P}{B_\infty} \right)_{\perp} B_{\infty \perp} + \hat{e}_n \left( \frac{B_P}{B_\infty} \right)_n B_{\infty n} \quad (42)$$

where the subscripts ( $\parallel$ ,  $\perp$ ,  $n$ ) refer respectively to the contributions associated with the components of  $\underline{B}_\infty$  parallel to  $\underline{V}_\infty$ ; perpendicular to  $\underline{V}_\infty$  in the plane that contains the point P, the center of the planet, and the vector  $\underline{V}_\infty$ ; and normal to the latter plane.

For the contribution associated with the parallel component  $B_{\infty \parallel}$ , it has been shown (refs. 28,29) that  $\left( \frac{B_P}{B_\infty} \right)_{\parallel}$  is proportional to  $\rho \underline{V}$  throughout the entire flow field. Consequently, this component can be calculated directly from the gasdynamic solution by the expression

$$\left( \frac{B_P}{B_\infty} \right)_{\parallel} = \frac{\rho_p \underline{V}_p}{\rho_\infty |\underline{V}_\infty|} \quad (43)$$

Similarly, the normal component  $(B_P/B_\infty)_n$  can be shown to be equal to

$$\left( \frac{B_P}{B_\infty} \right)_n = \frac{R_P \rho_P}{R_{P_\infty} \rho_\infty} \quad (44)$$

where  $R_P$  is the radial cylindrical coordinate of the streamline, as indicated in figure 4.

The determination of the contribution  $(B_P/B_\infty)_t$  cannot be made directly from the gasdynamic properties as can the other two components. For this component, recourse must be made to the general computation associated with equation (41). Details of the calculation procedure for  $(B_P/B_\infty)_t$  are provided in the user's manual section of this report.

## RESULTS AND DISCUSSION

In order both to verify the correctness of the procedures developed under this study as well as to demonstrate their flexibility and power for calculating solar wind flows for a variety of conditions, a large number of test cases have been run. A representative sample of the results obtained from those calculations is reported here. Because the implicit blunt-body procedure (IMP code) is new, that code was tested and compared to previously established theoretical methods to substantiate its validity prior to solar wind applications. We have prepared figure 5 to exhibit such a comparison. Here, flow field results predicted by the present implicit method are compared with those of other theoretical techniques and also experimental data for supersonic flow past a sphere with  $M_\infty = 4.926$  and  $\gamma = 1.4$ . The variation of density and Mach number along the stagnation streamline are provided in the two plots on the left, while the variation of surface pressure and shock standoff distance with spherical angle are given in the two plots on the right. In all of these comparisons, the present theoretical results are in excellent agreement with both established theoretical methods and experiment.

Figure 6 exhibits a comparison of results predicted by the implicit method for a solar wind calculation. The upper plot of the figure displays the locations of the bow wave and sonic line for flow past the equatorial trace of the magnetopause for  $M_\infty = 8$  and  $\gamma = 5/3$ . The density distribution along the magnetosphere boundary and along the shock wave for this flow are given in the lower plot. Included in both of these figures is the solution calculated by Spreiter et al. (ref. 3) using the inverse method of Inouye and Lomax (ref. 30). Excellent agreement is obtained between the present implicit technique and the inverse method. Figure 7 provides analogous results for the equatorial trace of the magnetopause for a variety of Mach numbers typical of solar wind flows, and illustrates the Mach number capability of the present IMP code.

With regard to solar wind flows past nonmagnetic planets, figure 8 displays results for the bow shock location for  $M_\infty = 8$  and  $\gamma = 5/3$  flow past various ionopause shapes with  $H/R_0 = 0.01, 0.1, 0.2, 0.25, 0.50, 0.75$  and  $1.0$ . Not included in that figure for clarity of presentation are the results of Spreiter et al. (ref. 5) obtained by using the inverse method. Those results and the predictions of the present implicit method given in figure 8 are essentially indistinguishable.



As an illustration of the geometric flexibility of the present implicit method and also as a critical test of its ability to capture embedded shock waves besides the bow shock, a feature which the inverse method cannot duplicate, figures 9 and 10 have been prepared. This calculation corresponds to the  $M_\infty = 5$  and  $\gamma = 5/3$  flow around the axisymmetric shape generated by rotating the principal meridian of the magnetopause about its axis and compares with an experimental test by Spreiter et al. (ref. 3). This particular profile shape contains a pronounced dent with a concave corner in the vicinity of the neutral point. Spreiter et al. (ref. 3) have argued that the presence of a concave corner in the magnetopause is unrealistic and would not occur in nature, but should be replaced by a free surface created by drawing a tangent line across the corner. In figure 9, we present results for both the concave and the free surfaces, denoted by solid and dashed lines, respectively. For the concave surface, a pocket of embedded subsonic flow is seen to form behind the embedded shock wave which was caused by the indented profile. If the surface is modified to the free surface shape, the embedded wave disappears completely as expected. The corresponding pressure coefficients on the magnetosphere boundary are presented in figure 10. For the concave surface, the shock wave is located on the body at approximately  $\beta = 80^\circ$ , while for the free surface, the pressure coefficient displays a constant value as anticipated. Finally, we note that the calculation of a supersonic flow with an embedded shock and subsequent subsonic pocket provides a severe test for any blunt body procedure. The ability of the present code to provide convergent results for such a flow demonstrates the capability for further extension and application to more generalized profiles than was heretofore possible.

As a final indication of the range of solar wind flows over which the implicit code has been tested, we have prepared figure 11 which displays the variation of shock stand-off distance with oncoming Mach number and ratio of specific heats for three different magneto/ionopause shapes. These include the rotated equatorial trace of the magnetopause, and the ionopause shapes for  $H/R_\odot = 0.01$  and  $0.5$ . Those shapes and the corresponding ranges of  $M_\infty$  and  $\gamma$  essentially span the entire range of interest of geometry and solar wind conditions for which the computer programs developed herein would be normally applied.

In order to demonstrate the ability of the marching code to continue the blunt-body IMP solution downstream to some arbitrarily-specified

downstream location, and also to verify its stability and convergence for application to these classes of flows, we have calculated marching solutions for a variety of cases typical of solar wind interactions. Figure 12 exhibits the location of the bow wave for flows with  $\gamma = 5/3$  and  $M_\infty = 3, 8, \text{ and } 25$  past the rotated equatorial trace of the magnetopause as the flow proceeds downstream from the nose region to  $x/D = -11$ . For this calculation, starting conditions for the marching code (SCT) have been provided by the blunt-body (IMP) code on the line  $x/D = 0.0$ , which is the usual location at which the two solutions are joined by the computer program. The marching code then determines the remainder of the flow field back to the specified downstream location. Since for the particular shapes considered herein the downstream flows are quite smooth, the marching calculation is very efficient (less than 30 sec., CDC 7600, OPT=2 compiler). Similar results are presented in figure 13 for  $M_\infty = 8$  and  $\gamma = 5/3$  flow past an ionopause shape with  $H/R_0 = 0.1$ . Those results have been carried downstream to  $x/R_0 = -20$  since this distance is more typical of the region of interest for nonmagnetic planets. This is so because of the different scalings ( $D, R_0$ ) used for the magnetic and nonmagnetic applications. For Venus and Mars, the location of the ionopause nose is at a distance only slightly greater than the planetary radius, as compared with the location of the magnetopause nose for the Earth which is of the order of 10 planetary radii.

In order to illustrate the capability of the present procedures to determine streamlines, contour maps of various flow properties, and magnetic field lines and contours, as well as to demonstrate the automated plotting capability for displaying these results, figures 14 and 15 have been prepared. Figure 14 illustrates the computer generated streamline locations and contour maps of density  $\rho/\rho_\infty$  and velocity ratio  $V/V_\infty$  for the complete near and far field flow about the equatorial trace of the magnetosphere for  $M = 8$  and  $\gamma = 5/3$ . Based on this gasdynamic solution, figure 15 exhibits the corresponding results for the magnetic field components  $(B/B_\infty)_\perp$  and  $(B/B_\infty)_\parallel$  in the plane of symmetry. Both magnetic field line locations and contours are provided. In addition to demonstrating the overall smoothness of the computed results, these two figures illustrate the ability of the present techniques to provide the completely automated production of report quality plots of both gasdynamic and magnetic field properties for solar wind flows past axisymmetric magneto/ionopause shapes

## CONCLUDING REMARKS

Theoretical analysis and associated development of computer programs were carried out for the purpose of developing computational techniques for predicting the interaction of solar wind flows with both magnetic and nonmagnetic terrestrial planets. Based on the identical theoretical model employed in previous work, i.e. the steady, dissipationless, magnetohydrodynamic model for axisymmetric, supersonic, super-Alfvénic solar wind flow a new and more powerful solution procedure has been developed. The procedure is built upon an assemblage of computer codes, including:

- Blunt-body code - to determine gasdynamic solution near obstacle nose
- Marching code - to determine gasdynamic solution downstream of obstacle nose
- Streamline code - to determine flow field streamlines
- Contour code - to determine contour maps of flow and magnetic field properties
- Magnetic field code - to determine frozen-in magnetic field
- Plotting code - to plot selected flow and magnetic field results

Comparisons are reported which demonstrate the accuracy of the present techniques by comparison with previously-established theoretical methods as well as limited experimental data. Furthermore, new results are presented for a variety of solar wind flows which illustrate the flexibility and generality of the component methods. The computational procedures are fully automated and provide detailed flow field and magnetic field properties in convenient output format, including an automatic plot capability. The programs are documented and are presented in a general user's manual included as part of this report.

With regard to improvements of the present techniques to provide a more accurate mathematical representation of solar wind flow, a number of items for further study are recommended. The first of these involves extension of the present capability from axisymmetric to three-dimensional nonaxisymmetric obstacle shapes representative of planetary magnetopauses. The second involves the merging of the present procedures for determining the magnetic field exterior to the magnetosphere boundary with a method, such as the Olsen-Pfitzer model, for calculating the confined magnetic field so as to provide a complete magnetic field representation. Lastly, the capability for determining numerical solutions of the complete magnetohydrodynamic equations, rather than the frozen magnetic field approximation,

should be actively pursued. Although this extension represents a major advance in magnetospheric physics and computational fluid dynamics, in view of the success of the currently employed methods, its successful achievement appears highly promising. The component methods on which the present procedure is based are directly capable of extension in these as well as other directions. Moreover, the efficiency of the present calculations indicates that the improved representation achieved by these improvements will not result in prohibitive computational costs.

## APPENDIX A

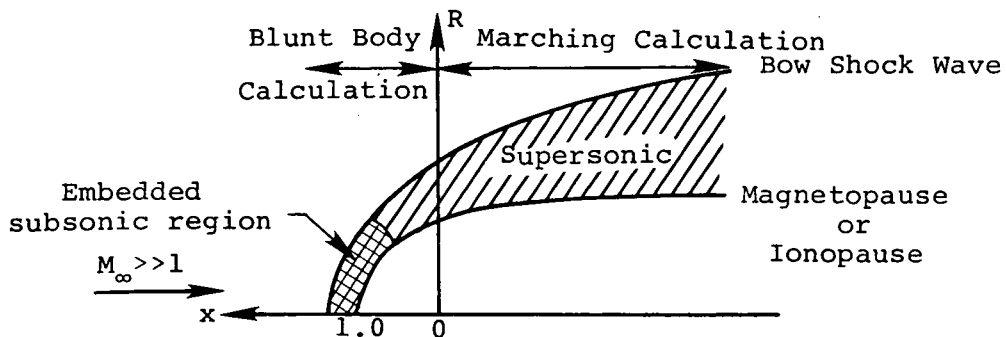
### A.1 Introduction

The purpose of this appendix is to describe the operation of the assemblage of computer codes which were developed in conjunction with the theoretical work presented in this report and organized into one program, and to provide sufficient detail to permit understanding and use of the program. The program computes the flow field of the solar wind about a terrestrial planet, using a procedure for the calculation of supersonic/hypersonic flow about an axisymmetric blunt body. The corresponding frozen-in magnetic field is then calculated from the previously determined velocity and density fields. Streamlines and contour lines of various flow field properties and magnetic field components are also determined.

A description of the general operating procedure of the program is given, with descriptions of input and output. The program is written in FORTRAN IV and has been developed on a CDC 7600 computer. University Computing Company (UCC) Standard Plotting Software and Functional Software packages are used to produce automated plots. Files used, besides TAPE5 for INPUT and TAPE6 for OUTPUT, are TAPE1 for the plot file (system default), TAPE4 for input file for rerun option, and TAPE9 for storing data for rerun. Typical run times for cases using the default parameters are 40 to 50 seconds, using the OPT=2 compiler. For a case using the rerun option, which employs a previously calculated flow field, the run time is approximately 5 seconds.

### A.2 Program Description

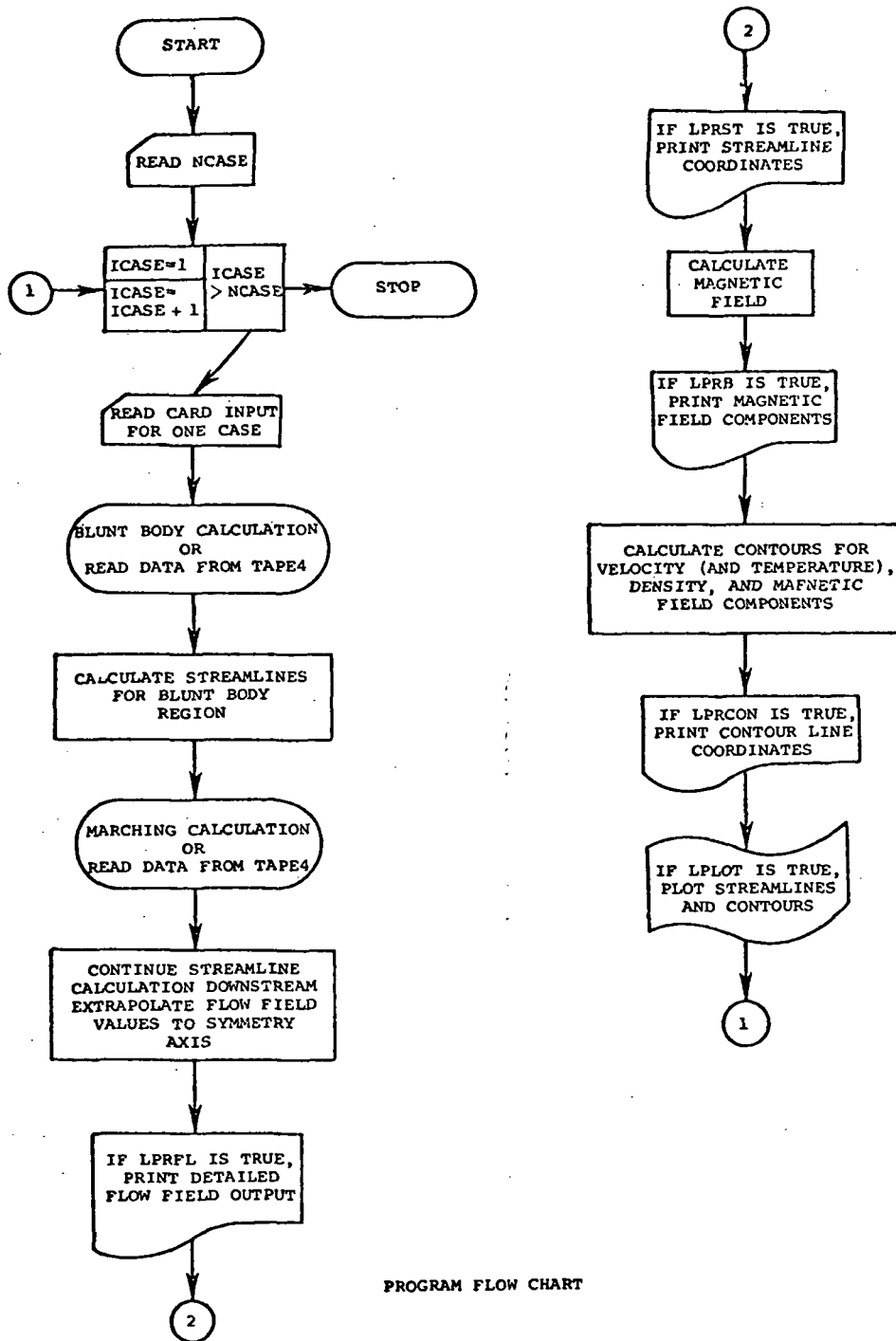
For computational purposes, the flow is subdivided into two regions, as indicated in the sketch below, with the center of the planet as origin.



The region near the nose of the magnetopause/ionopause includes all of the imbedded subsonic flow and part of the supersonic flow. An axisymmetric

implicit unsteady Euler equation solver is used to calculate this part of the flow field. Using the solution plane at  $x = 0.0$  to provide starting conditions, the flow field in the purely supersonic downstream region is determined by integrating the steady Euler equations using a spatial marching procedure. Streamlines, the magnetic field, and contours are calculated using the entire flow field, distinguishing between the two regions as required by the different forms of the computational grids. A rerun capability is provided, where flow field data is read from a file written on a previous run, rather than repeating the blunt body and marching calculations. The computations proceed as shown in the sketch below, which provides an overall flow chart of the complete program. The program provides for several cases to be run consecutively.

APPENDIX A

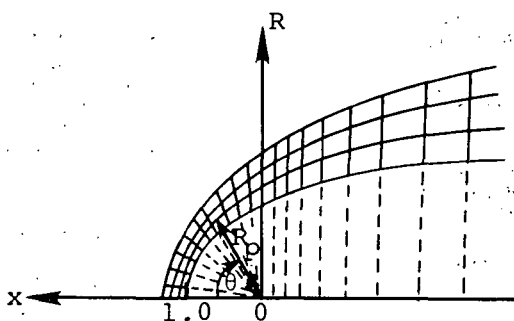


PROGRAM FLOW CHART

## A.2.1 Calculation Procedure

After reading in the number of cases in the run, each case is calculated independently. Subroutine INPUT reads in all card input required for one case, viz. a title, flow conditions, obstacle geometry, calculation and print control parameters, and desired contour values. The user may supply the obstacle geometry in the form of a shape table for an axisymmetric body, or use one of the default shapes which are calculated internally by the program. These default shapes are the magnetopause equatorial trace and a constant scale-height ionopause for which  $H/R_0$  is specified by the user. The input is printed as the first item of output.

A computational mesh in polar  $(R_p, \theta)$  coordinates is established for the blunt body calculation; then, for the marching calculation, this is extended into a cylindrical  $(x, R)$  system, as indicated below:



All lengths,  $x$ ,  $R$ ,  $R_p$ , are scaled so that the nose of the obstacle is at  $x = 1.0$ . For the default shapes, rays at equal angular increments of  $\Delta\theta$  are used, starting at  $-\Delta\theta/2$ , up to  $90^\circ + \Delta\theta$ , where  $\Delta\theta = 90^\circ / (NBLUNT - 1.5)$  and NBLUNT is an input parameter describing the number of angular mesh points to be used in the blunt-body calculation. Program default value is NBLUNT = 24, so that for the default mesh,  $\Delta\theta = 4^\circ$ . The obstacle shape is determined by integrating the appropriate differential equation by a trapezoidal predictor-corrector method. For a user-supplied shape, the  $\theta$  grid is determined by rays from the origin through the first NBLUNT points, and the reflection of the first ray in the x-axis. Values for  $R_p$  are determined by dividing the line segments between the body and bow shock wave into  $NR - 1$  equal intervals. Thus, including the obstacle and bow shock wave, the grid forms  $NR$  arcs around the obstacle. A starting solution for the blunt-body calculation is obtained by guessing a bow shock shape and by prescribing a Newtonian pressure distribution on the body.



## APPENDIX A

Noting that the maximum entropy streamline wets the body, other flow properties on the body surface can then be calculated. An initial flow field is then established by linear interpolation between the obstacle and the guessed bow shock, where the Rankine-Hugoniot relations hold. The integration proceeds in time for ITER steps. The initial bow shock shape used for the magnetopause equatorial trace and for an ionopause with  $H/R_0 \geq 0.1$  is a correlation shape depending on  $(M_\infty, \gamma, H/R_0)$  and given by the parabola  $R_p = \delta_1 \sqrt{\delta_0 - x} / \sqrt{\delta_0}$  where

$$\delta_0 = 1.0 + 1.1 \left[ ((\gamma-1)M_\infty^2 + 2) / (\gamma+1)M_\infty^2 \right] \times (0.9 + 0.5 H/R_0)$$

$$\delta_1 = \Delta_0 \{ (1.273 + 0.009 M_\infty^2) (0.904 + 0.655 H/R_0)$$

$$\times (3.95 - 5.3 H/R_0 + 3.85 (H/R_0)^2) \} + (R_{\text{body}})_x = 0.0$$

$$\Delta_0 = \left[ (\gamma-1)M_\infty^2 + 2 \right] / \left[ (\gamma+1)M_\infty^2 \right] \times 0.78$$

For a user-supplied obstacle shape and for an ionopause with  $H/R_0 < 0.1$ , the initial shock shape used is the curve  $R_p = \sqrt{(1 + \Delta_0 (1 + 0.680^2 + 0.160^4))}$ . Information on convergence, the final sonic line locations, and the body and final bow shock shape are printed from this calculation.

The results at  $\theta = 90^\circ$ , i.e. at  $x = 0.0$ , are used as starting conditions for the marching calculation, after proper normalization. For default geometries, the integration of the appropriate differential equation is continued downstream at equal  $\theta$  increments to form a body shape table. The stepsize along the x-axis is recalculated at every ICØNST(49) with ICØNST(49) being set to 10. At each x-location,  $R_{\text{body}}$  is determined by linear interpolation. The computational mesh is extended by adding the line perpendicular to the x-axis at each step, divided in the same manner as for the blunt nose. The calculation marches downstream with a maximum stepsize of 1.0 until the terminal location specified by the user has been passed. However, the number of steps is limited to 75, after which the calculation will end regardless of the x-location. The coordinates of the obstacle and bow shock are printed at each step.

The grid coordinates and flow field values are written to a file, TAPE9, which may be saved to use as input for a later run. This rerun option, which replaces constructing the computational mesh and performing

the blunt body and marching calculations with reading the rerun input file, TAPE4, is described in section A.2.2.

The streamlines are calculated in two sections, following each of the flow field calculations. Using the results of the blunt body calculation, i.e. the  $(x, R)$  grid coordinates,  $(R_p, \theta)$  grid coordinates, density  $\rho/\rho_\infty$ , and velocity components  $v_X/v_\infty$  and  $v_R/v_\infty$ , the velocity magnitude  $|v|/v_\infty$  and flow angle are calculated. Density  $\rho/\rho_\infty$  and velocity  $|v|/v_\infty$  are smoothed along the rays of constant- $\theta$ , using a third degree least squares fit with respect to  $R_p$ . Streamlines are then calculated downstream to  $x = 0.0$ , using the trajectory method, integrating through the velocity field by means of a third-order modified Euler integration procedure, using the grid locations on the bow shock as starting positions. The flow angle  $\phi = \tan^{-1}(v_R/v_X)$  at each point is determined using bivariate linear interpolation in  $\theta$ , then  $R_p$ . Points for which  $\theta < 0^\circ$  or  $\theta > 90^\circ$  are discarded in the interpolation.

The marching calculation provides  $(x, R)$  grid coordinates, and values of density  $\rho/\rho_t$ , and velocity components  $v_X/v_t$  and  $v_R/v_t$ , where  $t$  denotes free-stream stagnation conditions. For compatibility with the blunt body solution, the flow field values are converted to  $\rho/\rho_\infty$ ,  $v_X/v_\infty$ ,  $v_R/v_\infty$  before calculating the resultant velocity magnitude  $|v|/v_\infty$  and flow angle  $\phi$ . The streamline calculation is continued downstream, employing the same method as in the nose region. Starting positions on the shock wave for the streamline calculation in the marching zone are set at equal  $R$ -increments, with a maximum of 50 streamlines calculated. The flow angle is determined using bivariate linear interpolation first in  $x$ , then in  $R$ .

Along the symmetry axis, values of  $x$ ,  $\rho/\rho_\infty$ , and  $|v|/v_\infty$  are determined by extrapolation, using a third-order Lagrangian polynomial in  $\theta$  on each arc of the computational grid. Exact values for the stagnation streamline are used where possible, viz.

at the bow shock

$$\rho/\rho_\infty = (\gamma+1)M_\infty^2 / \left[ (\gamma-1)M_\infty^2 + 2 \right]$$

$$|v|/v_\infty = 1/(\rho/\rho_\infty)$$

APPENDIX A

at the body surface

$$\rho/\rho_\infty = (\rho/\rho_\infty)_{\text{shock}} \left\{ \left[ \frac{(\gamma+1)M_\infty^2}{4\gamma M_\infty^2 - 2(\gamma-1)} \right]^{1/(\gamma-1)} \right\}$$

$$|\vec{v}|/v_\infty = 0.0$$

$$x = 1.0$$

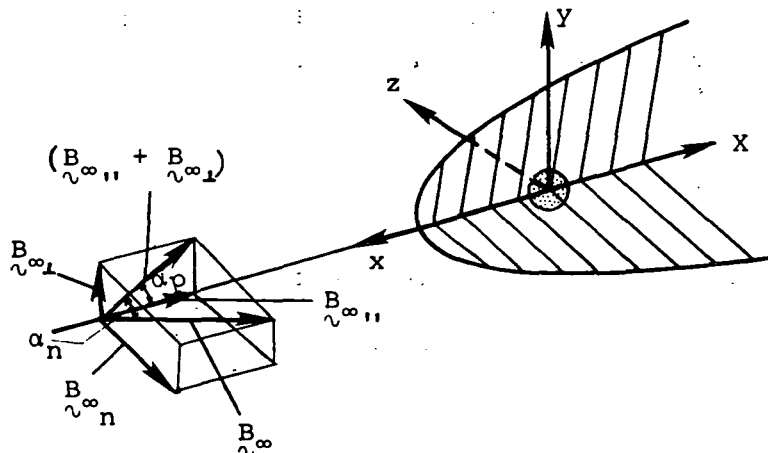
Detailed flow field output may now be printed by subroutine FLØUT, with LPRFL as print control variable. In addition to grid coordinates, density, velocities and flow angle, values of temperature  $T/T_\infty$  and pressure  $P/P_\infty$  are output, where

$$T/T_\infty = 1 + \left[ (\gamma-1)/2 \right] M_\infty^2 \left[ 1 - (|\vec{v}|/v_\infty)^2 \right]$$

$$P/P_\infty = (\rho/\rho_\infty) (T/T_\infty)$$

Streamline coordinates may also be printed by subroutine STØUT, with LPRST as print control variable.

The magnetic field is determined by separately calculating the components whose field lines are parallel, perpendicular, and normal to the flow, in the undisturbed solar wind. These components are then added vectorially, the resultant being expressed in orthogonal  $(x,y,z)$  components. The angles in the free stream  $\alpha_p$  and  $\alpha_n$  between the magnetic field and the flow, as shown in the sketch below, are input variables. The components are calculated using the following formulae, in which  $\vec{e}$  signifies a vector of magnitude  $e$ , in the direction of the component field line, and  $\hat{n}$  the unit normal vector.



$$\left(\frac{B}{B_\infty}\right)_{\parallel} = \left(\frac{V}{V_\infty}\right) \left(\frac{\rho}{\rho_\infty}\right); \quad \left(\frac{B}{B_\infty}\right)_{\perp} = \left(\frac{\Delta\ell}{\Delta\ell_\infty}\right) \left(\frac{\rho}{\rho_\infty}\right); \quad \left(\frac{B}{B_\infty}\right)_n = \left(\frac{R}{R_\infty}\right) \left(\frac{\rho}{\rho_\infty}\right)$$

$$\left(\frac{B}{B_\infty}\right) = \left(\frac{B}{B_\infty}\right)_{\parallel} \left(\frac{B_{\infty\parallel}}{B_\infty}\right) + \left(\frac{B}{B_\infty}\right)_{\perp} \left(\frac{B_{\infty\perp}}{B_\infty}\right) + \hat{n} \left(\frac{B}{B_\infty}\right)_n \left(\frac{B_{\infty n}}{B_\infty}\right)$$

The magnetic field line vector component  $B_{\parallel}$ , which results from the interplanetary component  $B_{\infty\parallel}$ , that is parallel to the undisturbed solar flow has local magnitude given by  $(|V|/V_\infty)(\rho/\rho_\infty)$ , and the same local direction  $\phi$  as the fluid flow. Determination of the normal magnetic field component  $B_n$  requires calculation of  $R/R_\infty$ , where  $R_\infty$  is the free stream cylindrical R-ordinate of the streamline through the point under consideration. This is calculated by linearly interpolating in the local radial cylindrical coordinate  $R$  between the streamlines, with  $R/R_\infty = 1.0$  along the x-axis. The magnetic field vector component  $B_{\perp}$  resulting from the interplanetary component  $B_{\infty\perp}$  which is perpendicular to the undisturbed solar wind flow requires the distance vector  $\Delta\ell/\Delta\ell_\infty$ , whose magnitude is  $\Delta\ell/\Delta\ell_\infty$  and direction is  $\psi$ , where  $\Delta\ell/\Delta\ell_\infty$  is the stretching factor of the perpendicular field at the point, and  $\psi$  is the direction of the field line through the point. The perpendicular field lines are determined by integrating  $\int v dt$  along each streamline, using trapezoidal integration to locate points along the streamline at regular increments in time,  $\Delta t$ , starting at a perpendicular field line ahead of the bow shock. Values for  $\Delta\ell/\Delta\ell_\infty$  and  $\psi$  are calculated at the points where the perpendicular field lines and streamlines intersect, interpolating only along the field lines. A generalized quadrilateral interpolation scheme is then employed to determine  $\Delta\ell/\Delta\ell_\infty$  and  $\psi$  at the computational grid points, using the quadrilateral containing the point formed by the intersection of pairs of adjacent streamlines and perpendicular field lines. At the bow shock, an exact formula is used, viz.

$$(\Delta\ell/\Delta\ell_\infty)^2 = 1 + \cot^2\theta(1+D^2) - 2D \times \csc\theta \times \cot\theta \times \cos(\theta-\delta)$$

$$\psi = \theta + \sin^{-1}\{D \times \cot\theta \times \sin(\theta-\delta)/(\Delta\ell/\Delta\ell_\infty)\}$$

## APPENDIX A

where

$$D^2 = 1 - 4(M_\infty^2 \sin^2 \theta - 1)(\gamma M_\infty^2 \sin^2 \theta + 1) / \left\{ (\gamma + 1)^2 M_\infty^4 \sin^2 \theta \right\}$$

$$\cot \delta = \tan \theta \times \left\{ (\gamma + 1) M_\infty^2 / \left[ 2(M_\infty^2 \sin^2 \theta - 1) \right] - 1 \right\}$$

$$\theta = \tan^{-1} \left\{ \frac{dR_{\text{shock}}}{dx} \right\}$$

The values of  $\Delta l / \Delta l_\infty$  at the grid points are smoothed using fifth-order least squares fit with respect to arc length along the arcs of the grid. The resultant magnetic field is expressed in orthogonal (x,y,z) components, where

$$B_x / B_\infty = \cos \alpha_n \times \left( \cos \phi \times \cos \alpha_p \times (|B| / B_\infty)_n + \cos \psi \times \sin \alpha_p \times (|B| / B_\infty)_\perp \right)$$

$$B_y / B_\infty = \cos \alpha_n \times \left( \sin \phi \times \cos \alpha_p \times (|B| / B_\infty)_n + \sin \psi \times \sin \alpha_p \times (|B| / B_\infty)_\perp \right)$$

$$B_z / B_\infty = \sin \alpha_n \times (B / B_\infty)_n$$

Magnetic field components may now be printed by subroutine BOUT, with LPRB as print control parameter. The magnetic field is not calculated when LPRB = .FALSE. and KBCON=0.

Contours are calculated for velocity  $|v|/v_\infty$ , density  $\rho/\rho_\infty$ , and magnetic field components  $(B/B_\infty)_n$  and  $(B/B_\infty)_\perp$ . The method used is a modified version of a procedure developed by R. Sorenson of NASA/Ames Research Center. The boundary is searched for intervals which bracket a contour point. Having found one point, the remainder of the contour is determined by 'walking' around the contour, searching at each step for the interval through which the contour line next passes, until a boundary point is reached. Then closed contours are found in a similar manner. Linear interpolation is used throughout the process. Note that since  $T/T_\infty$  is a function of  $|v|/v_\infty$  only, velocity contours may also be considered as temperature contours. The coordinates of the contour lines can be printed by subroutine CONOUT, with LPRCON as print control parameter. The section of the program which creates the plots is accessed only when the control parameter LPLOT = .TRUE.

### A.2.2 Rerun Option

The rerun option is used when `LRERUN = .TRUE.` The blunt body and marching calculations are replaced with reading the grid coordinates and flow field values from the rerun file, TAPE4, which contains data written to TAPE9, then saved, on a previous run. Different values for any parameter not used in the flow field calculations may be specified, viz. contour values, plot length, magnetic field angles, and output options. Values of `AMACH`, `GAMMA`, and `HRØ` are required input, to ensure that the input rerun file does contain the case desired for rerun. If the geometry is user-supplied, the body shape table will be read from TAPE4, and should not be input from cards.

After reading the card input, `AMACH`, `GAMMA`, and `HRØ` are tested against values from TAPE4. The grid coordinates and flow field values from the blunt body calculation are read in, then smoothed, and streamlines calculated for this region, as previously described. The results of the marching calculation are then read, and the streamline calculation continued downstream. The calculations then proceed as described in section A.2.1.

A run must not contain more than one case which uses the rerun option.

### A.2.3 Program Limitations and Precautions

The program makes some assumptions about the geometry of the obstacle shape around which flow is to be calculated, and about the flow field. The obstacle shape is assumed to be monotonically increasing in  $R$ , going downstream. The nose of the obstacle is at  $x = 1.0$ . The origin of the  $(x, R)$  coordinate system is the center of the planet. Obstacle shapes with sharp corners should be avoided. The flow at  $x = 0.0$ , which is used as the starting plane for the marching calculation, must be such that the axial ( $x$ -direction) Mach number is purely supersonic. This is a basic requirement of the marching code and is associated with the manner in which the code advances the solution. That condition is violated for ionopause shapes with  $H/RØ > 0.5$ , so that with the present joining procedure employed (i.e. at  $x = 0.0$ ) those shapes cannot be treated. In the magnetic field calculation, the first streamline is assumed to be inside the arc described by the grid points immediately off the body, downstream of  $x = 0.0$ . To reduce computational costs, a grid using  $NR = 10$  may be used, in which case a lower value of  $CN$  may be required. This would

## APPENDIX A

reduce the running line by approximately 40 percent. A free stream Mach number less than 3.0 is not advised.

### A.2.4 Convergence Criteria for Blunt Body Calculation

The output provides two measures of the convergence of the blunt body calculation. The RMS of shock speed and maximum shock speed are printed at each iteration. These quantities should both tend to zero. A value for  $q_{\text{RMS}}$ , RMS of shock speed, of

$$q_{\text{RMS}} < \sqrt{\gamma} \times M_{\infty} \times 10^{-3}$$

where  $\gamma$  is the specific heat ratio, and  $M_{\infty}$  is the free stream Mach number, usually indicates a converged solution. The RMS of error in enthalpy, HT, should be less than 1 percent, with the maximum enthalpy error also of that order.

The Courant number, CN, determines the time step size used by the calculation. A value not greater than the default of 3.0 should be used. For low Mach numbers or a coarser mesh than the default, a lower value may be preferable. If the default value does not generate a converged solution, or if the error message from subroutine SHOCK is printed, try lowering CN in increments of 0.5 to find a better value of CN. User-supplied bodies may also require a lower Courant number.

### A.3 Description of Input

This section describes the card input for the program. An alphabetized dictionary of input variables is provided, defining the variables, listing default values and limitations. A discussion of the preparation of the card input is then presented, followed by a description of the input card format.

#### A.3.1 Dictionary of Input Variables

AMACH	free-stream Mach number; $3.0 \leq \text{AMACH} \leq 25.0$ is recommended
ANGN	the angle, in degrees, measuring the deviation of the free-stream magnetic field from the plane in which $B_{\infty 0}$ and $B_{\infty 1}$ lie; equal to $\tan^{-1}(B_{\infty 0} / \sqrt{ B_{\infty 0} ^2 +  B_{\infty 1} ^2})$
ANGP	the angle, in degrees, measuring the deviation of the in-plane magnetic component ( $B_{\infty 0} + B_{\infty 1}$ ) from the direction of flow; equal to $\tan^{-1}(B_{\infty 1} / B_{\infty 0})$

BCØN(I) KBCØN-dimensional array specifying values to be used for mag-  
 netic field strength contours

CN Courant number used for blunt body calculation; program default  
 value is 3.0

GAMMA free-stream ratio of specific heats

HRØ obstacle geometry indicator:
 

- HRØ > 0 - ionopause with  $H/R_0 = HRØ$
- HRØ = 0 - magnetopause equatorial trace
- HRØ < 0 - geometry is user-supplied

ITER integer, number of iterations for blunt body calculation;  
 program default value is 300

KBCØN integer, number of values specified for magnetic field contours;  
 $0 \leq KBCØN \leq 20$

KRCØN integer, number of values specified for density contours;  
 $0 \leq KRCØN \leq 20$

KVCØN integer, number of values specified for velocity contours;  
 $0 \leq KVCØN \leq 20$

LPLOT logical variable indicating whether to create plots or plot file
 

- FALSE - no
- TRUE - yes

LPRB logical variable indicating whether to print magnetic field  
 output
 

- FALSE - no
- TRUE - yes

LPRCØN logical variable indicating whether to print coordinates of  
 contour lines
 

- FALSE - no
- TRUE - yes

LPRFL logical variable indicating whether to print detailed flow field  
 output
 

- FALSE - no
- TRUE - yes

LPRST logical variable indicating whether to print coordinates of  
 streamlines
 

- FALSE - no
- TRUE - yes



## APPENDIX A

LRERUN	logical variable indicating whether this case uses rerun option FALSE - perform blunt body and marching calculations TRUE - read results of a previous calculation from TAPE4
NBLUNT	integer, number of angular mesh points for blunt body calculation; for user-supplied geometry, $XX(NBLUNT-1)=0.0$ ; program default value, and maximum, is 24
NBØD	integer, number of points in body shape table when geometry is user-supplied; $1 \leq NBØD \leq 100$
NCASE	integer, number of cases to be run consecutively; $NCASE \geq 1$
NR	integer, number of radial mesh points; program default value, and maximum, is 19
RCØN(I)	KRCØN - dimensional array specifying values to be used for density contours
RR(I)	NBØD - dimensional array representing the R-locations, in cylindrical (x,R) coordinates, of the user-supplied body shape
TITLE	descriptive heading of the case, to be printed on the first page of output; may contain up to 80 characters, including blanks
VCØN(I)	KVCØN - dimensional array specifying values to be used for velocity contours
XCALC	terminal downstream x-location for marching calculation of flow field; $XCALC < 0.0$ ; program default value is -1.0
XPLØT	terminal downstream x-location for calculation of streamlines, magnetic field, and contours; $XCALC \leq XPLØT < 0.0$ ; program default value is -1.0
XX(I)	NBØD - dimensional array representing the x-locations, in cylindrical (x,R) coordinates, of the user-supplied body shape

### A.3.2 Preparation of Input Data

The card input for a run consists of one card containing the number of cases to be run consecutively, Item 0, followed by a set of input for each case, Item 1 through Item 7, and Item 8 if required. Where a default value is to be used, the input field should be left blank. For each case, all required variables which do not assume their default values should be specified. The input format for all cards is described in section A.3.3.

Item 0 - This item consists of one card, containing the number of cases in this run, NCASE.

Item 1 - This card provides identification of the case, TITLE, which is printed on the first page of the output for this case.

Item 2 - This card contains information on the flow conditions and body geometry, and parameters required for the blunt body and marching calculations. AMACH, GAMMA, and HRØ must be specified for each case. For the rerun option, the values are tested against the values from the rerun file. The parameters XCALC, NR, NBLUNT, CN, ITER are used only when the flow field is to be calculated. These variables each assume a default value if the input field is blank.

Item 3 - This item consists of one card containing the rerun indicator, LRERUN, and the output control variables LPRFL, LPRST, LPRCØN, LPRB, and LPLØT.

Item 4 - This card contains the variables XPLØT, ANGP, and ANGN. The value for XPLØT is changed by the program to be the x-location of the marching calculation immediately upstream of the input value for XPLØT. The angles describing the deviation of the magnetic field from the flow, ANGP and ANGN, are not required when LPRB=.FALSE. and KBCØN=0, since the magnetic field is not calculated under these conditions. ANGP is the angle between the vectors  $(B_{\infty\perp} + B_{\infty\parallel})$  and  $v_{\infty}$ , while ANGN is the angle between  $B_{\infty}$  and  $(B_{\infty\perp} + B_{\infty\parallel})$ , where  $B_{\infty\parallel}$ ,  $B_{\infty\perp}$ ,  $B_{\infty n}$  are the components of the free-stream magnetic field,  $B_{\infty}$ , which are parallel, perpendicular, and normal to  $v_{\infty}$ , and are as indicated in figure 4 of the text. The two angles ANGP and ANGN fully determine the half plane for which the magnetic field is to be calculated. The magnetic field for the other half of the plane may be calculated by rerunning with the sign of ANGP reversed. When  $(B_{\infty\perp} + B_{\infty\parallel}) = 0$ ,  $ANGN = \pm 90^\circ$ ,  $ANGP = 0^\circ$ ; and, when  $B_{\infty n} = 0$ ,  $ANGN = 0^\circ$ .

Item 5 - This item contains the values for the velocity contours. The first card contains KVCØN, the number of values specified for VCØN. If KVCØN=0, only this card is required, and no velocity contours are calculated. If KVCØN > 0, the contour values are then read. Up to three cards may be required to accommodate the values, eight per card, maximum of 20. The contour values should be monotonically increasing, with at least one value within the range of the magnitude of the velocity in the region for which contours are to be calculated.

Item 6 - This item contains the values for the density contours. The description is similar to that for item 5, with KRCØN being the number of values specified, and RCØN the array of values.

Item 7 - This item contains the values for the magnetic field contours. The description is similar to that for item 5, with KBCØN

## APPENDIX A

being the number of values specified, and BCØN the array of values. Note that the same contour values are used for the parallel and perpendicular components.

Item 8 - This optional item is required when  $HRØ < 0.0$  and  $LRERUN = .FALSE.$ , and contains the body shape table for the user-supplied geometry. The first card contains NBØD, the number of points in the shape table. The next NBØD cards contain the cylindrical (x,R) coordinates of these points, (XX(I), RR(I)), one point per card. The points supplied by the user determine the  $\theta$ -spacing of the mesh used for the blunt body calculation. The first point should be near, but not on, the x-axis. A suggested location is such that the  $\theta$ -spacing between the first point and the x-axis is half the  $\theta$ -spacing between the first two points. The blunt body calculation adds a point which is the reflection about the x-axis of the first point in the body shape table. The (NBLUNT-1)<sup>th</sup> point should be at  $x=0.0$ . The BLUNT<sup>th</sup> point is also used to create the grid for the blunt body calculation. The coordinates must be normalized so that the planet center is at (0.,0.) and the nose of the body at (1.,0.).

### A.3.3 Format of Input Data

Four format types are used for the input data. For real numbers (F-format), a decimal point is required. Integers (I-format) should be right-adjusted in the field. For logical variables (L-format), the first non-blank character in the field, which should be 'T' or 'F', determines the value. Note that a blank input field is interpreted as 'FALSE'. The title, which is in A-format, may contain any valid character.

A description of the card format of the input data follows, with item numbers corresponding to those in section A.3.2:



Item No. 6:

(1) 1 card

Variable	KRCØN
Card Column	10
Format Type	I

(2) 0 to 3 cards as needed for up to 20 values, 8 per card

Variable	RCØN(1)	RCØN(2)	RCØN(KRCØN)
Card Column	10	20	30
Format Type	F	F	F
			40
			50
			60
			70
			80

Item No. 7:

(1) 1 card

Variable	KRCØN
Card Column	10
Format Type	I

(2) 0 to 3 cards as needed for up to 20 values, 8 per card

Variable	BCØN(1)	BCØN(2)	BCØN(KBCØN)
Card Column	10	20	30
Format Type	F	F	F
			40
			50
			60
			70
			80

Item No. 8:

(required only when HRØ < 0.0 and LRERUN=.FALSE.)

(1) 1 card

Variable	NBØD
Card Column	10
Format Type	I

(2) I = 1 to NBØD; NBØD cards

Variable	XX(I)	RR(I)
Card Column	10	20
Format Type	F	F

#### A.4 Description of Output

This section describes the output of the computer program. The contents of each output item are specified and discussed. The printed output consists of six items, four of which are optional, with input control parameters. Plotted output is also optional.

The first output item consists of the input data. The title for the case is printed first, followed by all input variables, with identification of each variable. Default values are printed as if they were input. Parameters CN, NR, NBLUNT, ITER for the blunt body calculation and XCALC, the terminal location for the marching calculation, are printed only when the flow field is to be calculated. When the geometry is user-supplied, the input body shape table is printed. For a default geometry, the body shape is indicated by the description "default magnetopause coordinates - equatorial trace" or "default ionopause coordinates -  $H/R\emptyset =$  ".

The second output item is not printed when LRERUN=.TRUE. From the blunt body calculation, the shock speed at each iteration, the final enthalpy error, final sonic line location, and body and final bow shock shape are printed. For convergence criteria of this calculation, the downstream location and body and shock ordinates are output. There is no control variable allowing the user to suppress this item of output when the flow field is calculated.

Detailed flow field output is the third item, and is printed only when LPRFL=.TRUE. Coordinates are labeled as X/D, R/D, RP/D, or X/RO, R/RO, RP/RO, to emphasize that distances are normalized by the distance from the center of the planet to the nose of the body, D for the magnetopause, RO for an ionopause. Along the symmetry axis, the values printed are velocity magnitude  $V/V_{\infty}$ , density  $\rho/\rho_{\infty}$ , temperature  $T/T_{\infty}$ , and pressure  $P/P_{\infty}$ . Over the rest of the flow field values are also given for velocity components  $V_x/V_{\infty}$ ,  $V_r/V_{\infty}$ , and flow angle  $\phi$ . Note that the flow angle is the deviation of the flow about the obstacle, and so  $0^\circ \leq \phi < 90^\circ$ .

The next output item is the (x,R) coordinates of the streamlines. For the blunt body region, the  $(R_p, \theta)$  coordinates of the starting position on the bow shock wave are also given. This item is printed only when LPRST=.TRUE.

## APPENDIX A

The magnetic field components are then printed, if LPRB=.TRUE. . The location of each point is defined in  $(R_p, \theta)$  coordinates for the blunt body region, and  $(x, R)$  coordinates for the downstream marching region. The components along field lines parallel, perpendicular, and normal to the flow in the free stream are printed as B/BINF(PARALLEL), B/BINF(PERP), B/BINF(NORMAL). The orthogonal  $(x, y, z)$  components of the resultant are printed as BX/BINF(RESULTANT), BY/BINF(RESULTANT), BZ/BINF(RESULTANT). The magnetic field in the symmetry  $(x, y)$  plane, defined by the vector sum  $\{(B/B_\infty)_x + (B/B_\infty)_y\}$ , is also printed, and is given by the magnitude B/BINF(IN-PLANE) and direction B-ANGLE(IN-PLANE) of the vector. The B-ANGLE  $\psi$  is the angle between the magnetic field and the flow, and generally has the same sign as ANGP.

The last item printed is the  $(x, R)$  coordinates of the contours, for which LPRCON is the logical control variable. Noting that temperature and velocity contours coincide, the corresponding value of T/TINF is printed along with V/VINF for the velocity contours. There are three nonfatal error messages which may occur - see section A.5.

The program also has the capability of producing plotted output, using UCC plot routines AXIS, CHAR, DASH, DDTLN, ENPLT, GREEK, MATH, NUMPLT, PLOT, PLTLN, POLAR, SCALF, VECTOR. Plots are not produced when LPLDT=.FALSE. The plots provide pictorial representation of the streamlines and contours, with a maximum of six frames produced. The first frame is a plot of the streamlines. Then contour plots of velocity, temperature, and density are drawn. The last two frames are contour plots of the parallel and perpendicular magnetic field components, with field lines added to indicate direction. Frames are omitted when no contour levels are provided.

### A.5 Program Error Messages

This section lists the messages printed by the program, and indicates what action should be taken by the user.

- (1) \*\*\*\*\* EXECUTION TERMINATED \*\*\*\*\*  
 RERUN DATA ON TAPE4 DOES NOT AGREE  
 WITH CASE SPECIFIED ON CARD INPUT:  
 MACH NØ. GAMMA M/RO

FROM CARDS  
 FROM TAPE4

The first three parameters of item 2 of the input for a case using the rerun option should agree with those used when creating the file. The tolerance used in comparing the values is  $10^{-5}$ . For a user-supplied geometry, it is sufficient for both values of  $H/R_0$  to be negative.

- (2) \*\*\*\*\* EXECUTION TERMINATED \*\*\*\*\*  
 ARRAY OF CONTOUR VALUES IMPROPERLY SPECIFIED

When specified, the contour values should be monotonically increasing, with at least one value in the range of the velocity, density, or magnetic field strength for the region under consideration. This error does not inhibit generation of the rerun file.

- (3) CONTOUR SEARCH ABORTED - TABLE OVERFLOW IN NAD

The program allows for 29 contour lines to be found, storing the starting address of each contour in array NAD. This message indicates that at least one more contour line could be found. If the user requires all the contours of the levels specified, the case should be rerun in two parts. Otherwise, reduce the number of contour levels specified.

- (4) CONTOUR SEARCH ABORTED - TABLE OVERFLOW IN (X,Y)

The contour lines may be described by up to 1000 points, stored in arrays X and Y. This message indicates that more points would be required for the contour lines requested. The last contour line found will be incomplete. As with (3), either reduce the number of contour levels or run as two cases.

- (5) NEGATIVE PRESSURE DETECTED BY SHOCK AT J=  
 PN= PØ= PTAU=

This message is printed when a negative pressure has been calculated at the shock on this iteration, at radial location J. The quantities printed are: PN, the pressure calculated on this step; PØ, the pressure from the previous step; and PTAU, the partial derivative of pressure with



## APPENDIX A

respect to time. This condition indicates that the shock wave motion is too extreme. Lowering the value of CN, and thus reducing the time step, may remove the problem.

The following messages (6)-(10) usually result from using an obstacle geometry which is in some way too severe for the program to handle in its present form. The obstacle slope may be sufficiently high at  $x = 0.0$  that the axial Mach number becomes subsonic in the starting solution for the marching calculation, or there may be a sharp corner in the profile. Check input, particularly free stream Mach number and body geometry.

(6) NEGATIVE PRESSURE  $\emptyset$ N B $\emptyset$ DY DETECTED BY BNDRY, PB= AT J=

This message indicates that a negative pressure on the body, PB, has been calculated at radial location J.

(7) NEGATIVE PRESSURE  $\emptyset$ R DENSITY  $\emptyset$ N B $\emptyset$ DY DETECTED BY BNDRYM AT X=  
PB= RH $\emptyset$ B= VXB= VRB=

The program makes internal corrections when this condition occurs, resulting pressure PB, density RH $\emptyset$ B, and velocity components VXB and VRB.

(8) NEGATIVE SIGMA-BAR-1 IN EIGENM INDICATES SUBS $\emptyset$ NIC FL $\emptyset$ W AT I=

(9) NEGATIVE SIGMA-BAR-2 IN EIGENM INDICATES SUBS $\emptyset$ NIC FL $\emptyset$ W AT I=

These messages are printed when subsonic flow is detected by the marching calculation. The computed stepsize for this region will be quite small.

(10) -----BODY TURN STOPPED AT M2=100-----

This message indicates that the body has a sharp corner, which has been limited to  $100^\circ$  when being transformed.

### A.6 Sample Case

A sample case is presented in this section. Figures A.1, A.2, and A.3 illustrate the input data, portions of the printed output, and the plotted output, respectively.

The sample case is run alone and is set up so as to produce all possible output. Flow is to be calculated about the rotated equatorial

trace of the magnetopause to a downstream location of  $x = -10.0$ , with  $M_\infty = 8$ ,  $\gamma = 5/3$ . Streamlines, magnetic field components, and contours are desired to a downstream location of  $x = -5.0$ . The magnetic field forms angles of  $\alpha_p = -45^\circ$ ,  $\alpha_n = 45^\circ$  with the solar wind flow. Contour values are specified for all quantities.

The input data is tabulated in figure A.1, with item numbers corresponding to those in sections A.3.2 and A.3.3. The first card, item 0, indicates that there is one case to be run. The remaining 13 cards provide the data required for this case. Item 1 contains the identifying title. On the next card, item 2, values are specified for AMACH, GAM, HRØ, and XCALC. The other data fields are left blank to indicate that the default values will be used. The values of the logical variables of item 3 specify that the flow field is to be calculated, and that full printed and plotted output is to be produced. Item 4 defines the plot length to be  $-5.0$ , and the magnetic field angles as ANGP =  $-45.0$  and ANGN =  $45.0$ . Items 5, 6, 7 specify the contour levels to be used - 12 for velocity and temperature, 10 for density, and 12 for magnetic field strength. Item 8 is omitted, since the obstacle geometry is one of the default shapes for which the coordinates are calculated internally by the program.

Figure A.2 presents portions of the printed output from the sample case using the data deck of figure A.1. The full printed output for this case is approximately 5,000 lines. The first item of printed output, figure A.2(a), is the input variables. Then in figure A.2(b), the output from the blunt body calculation is shown, omitting shock speed values for iterations 6 to 295. Note that the convergence criteria described in section A.2.4 are satisfied. Figure A.2(c) provides the output from the marching calculation. Figures A.2(d), (e), (f) show the detailed flow field output in four areas: near the symmetry axis; near  $x = 0.0$ , when the two calculation schemes are joined; around  $x = -5.0$ , the value of XPLØT; and the last two locations calculated. An example of the streamline output is shown in figures A.2(g), (h). Figures A.2(h), (i), (j) provide the magnetic field components at the same locations chosen to illustrate the flow field output. Examples of the printed output of the contour lines are shown in figures A.2(k), (l), (m), choosing two contour lines for each quantity. Note that for  $(|B|/B_\infty)_\perp$ , the different contour lines for the same contour level are considered to be two separate and distinct lines.

Figure A.3 shows the six plots which are produced by the program for this case.

APPENDIX A

Item No.	Column No.	10	20	30	40	50	60	70	80
0		1							
1		SAMPLE CASE		DEFAULT MAGNETØPAUSE EQUATØRIAL TRACE					
2	8.0	1.666666667	0.0	-10.0					
3	FALSE	TRUE	TRUE	TRUE	TRUE	TRUE			
4	-5.0	-45.0	45.0						
5		12							
	0.1	0.2	0.3	0.4	0.5	0.6	0.7	0.75	
	0.8	0.85	0.88	0.9					
6		-10							
	0.8	1.2	1.6	2.0	2.5	3.0	3.5	3.8	
	4.0	4.2							
7		12							
	0.5	0.75	1.0	1.25	1.5	2.0	2.5	3.0	
	3.5	4.0	5.0	6.0					

Figure A-1. - Card input for sample case.

FIGURE A.2

## ABBREVIATED OUTPUT FOR SAMPLE CASE

SAMPLE CASE      DEFAULT MAGNETOPAUSE EQUATORIAL TRACE

INPUT VARIABLES  
\*\*\*\*\*

FREESTREAM MACH NO. = 8.00  
 SPECIFIC HEAT RATIO = 1.667  
 OBSTACLE GEOMETRY: DEFAULT MAGNETOPAUSE COORDINATES - EQUATORIAL TRACE  
 PARAMETERS FOR BLUNT BODY CALCULATION  
     NO. OF RADIAL MESH POINTS = 17  
     NO. OF ANGULAR MESH POINTS = 24  
     COURANT NUMBER            = 3.00  
     NO. OF ITERATIONS         = 300  
 TERMINAL DOWNSTREAM LOCATION FOR MARCHING CALCULATION = -10.00  
 TERMINAL DOWNSTREAM LOCATION FOR PLOTTING = -5.00  
 IN-PLANE DEVIATION OF MAGNETIC FIELD FROM FLOW = -45.00 DEGREES  
 DEVIATION OF MAGNETIC FIELD FROM PLANE OF FLOW = 45.00 DEGREES  
 LRRUN = F  
 LPRFL = T  
 LPRST = T  
 LPRCON = T  
 LPRB = T  
 LPLUT = T

VALUES SPECIFIED FOR CONTOUR CALCULATION  
\*\*\*\*\*

## 12 CONTOUR LEVELS FOR VELOCITY:

.200	.250	.300	.400	.500	.600
.700	.750	.800	.850	.900	.950

## 10 CONTOUR LEVELS FOR DENSITY:

.800	1.200	1.600	2.000	2.500	3.000
3.500	3.600	4.100	4.200		

## 12 CONTOUR LEVELS FOR MAGNETIC FIELD STRENGTH:

.500	.750	1.000	1.250	1.500	2.000
2.500	3.000	3.500	4.000	5.000	6.000

Figure A.2(a)

BLUNT BODY CALCULATION  
\*\*\*\*\*

ITERATION 1	RMS OF SHOCK SPEED= 1.2458E-02	MAXIMUM SHOCK SPEED= 3.6519E-02 AT J=25
ITERATION 2	RMS OF SHOCK SPEED= 1.2445E-02	MAXIMUM SHOCK SPEED= 3.1748E-02 AT J=25
ITERATION 3	RMS OF SHOCK SPEED= 2.1994E-02	MAXIMUM SHOCK SPEED= 3.2075E-02 AT J=25
ITERATION 4	RMS OF SHOCK SPEED= 3.4842E-02	MAXIMUM SHOCK SPEED= 5.0377E-02 AT J=16
ITERATION 5	RMS OF SHOCK SPEED= 4.9444E-02	MAXIMUM SHOCK SPEED= 7.2239E-02 AT J=16
ITERATION 296	RMS OF SHOCK SPEED= 3.7908E-03	MAXIMUM SHOCK SPEED= 9.6232E-03 AT J=10
ITERATION 297	RMS OF SHOCK SPEED= 3.7524E-03	MAXIMUM SHOCK SPEED= 9.1111E-03 AT J=15
ITERATION 298	RMS OF SHOCK SPEED= 3.7140E-03	MAXIMUM SHOCK SPEED= 9.1274E-03 AT J=17
ITERATION 299	RMS OF SHOCK SPEED= 3.6752E-03	MAXIMUM SHOCK SPEED= 8.9772E-03 AT J=17
ITERATION 300	RMS OF SHOCK SPEED= 3.6352E-03	MAXIMUM SHOCK SPEED= 8.6374E-03 AT J=14

FINAL SONIC LINE LOCATION

XSL= .5982	RSL= .9649
XSL= .6171	RSL= .9571
XSL= .6347	RSL= .9702
XSL= .6541	RSL= .9812
XSL= .6742	RSL= .9909
XSL= .6959	RSL= .9988
XSL= .7187	RSL= 1.0043
XSL= .7425	RSL= 1.0081
XSL= .7665	RSL= 1.0117
XSL= .7914	RSL= 1.0154
XSL= .8172	RSL= 1.0191
XSL= .8437	RSL= 1.0228
XSL= .8694	RSL= 1.0264
XSL= .8967	RSL= .9951
XSL= .9246	RSL= .9871
XSL= .9518	RSL= .9774
XSL= .9795	RSL= .9661
XSL= 1.0077	RSL= .9529
XSL= 1.0370	RSL= .9372

<<<< X ERROR IN HT = .3822E+03 RMS OF X ERROR IN HT = .6475E-01 >>>>

BODY AND FINAL SHOCK SHAPE

J	X(BODY)	R(BODY)	X(SHOCK)	R(SHOCK)
2	-.9995	.0349	-1.2775	.0444
3	-.9597	.1046	-1.2662	.1331
4	-.9879	.1742	-1.2592	.2218
5	-.9754	.2434	-1.2456	.3136
6	-.9611	.3122	-1.2292	.3994
7	-.9447	.3815	-1.2032	.4882
8	-.9185	.4485	-1.1634	.5772
9	-.8925	.5147	-1.1137	.6661
10	-.8667	.5805	-1.0571	.7554
11	-.8250	.6453	-1.0014	.8449
12	-.7874	.7105	-1.0383	.9349
13	-.7448	.7713	-.9898	1.0250
14	-.6994	.8323	-.9357	1.1153
15	-.6480	.8939	-.8777	1.2082
16	-.5935	.9459	-.8130	1.3013
17	-.5359	1.0002	-.7418	1.3951
18	-.4723	1.0609	-.6643	1.4914
19	-.4054	1.1137	-.5793	1.5886
20	-.3340	1.1648	-.4844	1.6892
21	-.2531	1.2138	-.3819	1.7922
22	-.1772	1.2611	-.2668	1.8987
23	-.0973	1.3067	-.1415	2.0088
24	.0000	1.3491	-.0000	2.1245

Figure A.2(b) - continued

MARCHING CALCULATION  
 \*\*\*\*\*

STEP NO.	DOWNSTREAM LOCATION	BODY ORDINATE	SHOCK ORDINATE
1	-0.302	1.3622	2.1483
2	-0.604	1.3751	2.1719
3	-0.906	1.3874	2.1951
4	-1.206	1.3993	2.2181
5	-1.510	1.4108	2.2408
6	-1.812	1.4219	2.2633
7	-2.114	1.4326	2.2855
8	-2.416	1.4430	2.3074
9	-2.718	1.4531	2.3292
10	-3.023	1.4639	2.3511
11	-3.328	1.4743	2.4043
12	-3.632	1.4848	2.4409
13	-3.937	1.4949	2.4769
14	-4.242	1.5052	2.5123
15	-4.546	1.5148	2.5472
16	-4.851	1.5226	2.5815
17	-5.156	1.5308	2.6153
18	-5.460	1.5383	2.6487
19	-5.765	1.5463	2.6816
20	-6.069	1.5538	2.7359
21	-6.373	1.6139	2.7891
22	-6.676	1.6267	2.8412
23	-6.979	1.6384	2.8922
24	-7.282	1.6491	2.9423
25	-7.585	1.6587	2.9914
26	-7.888	1.6676	3.0397
27	-8.191	1.6757	3.0872
28	-8.494	1.6831	3.1339
29	-8.797	1.6899	3.1799
30	-9.100	1.6999	3.2537
31	-9.403	1.7306	3.3257
32	-9.706	1.7161	3.3962
33	-10.009	1.7228	3.4651
34	-10.312	1.7287	3.5327
35	-10.615	1.7338	3.5989
36	-10.918	1.7384	3.6640
37	-11.221	1.7425	3.7278
38	-11.524	1.7462	3.7906
39	-11.827	1.7494	3.8524
40	-12.130	1.7542	3.9245
41	-12.433	1.7582	4.0051
42	-12.736	1.7616	4.1513
43	-13.039	1.7545	4.2465
44	-13.342	1.7670	4.3396
45	-13.645	1.7691	4.4311
46	-13.948	1.7711	4.5206
47	-14.251	1.7726	4.6086
48	-14.554	1.7741	4.6951
49	-14.857	1.7753	4.7802
50	-15.160	1.7771	4.9198
51	-15.463	1.7766	5.0561
52	-15.766	1.7799	5.1894
53	-16.069	1.7809	5.3198
54	-16.372	1.7818	5.4476
55	-16.675	1.7826	5.5730
56	-16.978	1.7833	5.6961
57	-17.281	1.7839	5.8173
58	-17.584	1.7844	5.9364
59	-17.887	1.7848	6.0538
60	-18.190	1.7854	6.2394

Figure A.2(c) - continued

DETAILED FLOW FIELD OUTPUT  
\*\*\*\*\*

FLOW FIELD VALUES EXTRAPOLATED TO SYMMETRY AXIS, THETA = 0.00 DEGREES

I	X/D	V/VINF	RHO/RHOINF	T/TINF	P/PINF
1	1.0000	1.0000	4.2291	22.3333	94.4497
2	1.0150	.9814	4.2200	22.3276	94.2214
3	1.0300	.9627	4.2156	22.3133	94.0645
4	1.0450	.9451	4.2089	22.2899	93.8164
5	1.0600	.9297	4.1998	22.2572	93.4765
6	1.0750	.9165	4.1883	22.2149	93.0430
7	1.0900	.9049	4.1744	22.1629	92.5177
8	1.1050	.8943	4.1582	22.1012	91.9079
9	1.1200	.8846	4.1395	22.0300	91.1941
10	1.1350	.8754	4.1185	21.9494	90.3992
11	1.1500	.8666	4.0951	21.8599	89.5189
12	1.1650	.8581	4.0693	21.7618	88.5562
13	1.1800	.8500	4.0412	21.6558	87.5148
14	1.1950	.8421	4.0106	21.5424	86.3989
15	1.2100	.8344	3.9777	21.4225	85.2129
16	1.2250	.8269	3.9424	21.2969	83.9618
17	1.2400	.8196	3.9048	21.1666	82.6538
18	1.2550	.8124	3.8647	21.0326	81.2894
19	1.2700	.8054	3.8209	20.8721	79.7595

FLOW FIELD VALUES FROM BLUNT BODY CALCULATION

ANGULAR LOCATION NO. 2, AT THETA = 2.0000 DEGREES

I	RP/D	R/D	X/D	VR/VINF	VX/VINF	FLOW ANGLE	V/VINF	RHO/RHOINF	T/TINF	P/PINF
1	1.0000	.0349	.9995	.0117	.0003	88.4170	.0103	4.2264	22.3311	94.3802
2	1.0150	.0354	1.0146	.0179	.0159	48.3361	.0245	4.2230	22.3206	94.2596
3	1.0300	.0360	1.0296	.0298	.0315	32.0664	.0386	4.2175	22.3016	94.0567
4	1.0450	.0365	1.0446	.0446	.0486	21.7493	.0526	4.2099	22.2742	93.7714
5	1.0600	.0370	1.0597	.0784	.0638	16.1277	.0667	4.2001	22.2384	93.4034
6	1.0750	.0375	1.0747	.0981	.0788	12.9421	.0808	4.1982	22.1941	92.9527
7	1.0900	.0381	1.0898	.0979	.0934	10.8570	.0948	4.1740	22.1415	92.4194
8	1.1050	.0386	1.1048	.0977	.1079	9.3428	.1088	4.1577	22.0806	91.8036
9	1.1200	.0391	1.1199	.0976	.1221	8.1878	.1228	4.1390	22.0114	91.1056
10	1.1350	.0396	1.1349	.0974	.1361	7.2935	.1368	4.1181	21.9339	90.3258
11	1.1500	.0402	1.1499	.0973	.1501	6.5784	.1508	4.0948	21.8482	89.4648
12	1.1650	.0407	1.1650	.0972	.1639	5.9916	.1648	4.0692	21.7542	88.5233
13	1.1800	.0412	1.1800	.0971	.1778	5.4997	.1787	4.0413	21.6521	87.5019
14	1.1950	.0417	1.1951	.0970	.1916	5.0828	.1926	4.0109	21.5419	86.4017
15	1.2100	.0423	1.2101	.0970	.2054	4.7228	.2065	3.9780	21.4235	85.2237
16	1.2250	.0428	1.2252	.0969	.2193	4.4117	.2204	3.9428	21.2970	83.9689
17	1.2400	.0433	1.2402	.0969	.2334	4.1354	.2343	3.9050	21.1625	82.6387
18	1.2550	.0438	1.2553	.0969	.2474	3.9001	.2481	3.8646	21.0200	81.2346
19	1.2700	.0444	1.2703	.0969	.2621	3.6835	.2620	3.8218	20.8695	79.7581

ANGULAR LOCATION NO. 3, AT THETA = 6.0000 DEGREES

I	RP/D	R/D	X/D	VR/VINF	VX/VINF	FLOW ANGLE	V/VINF	RHO/RHOINF	T/TINF	P/PINF
1	1.0000	.1046	.9957	.0350	.0029	85.2522	.0409	4.2139	22.2977	93.9609
2	1.0150	.1052	1.0117	.0543	.0185	71.1386	.0525	4.2102	22.2745	93.7792
3	1.0300	.1058	1.0257	.0585	.0369	58.4397	.0642	4.2045	22.2454	93.5316
4	1.0450	.1064	1.0408	.0573	.0516	48.0188	.0760	4.1970	22.2102	93.2169
5	1.0600	.1070	1.0558	.0559	.0670	39.4164	.0878	4.1875	22.1689	92.8335
6	1.0750	.1075	1.0708	.0541	.0817	33.5384	.0997	4.1761	22.1212	92.3799
7	1.0900	.1081	1.0859	.0536	.0953	29.0690	.1117	4.1625	22.0670	91.8546
8	1.1050	.1087	1.1009	.0531	.1107	25.6199	.1239	4.1469	22.0058	91.2559
9	1.1200	.1093	1.1159	.0526	.1249	22.8317	.1362	4.1291	21.9376	90.5823
10	1.1350	.1099	1.1309	.0522	.1389	20.5983	.1487	4.1091	21.8619	89.8321
11	1.1500	.1104	1.1459	.0519	.1529	18.7485	.1613	4.0868	21.7784	89.0035
12	1.1650	.1110	1.1610	.0516	.1667	17.2044	.1741	4.0622	21.6886	88.0951
13	1.1800	.1116	1.1760	.0514	.1806	15.8878	.1871	4.0352	21.5863	87.1050
14	1.1950	.1122	1.1911	.0512	.1944	14.7565	.2004	4.0058	21.4768	86.0317
15	1.2100	.1128	1.2061	.0510	.2083	13.7666	.2139	3.9739	21.3576	84.8737
16	1.2250	.1134	1.2211	.0509	.2222	12.8966	.2276	3.9395	21.2282	83.6293
17	1.2400	.1140	1.2362	.0507	.2364	12.1097	.2416	3.9025	21.0881	82.2972
18	1.2550	.1146	1.2512	.0506	.2504	11.4144	.2559	3.8629	20.9364	80.8760
19	1.2700	.1152	1.2662	.0503	.2652	10.7386	.2705	3.8206	20.7726	79.3645

Figure A.2(d) - continued

ANGULAR LOCATION NO.23, AT THETA = 86.0000 DEGREES

Table with 11 columns: I, RP/D, R/D, X/D, VR/VINF, VX/VINF, FLOW ANGLE, V/VINF, RHO/RHOINF, T/TINF, P/PINF. Rows 1-19.

ANGULAR LOCATION NO.24, AT THETA = 90.0000 DEGREES

Table with 11 columns: I, RP/D, R/D, X/D, VR/VINF, VX/VINF, FLOW ANGLE, V/VINF, RHO/RHOINF, T/TINF, P/PINF. Rows 1-19.

FLOW FIELD VALUES FROM MARCHING CALCULATION

ADDITIONAL AXIAL LOCATION NO. 1, AT X/D = -0.300

Table with 9 columns: I, R/D, VR/VINF, VX/VINF, FLOW ANGLE, V/VINF, RHO/RHOINF, T/TINF, P/PINF. Rows 1-19.

ADDITIONAL AXIAL LOCATION NO. 2, AT X/D = -0.674

Table with 9 columns: I, R/D, VR/VINF, VX/VINF, FLOW ANGLE, V/VINF, RHO/RHOINF, T/TINF, P/PINF. Rows 1-19.

Figure A.2(e) - continued



APPENDIX A

ADDITIONAL AXIAL LOCATION NO.45, AT X/D = -4.6689

I	R/D	VR/VINF	VX/VINF	FLOW ANGLE	V/VINF	RHO/RHOINF	T/TINF	P/PINF
1	1.7691	.0073	.6043	.607	.9044	.4326	4.8848	2.1132
2	1.9171	.0155	.9173	.3494	.9077	.4504	4.7561	2.1421
3	2.0649	.0210	.9112	1.2599	.9114	.4728	4.6136	2.1813
4	2.2128	.0272	.9144	1.7062	.9148	.4989	4.4819	2.2358
5	2.3616	.0354	.9175	2.2076	.9182	.5317	4.3473	2.3116
6	2.5095	.0447	.9203	2.7800	.9214	.5726	4.2267	2.4167
7	2.6584	.0553	.9228	3.4322	.9244	.6236	4.1024	2.5584
8	2.8043	.0672	.9248	4.1552	.9272	.6871	3.9912	2.7422
9	2.9522	.0800	.9255	4.9335	.9299	.7652	3.8848	2.9725
10	3.1000	.0934	.9279	5.7464	.9325	.8603	3.7812	3.2531
11	3.2479	.1071	.9289	6.5772	.9351	.9753	3.6795	3.5887
12	3.3958	.1209	.9297	7.4113	.9376	1.1128	3.5822	3.9859
13	3.5437	.1347	.9302	8.2382	.9399	1.2753	3.4885	4.4499
14	3.6916	.1482	.9312	9.0545	.9419	1.4658	3.4052	4.9915
15	3.8394	.1614	.9299	9.8443	.9438	1.6853	3.3316	5.6155
16	3.9873	.1743	.9290	10.6241	.9452	1.9374	3.2740	6.3429
17	4.1352	.1872	.9275	11.3488	.9464	2.2159	3.2265	7.1496
18	4.2831	.1985	.9258	12.0335	.9468	2.5309	3.2022	8.1195
19	4.4310	.2049	.9240	12.7372	.9473	2.8557	3.1897	9.1089

ADDITIONAL AXIAL LOCATION NO.46, AT X/D = -4.9175

I	R/D	VR/VINF	VX/VINF	FLOW ANGLE	V/VINF	RHO/RHOINF	T/TINF	P/PINF
1	1.7710	.0113	.9155	.4016	.9055	.4269	4.8417	2.0669
2	1.9237	.0124	.9089	.7818	.9099	.4444	4.7070	2.1317
3	2.0765	.0168	.9125	1.1776	.9128	.4663	4.5583	2.2256
4	2.2293	.0220	.9161	1.6032	.9154	.4918	4.4183	2.3171
5	2.3820	.0334	.9194	2.0776	.9200	.5238	4.2764	2.2398
6	2.5348	.0422	.9225	2.5194	.9234	.5635	4.1412	2.3334
7	2.6875	.0514	.9252	3.2396	.9256	.6131	4.0151	2.4518
8	2.8403	.0630	.9274	3.9352	.9276	.6752	3.8974	2.6314
9	2.9931	.0743	.9293	4.6915	.9324	.7519	3.7863	2.8468
10	3.1456	.0854	.9309	5.4892	.9351	.8458	3.6798	3.1124
11	3.2981	.1030	.9320	6.3093	.9377	.9596	3.5770	3.4325
12	3.4512	.1116	.9328	7.1363	.9401	1.0960	3.4790	3.8131
13	3.6040	.1315	.9333	7.9591	.9424	1.2576	3.3879	4.2606
14	3.7568	.1444	.9333	8.7735	.9444	1.4472	3.3073	4.7862
15	3.9095	.1572	.9330	9.5833	.9461	1.6659	3.2371	5.3925
16	4.0623	.1701	.9320	10.3447	.9474	1.9168	3.1836	6.1223
17	4.2151	.1821	.9309	11.0702	.9485	2.1937	3.1406	6.8896
18	4.3678	.1945	.9287	11.8280	.9488	2.5068	3.1272	7.8393
19	4.5206	.2049	.9268	12.4041	.9492	2.8289	3.1137	8.8081

ADDITIONAL AXIAL LOCATION NO.59, AT X/D = -9.8284

I	R/D	VR/VINF	VX/VINF	FLOW ANGLE	V/VINF	RHO/RHOINF	T/TINF	P/PINF
1	1.7848	.0049	.9296	.5577	.9196	.3564	4.2931	1.5302
2	2.0220	.0043	.9249	.3892	.9245	.3738	4.0994	1.9322
3	2.2591	.0111	.9296	.5816	.9297	.3953	3.8951	1.5398
4	2.4963	.0177	.9348	.9635	.9349	.4208	3.6854	1.5508
5	2.7335	.0273	.9402	1.2367	.9404	.4519	3.4675	1.5671
6	2.9706	.0350	.9454	1.5168	.9458	.4890	3.2515	1.5922
7	3.2078	.0430	.9510	1.8183	.9509	.5334	3.0425	1.6229
8	3.4450	.0511	.9531	2.1318	.9557	.5867	2.8474	1.6705
9	3.6821	.0621	.9590	2.5163	.9600	.6516	2.6742	1.7426
10	3.9193	.0742	.9622	2.9890	.9635	.7321	2.5288	1.8514
11	4.1565	.0856	.9645	3.5531	.9663	.8218	2.4129	2.0069
12	4.3936	.1017	.9639	4.1939	.9685	.9536	2.3246	2.2466
13	4.6308	.1223	.9655	4.8797	.9711	1.0988	2.2598	2.4831
14	4.8680	.1444	.9664	5.6022	.9711	1.2693	2.2180	2.8154
15	5.1051	.1664	.9658	6.3153	.9726	1.4622	2.1942	3.2084
16	5.3423	.1886	.9643	7.0594	.9726	1.6837	2.1949	3.6890
17	5.5795	.2102	.9625	7.7513	.9713	1.9134	2.2068	4.2225
18	5.8166	.2324	.9598	8.4982	.9703	2.1720	2.2468	4.8000
19	6.0538	.2527	.9573	9.1393	.9694	2.4354	2.2863	5.5565

ADDITIONAL AXIAL LOCATION NO.60, AT X/D = -10.5003

I	R/D	VR/VINF	VX/VINF	FLOW ANGLE	V/VINF	RHO/RHOINF	T/TINF	P/PINF
1	1.7854	.0000	.9209	.0476	.9209	.3501	4.2424	1.4854
2	2.0329	.0000	.9209	.3733	.9209	.3676	4.0439	1.4866
3	2.2803	.0117	.9311	.6598	.9312	.3894	3.8350	1.4935
4	2.5278	.0182	.9360	.9330	.9356	.4154	3.6203	1.5039
5	2.7752	.0267	.9419	1.2185	.9421	.4472	3.3972	1.5191
6	3.0227	.0342	.9473	1.4646	.9476	.4851	3.1763	1.5447
7	3.2702	.0416	.9524	1.7406	.9529	.5302	2.9028	1.5710
8	3.5175	.0491	.9572	2.0435	.9578	.5841	2.7637	1.6143
9	3.7650	.0565	.9613	2.3948	.9621	.6491	2.5869	1.6799
10	4.0124	.0640	.9645	2.8313	.9667	.7288	2.4391	1.7777
11	4.2599	.0714	.9668	3.3631	.9695	.8273	2.3227	1.9215
12	4.5073	.0788	.9683	3.9775	.9716	.9475	2.2500	2.1186
13	4.7548	.0862	.9689	4.6829	.9721	1.0908	2.1742	2.3716
14	5.0022	.0936	.9688	5.3477	.9730	1.2587	2.1365	2.6891
15	5.2496	.1010	.9691	6.0493	.9735	1.4478	2.1171	3.0653
16	5.4971	.1084	.9690	6.7819	.9733	1.6615	2.1223	3.5262
17	5.7445	.1157	.9688	7.5449	.9730	1.8881	2.1385	4.0377
18	5.9920	.1231	.9681	8.3205	.9719	2.1395	2.1818	4.6679
19	6.2394	.1305	.9665	9.1371	.9709	2.3901	2.2247	5.3173

Figure A.2(f) - continued

STREAMLINE TRAJECTORY CALCULATION  
 \*\*\*\*\*

43 STREAMLINES CALCULATED

STREAMLINE NO. 1, STARTING AT X/D = 1.2723, R/D = .0444  
 (CORRESPONDS TO THETA = 2.00 DEGREES, RP/D = 1.2711)

X/D	R/D
1.2703	.0444
1.2403	.0465
1.2153	.0483
1.1903	.0515
1.1653	.0552
1.1403	.0600
1.1153	.0670
1.0903	.0730
1.0653	.0988
1.0403	.1233
1.0153	.1688
.9903	.2680
.9653	.3498
.9353	.4353
.9103	.4954
.8853	.5509
.8603	.6002
.8353	.6454
.8103	.6859
.7853	.7257
.7603	.7621
.7353	.7961
.7103	.8284
.6853	.8539
.6603	.8879
.6303	.9209
.6053	.9471
.5803	.9721
.5553	.9961
.5303	1.0191
.5053	1.0412
.4803	1.0624
.4553	1.0829
.4303	1.1026
.4053	1.1216
.3803	1.1400
.3553	1.1577
.3253	1.1782
.3003	1.1947
.2753	1.2106
.2503	1.2260
.2253	1.2409
.2003	1.2554
.1753	1.2694
.1503	1.2831
.1253	1.2962
.1003	1.3090
.0753	1.3214
.0503	1.3334
.0253	1.3451
-.0047	1.3580
-.0216	1.3742
-.0426	1.3977
-.0684	1.4230
-.0920	1.4509
-.1131	1.4803
-.12129	1.5053
-.14243	1.5273
-.15755	1.5493
-.18170	1.5703
-.20284	1.5923
-.22096	1.6116
-.24210	1.6307
-.26325	1.6484
-.28137	1.6641
-.30251	1.6797
-.32164	1.6939
-.34278	1.7081
-.36292	1.7213
-.38104	1.7346
-.40219	1.7474
-.42333	1.7599
-.44145	1.7719
-.46259	1.7839
-.48372	1.7959
-.49175	1.7865

Figure A.2(g) - continued

APPENDIX A

STREAMLINE NO.42, STARTING AT X/D = -4.3769, R/D = 4.3233

X/D	R/D
-4.3769	4.3233
-4.5683	4.3717
-4.7998	4.4187
-4.9175	4.4442

STREAMLINE NO.43, STARTING AT X/D = -4.6915, R/D = 4.4391

X/D	R/D
-4.6915	4.4391
-4.9029	4.4861
-4.9175	4.4893

MAGNETIC FIELD COMPONENTS  
\*\*\*\*\*

ANGULAR LOCATION NO. 1, AT THETA = 0.000 DEGREES

I	RP/D	B/BINF (PARALLEL)	B/BINF (PERP)	B/BINF (IN-PLANE)	B-ANGLE (IN-PLANE)	B/BINF (NORMAL)	BX/BINF (RESULTANT)	BY/BINF (RESULTANT)	BZ/BINF (RESULTANT)
1	1.0000	0.0000	0.0000	0.0000	0.0000	0.0000	0.0000	0.0000	0.0000
2	1.0156	0.0693	19.5088	13.7949	-89.7964	4.2200	0.0347	-9.7544	2.9846
3	1.0321	0.2292	15.3355	11.5321	-89.5076	4.2156	0.0646	-7.5177	2.9809
4	1.0485	0.4866	11.7067	8.2804	-89.0712	4.2089	0.0949	-5.8544	2.9761
5	1.0652	0.7519	8.6738	6.9841	-88.5445	4.1998	0.1254	-4.9369	2.9697
6	1.0792	1.0221	6.5664	6.0615	-87.9137	4.1885	0.1561	-4.0283	2.9616
7	1.0903	1.3031	4.7505	5.3667	-87.1821	4.1744	0.1865	-3.7903	2.9518
8	1.1003	1.5937	3.4844	4.8521	-86.3759	4.1582	0.2169	-3.4241	2.9403
9	1.1204	1.8956	2.6933	4.4951	-85.5100	4.1395	0.2468	-3.1476	2.9271
10	1.1354	2.2129	2.1691	4.2847	-84.6424	4.1185	0.2762	-2.9456	2.9122
11	1.1541	2.5529	1.8719	3.9241	-83.6888	4.0951	0.3052	-2.7580	2.8957
12	1.1655	2.9201	1.6239	3.7157	-82.7222	4.0693	0.3330	-2.6369	2.8775
13	1.1805	3.3212	1.4042	3.5301	-81.7056	4.0412	0.3601	-2.4721	2.8575
14	1.1926	3.7522	1.2054	3.3875	-80.7244	4.0106	0.3861	-2.3042	2.8360
15	1.2104	4.2129	1.0244	3.2454	-79.6958	3.9777	0.4111	-2.2096	2.8127
16	1.2257	4.6966	0.8694	3.1101	-78.6277	3.9424	0.4345	-2.1602	2.7877
17	1.2407	5.2052	0.7352	3.0185	-77.6478	3.9248	0.4566	-2.0850	2.7611
18	1.2558	5.7445	0.6179	2.9202	-76.6392	3.8647	0.4772	-2.0093	2.7328
19	1.2706	6.3111	0.5249	2.7928	-75.3336	3.8209	0.5000	-1.9104	2.7018

ANGULAR LOCATION NO. 2, AT THETA = 2.000 DEGREES

I	RP/D	B/BINF (PARALLEL)	B/BINF (PERP)	B/BINF (IN-PLANE)	B-ANGLE (IN-PLANE)	B/BINF (NORMAL)	BX/BINF (RESULTANT)	BY/BINF (RESULTANT)	BZ/BINF (RESULTANT)
1	1.0000	0.0000	0.0000	0.0000	0.0000	0.0000	0.0000	0.0000	0.0000
2	1.0152	0.0637	19.6130	13.3129	-91.2200	6.8133	-0.2680	-9.7650	4.8177
3	1.0302	0.1600	14.9735	11.5251	-93.7384	6.6524	-0.0959	-7.4417	4.7039
4	1.0453	0.2216	11.6901	8.2968	-97.0175	6.4249	-0.6118	-5.8231	4.5431
5	1.0603	0.2802	8.6697	6.9237	-99.2630	6.2297	0.0630	-4.8954	4.4051
6	1.0754	0.3363	6.5682	6.0071	-88.4334	6.0636	0.1172	-4.2450	4.2452
7	1.0904	0.3908	4.7569	5.3183	-87.0814	5.7595	0.1587	-3.7571	4.0514
8	1.1055	0.4522	3.4836	4.8053	-86.0891	5.5336	0.1962	-3.3922	3.9129
9	1.1205	0.5084	2.6959	4.4193	-85.7462	5.3252	0.2318	-3.1167	3.7655
10	1.1356	0.5639	2.0903	4.1393	-84.8951	5.1444	0.2602	-2.9123	3.6378
11	1.1507	0.6175	1.6201	3.8743	-84.0020	4.9735	0.2803	-2.7246	3.5168
12	1.1657	0.6714	1.2660	3.5645	-83.1898	4.8030	0.3073	-2.5729	3.3962
13	1.1806	0.7241	0.9449	3.4755	-82.3421	4.6355	0.3276	-2.4357	3.2916
14	1.1958	0.7725	0.7240	3.3267	-81.4203	4.5090	0.3512	-2.3275	3.1841
15	1.2109	0.8219	0.5331	3.1872	-80.4476	4.3604	0.3740	-2.2225	3.0830
16	1.2259	0.8690	0.3112	3.0529	-79.4317	4.2117	0.3971	-2.1219	2.9822
17	1.2410	0.9148	0.1574	2.9234	-78.3632	4.0825	0.4212	-2.0454	2.8888
18	1.2561	0.9589	0.0749	2.8555	-77.2813	3.9556	0.4446	-1.9696	2.7971
19	1.2711	1.0011	0.5248	2.7358	-75.0273	3.8218	0.4673	-1.8786	2.7024

Figure A.2(h) - continued

## ANGULAR LOCATION NO. 3, AT THETA = 6.0000 DEGREES

I	RP/D	B/BINF (PARALLEL)	B/BINF (PERP)	B/BINF (IN-PLANE)	B-ANGLE (IN-PLANE)	B/BINF (NORMAL)	BX/BINF (RESULTANT)	BY/BINF (RESULTANT)	BZ/BINF (RESULTANT)
1	1.0011	.1723							
2	1.0163	.2211	19.7354	13.8038	-94.0993	12.0951	-.6977	-0.7358	8.5525
3	1.0314	.2700	14.8020	10.2979	-93.4057	11.6519	-.4326	-7.2588	8.2391
4	1.0465	.3188	11.6097	8.8349	-92.1443	10.9525	-.2126	-5.6776	7.7466
5	1.0616	.3676	9.8224	6.7739	-91.0505	10.3597	-.0878	-4.7891	7.3254
6	1.0767	.4164	8.5379	5.8698	-89.9227	8.6352	.0096	-4.1506	6.1060
7	1.0918	.4651	7.5758	5.1945	-88.9634	7.5921	.0664	-3.6725	5.3048
8	1.1069	.5138	6.8514	4.6877	-87.9932	6.8321	.1161	-3.3127	4.8310
9	1.1221	.5624	6.3034	4.3063	-87.0325	6.3063	.1576	-3.0459	4.4592
10	1.1372	.6108	5.8859	4.0167	-86.1842	5.9080	.1890	-2.8339	4.1776
11	1.1523	.6592	5.5298	3.7568	-85.2620	5.5322	.2194	-2.6474	3.9119
12	1.1674	.7073	5.2036	3.5460	-84.4222	5.1748	.2437	-2.4955	3.6591
13	1.1825	.7551	4.9275	3.3572	-83.4894	4.9048	.2692	-2.3586	3.4682
14	1.1976	.8027	4.7026	3.2041	-82.6489	4.6555	.2899	-2.2470	3.2919
15	1.2128	.8499	4.4867	3.0578	-81.7828	4.4481	.3098	-2.1399	3.1453
16	1.2279	.8966	4.2843	2.9220	-80.7752	4.2662	.3312	-2.0395	3.0166
17	1.2430	.9429	4.1259	2.8199	-79.6469	4.0980	.3583	-1.9615	2.8977
18	1.2581	.9885	3.9738	2.7231	-78.4669	3.9595	.3850	-1.8866	2.7998
19	1.2732	1.0334	3.8123	2.6216	-77.1723	3.8206	.4116	-1.8075	2.7016

## ANGULAR LOCATION NO. 23, AT THETA = 86.0000 DEGREES

I	RP/D	B/BINF (PARALLEL)	B/BINF (PERP)	B/BINF (IN-PLANE)	B-ANGLE (IN-PLANE)	B/BINF (NORMAL)	BX/BINF (RESULTANT)	BY/BINF (RESULTANT)	BZ/BINF (RESULTANT)
1	1.3092	1.1539							
2	1.3484	1.2145	8.5172	5.1726	-149.3591	11.8723	-3.1469	-1.8541	8.3950
3	1.3875	1.2577	5.7915	5.2113	-146.2984	7.1832	-1.8891	-1.2599	5.0793
4	1.4266	1.3240	4.5546	2.3029	-142.7691	5.6294	-1.2965	-.9952	3.9806
5	1.4658	1.3738	3.6240	1.7525	-138.9333	4.8498	-.9343	-.8141	3.4293
6	1.5049	1.4376	3.3967	1.4204	-133.7244	4.3286	-.6942	-.7258	3.0698
7	1.5441	1.5057	3.1593	1.1903	-127.5731	4.0145	-.5132	-.6671	2.8387
8	1.5832	1.5787	2.9117	1.0309	-120.5963	3.7970	-.3707	-.6269	2.6849
9	1.6223	1.6509	2.7665	.9111	-112.9630	3.6526	-.2513	-.5931	2.5828
10	1.6615	1.7407	2.6534	.8274	-104.3051	3.5498	-.1446	-.5669	2.5101
11	1.7006	1.8307	2.5789	.7682	-95.5531	3.4850	-.0526	-.5437	2.4643
12	1.7397	1.9272	2.5202	.7392	-85.8703	3.4386	.0376	-.5213	2.4314
13	1.7789	2.0307	2.4826	.7373	-76.2889	3.4192	.1236	-.5065	2.4177
14	1.8180	2.1415	2.4593	.7494	-67.5293	3.4158	.2025	-.4897	2.4154
15	1.8571	2.2601	2.4524	.7576	-59.3933	3.4262	.2836	-.4793	2.4227
16	1.8963	2.3869	2.4456	.8376	-51.7332	3.4525	.3668	-.4650	2.4413
17	1.9354	2.5223	2.4446	.8986	-44.9234	3.4900	.4499	-.4487	2.4678
18	1.9745	2.6666	2.4489	.9694	-38.9013	3.5389	.5335	-.4305	2.5024
19	2.0137	2.8201	2.4452	1.0402	-33.6877	3.5964	.6162	-.4015	2.5430

## ANGULAR LOCATION NO. 24, AT THETA = 90.0000 DEGREES

I	RP/D	B/BINF (PARALLEL)	B/BINF (PERP)	B/BINF (IN-PLANE)	B-ANGLE (IN-PLANE)	B/BINF (NORMAL)	BX/BINF (RESULTANT)	BY/BINF (RESULTANT)	BZ/BINF (RESULTANT)
1	1.3491	1.1925							
2	1.3922	1.2443	7.7661	4.6839	-151.7632	10.8083	-2.9163	-1.5700	7.6424
3	1.4352	1.1989	5.3267	2.9243	-148.1538	6.5661	-1.7565	-1.0912	4.6430
4	1.4783	1.2567	4.1933	2.0885	-144.2240	5.1963	-1.1981	-.8634	3.6744
5	1.5214	1.3184	3.5221	1.5802	-139.7697	4.4745	-.8530	-.7216	3.1639
6	1.5645	1.3844	3.1343	1.2765	-133.7249	4.0266	-.6239	-.6523	2.8472
7	1.6076	1.4552	2.8746	1.0666	-127.0528	3.7522	-.4544	-.6019	2.6932
8	1.6506	1.5314	2.7021	.9232	-119.2654	3.5687	-.3191	-.5695	2.5234
9	1.6937	1.6133	2.5728	.8176	-110.9357	3.4484	-.2066	-.5400	2.4384
10	1.7368	1.7016	2.4808	.7494	-101.2532	3.3707	-.1034	-.5197	2.3834
11	1.7799	1.7968	2.4151	.7039	-91.6648	3.3186	-.0145	-.4975	2.3466
12	1.8230	1.8992	2.3690	.6984	-80.6905	3.2934	.0799	-.4873	2.3302
13	1.8660	2.0195	2.3428	.6981	-71.5558	3.2924	.1562	-.4862	2.3281
14	1.9091	2.1281	2.3295	.7355	-62.1816	3.3035	.2427	-.4800	2.3359
15	1.9522	2.2554	2.3311	.7869	-54.2423	3.3327	.3251	-.4513	2.3565
16	1.9953	2.3920	2.3315	.8436	-46.9440	3.3742	.4073	-.4359	2.3859
17	2.0384	2.5383	2.3372	.9186	-40.4107	3.4282	.4946	-.4211	2.4241
18	2.0814	2.6946	2.3469	.9964	-34.6920	3.4919	.5793	-.4010	2.4691
19	2.1245	2.8613	2.3530	1.0732	-29.3214	3.5676	.6617	-.3716	2.5226

Figure A.2(1) - continued



VELOCITY AND TEMPERATURE CONTOURS  
\*\*\*\*\*

12 VELOCITY (TEMPERATURE) CONTOUR LINES FOUND

11 POINTS IN CONTOUR LINE OF V/VINF = .100, T/TINF = 22.120

X/D	R/D
.9853	.1901
1.0019	.1832
1.0109	.1783
1.0186	.1740
1.0353	.1664
1.0527	.1405
1.0707	.1133
1.0712	.1126
1.0856	.0614
1.0933	.0353
1.1010	0.0000

20 POINTS IN CONTOUR LINE OF V/VINF = .200, T/TINF = 21.480

X/D	R/D
.9447	.3697
.9614	.3689
.9785	.3662
.9961	.3617
1.0142	.3552
1.0328	.3466
1.0453	.3396
1.0516	.3356
1.0704	.3215
1.0897	.3144
1.1095	.2942
1.1151	.2878
1.1294	.2777
1.1498	.2553
1.1614	.2448
1.1705	.1811
1.1806	.1251
1.1913	.1212
1.2031	.0920
1.2136	0.0000

DENSITY CONTOURS  
\*\*\*\*\*

10 DENSITY CONTOUR LINES FOUND

9 POINTS IN CONTOUR LINE OF RHO/RHOINF = 4.200

X/D	R/D
.9930	.1282
1.0036	.1251
1.0247	.1171
1.0346	.1086
1.0417	.0925
1.0597	.0376
1.0598	.0376
1.0599	.0242
1.0599	0.0000

Figure A.2(k) - continued

APPENDIX A

27 POINTS IN CONTOUR LINE OF  $\rho/\rho_{\infty} = 4.000$

X/D	R/D
.9483	.3572
.9617	.3678
.9754	.3776
.9895	.3861
1.0039	.3933
1.0189	.3986
1.0344	.4016
1.0508	.4026
1.0681	.3977
1.0867	.3886
1.1071	.3722
1.1284	.3426
1.1508	.3406
1.1559	.2882
1.1795	.2881
1.1874	.2182
1.1933	.1641
1.2101	.1255
1.2005	.0419
	0.0000

MAGNETIC FIELD CONTOURS  
\*\*\*\*\*

11 MAGNETIC FIELD CONTOUR LINES FOUND  
(FOR COMPONENT ALONG FIELD LINES PARALLEL TO FLOW IN FREESTREAM)

13 POINTS IN CONTOUR LINE OF  $B/B_{\infty}$  (PARALLEL) = .900

X/D	R/D
.9789	.2283
.9954	.2226
1.0123	.2144
1.0296	.2033
1.0473	.1892
1.0654	.1854
1.0849	.1689
1.0831	.1405
1.0966	.1153
1.1018	.0983
1.1176	.0791
1.1202	.0668
1.1220	0.0000

19 POINTS IN CONTOUR LINE OF  $B/B_{\infty}$  (PARALLEL) = .750

X/D	R/D
.9513	.3464
.9684	.3437
.9860	.3391
1.0041	.3326
1.0122	.3289
1.0222	.3242
1.0403	.3126
1.0589	.3004
1.0780	.2845
1.0911	.2721
1.0973	.2651
1.1166	.2406
1.1364	.2116
1.1427	.2015
1.1564	.1691
1.1744	.1234
1.1767	.1108
1.1883	.0419
1.1892	0.0000

Figure A.2(1) - continued

12 MAGNETIC FIELD CONTOUR LINES FOUND  
 (FOR COMPONENT ALONG FIELD LINES PERPENDICULAR TO FLOW IN FREESTREAM)

45 POINTS IN CONTOUR LINE OF  $\delta/BIN$  (PERPENDICULAR) = 2.200

X/D	R/D
-1.8975	1.7899
-1.8527	1.7957
-1.7055	1.8142
-1.6156	1.8226
-1.5257	1.8283
-1.5027	1.8293
-1.4359	1.8346
-1.3459	1.8394
-1.2964	1.8414
-1.2667	1.8407
-1.1279	1.8396
-1.0762	1.8425
-0.9863	1.8446
-0.8404	1.8430
-0.8542	1.8409
-0.8165	1.8453
-0.7530	1.8480
-0.6996	1.8499
-0.6814	1.8500
-0.6461	1.8559
-0.5926	1.8625
-0.5428	1.8651
-0.5392	1.8728
-0.4857	1.8677
-0.4838	1.8882
-0.4322	1.9140
-0.4277	1.9165
-0.3885	1.9497
-0.3786	1.9667
-0.3651	1.9890
-0.3355	2.0345
-0.3628	2.0697
-0.3788	2.1363
-0.3845	2.1924
-0.4257	2.2261
-0.4322	2.2404
-0.4766	2.3274
-0.4857	2.3311
-0.5307	2.3978
-0.5392	2.4695
-0.5926	2.4803
-0.6496	2.5617
-0.6461	2.5431
-0.6996	2.6170
-0.7337	2.6567

6 POINTS IN CONTOUR LINE OF  $\delta/BIN$  (PERPENDICULAR) = 2.000

X/D	R/D
-3.6973	1.8865
-3.4232	1.9133
-4.1718	1.9388
-4.4214	1.9599
-4.6655	1.9766
-4.9175	1.9883

Figure A.2(m) - concluded



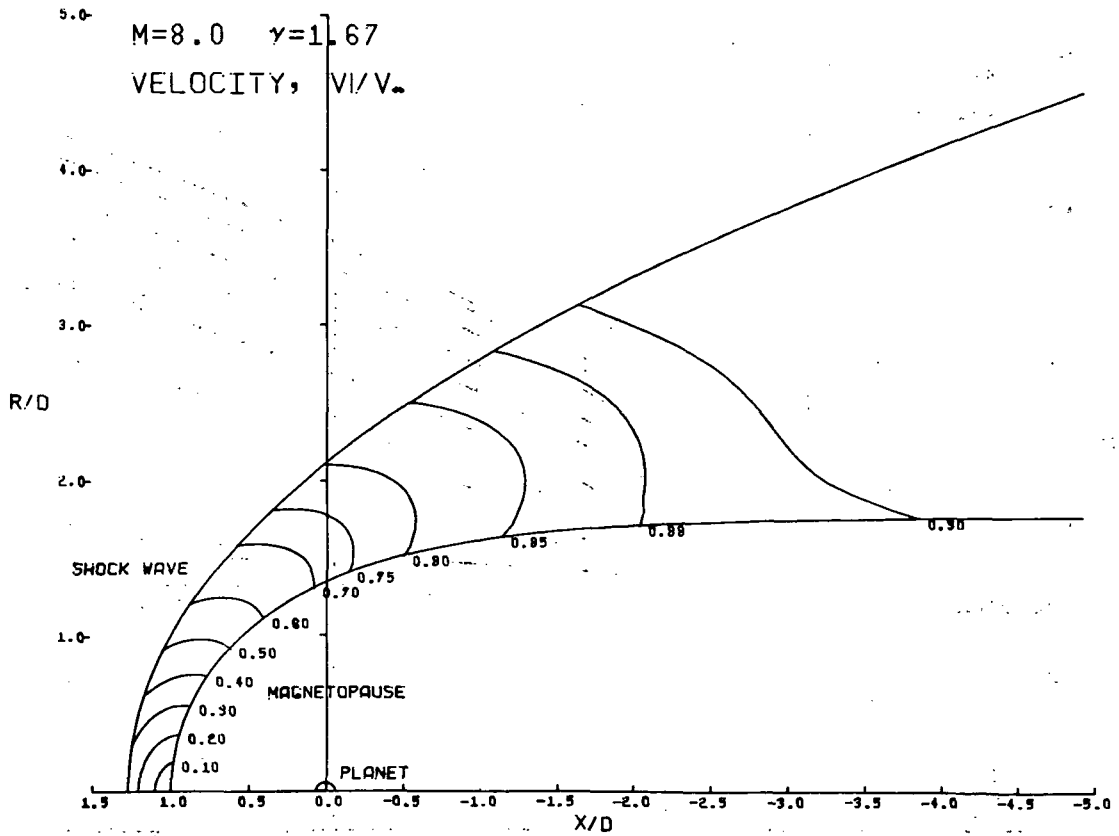
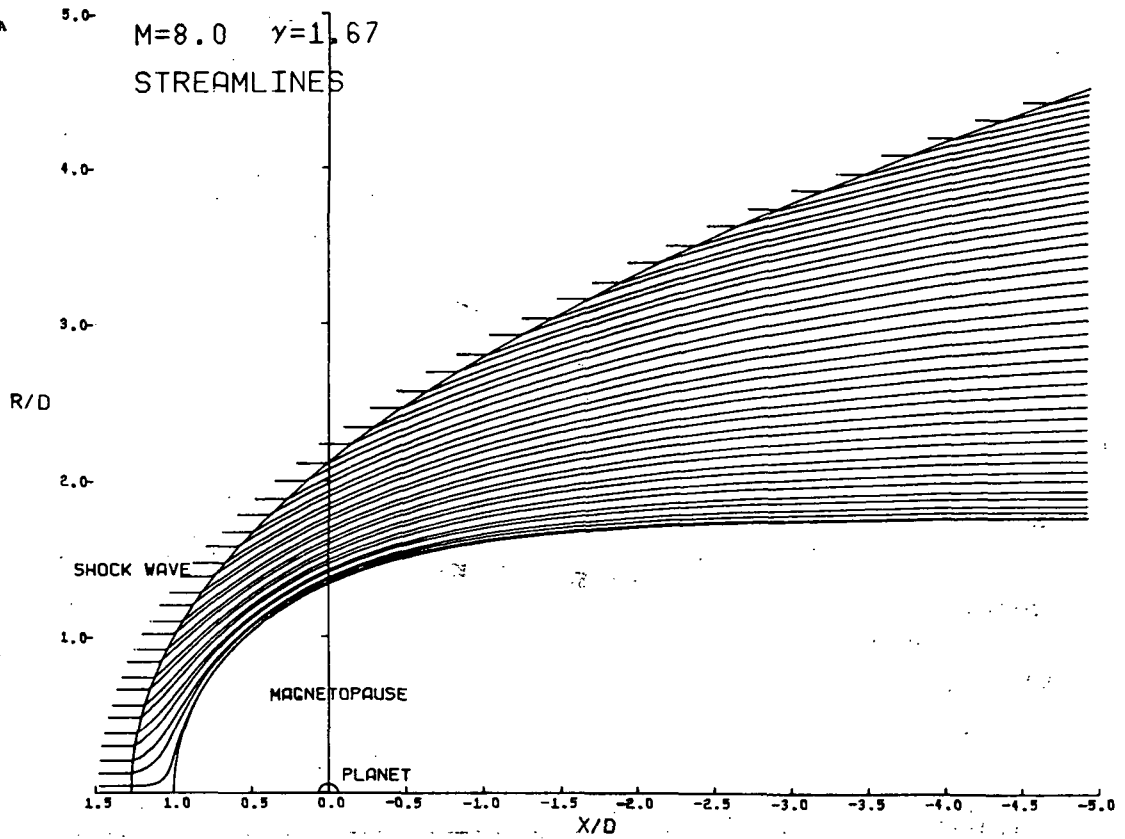


Figure A.3. - Plot output for sample case.

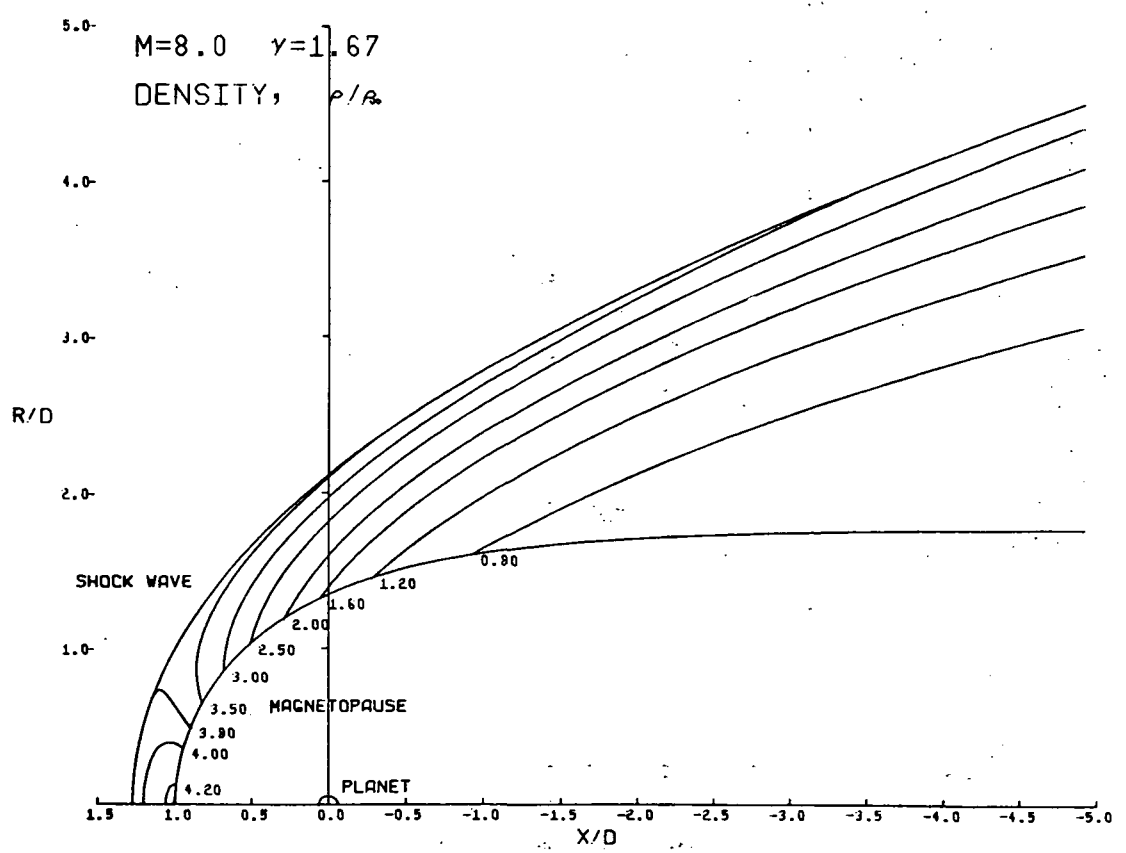
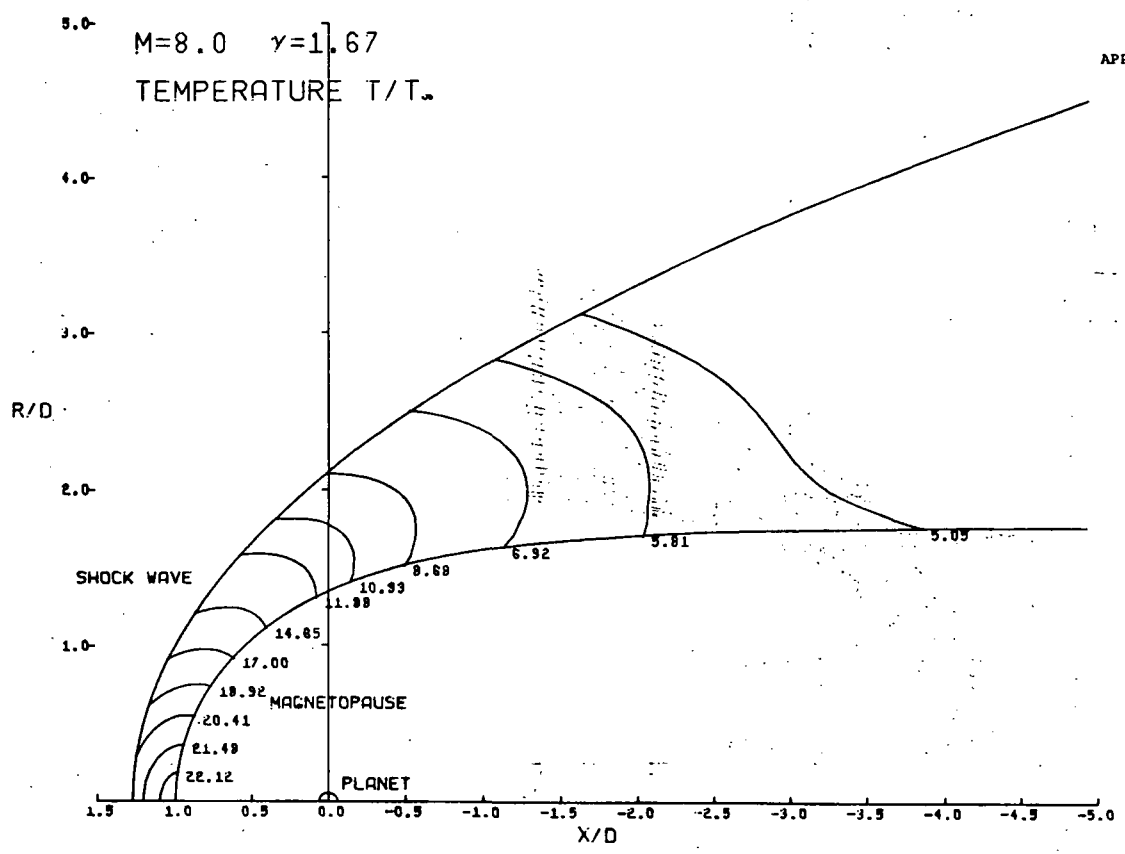


Figure A.3. - Continued.

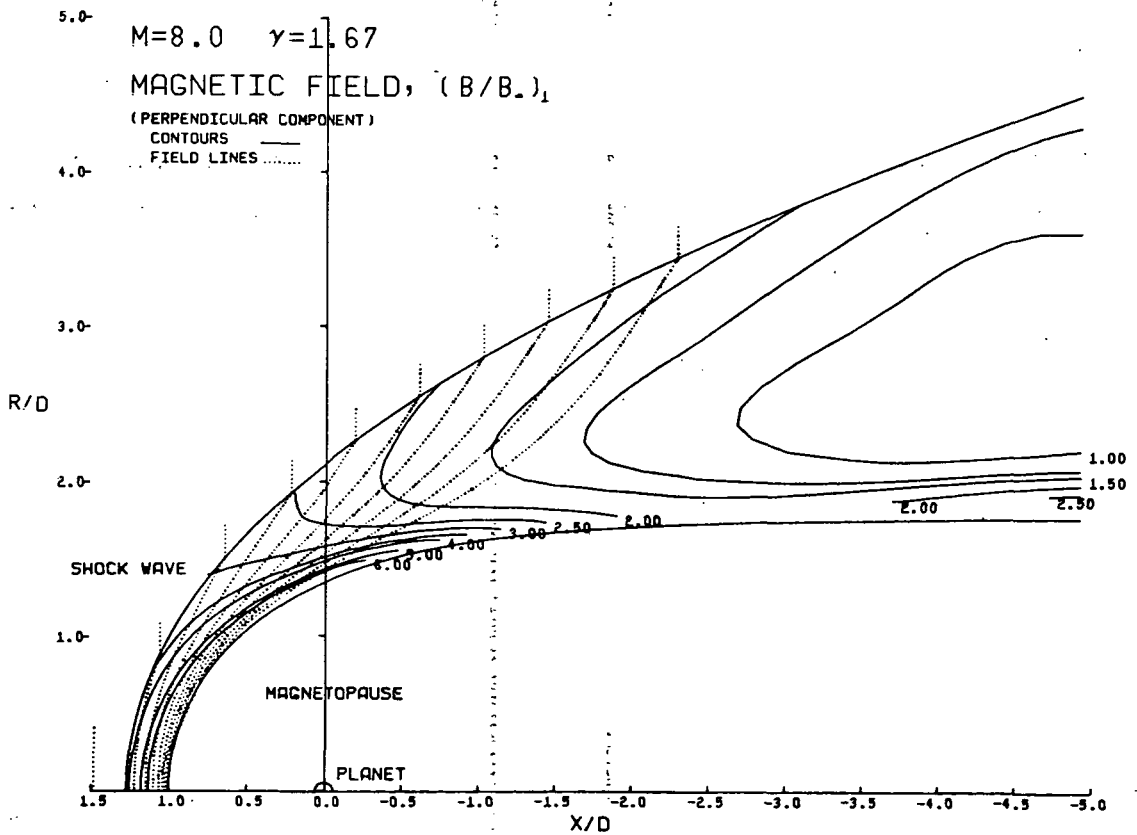
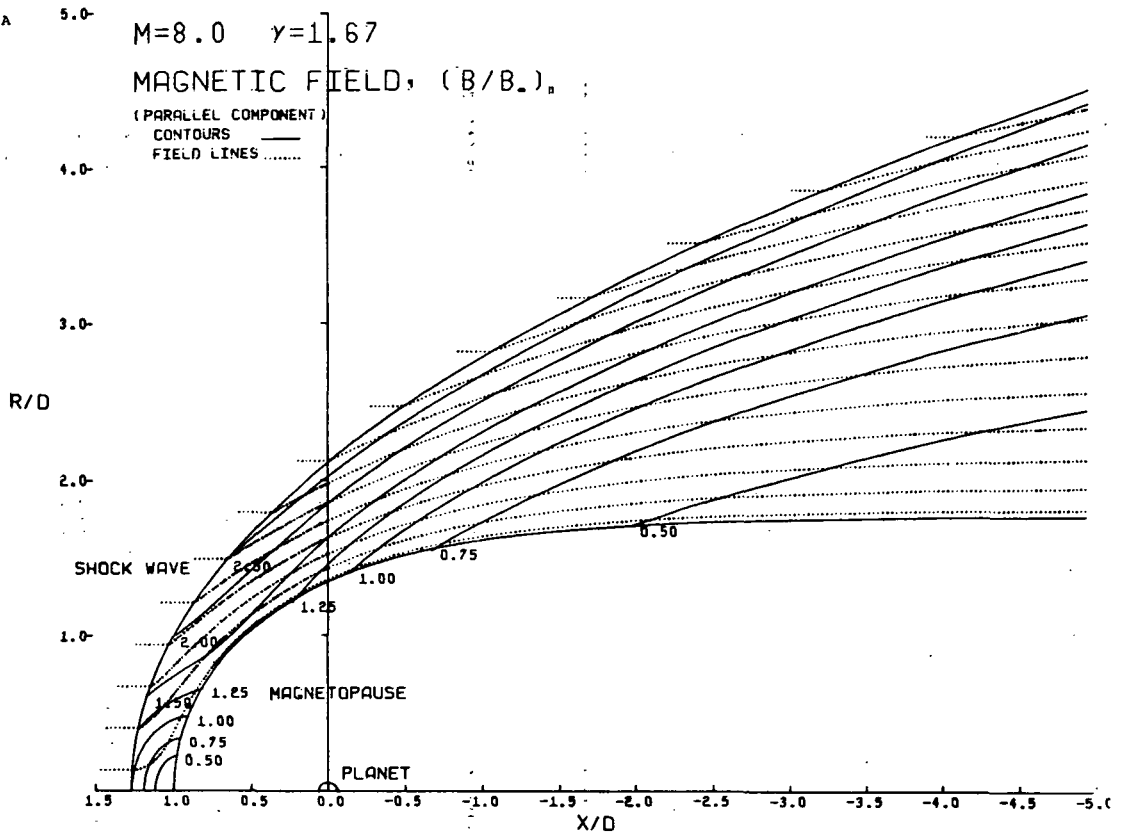


Figure A.3. - Concluded.

APPENDIX B

LISTING OF COMPUTER PROGRAM

```

PROGRAM MAIN (INPUT,OUTPUT,TAPE=INPUT,TAPE=OUTPUT,
* LOGICAL LRBUN,LRPFL,LRPST,LRPCOM,LRPB,LPLOT
COMMON /PROG/ LRBUN,LRPFL,LRPST,LRPCOM,LRPB,LPLOT
READ(5,1) I, N
DO 20 I=1, N
CALL LTRUN
CALL LPLB
CALL LPRB
CALL LPRC
CALL LPRP
GO TO 10
10 CALL LTRUN
11 CALL LPLB
12 CALL LPRB
13 CALL LPRC
14 CALL LPRP
15 CALL LTRUN
16 CALL LPLB
17 CALL LPRB
18 CALL LPRC
19 CALL LPRP
20 CONTINUE
STOP
END

SUBROUTINE BCMP
* THIS SUBROUTINE CALCULATES THE COMPONENTS OF THE MAGNETIC FIELD
* PARALLEL, PERPENDICULAR AND NORMAL TO THE FLOW.
COMMON /BCMP/ KYCOM, XCOM(20), XCI(20), YCOM(20), YCI(20), I0J,
* VLEG(100), RR(20,100),
COMMON /BLUNT/ IMETA(20), RP(20,20)
LEVEL 2, XST, RST, NUM, NST
COMMON /OVAL/ NB, NMBF(11), XBF(51,100), RBF(51,100), ELBF(51,100),
* GAMBF(51,100)
COMMON /DMS1/ KM, ZPLOT, NBLUNT, NZEND, NZADO
LEVEL 2, XST, RST, NUM, NST
COMMON /STREAM/ XST(50,150), RST(50,150), NUM(50), NST
COMMON /SHOCKS/ DRSD(100), DST(50)
DATA P10Z /1.5707963277/
* THIS SUBROUTINE CALCULATES THE MAGNITUDE AND DIRECTION OF
* FLUX LINE AT THE POINTS WHERE THE STREAMLINES INTERSECT THE
* MAGNETIC FIELD LINES WHICH ARE PERPENDICULAR TO THE FLOW
* IN FREESTREAM
DST(11)=*.5/DST(1,1)
DO 40 I=2,NST
DST(11)=DST(1,1)-NST(I-1,1)
40 CONTINUE
* SET AFFAYS TO FREE STREAM VALUES
NSTP=NST+1
JBFMAX=NBF(1,1)
DO 30 I=2,NSTPI
IF (NBF(I,1) .LT. JBFMAX) GO TO 30
30 CONTINUE
DO 20 I=3,JBFMAX
:LEBF(I,1)=I+5
:EMFF(I,1)=P10Z
20 CONTINUE
* VALUES ALONG FIELD LINES WHICH CROSS SHOCK
DO 10 J=3,NB
IF (J .GT. NBF(1,1)) GO TO 10C
I3=ISORT(I,2,J)-XBF(1,1)+2+RBF(2,J)+21*2.0
:LEFF(I,1)=LEUST(I)
GAP=P10Z
DZ=XBF(3,1)-XBF(2,J)
PZ=XBF(3,1)-RBF(2,J)
LE=SCAT(IONZ*GAZ+DRZ+GRZ)
SAP=AFIN(I,2,OXZ)
:LEFF(2,J)=LE+GZ*(OXZ-IO1+OZ1)+DST(21)*GST(11)
GAMBF(2,J)=GAM1+DZ*(ANZ*O1)/(OI+OZ1)
GO TO 20
20 CONTINUE
DI=ISORT(I,2,J)-XBF(2,J)+2+RBF(2,2)+21*2.0
DZ=XBF(3,1)-XBF(2,J)
PZ=XBF(3,1)-RBF(2,J)
LE=SCAT(IONZ*GAZ+DRZ+GRZ)
SAP=AFIN(I,2,OXZ)
:LEFF(2,J)=LE+GZ*(OXZ-IO1+OZ1)+DST(21)*GST(11)
GAMBF(2,J)=GAM1+DZ*(ANZ*O1)/(OI+OZ1)
GO TO 20
20 CONTINUE
DO 10C I=3,NJ
DI=OZ
GAP=GAMZ
IF (XFF(I+1,1) .LT. XST(I,1)) GO TO 10C
PZ=XBF(I+1,1)-XBF(I,1)
PZ=XBF(I+1,1)-RBF(I,1)
PZ=SCAT(IONZ*GAZ+DRZ+GRZ)
:LEFF(2,J)=LE+GZ*(OXZ-IO1+OZ1)+DST(21)*GST(11)
GAMBF(2,J)=GAM1+DZ*(ANZ*O1)/(OI+OZ1)
CONTINUE
DO 10C I=3,NJ
DI=OZ
CALL 61M(LRBY,5,5,LRBY,LS+1)
12. ASXVBF(I,1,1)
13. ASXVBF(I,1,1)
END

```

BCMP	52
BCOMP	53
BCOMP	54
BCOMP	55
BCOMP	56
BCOMP	57
BCOMP	58
BCOMP	59
BCOMP	60
BCOMP	61
BCOMP	62
BCOMP	63
BCOMP	64
BELGAM	2
BVAL	3
BVAL	4
BVAL	5
DMSTRM	2
STREAM	2
STREAM	3
SHOCKS	7
BELGAM	8
BELGAM	9
BELGAM	10
BELGAM	11
BELGAM	12
BELGAM	13
BELGAM	14
BELGAM	15
BELGAM	16
BELGAM	17
BELGAM	18
BELGAM	19
BELGAM	20
BELGAM	21
BELGAM	22
BELGAM	23
BELGAM	24
BELGAM	25
BELGAM	26
BELGAM	27
BELGAM	28
BELGAM	29
BELGAM	30
BELGAM	31
BELGAM	32
BELGAM	33
BELGAM	34
BELGAM	35
BELGAM	36
BELGAM	37
BELGAM	38
BELGAM	39
BELGAM	40
BELGAM	41
BELGAM	42
BELGAM	43
BELGAM	44
BELGAM	45
BELGAM	46
BELGAM	47
BELGAM	48
BELGAM	49
BELGAM	50
BELGAM	51
BELGAM	52
BELGAM	53
BELGAM	54
BELGAM	55
BELGAM	56
BELGAM	57
BELGAM	58
BELGAM	59
BELGAM	60
BELGAM	61
BELGAM	62
BELGAM	63
BELGAM	64
BELGAM	65
BELGAM	66
BELGAM	67
BELGAM	68











APPENDIX B

```

N=NINUR(K)
XS(1)=XSTP(K,1)-J,2
YS(1)=YSTP(K,1)
DO 120 N=1,NN
  XS(N+1)=XSTR(K,N)
  YS(N+1)=YSTR(K,N)
120 CONTINUE
DO 130 N=1,NN
  CALL DUTLN(XS(N),YS(N),XS(N+1),YS(N+1),Z0,0)
130 CONTINUE
1310 CONTINUE
K1TORN
C
C (K=K) PERPENDICULAR FIELD LINES FOR MAGNETIC FIELD PLOT
C
1320 CONTINUE
  XS(1)=XBF(1,2)
  YS(1)=YBF(1,1)
  YS(1)=0
  YS(2)=0.4
  YS(12)=0.4
  NS=NRF(1,1)-7
  CALL DUTLN(XS(1),YS(1),XS(12),YS(12),Z0,0)
  DO 135 K=2,NB*2
  DO 170 J=1,NMAX
  IF (XSH(J) .LE. XDF(NS+1,K)) GO TO 170
  GO TO 130
170 CONTINUE
  J=NTMAX
180 CONTINUE
  P5H=YSHK(J=1)+XBF(NS+1,K)-YSHK(J=1)+(YSHK(J)-YSHK(J=1))
  /XSHK(J)-YSHK(J=1)
  DO 190 J=1,NT
  IF (XBF(J,K) .GT. RSM) GO TO 200
  YS(1)=XBF(J,K)
  YS(1)=YBF(J,K)
  YS(1)=XBF(J,K)
190 CONTINUE
  XSF(J)=XBF(NS+1,K)
  YS(J)=YBF(J,K)
  XSF(J)=XSF(J)
  YS(J)=YBF(J,K)
  XSF(J)=XBF(NS+1,K)
  YS(J)=YBF(J,K)
  N=NJ
200 CONTINUE
  DO 210 N=1,NN
  CALL DUTLN(XS(N),YS(N),XS(N+1),YS(N+1),Z0,0)
210 CONTINUE
  IF (NS .LT. K) RETURN
  NS=N+1+MOD(NB,2)
  NFR=INT(NB*(NS-1)/2)
  DO 220 K=NS,N*2
  DO 230 J=1,NT
  XS(J)=XBF(J,K)
  YS(J)=YBF(J,K)
  IF (XBF(J,1) .LE. K) GO TO 240
230 CONTINUE
  XSF(NN+1)=ZPLUT
  YS(NN+1)=YSTR(K,XS(NN+1)-XS(NN),YS(NN+1)+YS(NN)-1)
  /XS(NN)-XS(NN-1)
  DO 250 N=1,NN
  CALL DUTLN(XS(N),YS(N),XS(N+1),YS(N+1),Z0,0)
250 CONTINUE
220 CONTINUE
  RETURN
C
END
SUBROUTINE CONTOUR
SURFROUTINE CONTOUR CONTROLS CALCULATING AND PRINTING THE COUNTOURS
AND CREATING THE PLOTS
C
COMMON /BIN/ ANP,ANON,K8CON,B8CON,Z0
C
C LUCIL,Z,BANG,BPFP,OBDR,BRAG,BANG
C
C COMON /BCOMP3/ BKMTAL,Z0,0,0,0,0,0,0,0,0,0,0,0,0,0,0,0
C
C COMON /BCOMP4/ BKMTAL,Z0,0,0,0,0,0,0,0,0,0,0,0,0,0,0,0
C
C COMON /BCOMP5/ BKMTAL,Z0,0,0,0,0,0,0,0,0,0,0,0,0,0,0,0
C
C COMON /BVAL/ NB,MB,MBE,MBE,MBE,MBE
C
C COMON /BVAL1/ NB,F5,1,1,1,1,1,1,1,1,1,1,1,1,1,1,1,1,1,1,1,1,1
C
C COMON /CON1/ KCON,KCON(2),KCON,KCON(2),KCON,KCON(2),KCON,KCON(2)
C
C * VF(ZC,10,1),KMBF(ZC,10,1)
  CONTR 110
  CONTR 111
  CONTR 112
  CONTR 113
  CONTR 114
  CONTR 115
  CONTR 116
  CONTR 117
  CONTR 118
  CONTR 119
  CONTR 120
  CONTR 121
  CONTR 122
  CONTR 123
  CONTR 124
  CONTR 125
  CONTR 126
  CONTR 127
  CONTR 128
  CONTR 129
  CONTR 130
  CONTR 131
  CONTR 132
  CONTR 133
  CONTR 134
  CONTR 135
  CONTR 136
  CONTR 137
  CONTR 138
  CONTR 139
  CONTR 140
  CONTR 141
  CONTR 142
  CONTR 143
  CONTR 144
  CONTR 145
  CONTR 146
  CONTR 147
  CONTR 148
  CONTR 149
  CONTR 150
  CONTR 151
  CONTR 152
  CONTR 153
  CONTR 154
  CONTR 155
  CONTR 156
  CONTR 157
  CONTR 158
  CONTR 159
  CONTR 160
  CONTR 161
  CONTR 162
  CONTR 163
  CONTR 164
  CONTR 165
  CONTR 166
  CONTR 167
  CONTR 168
  CONTR 169
  CONTR 170
  CONTR 171
  CONTR 172
  CONTR 173
  CONTR 174
  CONTR 2
  CONTR 3
  CONTR 4
  CONTR 5
  CONTR 6
  CONTR 7
  CONTR 8
  CONTR 9
  CONTR 10
  CONTR 11
  CONTR 12
  CONTR 13
  CONTR 14
  CONTR 15
  CONTR 16
  CONTR 17
  CONTR 18
  CONTR 19
  CONTR 20
  CONTR 21
  CONTR 22
  CONTR 23
  CONTR 24
  CONTR 25
  CONTR 26
  CONTR 27
  CONTR 28
  CONTR 29
  CONTR 30
  CONTR 31
  CONTR 32
  CONTR 33
  CONTR 34
  CONTR 35
  CONTR 36
  CONTR 37
  CONTR 38
  CONTR 39
  CONTR 40
  CONTR 41
  CONTR 42
  CONTR 43
  CONTR 44
  CONTR 45
  CONTR 46
  CONTR 47
  CONTR 48
  CONTR 49
  CONTR 50
  CONTR 51
  CONTR 52
  CONTR 53
  CONTR 54
  CONTR 55
  CONTR 56
  CONTR 57
  CONTR 58
  CONTR 59
  CONTR 60
  CONTR 61
  CONTR 62
  CONTR 63
  CONTR 64
  CONTR 65
  CONTR 66
  CONTR 67
  CONTR 68
  CONTR 69
  CONTR 70
  CONTR 71
  CONTR 72
  CONTR 73
  CONTR 74
  CONTR 75
  CONTR 76
  DRDX 2
  DRDX 3
  DRDX 4
  DRDX 5
  DRDX 6
  DRDX 7
  DRDX 8
  DRDX 9
  DRDX 10
  DRDX 11
  DRDX 12
  DRDX 13
  DRDX 14
  DRDX 15
  DRDX 16
  DRDX 17
  DRDX 18
  DRDX 19
  FUNCTION DROX(X,R)
  THIS ROUTINE DETERMINES THE SLOPE OF THE FLOW ANGLE AT
  POINT (X,R) IN THE PLUNT BODY REGION
  COMMON /BOUND/ THETA(20),R(20,20)
  COMMON /BOUND1/ X0D(100),Y0D(100),XSHK(100),YSHK(100),NMKMAX,
  & NTHETA,AMACH,GAM,HD,MMINDX
  COMMON /DRD/ ANG(20,100),DTH(100),DRS(100),R1,JS,DEG
  DETERMINE RP AND THETA FROM R AND X
  THETA=GG*ATAN2(R,1-X)
  RPP=SORT((R1-X)*R**2+R**2)
  USE BIVARIATE LINEAR INTERPOLATION IN THETA THEN RP
  DO 3 J=JS,NTMETHA
  DRDX 2
  DRDX 3
  DRDX 4
  DRDX 5
  DRDX 6
  DRDX 7
  DRDX 8
  DRDX 9
  DRDX 10
  DRDX 11
  DRDX 12
  DRDX 13
  DRDX 14
  DRDX 15
  DRDX 16
  DRDX 17
  DRDX 18
  DRDX 19

```







```

COMPON/CONT/ KVCOM,VC(120),NRCON,VC(20),X(C(20),Y(C(20),Z(C(20))),Y(C(20),Z(C(20))),
* VFC(20,100),R(DF(20,100)),RPF(20,20)
COMMON /BLUNT/ THETA(20),RPF(20,20)
LEVEL 2, V*V*Y
COMMON /VGRIP/ VY(20,100),VY(20,100)
COMMON /ORP/ ANGLE(20,100),DT(100),RHS(100),RL,JA,DFG
COMMON /INSTHM/ ZBLDT,NGLUNT,NZENG,NZADD
COMMON /STRM/ V(150),X(150),P(150),NUM(150),NST
LEVEL 2, X(150),R(150),NST
DATA WZ0,100
C
C INPUT CYLINDRICAL VELOCITY COMPONENTS AND POLAR GRID POINTS
C
C
R1=0
DA=0.1015627
DA=0.1015627
FAC1=1/(AMAC+SQR(GAM))
THETA(1)=0
NTH=NTHTA
DC 2 J=2,NTP
THEJA(J)=DC*THETA(1)
DC 1 I=1,NMAX
VY(I,J)=EACV(I,J)
VY(I,J)=EACV(I,J)
VY(I,J)=505*(V(X(I,J))+2*V(Y(I,J)))*2
IF(DAS(V(Z(I,J))),C(50000)) GO TO 6
ANG(I,J)=V(Y(I,J)/V(X(I,J)))
GO TO 1
C
C SMOOTH RHC AND V ALONG CONSTANT-THETA LINES.
C
C
DO 3 J=2,NTP
CALL FLSOY(NMAX,J,R(I,J),WDF(I,J),WZ,SP,AR,IEI)
CALL FLSOY(NMAX,J,R(I,J),V(I,J),WZ,SP,AR,IEI)
DO 3 I=1,NMAX
XPR=RP(I,J)
RDEF(I,J)=((AR(4)*XPR+AR(3))*XPR+AR(2))*XPR+AR(1)
V(I,J)=((AR(4)*XPR+V(I,J))*XPR+V(I))
3 CONTINUE
C
C TRAJECTORY STREAMLINE CALCULATION
C
C
DA=AMINI(DRS(2)/2,,GOS)
J=2
NST=NTHTA-1
NLIM=X(NMAX,2)/DA*10.
J=JST+1
RS=YC(NMAX,J)
XS=XC(NMAX,J)
CXP=X(NMAX,2)*.02
XRT=X+D*FX
IF(JST.EQ.4) DA=AMINI(DRS(2)/2,,D*HKA)
DO 10 N=1,NLIM
X=XS
R=R5
C
C THIRD-ORDER MODIFIED EULER INTEGRATION PROCEDURE
C
C
DPX=OROX(XS,RS)
KS1=RS+DRX*DX
XS=XS+DX
SLOPE=.5*(URX+DKOX(XS,RS1))
RS=RS+SLOPE*DX
IF(N.EQ.1) GO TO 13
IF(XS.GT.XF) GO TO 11
IF(XS.LT.XMRT) GO TO 10
NN=NN+1
XXX(JST,NN)=XS
RRR(JST,NN)=RS
XVRT=XRT+D*HXX
GO TO 10
NN=1
XXX(JST,NN)=X
RRR(JST,NN)=R
10 CONTINUE
11 CONTINUE
13 NN=NN+1

```

```

TRANSF1 2
TRANSF1 3
TRANSF1 4
TRANSF1 5
TRANSF1 6
TRANSF1 12
DISTRM 12
FLOM8 13
FLOM8 14
FLOM8 15
FLOM8 16
FLOM8 17
FLOM8 18
FLOM8 19
FLOM8 20
FLOM8 21
FLOM8 22
FLOM8 23
FLOM8 24
FLOM8 25
FLOM8 26
FLOM8 27
FLOM8 28
FLOM8 29
FLOM8 30
FLOM8 31
FLOM8 32
FLOM8 33
FLOM8 34
FLOM8 35
FLOM8 36
FLOM8 37
FLOM8 38
FLOM8 39
FLOM8 40
FLOM8 41
FLOM8 42
FLOM8 43
FLOM8 44
FLOM8 45
FLOM8 46
FLOM8 47
FLOM8 48
FLOM8 49
FLOM8 50
FLOM8 51
FLOM8 52
FLOM8 53
FLOM8 54
FLOM8 55
FLOM8 56
FLOM8 57
FLOM8 58
FLOM8 59
FLOM8 60
FLOM8 61
FLOM8 62
FLOM8 63
FLOM8 64
FLOM8 65
FLOM8 66
FLOM8 67
FLOM8 68
FLOM8 69
FLOM8 70
FLOM8 71
FLOM8 72
FLOM8 73
TRANSF1 2
TRANSF1 3
TRANSF1 4
TRANSF1 5
TRANSF1 6
TRANSF1 12
DISTRM 12
FLOM8 13
FLOM8 14
FLOM8 15
FLOM8 16
FLOM8 17
FLOM8 18
FLOM8 19
FLOM8 20
FLOM8 21
FLOM8 22
FLOM8 23
FLOM8 24
FLOM8 25
FLOM8 26
FLOM8 27
FLOM8 28
FLOM8 29
FLOM8 30
FLOM8 31
FLOM8 32
FLOM8 33
FLOM8 34
FLOM8 35
FLOM8 36
FLOM8 37
FLOM8 38
FLOM8 39
FLOM8 40
FLOM8 41
FLOM8 42
FLOM8 43
FLOM8 44
FLOM8 45
FLOM8 46
FLOM8 47
FLOM8 48
FLOM8 49
FLOM8 50
FLOM8 51
FLOM8 52
FLOM8 53
FLOM8 54
FLOM8 55
FLOM8 56
FLOM8 57
FLOM8 58
FLOM8 59
FLOM8 60
FLOM8 61
FLOM8 62
FLOM8 63
FLOM8 64
FLOM8 65
FLOM8 66
FLOM8 67
FLOM8 68
FLOM8 69
FLOM8 70
FLOM8 71
FLOM8 72
FLOM8 73
TRANSF1 2
TRANSF1 3
TRANSF1 4
TRANSF1 5
TRANSF1 6
TRANSF1 12
DISTRM 12
FLOM8 13
FLOM8 14
FLOM8 15
FLOM8 16
FLOM8 17
FLOM8 18
FLOM8 19
FLOM8 20
FLOM8 21
FLOM8 22
FLOM8 23
FLOM8 24
FLOM8 25
FLOM8 26
FLOM8 27
FLOM8 28
FLOM8 29
FLOM8 30
FLOM8 31
FLOM8 32
FLOM8 33
FLOM8 34
FLOM8 35
FLOM8 36
FLOM8 37
FLOM8 38
FLOM8 39
FLOM8 40
FLOM8 41
FLOM8 42
FLOM8 43
FLOM8 44
FLOM8 45
FLOM8 46
FLOM8 47
FLOM8 48
FLOM8 49
FLOM8 50
FLOM8 51
FLOM8 52
FLOM8 53
FLOM8 54
FLOM8 55
FLOM8 56
FLOM8 57
FLOM8 58
FLOM8 59
FLOM8 60
FLOM8 61
FLOM8 62
FLOM8 63
FLOM8 64
FLOM8 65
FLOM8 66
FLOM8 67
FLOM8 68
FLOM8 69
FLOM8 70
FLOM8 71
FLOM8 72
FLOM8 73

```

```

74 FLOWM
75 FLOWM
76 FLOWM
77 FLOWM
78 FLOWM
79 FLOWM
80 FLOWM
81 FLOWM
82 FLOWM
83 FLOWM
84 FLOWM
85 FLOWM
86 FLOWM
87 FLOWM
88 FLOWM
89 FLOWM
90 FLOWM
91 FLOWM
92 FLOWM
93 FLOWM
94 FLOWM
95 FLOWM
96 FLOWM
97 FLOWM
98 FLOWM
99 FLOWM
100 FLOWM
101 FLOWM
102 FLOWM
103 FLOWM

C *****
C SUBROUTINE FLSQFY (N,NX,NY,NZ,NI,SI,SI,IER)
C
C PURPOSE
C   FLSQFY CONSTRUCTS A LEAST SQUARES POLYNOMIAL APPROXIMATION
C   OF SPECIFIED DEGREE TO A GIVEN SET OF DATA POINTS WITH
C   COLUMN WEIGHTS USING ORTHOGONAL POLYNOMIALS.
C
C USAGE
C   DIMENSION X(N),Y(N),Z(N),SI(NM1),SI(NM2)
C   CALL FLSQFY (N,NX,NY,NZ,NI,SI,SI,IER)
C
C INPUT PARAMETERS
C   N - NUMBER OF DATA POINTS
C   NX - DEGREE OF POLYNOMIAL DESIRED, N<=LT.M
C   NY - ARRAY OF INDEPENDENT VARIABLE
C   NZ - ARRAY OF DEPENDENT VARIABLE
C   NI - ARRAY OF POSITIVE WEIGHTS
C   NM1 - ROW DIMENSION OF SCRATCH ARRAY SI, NM1<=65.M
C   SI - SCRATCH ARRAY
C
C   IN THE COLUMN DEFINITIONS BELOW,
C   1 - REFERS TO POLYNOMIAL ORDER
C   COL J - REFERS TO ROW INDEXING WITHIN A COLUMN
C   COL 1 - POLYNOMIAL P(I-1), VALUE AT EACH X(I) I THRU 24
C   COL 2 - COEFFICIENT OF EACH X**(J-1) TERM AFTER 24
C   COL 3 - POLYNOMIAL P(I), SAME FORM AS COL 1.
C   COL 4 - ALPHA(I,1), WHERE I=J-1
C   COL 5 - S(I), WHERE I=J-1
C   COL 6 - SIGMA**2, WHERE I=J-1
C
C OUTPUT PARAMETERS
C   A - ARRAY OF COMPUTED COEFFICIENTS
C   ALL THRU A(N+1) CONTAIN COMPUTED POLYNOMIAL
C   COEFFICIENTS IN ORDER OF INCREASING DEGREE.
C   IER - ERROR INDICATOR
C     .EQ.0 SUCCESS
C     .EQ.1 (N<=65).OR.(N<=L.O)
C     .EQ.2 N*LT.M
C     .EQ.3 M*LT.L
C     .EQ.4 M*LT.L<O
C
C REFERENCE
C   FORSTNER, G. E., GENERATION AND USE OF ORTHOGONAL
C   POLYNOMIALS FOR DATA-FITTING WITH A DIGITAL COMPUTER,
C   J. SIAM, VOL. 5, NO. 2, (JUNE 1957) PP. 74-88.
C   NOTE - MOST NOTATION AND MOST LOCAL VARIABLE NAMES ARE
C   BASED ON THE REFERENCES, IE MPP IS M(I),I=1(I),P(I),
C   BUT M, WT AND W(I) REFER TO THE WEIGHTS ARRAY.
C *****
C DIMENSION X(I),Y(I),Z(I),SI(NM1),SI(NM2),A(I)
C
C *** INITIAL SET-UP ***
C IER = 0
C IF (N<=65).OR.(N<=L.O) IER=1
C IF (M*LT.M) IER=2
C IF (M*LT.L) IER=3

```

```

C *****
C THIRD ORDER MODIFIED EULER INTEGRATION PROCEDURE
C
C DO 10 A=1,NLIM
C   ORX=ORX(MIXS)
C   IF (IAS*DX .GT. XF) GO TO 11
C   RS=RS+URA*DX
C   XS=XS+DX
C   SLOPE=S*(URK+ORAMIXS+XSI1)
C   RS=RS+SLOPE*DX
C   IF (X<=L*WMT) GO TO 10
C   M=N*NN+1
C   XX(I,NN)=XS
C   RPL(I,NN)=RS
C   XRT=XRT+ORX
C 10 CONTINUE
C 11 CONTINUE
C
C SLOPE=S*(DRX+(XK-XS))
C SLOPE=S*(DRX+UKOXK(XK+RS1))
C PS=RS+SLOPE*(XK-XS)
C NN=NN+1
C XX(I,NN)=XK
C RPL(I,NN)=KS
C NUM(I)=NN
C 12 CONTINUE
C 13 RETURN
C 14 END

```

```

C *****
C SUBROUTINE FLSQFY (N,NX,NY,NZ,NI,SI,SI,IER)
C
C PURPOSE
C   FLSQFY CONSTRUCTS A LEAST SQUARES POLYNOMIAL APPROXIMATION
C   OF SPECIFIED DEGREE TO A GIVEN SET OF DATA POINTS WITH
C   COLUMN WEIGHTS USING ORTHOGONAL POLYNOMIALS.
C
C USAGE
C   DIMENSION X(N),Y(N),Z(N),SI(NM1),SI(NM2)
C   CALL FLSQFY (N,NX,NY,NZ,NI,SI,SI,IER)
C
C INPUT PARAMETERS
C   N - NUMBER OF DATA POINTS
C   NX - DEGREE OF POLYNOMIAL DESIRED, N<=LT.M
C   NY - ARRAY OF INDEPENDENT VARIABLE
C   NZ - ARRAY OF DEPENDENT VARIABLE
C   NI - ARRAY OF POSITIVE WEIGHTS
C   NM1 - ROW DIMENSION OF SCRATCH ARRAY SI, NM1<=65.M
C   SI - SCRATCH ARRAY
C
C   IN THE COLUMN DEFINITIONS BELOW,
C   1 - REFERS TO POLYNOMIAL ORDER
C   COL J - REFERS TO ROW INDEXING WITHIN A COLUMN
C   COL 1 - POLYNOMIAL P(I-1), VALUE AT EACH X(I) I THRU 24
C   COL 2 - COEFFICIENT OF EACH X**(J-1) TERM AFTER 24
C   COL 3 - POLYNOMIAL P(I), SAME FORM AS COL 1.
C   COL 4 - ALPHA(I,1), WHERE I=J-1
C   COL 5 - S(I), WHERE I=J-1
C   COL 6 - SIGMA**2, WHERE I=J-1
C
C OUTPUT PARAMETERS
C   A - ARRAY OF COMPUTED COEFFICIENTS
C   ALL THRU A(N+1) CONTAIN COMPUTED POLYNOMIAL
C   COEFFICIENTS IN ORDER OF INCREASING DEGREE.
C   IER - ERROR INDICATOR
C     .EQ.0 SUCCESS
C     .EQ.1 (N<=65).OR.(N<=L.O)
C     .EQ.2 N*LT.M
C     .EQ.3 M*LT.L
C     .EQ.4 M*LT.L<O
C
C REFERENCE
C   FORSTNER, G. E., GENERATION AND USE OF ORTHOGONAL
C   POLYNOMIALS FOR DATA-FITTING WITH A DIGITAL COMPUTER,
C   J. SIAM, VOL. 5, NO. 2, (JUNE 1957) PP. 74-88.
C   NOTE - MOST NOTATION AND MOST LOCAL VARIABLE NAMES ARE
C   BASED ON THE REFERENCES, IE MPP IS M(I),I=1(I),P(I),
C   BUT M, WT AND W(I) REFER TO THE WEIGHTS ARRAY.
C *****
C DIMENSION X(I),Y(I),Z(I),SI(NM1),SI(NM2),A(I)
C
C *** INITIAL SET-UP ***
C IER = 0
C IF (N<=65).OR.(N<=L.O) IER=1
C IF (M*LT.M) IER=2
C IF (M*LT.L) IER=3

```

```

C *****
C SUBROUTINE FLSQFY (N,NX,NY,NZ,NI,SI,SI,IER)
C
C PURPOSE
C   FLSQFY CONSTRUCTS A LEAST SQUARES POLYNOMIAL APPROXIMATION
C   OF SPECIFIED DEGREE TO A GIVEN SET OF DATA POINTS WITH
C   COLUMN WEIGHTS USING ORTHOGONAL POLYNOMIALS.
C
C USAGE
C   DIMENSION X(N),Y(N),Z(N),SI(NM1),SI(NM2)
C   CALL FLSQFY (N,NX,NY,NZ,NI,SI,SI,IER)
C
C INPUT PARAMETERS
C   N - NUMBER OF DATA POINTS
C   NX - DEGREE OF POLYNOMIAL DESIRED, N<=LT.M
C   NY - ARRAY OF INDEPENDENT VARIABLE
C   NZ - ARRAY OF DEPENDENT VARIABLE
C   NI - ARRAY OF POSITIVE WEIGHTS
C   NM1 - ROW DIMENSION OF SCRATCH ARRAY SI, NM1<=65.M
C   SI - SCRATCH ARRAY
C
C   IN THE COLUMN DEFINITIONS BELOW,
C   1 - REFERS TO POLYNOMIAL ORDER
C   COL J - REFERS TO ROW INDEXING WITHIN A COLUMN
C   COL 1 - POLYNOMIAL P(I-1), VALUE AT EACH X(I) I THRU 24
C   COL 2 - COEFFICIENT OF EACH X**(J-1) TERM AFTER 24
C   COL 3 - POLYNOMIAL P(I), SAME FORM AS COL 1.
C   COL 4 - ALPHA(I,1), WHERE I=J-1
C   COL 5 - S(I), WHERE I=J-1
C   COL 6 - SIGMA**2, WHERE I=J-1
C
C OUTPUT PARAMETERS
C   A - ARRAY OF COMPUTED COEFFICIENTS
C   ALL THRU A(N+1) CONTAIN COMPUTED POLYNOMIAL
C   COEFFICIENTS IN ORDER OF INCREASING DEGREE.
C   IER - ERROR INDICATOR
C     .EQ.0 SUCCESS
C     .EQ.1 (N<=65).OR.(N<=L.O)
C     .EQ.2 N*LT.M
C     .EQ.3 M*LT.L
C     .EQ.4 M*LT.L<O
C
C REFERENCE
C   FORSTNER, G. E., GENERATION AND USE OF ORTHOGONAL
C   POLYNOMIALS FOR DATA-FITTING WITH A DIGITAL COMPUTER,
C   J. SIAM, VOL. 5, NO. 2, (JUNE 1957) PP. 74-88.
C   NOTE - MOST NOTATION AND MOST LOCAL VARIABLE NAMES ARE
C   BASED ON THE REFERENCES, IE MPP IS M(I),I=1(I),P(I),
C   BUT M, WT AND W(I) REFER TO THE WEIGHTS ARRAY.
C *****
C DIMENSION X(I),Y(I),Z(I),SI(NM1),SI(NM2),A(I)
C
C *** INITIAL SET-UP ***
C IER = 0
C IF (N<=65).OR.(N<=L.O) IER=1
C IF (M*LT.M) IER=2
C IF (M*LT.L) IER=3

```

```

C *****
C SUBROUTINE FLSQFY (N,NX,NY,NZ,NI,SI,SI,IER)
C
C PURPOSE
C   FLSQFY CONSTRUCTS A LEAST SQUARES POLYNOMIAL APPROXIMATION
C   OF SPECIFIED DEGREE TO A GIVEN SET OF DATA POINTS WITH
C   COLUMN WEIGHTS USING ORTHOGONAL POLYNOMIALS.
C
C USAGE
C   DIMENSION X(N),Y(N),Z(N),SI(NM1),SI(NM2)
C   CALL FLSQFY (N,NX,NY,NZ,NI,SI,SI,IER)
C
C INPUT PARAMETERS
C   N - NUMBER OF DATA POINTS
C   NX - DEGREE OF POLYNOMIAL DESIRED, N<=LT.M
C   NY - ARRAY OF INDEPENDENT VARIABLE
C   NZ - ARRAY OF DEPENDENT VARIABLE
C   NI - ARRAY OF POSITIVE WEIGHTS
C   NM1 - ROW DIMENSION OF SCRATCH ARRAY SI, NM1<=65.M
C   SI - SCRATCH ARRAY
C
C   IN THE COLUMN DEFINITIONS BELOW,
C   1 - REFERS TO POLYNOMIAL ORDER
C   COL J - REFERS TO ROW INDEXING WITHIN A COLUMN
C   COL 1 - POLYNOMIAL P(I-1), VALUE AT EACH X(I) I THRU 24
C   COL 2 - COEFFICIENT OF EACH X**(J-1) TERM AFTER 24
C   COL 3 - POLYNOMIAL P(I), SAME FORM AS COL 1.
C   COL 4 - ALPHA(I,1), WHERE I=J-1
C   COL 5 - S(I), WHERE I=J-1
C   COL 6 - SIGMA**2, WHERE I=J-1
C
C OUTPUT PARAMETERS
C   A - ARRAY OF COMPUTED COEFFICIENTS
C   ALL THRU A(N+1) CONTAIN COMPUTED POLYNOMIAL
C   COEFFICIENTS IN ORDER OF INCREASING DEGREE.
C   IER - ERROR INDICATOR
C     .EQ.0 SUCCESS
C     .EQ.1 (N<=65).OR.(N<=L.O)
C     .EQ.2 N*LT.M
C     .EQ.3 M*LT.L
C     .EQ.4 M*LT.L<O
C
C REFERENCE
C   FORSTNER, G. E., GENERATION AND USE OF ORTHOGONAL
C   POLYNOMIALS FOR DATA-FITTING WITH A DIGITAL COMPUTER,
C   J. SIAM, VOL. 5, NO. 2, (JUNE 1957) PP. 74-88.
C   NOTE - MOST NOTATION AND MOST LOCAL VARIABLE NAMES ARE
C   BASED ON THE REFERENCES, IE MPP IS M(I),I=1(I),P(I),
C   BUT M, WT AND W(I) REFER TO THE WEIGHTS ARRAY.
C *****
C DIMENSION X(I),Y(I),Z(I),SI(NM1),SI(NM2),A(I)
C
C *** INITIAL SET-UP ***
C IER = 0
C IF (N<=65).OR.(N<=L.O) IER=1
C IF (M*LT.M) IER=2
C IF (M*LT.L) IER=3

```







```

36 MAP 188 C KOD5=1 GO TO 41
MAP 189 TO 29 NVAL=NMIN,NMAX
MAP 190 VAL=ACON(I,NVAL)
MAP 191 GO TO (37,20),KOD5
MAP 192 IF (VAL,LT,AL) GO TO 29
MAP 193 KOD5=2
MAP 194 IF (VAL,GT,AL) GO TO 2C
MAP 195
MAP 196 CHECK TO SEE IF THE CONTOUR LINE POINT JUST FOUND IS A
MAP 197 NEW LINE, OR THE TRAIL END OF ONE ALREADY FOUND.
MAP 198 IF (KOD5,EG,2) GO TO 29
MAP 199
MAP 200 DLT=NMIN,AL AND 22
MAP 201 IF (KOD7,EG,1),OK,KOD7,EG,4) GO TO 32
MAP 202 A2=AA
MAP 203 A3=AB
MAP 204 GO TO 33
MAP 205 A2=AB
MAP 206 A1=AA
MAP 207
MAP 208 ENT: P IN TH. TABLES TH. POINT JUST FOUND.
MAP 209 NOUN=NAD(I)+1
MAP 210 IF (NOUN,GT,ISIZ2) GO TO 35
MAP 211 NAD(I)=NOUN
MAP 212 CALL ENTER(KUD2,J,K,NVAL,A1,A2,JMIN,KMIN,ICHK,KOD4,X,Y,NXY,ACONT,
MAP 213 L,I,IZ2)
MAP 214 IF (KOD4,IC,2) GO TO 70
MAP 215 NAD(INDEX)=NXY
MAP 216
MAP 217
MAP 218
MAP 219
MAP 220
MAP 221
MAP 222
MAP 223
MAP 224
MAP 225
MAP 226
MAP 227
MAP 228
MAP 229
MAP 230
MAP 231
MAP 232
MAP 233
MAP 234
MAP 235
MAP 236
MAP 237
MAP 238
MAP 239
MAP 240
MAP 241
MAP 242
MAP 243
MAP 244
MAP 245
MAP 246
MAP 247
MAP 248
MAP 249
MAP 250
MAP 251
MAP 252
MAP 253
MAP 254
MAP 255
MAP 256
MAP 257
MAP 258
MAP 259
MAP 260
MAP 261
MAP 262
MAP 263
MAP 264
MAP 265
MAP 266
MAP 267
MAP 268
MAP 269
MAP 270
MAP 271
MAP 272
MAP 273
MAP 274
MAP 275
MAP 276
MAP 277
MAP 278
MAP 279
MAP 280
MAP 281
MAP 282
MAP 283
MAP 284
MAP 285
MAP 286
MAP 287
MAP 288
MAP 289
MAP 290
MAP 291
MAP 292
MAP 293
MAP 294
MAP 295
MAP 296
MAP 297
MAP 298
MAP 299
MAP 300
MAP 301
MAP 302
MAP 303
MAP 304
MAP 305
MAP 306
MAP 307
MAP 308
MAP 309
MAP 310
MAP 311
MAP 312
MAP 313
MAP 314
MAP 315
MAP 316
MAP 317
MAP 318
MAP 319
MAP 320
MAP 321
MAP 322
MAP 323
MAP 324
MAP 325
MAP 326
MAP 327
MAP 328
MAP 329
MAP 330
MAP 331
MAP 332
MAP 333
MAP 334
MAP 335
MAP 336
MAP 337
MAP 338
MAP 339
MAP 340
MAP 341
MAP 342
MAP 343
MAP 344
MAP 345
MAP 346
MAP 347
MAP 348
MAP 349
MAP 350
MAP 351
MAP 352
MAP 353
MAP 354
MAP 355
MAP 356
MAP 357
MAP 358
MAP 359
MAP 360
MAP 361
MAP 362
MAP 363
MAP 364
MAP 365
MAP 366
MAP 367
MAP 368
MAP 369
MAP 370
MAP 371
MAP 372
MAP 373
MAP 374
MAP 375
MAP 376
MAP 377
MAP 378
MAP 379
MAP 380
MAP 381
MAP 382
MAP 383
MAP 384
MAP 385
MAP 386
MAP 387
MAP 388
MAP 389
MAP 390
MAP 391
MAP 392
MAP 393
MAP 394
MAP 395
MAP 396
MAP 397
MAP 398
MAP 399
MAP 400
MAP 401
MAP 402
MAP 403
MAP 404
MAP 405
MAP 406
MAP 407
MAP 408
MAP 409
MAP 410
MAP 411
MAP 412
MAP 413
MAP 414
MAP 415
MAP 416
MAP 417
MAP 418
MAP 419
MAP 420
MAP 421
MAP 422
MAP 423
MAP 424
MAP 425
MAP 426
MAP 427
MAP 428
MAP 429
MAP 430
MAP 431
MAP 432
MAP 433
MAP 434
MAP 435
MAP 436
MAP 437
MAP 438
MAP 439
MAP 440
MAP 441
MAP 442
MAP 443
MAP 444
MAP 445
MAP 446
MAP 447
MAP 448
MAP 449
MAP 450
MAP 451
MAP 452
MAP 453
MAP 454
MAP 455
MAP 456
MAP 457
MAP 458
MAP 459
MAP 460
MAP 461
MAP 462
MAP 463
MAP 464
MAP 465
MAP 466
MAP 467
MAP 468
MAP 469
MAP 470
MAP 471
MAP 472
MAP 473
MAP 474
MAP 475
MAP 476
MAP 477
MAP 478
MAP 479
MAP 480
MAP 481
MAP 482
MAP 483
MAP 484
MAP 485
MAP 486
MAP 487
MAP 488
MAP 489
MAP 490
MAP 491
MAP 492
MAP 493
MAP 494
MAP 495
MAP 496
MAP 497
MAP 498
MAP 499
MAP 500
MAP 501
MAP 502
MAP 503
MAP 504
MAP 505
MAP 506
MAP 507
MAP 508
MAP 509
MAP 510
MAP 511
MAP 512
MAP 513
MAP 514
MAP 515
MAP 516
MAP 517
MAP 518
MAP 519
MAP 520
MAP 521
MAP 522
MAP 523
MAP 524
MAP 525
MAP 526
MAP 527
MAP 528
MAP 529
MAP 530
MAP 531
MAP 532
MAP 533
MAP 534
MAP 535
MAP 536
MAP 537
MAP 538
MAP 539
MAP 540
MAP 541
MAP 542
MAP 543
MAP 544
MAP 545
MAP 546
MAP 547
MAP 548
MAP 549
MAP 550
MAP 551
MAP 552
MAP 553
MAP 554
MAP 555
MAP 556
MAP 557
MAP 558
MAP 559
MAP 560
MAP 561
MAP 562
MAP 563
MAP 564
MAP 565
MAP 566
MAP 567
MAP 568
MAP 569
MAP 570
MAP 571
MAP 572
MAP 573
MAP 574
MAP 575
MAP 576
MAP 577
MAP 578
MAP 579
MAP 580
MAP 581
MAP 582
MAP 583
MAP 584
MAP 585
MAP 586
MAP 587
MAP 588
MAP 589
MAP 590
MAP 591
MAP 592
MAP 593
MAP 594
MAP 595
MAP 596
MAP 597
MAP 598
MAP 599
MAP 600
MAP 601
MAP 602
MAP 603
MAP 604
MAP 605
MAP 606
MAP 607
MAP 608
MAP 609
MAP 610
MAP 611
MAP 612
MAP 613
MAP 614
MAP 615
MAP 616
MAP 617
MAP 618
MAP 619
MAP 620
MAP 621
MAP 622
MAP 623
MAP 624
MAP 625
MAP 626
MAP 627
MAP 628
MAP 629
MAP 630
MAP 631
MAP 632
MAP 633
MAP 634
MAP 635
MAP 636
MAP 637
MAP 638
MAP 639
MAP 640
MAP 641
MAP 642
MAP 643
MAP 644
MAP 645
MAP 646
MAP 647
MAP 648
MAP 649
MAP 650
MAP 651
MAP 652
MAP 653
MAP 654
MAP 655
MAP 656
MAP 657
MAP 658
MAP 659
MAP 660
MAP 661
MAP 662
MAP 663
MAP 664
MAP 665
MAP 666
MAP 667
MAP 668
MAP 669
MAP 670
MAP 671
MAP 672
MAP 673
MAP 674
MAP 675
MAP 676
MAP 677
MAP 678
MAP 679
MAP 680
MAP 681
MAP 682
MAP 683
MAP 684
MAP 685
MAP 686
MAP 687
MAP 688
MAP 689
MAP 690
MAP 691
MAP 692
MAP 693
MAP 694
MAP 695
MAP 696
MAP 697
MAP 698
MAP 699
MAP 700
MAP 701
MAP 702
MAP 703
MAP 704
MAP 705
MAP 706
MAP 707
MAP 708
MAP 709
MAP 710
MAP 711
MAP 712
MAP 713
MAP 714
MAP 715
MAP 716
MAP 717
MAP 718
MAP 719
MAP 720
MAP 721
MAP 722
MAP 723
MAP 724
MAP 725
MAP 726
MAP 727
MAP 728
MAP 729
MAP 730
MAP 731
MAP 732
MAP 733
MAP 734
MAP 735
MAP 736
MAP 737
MAP 738
MAP 739
MAP 740
MAP 741
MAP 742
MAP 743
MAP 744
MAP 745
MAP 746
MAP 747
MAP 748
MAP 749
MAP 750
MAP 751
MAP 752
MAP 753
MAP 754
MAP 755
MAP 756
MAP 757
MAP 758
MAP 759
MAP 760
MAP 761
MAP 762
MAP 763
MAP 764
MAP 765
MAP 766
MAP 767
MAP 768
MAP 769
MAP 770
MAP 771
MAP 772
MAP 773
MAP 774
MAP 775
MAP 776
MAP 777
MAP 778
MAP 779
MAP 780
MAP 781
MAP 782
MAP 783
MAP 784
MAP 785
MAP 786
MAP 787
MAP 788
MAP 789
MAP 790
MAP 791
MAP 792
MAP 793
MAP 794
MAP 795
MAP 796
MAP 797
MAP 798
MAP 799
MAP 800
MAP 801
MAP 802
MAP 803
MAP 804
MAP 805
MAP 806
MAP 807
MAP 808
MAP 809
MAP 810
MAP 811
MAP 812
MAP 813
MAP 814
MAP 815
MAP 816
MAP 817
MAP 818
MAP 819
MAP 820
MAP 821
MAP 822
MAP 823
MAP 824
MAP 825
MAP 826
MAP 827
MAP 828
MAP 829
MAP 830
MAP 831
MAP 832
MAP 833
MAP 834
MAP 835
MAP 836
MAP 837
MAP 838
MAP 839
MAP 840
MAP 841
MAP 842
MAP 843
MAP 844
MAP 845
MAP 846
MAP 847
MAP 848
MAP 849
MAP 850
MAP 851
MAP 852
MAP 853
MAP 854
MAP 855
MAP 856
MAP 857
MAP 858
MAP 859
MAP 860
MAP 861
MAP 862
MAP 863
MAP 864
MAP 865
MAP 866
MAP 867
MAP 868
MAP 869
MAP 870
MAP 871
MAP 872
MAP 873
MAP 874
MAP 875
MAP 876
MAP 877
MAP 878
MAP 879
MAP 880
MAP 881
MAP 882
MAP 883
MAP 884
MAP 885
MAP 886
MAP 887
MAP 888
MAP 889
MAP 890
MAP 891
MAP 892
MAP 893
MAP 894
MAP 895
MAP 896
MAP 897
MAP 898
MAP 899
MAP 900
MAP 901
MAP 902
MAP 903
MAP 904
MAP 905
MAP 906
MAP 907
MAP 908
MAP 909
MAP 910
MAP 911
MAP 912
MAP 913
MAP 914
MAP 915
MAP 916
MAP 917
MAP 918
MAP 919
MAP 920
MAP 921
MAP 922
MAP 923
MAP 924
MAP 925
MAP 926
MAP 927
MAP 928
MAP 929
MAP 930
MAP 931
MAP 932
MAP 933
MAP 934
MAP 935
MAP 936
MAP 937
MAP 938
MAP 939
MAP 940
MAP 941
MAP 942
MAP 943
MAP 944
MAP 945
MAP 946
MAP 947
MAP 948
MAP 949
MAP 950
MAP 951
MAP 952
MAP 953
MAP 954
MAP 955
MAP 956
MAP 957
MAP 958
MAP 959
MAP 960
MAP 961
MAP 962
MAP 963
MAP 964
MAP 965
MAP 966
MAP 967
MAP 968
MAP 969
MAP 970
MAP 971
MAP 972
MAP 973
MAP 974
MAP 975
MAP 976
MAP 977
MAP 978
MAP 979
MAP 980
MAP 981
MAP 982
MAP 983
MAP 984
MAP 985
MAP 986
MAP 987
MAP 988
MAP 989
MAP 990
MAP 991
MAP 992
MAP 993
MAP 994
MAP 995
MAP 996
MAP 997
MAP 998
MAP 999
MAP 1000

```

```

PLOTCH 2
PLOTCH 3
PLOTCH 4
PLOTCH 5
PLOTCH 6
PLOTCH 7
PLOTCH 8
PLOTCH 9
PLOTCH 10
PLOTCH 11
PLOTCH 12
PLOTCH 13
PLOTCH 14
PLOTCH 15
PLOTCH 16
SCALE 17
PLOTCH 18
PLOTCH 19
PLOTCH 20
PLOTCH 21
PLOTCH 22

```

```

C SURROUTINE SETUP ESTABLISHES PERMANENT PLOT ORIGIN
C DRAWS AXES, LABELS, AND TITLE
C SUPPLIES ROUND DRAWS AND LABELS STOCK WAY, PLANET,
C AND MAGNETOSPHERE (LBODY=J) UP LONGSPHERE
C (LBODY=1) BOUNDARY
C
C IF (PLPLOT=3) GO TO 14
CALL DASH(1,2,3,4,5,6,7,8,9,10)
CALL PLOT(1,2,3,4,5,6,7,8,9,10)
CALL SETUP(1,2,3,4,5,6,7,8,9,10)
CALL ROUND(1,2,3,4,5,6,7,8,9,10)
CALL CONT(1,2,3,4,5,6,7,8,9,10)
CALL SPLIT(LMAX,UBJ)
RETURN
C
C DRAW CONTOUR PLOTS
C CONTINUE
CALL PLOT(1,2,3,4,5,6,7,8,9,10)
CALL SETUP(1,2,3,4,5,6,7,8,9,10)
CALL ROUND(1,2,3,4,5,6,7,8,9,10)
CALL CONT(1,2,3,4,5,6,7,8,9,10)
CALL SPLIT(LMAX,UBJ)
RETURN
C
C CHANGE VELOCITY CONTOUR VALUES TO TEMPERATURE
C CONTINUE
C 20 I=1,4
FACT=100*(I-1)*PI/180
MPL=MAX(1, I)
DO 21 I=1,4
CONTINUE
GO TO 10
END
C
FUNCTION QUAD I,R,Y,T,XAP,YP
C THIS FUNCTION PERFORMS A GENERALIZED QUADRILATERAL INTERPOLATION
C GIVEN THE COORDINATES OF THE VERTICES, THE VALUES OF THE FUNCTION
C AT THOSE POINTS, AND THE COORDINATES OF THE POINT AT WHICH A
C VALUE OF THE FUNCTION IS DESIRED. (XAP,YP)
C X AND Y ARE THE DOMINANT ARRAYS AND F IS THE FUNCTION ARRAY
C DIMENSION X(4),Y(4),F(4)
S1=4-XAP*(X(1)+X(2)+X(3)+X(4))
S2=X(1)+X(2)+X(3)+X(4)
S3=X(1)+X(2)+X(3)+X(4)
S4=X(1)+X(2)+X(3)+X(4)
T1=4-Y*(Y(1)+Y(2)+Y(3)+Y(4))
T2=Y(1)+Y(2)+Y(3)+Y(4)
T3=Y(1)+Y(2)+Y(3)+Y(4)
T4=Y(1)+Y(2)+Y(3)+Y(4)
A=S2*B1-S3*B2
B=S1*B3-S2*B4
C=S1*B5-S4*B1
ETA=(B*B1/A)+C
IF (ABS(ETA) .GT. 1.0) ETA=ETA/DVA
X1=(S1+ETA*S2)/1.5+ETA*S3
QUAD=0.25*(F(1)+(1+ETA)*F(2)+(1+ETA)*F(4)+(1+ETA)*F(1)+C-X1)
RETURN
END
SUBROUTINE REKUN
COMMON /CONT/,KVCON,VCON(25),KRCOIN,PCOIN(20),XC(20,100),YC(20,100),
*VF(20,100),RHOJ(20,100)
COMMON /BLUNT/ THETA(25),RP(20,25)
LEVEL=2,VR,VY
COMMON /BOUND/ VAI(2,2),VBI(2,2),VCI(2,2)
COMMON /DNSTRM/ ZPLOI,NBLUNT,ZNEND,NZADD
COMMON /NUROD/ X(100),Y(100),NUROD
COMMON /BIN/ ANGP,ANGN,KBCON,PCOIN(20)
COMMON /BIN/ ANGP,ANGN,KBCON,PCOIN(20)
COMMON /PROPT/ LRURUN,LPRFL,LPRST,LPRCON,LPRBL,PLOT
COMMON /SHOCKS/ DRSDX(100),DST(50)
SUBPOTLINE READS DATA FROM TAP4 (WRITTEN TO TAP5 ON
DIFFERENT COUNTOUR VALUES), PLOT SIZE, AND/OR MAGNETIC FIELD
ANGLE. WITHOUT RECALCULATING THE CALCULATION OF THE VELOCITY
AND DENSITY FIELDS.
PEAR(1)=NBLUNT,NRMAX,AMAC*16,AMG*16,MDA
IF (ABS(GPAC+GAC*14)+ST*1.1) GO TO 10
IF (ABS(GAC+GAC*14)+ST*1.1) GO TO 10
IF (HKC*ALT*1.1) AND (AR0*1.1) JAGGO TO 2
IF (ABS(PLU-m*0.1) .GT. 1.1) GO TO 100
NZMAG=NBLUNT
GO TO 3
2 READ(4) NBLUN,IXX(1),IK(1),I=1,NBLUN
3 CONTINUE
C PRINT INPUT DATA
C
C SPLIT (L,UBJ) AMAC+1,GAN
4 WRITE(6,24) NBLUN,IXX(1),IK(1),I=1,NBLUN
GO TO 5
5 READ(4,21)
6 WRITE(6,21) MRO
9 CONTINUE
XPLOT=/PLOT
WRITE(6,23) XPLOT,ANGP,ANGN
WRITE(6,24) LKCON,LPKFL,LPST,LPCON,LPRL,PLOT
WRITE(6,24) KVCON
IF (KVCON .GT. 0)
WRITE(6,24) KCON WRITE(6,25) (VCUN(I),I=1,KVCON)
IF (KRCOIN .GT. 0)
WRITE(6,24) KBCON WRITE(6,25) (KCON(I),I=1,KBCON)
IF (KBCON .GT. 0)
WRITE(6,25) (BCON(I),I=1,KBCON)
210 FORMAT(//10X,'RHS STREAM MACH NO. ',E6.2
//10X,'SPECIAL CASE MACH NO. ',E6.2
//10X,'SUBJECTICLE GEOMETRY USED SUPPLIED COORDINATES --',
16,74,PUNTS(1:33),3HX(7:11),3HX(7:1)
//10X,'V=1, F=6.4')
216 FORMAT(//10X,'OBSTACLE GEOMETRY: DEFAULT MAGNETIC COORDINATE',
21MS = EQUATORIAL TRACE)
218 FORMAT(//10X,'OBSTACLE GEOMETRY: DEFAULT (UNPAUSE COORDINATE',
10H FOR 4/80, F4.2)
219 FORMAT(//10X,'MIN-PLANE DEVIATION OF MAGNETIC FIELD FROM FLOW ',
F7.2,PD4,DEGREES)
//10X,'MIN-PLANE DEVIATION OF MAGNETIC FIELD FROM FLOW ',
F7.2,PD4,DEGREES)
223 FORMAT(//10X,'HLENUR =L2//20,HLPRFL =L2//20,HLPKST =L2,
//10X,'HLPCON =L2//20,HLPRB =L2//20,HLPLUT =L2)
224 FORMAT(//10X,'HLENUR =L2//20,HLPRFL =L2//20,HLPKST =L2,
//10X,'HLPCON =L2//20,HLPRB =L2//20,HLPLUT =L2)
225 FORMAT(//10X,'CONTOUR LEVELS SPECIFIED FOR CONTOUR CALCULATION/
5X,40(IH*)')
226 FORMAT(//10X,'1-2-29H CONTOUR LEVELS FOR VLOCITY)')
227 FORMAT(//10X,'1-2-29H CONTOUR LEVELS FOR DENSITY)')
228 FORMAT(//10X,'1-2-29H CONTOUR LEVELS FOR MAGNETIC FIELD STRENGTH)')
230 FORMAT(//10X,'1-2-29H CONTOUR LEVELS FOR MAGNETIC FIELD STRENGTH)')
READ DATA GENERATED BY BLUNT JUDY CODE
DO 10 J=1,NBLUNT
JB=J+1
READ(4) J,THETA(J),DRSDX(JB)
DO 10 I=1,NBLUN
READ(4) I,XC(I),YC(I),RPL,JBI,YC(I),RPL,I,JBI,VAI(I,JBI),VBI(I,JBI),VCI(I,JBI)
CALL FLOWB
C
C READ DATA GENERATED BY MARCHEING CODE
NZADD=C
NZI=NBLUNT*1
DO 20 J=NZL,100
DO 20 I=NZL,100
READ(4) J,I,ZDRSDX(I,J)
IF (INT(DEF(5))) .NE. 0) GO TO 30
IF (Z .GT. ZPLOI) AND (NZADD .GT. 0) GO TO 33
NZADD=NZADD+1
DU 20 I=1,NBLUN
PEAR(4) I,YC(I),VAI(I,J),VBI(I,J),VCI(I,J),RHOJ(I,J)
XC(I),Y(J)
20 CONTINUE

```

```

30 CONTINUE
NZ=IND-NZADD
CALL FLGNR
RETURN
C PRINT LKRM MESSAGE IF TAPE4 IS NOT THE SAME CASE AS
C SPECIFIED IN CARD INPUT - PROGRAM IS STOPPED
C
100 WK1=1;WK2=2;WK3=3;WK4=4;WK5=5;WK6=6;WK7=7;WK8=8;
1100 FORMAT(10I10,19X,5(11X),2X,20M5,EXECUTION TERMINATED 23,5(11X),1/20X,
* 34HR1, RUN DATA UN TAPE4 DOES NOT AGREE WITH CASE
* 24M5,CYCLES UN CARD INPUT //23M5,FMACH NO,3X,5M5,MA,5X,
* 4M5//12M5,ICHRUM CAPD,3(14X,F10.4)/12M5,IOMHPRUM TAPE4,
* 3(XM5,F10.4))
STOP
END

```

```

FUNCTION RINF(I,J)
C THIS ROUTINE CALCULATES R/INF AT THE (I,J) GRID POINT
C
COMMON/EQUUD/ XBD0(100),ASHK(100),YSHK(100),XMKMAX,
1 COMMON/UMNT/ NCMX,AMAC,GM,HRU,MINDR
* VFZC,1EG,KAUF(20,100)
LEVEL 2, ASIP,ST,NUM,NST
COMMON /STREAM/ RST(50,250),RST1(50,250),NUM(50),NST
C IF POINT IS ON SHOULDER BOUNDARY R/INF=1.0
C IF (I.EI).AND.(J.EQ. J *GT. 1) GO TO 10
RINF=1.0
RETURN
C
C
10 CONTINUE
X=XCL(I,J)
Y=YCL(I,J)
Z=ZSU
GO TO JST,NST
N=NUM(JST)
OU SC R=PMN
IF (KST1(J),K) *GT. X) GO TO 4
30 CONTINUE
40 CONTINUE
J2=JST
I=JST-1
IF (K.EG. 1) R2=NST(J2,1)
IF (K.EG. 2) R2=NST(J2,K-1)+XN51(J2,K-1)+R3(J2,K)
* RST(J2,K-1)/RST(J2,K)-RST(J2,K-1)
20 CONTINUE
IF (R2 *GT. Y) GO TO 60
60 IF (R2.EG. 1) GO TO 100
C INTERPOLATE FOR R/INF
RINF=RST(J,1)
RINF2=RST(J,2)
RINFY=(RINF+RINF2-RINF1)*(Y-R1)/(R2-R1)
RETURN
C
C USE SYMMETRY AXIS AND BODY FOR ZERO-TH STREAMLINE
C
100 CONTINUE
IF (X.EG. -1.0) GO TO 110
RINF=1.0+Y/4*(R2/RST(1,1))-1.0
RETURN
110 GO TO 120
120 K=2-NMAX
IF (X.EG. XCL(1,K)) GO TO 130
130 K1=YCL(1,K)* (1-XC(1,K-1))/(YC(1,K)-YC(1,K-1))/ (XC(1,K)-XC(1,K-1))
RINF=0.0
GO TO 70
END
SUBROUTINE SEARCH(J,K,K02,MAP,JDIR,ICM,NXY,K0D3,NVAL,A1,A2,ACONT)
CONTOUR PROGRAMS MAP, WALK, SEARCH, ENTEK, AND CHECK

```

```

97 R/RUN
98 R/RUN
99 R/RUN
100 R/RUN
101 R/RUN
102 R/RUN
103 R/RUN
104 R/RUN
105 R/RUN
106 R/RUN
107 R/RUN
108 R/RUN
109 R/RUN
110 R/RUN
111 R/RUN
112 R/RUN
2 KRINF
3 KRINF
4 KRINF
5 KRINF
6 KRINF
7 KRINF
8 KRINF
9 KRINF
10 STREAM
11 KRINF
12 KRINF
13 KRINF
14 KRINF
15 KRINF
16 KRINF
17 KRINF
18 KRINF
19 KRINF
20 KRINF
21 KRINF
22 KRINF
23 KRINF
24 KRINF
25 KRINF
26 KRINF
27 KRINF
28 KRINF
29 KRINF
30 KRINF
31 KRINF
32 KRINF
33 KRINF
34 KRINF
35 KRINF
36 KRINF
37 KRINF
38 KRINF
39 KRINF
40 KRINF
41 KRINF
42 KRINF
43 KRINF
44 KRINF
45 KRINF
46 KRINF
47 KRINF
48 KRINF
49 KRINF
50 KRINF
51 KRINF
52 KRINF
53 KRINF
54 KRINF
55 KRINF
56 KRINF
57 KRINF
58 KRINF
59 KRINF
60 KRINF
2 SERCH
3 SERCH
4 SERCH

```

```

2 SETUP
3 SETUP
4 SETUP
5 SETUP
6 SETUP
7 SETUP
8 SETUP
9 SETUP
10 SETUP
11 SETUP
12 SETUP
13 SETUP
14 SETUP
15 SETUP
16 SETUP
17 SETUP
18 SETUP
19 SETUP
20 SETUP
21 SETUP
22 SETUP
23 SETUP
24 SETUP
25 SETUP
26 SETUP
27 SETUP
28 SETUP
29 SETUP
30 SETUP
31 SETUP
32 SETUP
33 SETUP
34 SETUP
35 SETUP
36 SETUP
37 SETUP
38 SETUP
39 SETUP
40 SETUP
41 SETUP
42 SETUP
43 SETUP
44 SETUP
45 SETUP
46 SETUP

```

```

SUBROUTINE SETUP(IPLD,TMACH,GM,IBODY)
THIS ROUTINE ESTABLISHES PLOT ORIGIN, DRAWS
AND LABELS X-AXIS, AND WRITES TITLE.
ULC PLOT SUBROUTINE IS USED ARE
SCALE, XSCALE, YSCALE, PLTLN, DOTLN.
DIMENSION TITLE(2),TITLE4(2)
DIMENSION TITLE5(2),TITLE6(3),TITLE5(2)
DIMENSION TITLEF(2)
COMMON /SCALE/ XSF,YSF,XMAX,YMAX,XLNGTH,YLNGTH
DATA PI2/3.1415926537
DATA TITLE1,TITLE2,VEL,VELOCITY,RODENSITY,
DATA TITLE3,TITLE4,STREAMLINE,IMS/
DATA TITLE5(1),TITLE5(2),IOMHPRUM,IMS/
DATA TITLE6(1),TITLE6(2),IOMHPRUM,PARALLEL,ICOMPONENT/
DATA TITLE6(3),TITLE6(4),IOMHPRUM,PERPENDIC,ICOMPONENT/
DATA TITLE6(5),TITLE6(6),IOMHPRUM,SHIELD,
DATA TITLE6(7),TITLE6(8),IOMHPRUM,MAGNETIC F,SHIELD,
DATA TITLE6(9),TITLE6(10),IOMHPRUM,CONTOURS,
TITLEF(1),TITLEF(2),IOMHPRUM,FIELD,IMS/
SET ORIGIN AT LEFT END OF X-AXIS
CALL PLOT(0,1,0,-3)
AS=XSF
YS=YSF
CALL SCALE(XS,YS,1)
DRAW AND LABEL X-AXIS. NOTE THAT SUBROUTINE AXIS
REQUIRES PARAMETERS IN INCHES, NOT USER UNITS.
NTC=INT(2.5*(XMAX-XMIN)/1.0)
CALL AXIS(X0,X1,X2,X3,XLNGTH,-NTC,1,0,0)
SET PERMANENT ORIGIN AT X=0
CALL PLOT(1,0,0,-3)
AS=XSF
YS=YSF
CALL SCALE(XS,YS,1)
DRAW Y-AXIS
NTC=INT(YMAX)+1

```

```

2 SETUP
3 SETUP
4 SETUP
5 SETUP
6 SETUP
7 SETUP
8 SETUP
9 SETUP
10 SETUP
11 SETUP
12 SETUP
13 SETUP
14 SETUP
15 SETUP
16 SETUP
17 SETUP
18 SETUP
19 SETUP
20 SETUP
21 SETUP
22 SETUP
23 SETUP
24 SETUP
25 SETUP
26 SETUP
27 SETUP
28 SETUP
29 SETUP
30 SETUP
31 SETUP
32 SETUP
33 SETUP
34 SETUP
35 SETUP
36 SETUP
37 SETUP
38 SETUP
39 SETUP
40 SETUP
41 SETUP
42 SETUP
43 SETUP
44 SETUP
45 SETUP
46 SETUP
47 SETUP
48 SETUP
49 SETUP
50 SETUP
51 SETUP
52 SETUP
53 SETUP
54 SETUP
55 SETUP
56 SETUP
57 SETUP
58 SETUP
59 SETUP
60 SETUP

```

```

C     CALL AXIS(0,0,0,1,4,0,0,YLNGT4,-N(C,2),PI2)
C     LABEL X=AXIS
C     YCM=0.475F
C     XCM=0.5XMAX-0.75-21/ASF
C     IF (IPLOT.EQ.1) GO TO 2
C     CALL CHAR(XCM,YCM,0.0,16,3HX/D.3)
C     GO TO 3
2  CALL CHAR(XCM,YCM,0.0,16,3HX/R.3)
C     XCM=XCM+2/ASF
C     CALL CHAR(XCM,YCM,0.0,16,3HX)
3  CONTINUE
C     ANNOTATE X=0.5 - NOTE ANNOTATION IS POSITIVE LEFT.
C     YC=0.475F
C     XCM=0.5
C     DLY=FLOAT(IX)*C.5
C     XCM=XCM+DELX
C     CALL NUMPLT(XCM,YC,0.0,-0.3,-4DR,1)
C     Z=ZA+1
C     IF (XMAX.LT.XMAX) GO TO 5
C     ANNOTATE Y=AXIS AT SIDO EDGE OF PLOT
C     YC=0.6
C     YC=YC+1.0
C     XCM=0.5+2/ASF
C     CALL NUMPLT(XCM,YC,0.0,16,3HX/D.3)
C     XCM=XCM+2/ASF
C     CALL CHAR(XCM,YCM,0.0,16,3HX/R.3)
C     IF (YMAX.LT.YMAX) GO TO 10
C     LABEL Y=AXIS.
C     XCM=0.5+0.95/ASF
C     YCM=ANINT((YMAX-1.0)/C.0)*0.5-0.7/YSF
C     IF (IBODY.EQ.1) GO TO 12
C     CALL CHAR(XCM,YCM,0.0,16,3HX/D.3)
C     GO TO 13
12  CALL CHAR(XCM,YCM,0.0,16,3HR/R.3)
C     XCM=XCM+2/ASF
C     CALL CHAR(XCM,YCM,0.0,16,4.0,1)
13  CONTINUE
C     DRAW TITLE. PLOT DETERMINES WHICH TITLE
C     SHOULD BE DRAWN.
C     YCM=YMAX-0.8/YSF
C     XCM=0.5+0.475F
C     IF (PLOT.EQ.2) GO TO 15
C     IF (PLOT.EQ.3) GO TO 20
C     IF (PLOT.EQ.4) GO TO 14
C     VELOCITY PLOT
C     IF (PLOT.EQ.4) GO TO 21
C     CALL CHAR(XCM,YCM,0.0,20,TITLE,9)
C     XCM=XCM+2/ASF
C     CALL PLOT(XCM,YCM,XCM,YCM,0.0,2,1HV,1)
C     CALL CHAR(XCM,YCM,0.0,2,1HV,1)
C     XCM=XCM+2/ASF
C     CALL PLOT(XCM,YCM,XCM,YCM,0.0,2,1HV,2)
C     CALL CHAR(XCM,YCM,0.0,2,2H/R,2)
C     CALL MATH(XCM+0.5/YSF,YCM-0.5/YSF,0.0,0,19)
C     GO TO 23
C     TEMPERATURE PLOT
C     CALL CHAR(XCM,YCM,0.0,20,TITLE,11)
C     XCM=XCM+2/ASF
C     CALL CHAR(XCM,YCM,0.0,2,3MT/I,3)
C     CALL MATH(XCM+0.5/YSF,YCM-0.5/YSF,0.0,0,19)
C     GO TO 25
C     DENSITY PLOT
C     CALL CHAR(XCM,YCM,0.0,2,1TLE,2,8)
C     XCM=XCM+2/ASF
C     CALL GREEN(XCM,YCM,0.0,0,17)
5  CALL AXIS(0,0,0,1,4,0,0,YLNGT4,-N(C,2),PI2)
6  LABEL X=AXIS
7  YCM=0.475F
8  XCM=0.5XMAX-0.75-21/ASF
9  IF (IPLOT.EQ.1) GO TO 2
10 CALL CHAR(XCM,YCM,0.0,16,3HX/D.3)
11 GO TO 3
12 CALL CHAR(XCM,YCM,0.0,16,3HX/R.3)
13 XCM=XCM+2/ASF
14 CALL CHAR(XCM,YCM,0.0,16,3HX)
15 CONTINUE
16 ANNOTATE X=0.5 - NOTE ANNOTATION IS POSITIVE LEFT.
17 YC=0.475F
18 XCM=0.5
19 DLY=FLOAT(IX)*C.5
20 XCM=XCM+DELX
21 CALL NUMPLT(XCM,YC,0.0,-0.3,-4DR,1)
22 Z=ZA+1
23 IF (XMAX.LT.XMAX) GO TO 5
24 ANNOTATE Y=AXIS AT SIDO EDGE OF PLOT
25 YC=0.6
26 YC=YC+1.0
27 XCM=0.5+2/ASF
28 CALL NUMPLT(XCM,YC,0.0,16,3HX/D.3)
29 XCM=XCM+2/ASF
30 CALL CHAR(XCM,YCM,0.0,16,3HX/R.3)
31 IF (YMAX.LT.YMAX) GO TO 10
32 LABEL Y=AXIS.
33 XCM=0.5+0.95/ASF
34 YCM=ANINT((YMAX-1.0)/C.0)*0.5-0.7/YSF
35 IF (IBODY.EQ.1) GO TO 12
36 CALL CHAR(XCM,YCM,0.0,16,3HX/D.3)
37 GO TO 13
38 CALL CHAR(XCM,YCM,0.0,16,3HR/R.3)
39 XCM=XCM+2/ASF
40 CALL CHAR(XCM,YCM,0.0,16,4.0,1)
39 CONTINUE
41 DRAW TITLE. PLOT DETERMINES WHICH TITLE
42 SHOULD BE DRAWN.
43 YCM=YMAX-0.8/YSF
44 XCM=0.5+0.475F
45 IF (PLOT.EQ.2) GO TO 15
46 IF (PLOT.EQ.3) GO TO 20
47 IF (PLOT.EQ.4) GO TO 14
48 VELOCITY PLOT
49 IF (PLOT.EQ.4) GO TO 21
50 CALL CHAR(XCM,YCM,0.0,20,TITLE,9)
51 XCM=XCM+2/ASF
52 CALL PLOT(XCM,YCM,XCM,YCM,0.0,2,1HV,1)
53 CALL CHAR(XCM,YCM,0.0,2,1HV,1)
54 XCM=XCM+2/ASF
55 CALL PLOT(XCM,YCM,XCM,YCM,0.0,2,1HV,2)
56 CALL CHAR(XCM,YCM,0.0,2,2H/R,2)
57 CALL MATH(XCM+0.5/YSF,YCM-0.5/YSF,0.0,0,19)
58 GO TO 23
59 TEMPERATURE PLOT
60 CALL CHAR(XCM,YCM,0.0,20,TITLE,11)
61 XCM=XCM+2/ASF
62 CALL CHAR(XCM,YCM,0.0,2,3MT/I,3)
63 CALL MATH(XCM+0.5/YSF,YCM-0.5/YSF,0.0,0,19)
64 GO TO 25
65 DENSITY PLOT
66 CALL CHAR(XCM,YCM,0.0,2,1TLE,2,8)
67 XCM=XCM+2/ASF
68 CALL GREEN(XCM,YCM,0.0,0,17)
20  CALL CHAR(XCM,YCM,0.0,2,1TLE,2,8)
21 CALL MATH(XCM+0.5/YSF,YCM-0.5/YSF,0.0,0,19)
22 GO TO 25
23 STREAMLINE'S PLOT
24 CONTINUE
25 CALL CHAR(XCM,YCM,0.0,2,1TLE,2,8)
26 GO TO 25
27 MAGNETIC FIELD PLOTS
28 CONTINUE
29 CALL CHAR(XCM,YCM,0.0,2,1TLE,2,8)
30 GO TO 25
31 CONTINUE
32 CALL CHAR(XCM,YCM,0.0,2,1TLE,2,8)
33 XCM=XCM+2/ASF
34 CALL CHAR(XCM,YCM,0.0,2,1TLE,2,8)
35 CALL MATH(XCM+0.5/YSF,YCM-0.5/YSF,0.0,0,19)
36 IF (IPLOT.EQ.1) GO TO 22
37 CALL MATH(XCM+0.5/YSF,YCM-0.5/YSF,0.0,0,19)
38 XCM=XCM+2/ASF
39 YCM=YCM+1/YSF
40 CALL CHAR(XCM,YCM,0.0,2,1TLE,2,8)
41 GO TO 25
42 CALL CHAR(XCM,YCM,0.0,2,1TLE,2,8)
43 YCM=YCM+0.475F
44 CALL CHAR(XCM,YCM,0.0,2,1TLE,2,8)
45 YCM=YCM+1/YSF
46 CALL CHAR(XCM,YCM,0.0,2,1TLE,2,8)
47 YCM=YCM+0.475F
48 CALL CHAR(XCM,YCM,0.0,2,1TLE,2,8)
49 YCM=YCM+1/YSF
50 CALL CHAR(XCM,YCM,0.0,2,1TLE,2,8)
51 YCM=YCM+0.475F
52 CALL CHAR(XCM,YCM,0.0,2,1TLE,2,8)
53 YCM=YCM+1/YSF
54 CALL CHAR(XCM,YCM,0.0,2,1TLE,2,8)
55 YCM=YCM+0.475F
56 CALL CHAR(XCM,YCM,0.0,2,1TLE,2,8)
57 YCM=YCM+1/YSF
58 CALL CHAR(XCM,YCM,0.0,2,1TLE,2,8)
59 YCM=YCM+0.475F
60 CALL CHAR(XCM,YCM,0.0,2,1TLE,2,8)
61 YCM=YCM+1/YSF
62 CALL CHAR(XCM,YCM,0.0,2,1TLE,2,8)
63 YCM=YCM+0.475F
64 CALL CHAR(XCM,YCM,0.0,2,1TLE,2,8)
65 YCM=YCM+1/YSF
66 CALL CHAR(XCM,YCM,0.0,2,1TLE,2,8)
67 YCM=YCM+0.475F
68 CALL CHAR(XCM,YCM,0.0,2,1TLE,2,8)
69 YCM=YCM+1/YSF
69  DRAW MACH NUMBER (M) AND RATIO OF SPECIFIC
70 HEATS (GAMMA).
71 CONTINUE
72 YCM=YMAX-0.3/YSF
73 XCM=0.5+0.475F
74 CALL CHAR(XCM,YCM,0.0,2,2HM,2)
75 CALL NUMPLT(XCM,YCM,0.0,2,2TMACH,1)
76 XCM=XCM+0.475F
77 CALL GREEN(XCM,YCM,0.0,2,1HV,3)
78 CALL CHAR(XCM,YCM,0.0,2,1HV,3)
79 CALL NUMPLT(XCM,YCM,0.0,2,2GAM,2)
80 RETURN
81 END
82 SUBROUTINE SFSCALE(XMK,YMK,NTRAX)
83 THIS ROUTINE DETERMINES SCALE FACTORS AND SIZE OF PLOT.
84 COMMON /SCALE/ XSF,YSF,XMAX,YMAX,XLNGTH,YLNGTH
85 DIMENSION XSF(1),YSF(1)
86 DATA YSIZE/800/
87 CALCULATE XMAX AND YMAX BASED ON LAST POINT OF SHOCK WAVE.
88 XMAX=INT(XKINTRAX)*0.5
89 YMAX=INT(YKINTRAX)*0.5
90 IF (XMAX.LT.0) XMAX=0
91 IF (YMAX.LT.0) YMAX=0
92 FIX PLOT SIZE IN Y-DIRECTION
93 ADJUST SCALE FACTORS FOR EQUAL X AND Y SCALE FACTORS
94 YLNGTH=YSIZE
95 XSF=YLNGTH/YMAX
96 YSF=XSF
97 XLNGTH=XSF*(XMAX+1.5)
98 RETURN
99 END
100 SUBROUTINE STUUT
101 THIS SUBROUTINE PRINTS THE STREAMLINES CALCULATED
102 IN SUBROUTINES FLOW AND FLOWM
103 END
104 STOUT
105 STOUT
106 STOUT
107 STOUT
108 STOUT
109 STOUT
110 STOUT
111 STOUT
112 STOUT
113 STOUT
114 STOUT
115 STOUT
116 STOUT
117 STOUT
118 STOUT
119 STOUT
120 STOUT
121 STOUT
122 STOUT
123 STOUT
124 STOUT
125 STOUT
126 STOUT
127 STOUT
128 STOUT
129 STOUT
130 STOUT
131 STOUT
132 STOUT
133 STOUT
134 STOUT
135 STOUT
136 STOUT
137 STOUT
138 STOUT
139 STOUT
140 STOUT
141 STOUT
142 STOUT
143 STOUT
144 STOUT
145 STOUT
146 STOUT
147 STOUT
148 STOUT
149 STOUT
150 STOUT
151 STOUT
152 STOUT
153 STOUT
154 STOUT
155 STOUT
156 STOUT
157 STOUT
158 STOUT
159 STOUT
160 STOUT
161 STOUT
162 STOUT
163 STOUT
164 STOUT
165 STOUT
166 STOUT
167 STOUT
168 STOUT
169 STOUT
170 STOUT
171 STOUT
172 STOUT
173 STOUT
174 STOUT
175 STOUT
176 STOUT
177 STOUT
178 STOUT
179 STOUT
180 STOUT
181 STOUT
182 STOUT
183 STOUT
184 STOUT
185 STOUT
186 STOUT
187 STOUT
188 STOUT
189 STOUT
190 STOUT
191 STOUT
192 STOUT
193 STOUT
194 STOUT
195 STOUT
196 STOUT
197 STOUT
198 STOUT
199 STOUT
200 STOUT
201 STOUT
202 STOUT
203 STOUT
204 STOUT
205 STOUT
206 STOUT
207 STOUT
208 STOUT
209 STOUT
210 STOUT
211 STOUT
212 STOUT
213 STOUT
214 STOUT
215 STOUT
216 STOUT
217 STOUT
218 STOUT
219 STOUT
220 STOUT
221 STOUT
222 STOUT
223 STOUT
224 STOUT
225 STOUT
226 STOUT
227 STOUT
228 STOUT
229 STOUT
230 STOUT
231 STOUT
232 STOUT
233 STOUT
234 STOUT
235 STOUT
236 STOUT
237 STOUT
238 STOUT
239 STOUT
240 STOUT
241 STOUT
242 STOUT
243 STOUT
244 STOUT
245 STOUT
246 STOUT
247 STOUT
248 STOUT
249 STOUT
250 STOUT
251 STOUT
252 STOUT
253 STOUT
254 STOUT
255 STOUT
256 STOUT
257 STOUT
258 STOUT
259 STOUT
260 STOUT
261 STOUT
262 STOUT
263 STOUT
264 STOUT
265 STOUT
266 STOUT
267 STOUT
268 STOUT
269 STOUT
270 STOUT
271 STOUT
272 STOUT
273 STOUT
274 STOUT
275 STOUT
276 STOUT
277 STOUT
278 STOUT
279 STOUT
280 STOUT
281 STOUT
282 STOUT
283 STOUT
284 STOUT
285 STOUT
286 STOUT
287 STOUT
288 STOUT
289 STOUT
290 STOUT
291 STOUT
292 STOUT
293 STOUT
294 STOUT
295 STOUT
296 STOUT
297 STOUT
298 STOUT
299 STOUT
300 STOUT
301 STOUT
302 STOUT
303 STOUT
304 STOUT
305 STOUT
306 STOUT
307 STOUT
308 STOUT
309 STOUT
310 STOUT
311 STOUT
312 STOUT
313 STOUT
314 STOUT
315 STOUT
316 STOUT
317 STOUT
318 STOUT
319 STOUT
320 STOUT
321 STOUT
322 STOUT
323 STOUT
324 STOUT
325 STOUT
326 STOUT
327 STOUT
328 STOUT
329 STOUT
330 STOUT
331 STOUT
332 STOUT
333 STOUT
334 STOUT
335 STOUT
336 STOUT
337 STOUT
338 STOUT
339 STOUT
340 STOUT
341 STOUT
342 STOUT
343 STOUT
344 STOUT
345 STOUT
346 STOUT
347 STOUT
348 STOUT
349 STOUT
350 STOUT
351 STOUT
352 STOUT
353 STOUT
354 STOUT
355 STOUT
356 STOUT
357 STOUT
358 STOUT
359 STOUT
360 STOUT
361 STOUT
362 STOUT
363 STOUT
364 STOUT
365 STOUT
366 STOUT
367 STOUT
368 STOUT
369 STOUT
370 STOUT
371 STOUT
372 STOUT
373 STOUT
374 STOUT
375 STOUT
376 STOUT
377 STOUT
378 STOUT
379 STOUT
380 STOUT
381 STOUT
382 STOUT
383 STOUT
384 STOUT
385 STOUT
386 STOUT
387 STOUT
388 STOUT
389 STOUT
390 STOUT
391 STOUT
392 STOUT
393 STOUT
394 STOUT
395 STOUT
396 STOUT
397 STOUT
398 STOUT
399 STOUT
400 STOUT
401 STOUT
402 STOUT
403 STOUT
404 STOUT
405 STOUT
406 STOUT
407 STOUT
408 STOUT
409 STOUT
410 STOUT
411 STOUT
412 STOUT
413 STOUT
414 STOUT
415 STOUT
416 STOUT
417 STOUT
418 STOUT
419 STOUT
420 STOUT
421 STOUT
422 STOUT
423 STOUT
424 STOUT
425 STOUT
426 STOUT
427 STOUT
428 STOUT
429 STOUT
430 STOUT
431 STOUT
432 STOUT
433 STOUT
434 STOUT
435 STOUT
436 STOUT
437 STOUT
438 STOUT
439 STOUT
440 STOUT
441 STOUT
442 STOUT
443 STOUT
444 STOUT
445 STOUT
446 STOUT
447 STOUT
448 STOUT
449 STOUT
450 STOUT
451 STOUT
452 STOUT
453 STOUT
454 STOUT
455 STOUT
456 STOUT
457 STOUT
458 STOUT
459 STOUT
460 STOUT
461 STOUT
462 STOUT
463 STOUT
464 STOUT
465 STOUT
466 STOUT
467 STOUT
468 STOUT
469 STOUT
470 STOUT
471 STOUT
472 STOUT
473 STOUT
474 STOUT
475 STOUT
476 STOUT
477 STOUT
478 STOUT
479 STOUT
480 STOUT
481 STOUT
482 STOUT
483 STOUT
484 STOUT
485 STOUT
486 STOUT
487 STOUT
488 STOUT
489 STOUT
490 STOUT
491 STOUT
492 STOUT
493 STOUT
494 STOUT
495 STOUT
496 STOUT
497 STOUT
498 STOUT
499 STOUT
500 STOUT

```



```

38 IF(K3IKUD6).NE.1) GO TO 9
   K=NODE
   GO TO 4
6  C ONE IN) ONE OUT, FIND WHERE OUT.
7  DD 3 K=J-1
8  IF(K3IKG)GOTO 1) GO TO 4
9  CONTINUE
C C SECOND THE POINT
4  CALL ENTER(K2(KS),J,J(KG),K(K6),MVAL,A1(K6),AZ(K6),J(JN),NMIN,ICHK,--
   KUD,J2,Y2,RY,RY,ACONT,ISIZ1)
C C RESET J AND K
C J=J(K6)
C K=K(K6)
C SEE IF WFRZ AT A BOUNDARY. IF SO, QUIT.
C IF(JG)GT(JMIN) GO TO 23
C GO TO (26,19,24,25),KOD5
C IF(J)GT(JMAX) GO TO 19
C GO TO (24,25,26,19),KOD5
24 IF(K6=EG=2) GO TO 1
C GO TO 19
25 IF(K6=EQ=2) GO TO 1
C GO TO 19
26 IF(K6=EQ=1) GO TO 1
C GO TO 1
27 IF(K6=KMIN) GO TO 27
C GO TO (30,30,49,49),KOD5
27 IF(K6=L1)KMAX) GO TO 6
C GO TO (29,29,30),KOD5
28 IF(K6=EQ=1) GO TO 1
C GO TO 1
29 IF(K6=EQ=2) GO TO 1
C GO TO 1
30 IF(K6=EQ=3) GO TO 1
C C PREPARE FOR NEXT STEP
6  KOD6=K6
   KOD5=KOD5+K6-2
   IF(KUD5.GT.4) KOD5=KOD5-4
   IF(KOD5.LT.1) KOD5=KUD5+4
   GO TO 31
C C CONTINUE
1  CONTINUE
5  RETURN
   END
SUBROUTINE BLUNTB
> COMMON/COM1/JMAX,KMAX,JY,KM,XMACH,ALPHA,GAM,GAMML,CN,DT,SMU,IPRT,
<RINF,GINF,CNF,ICS,IM,CLUS,PT,HUNK,KNODE,NCASE,NPUNCH
COMMON /COM2/ X(25,20),Y(25,20),Z(25,20),XET(25,20),YET(25,20),ZET(25,20)
COMMON /COM3/ J(25,20),I(25,20),K(25,20),L(25,20),M(25,20)
COMMON /COM4/ KVCUN,VCON(20),KRCUN,RCON(20),XC(20,100),YC(20,100),
* VF(20,100),RHO(120,100)
COMMON /BLUNT/ THETA(23),RPI(23,23)
LEVEL 2,VA,VY
COMMON/VCOMP/ VA(20,100),VY(20,100)
COMMON/MINETY/ AMACH,GAM,KRZ,PLINF,RLINE,VLINE,P9(120,3)
* RHOG(120,3),U90(20,3),V90(20,3),W90(20,3),RS90(3),
* RSZ90(3),KSP90(3),HRD,RD
COMMON /SHOCKS/ DRSDX(100),OST(150)
C...INITIALIZE
* WRITE(6,200)
200 FORMAT(1H,/,93X,22HBLUNT BODY CALCULATION/93X,22(1H)/)
CALL INITIA
C...DETERMINE SIZE
CALL EIGEN
C...INTEGRATE EQUATIONS
DO 1 I=1,ITER
  I=I+1
  CALL SHOCK
  CALL BNORY
  CALL INTEG
  CALL XIETAD(1)
  CONTINUE
1  CONTINUE
C...PRINT DATA
CALL OUTPUT(1)
C
BLUNTB 27
BLUNTB 28
BLUNTB 29
BLUNTB 30
BLUNTB 31
BLUNTB 32
BLUNTB 33
BLUNTB 34
BLUNTB 35
BLUNTB 36
BLUNTB 37
BLUNTB 38
BLUNTB 39
BLUNTB 40
BLUNTB 41
BLUNTB 42
BLUNTB 43
BLUNTB 44
BLUNTB 45
BLUNTB 46
BLUNTB 47
BLUNTB 48
BLUNTB 49
BLUNTB 50
BLUNTB 51
BLUNTB 52
BLUNTB 53
BLUNTB 54
BLUNTB 55
BLUNTB 56
BLUNTB 57
BLUNTB 58
BLUNTB 59
BLUNTB 60
BLUNTB 61
BLUNTB 62
BLUNTB 63
BLUNTB 64
BLUNTB 65
BLUNTB 66
BLUNTB 67
BLUNTB 68
BLUNTB 69
BLUNTB 70
BLUNTB 71
BLUNTB 72
BLUNTB 73
BLUNTB 74
BLUNTB 75
BLUNTB 76
BLUNTB 77
BLUNTB 78
BLUNTB 79
BLUNTB 80
BLUNTB 81
BLUNTB 82
BLUNTB 83
BLUNTB 84
BLUNTB 85
ABMATH 2
COM1 3
COM2 4
COM3 2
COM4 3
COMH2 6
COMH3 7
COMH4 8
COMH5 9
COMH6 10
COMH7 11
COMH8 12
COMH9 13
COMH10 14
COMH11 15
COMH12 16
COMH13 17
COMH14 18
COMH15 19
COMH16 20
COMH17 21
COMH18 22
COMH19 23
COMH20 24
COMH21 25
SUBROUTINE ABMATH(J,K,L)
> COMMON/COM1/JMAX,KMAX,JY,KM,XMACH,ALPHA,GAM,GAMML,CN,DT,SMU,IPRT,
<RINF,GINF,CNF,ICS,IM,CLUS,PT,HUNK,KNODE,NCASE,NPUNCH
COMMON /COM2/ X(25,20),Y(25,20),Z(25,20),XET(25,20),YET(25,20),ZET(25,20)
COMMON /COM3/ J(25,20),I(25,20),K(25,20),L(25,20),M(25,20)
COMMON /COM4/ KVCUN,VCON(20),KRCUN,RCON(20),XC(20,100),YC(20,100),
* VF(20,100),RHO(120,100)
COMMON /ABMATH/ AB(25,25)
LEVEL 1,VA,VY
COMMON/VCOMP/ VA(20,100),VY(20,100)
COMMON/MINETY/ AMACH,GAM,KRZ,PLINF,RLINE,VLINE,P9(120,3)
* RHOG(120,3),U90(20,3),V90(20,3),W90(20,3),RS90(3),
* RSZ90(3),KSP90(3),HRD,RD
COMMON /SHOCKS/ DRSDX(100),OST(150)
C...INITIALIZE
* WRITE(6,200)
200 FORMAT(1H,/,93X,22HBLUNT BODY CALCULATION/93X,22(1H)/)
CALL INITIA
C...DETERMINE SIZE
CALL EIGEN
C...INTEGRATE EQUATIONS
DO 1 I=1,ITER
  I=I+1
  CALL SHOCK
  CALL BNORY
  CALL INTEG
  CALL XIETAD(1)
  CONTINUE
1  CONTINUE
C...PRINT DATA
CALL OUTPUT(1)
C
ABMATH 7
ABMATH 8
ABMATH 9
ABMATH 10
ABMATH 11
ABMATH 12
ABMATH 13
ABMATH 14
ABMATH 15
ABMATH 16
ABMATH 17
ABMATH 18
ABMATH 19
ABMATH 20
ABMATH 21
C...STARTING PLANE FOR MARCHING CODE AT THETA=90 D-DEGREES
P40=YC(1),JPAK=1)
AMACH=XMACH
PLINF=PLINF
VLINE=VLINE
KMIN=KMIN
VMAX=VMAX
MPC=MPK
GAM=PCAN
GAM1=GAM*28.5*GAM
P42=1,GMPL=1-SAM/GAM1)
MPC1=MPC*1-SAM/GAM1)
MPC2=MPC*1-SAM/GAM1)
MPC3=MPC*1-SAM/GAM1)
MPC4=MPC*1-SAM/GAM1)
MPC5=MPC*1-SAM/GAM1)
MPC6=MPC*1-SAM/GAM1)
MPC7=MPC*1-SAM/GAM1)
MPC8=MPC*1-SAM/GAM1)
MPC9=MPC*1-SAM/GAM1)
MPC10=MPC*1-SAM/GAM1)
MPC11=MPC*1-SAM/GAM1)
MPC12=MPC*1-SAM/GAM1)
MPC13=MPC*1-SAM/GAM1)
MPC14=MPC*1-SAM/GAM1)
MPC15=MPC*1-SAM/GAM1)
MPC16=MPC*1-SAM/GAM1)
MPC17=MPC*1-SAM/GAM1)
MPC18=MPC*1-SAM/GAM1)
MPC19=MPC*1-SAM/GAM1)
MPC20=MPC*1-SAM/GAM1)
MPC21=MPC*1-SAM/GAM1)
MPC22=MPC*1-SAM/GAM1)
MPC23=MPC*1-SAM/GAM1)
MPC24=MPC*1-SAM/GAM1)
MPC25=MPC*1-SAM/GAM1)
MPC26=MPC*1-SAM/GAM1)
MPC27=MPC*1-SAM/GAM1)
MPC28=MPC*1-SAM/GAM1)
MPC29=MPC*1-SAM/GAM1)
MPC30=MPC*1-SAM/GAM1)
MPC31=MPC*1-SAM/GAM1)
MPC32=MPC*1-SAM/GAM1)
MPC33=MPC*1-SAM/GAM1)
MPC34=MPC*1-SAM/GAM1)
MPC35=MPC*1-SAM/GAM1)
MPC36=MPC*1-SAM/GAM1)
MPC37=MPC*1-SAM/GAM1)
MPC38=MPC*1-SAM/GAM1)
MPC39=MPC*1-SAM/GAM1)
MPC40=MPC*1-SAM/GAM1)
MPC41=MPC*1-SAM/GAM1)
MPC42=MPC*1-SAM/GAM1)
MPC43=MPC*1-SAM/GAM1)
MPC44=MPC*1-SAM/GAM1)
MPC45=MPC*1-SAM/GAM1)
MPC46=MPC*1-SAM/GAM1)
MPC47=MPC*1-SAM/GAM1)
MPC48=MPC*1-SAM/GAM1)
MPC49=MPC*1-SAM/GAM1)
MPC50=MPC*1-SAM/GAM1)
MPC51=MPC*1-SAM/GAM1)
MPC52=MPC*1-SAM/GAM1)
MPC53=MPC*1-SAM/GAM1)
MPC54=MPC*1-SAM/GAM1)
MPC55=MPC*1-SAM/GAM1)
MPC56=MPC*1-SAM/GAM1)
MPC57=MPC*1-SAM/GAM1)
MPC58=MPC*1-SAM/GAM1)
MPC59=MPC*1-SAM/GAM1)
MPC60=MPC*1-SAM/GAM1)
MPC61=MPC*1-SAM/GAM1)
MPC62=MPC*1-SAM/GAM1)
MPC63=MPC*1-SAM/GAM1)
MPC64=MPC*1-SAM/GAM1)
MPC65=MPC*1-SAM/GAM1)
MPC66=MPC*1-SAM/GAM1)
MPC67=MPC*1-SAM/GAM1)
MPC68=MPC*1-SAM/GAM1)
MPC69=MPC*1-SAM/GAM1)
MPC70=MPC*1-SAM/GAM1)
MPC71=MPC*1-SAM/GAM1)
MPC72=MPC*1-SAM/GAM1)
MPC73=MPC*1-SAM/GAM1)
MPC74=MPC*1-SAM/GAM1)
MPC75=MPC*1-SAM/GAM1)
MPC76=MPC*1-SAM/GAM1)
MPC77=MPC*1-SAM/GAM1)
MPC78=MPC*1-SAM/GAM1)
MPC79=MPC*1-SAM/GAM1)
MPC80=MPC*1-SAM/GAM1)
MPC81=MPC*1-SAM/GAM1)
MPC82=MPC*1-SAM/GAM1)
MPC83=MPC*1-SAM/GAM1)
MPC84=MPC*1-SAM/GAM1)
MPC85=MPC*1-SAM/GAM1)
MPC86=MPC*1-SAM/GAM1)
MPC87=MPC*1-SAM/GAM1)
MPC88=MPC*1-SAM/GAM1)
MPC89=MPC*1-SAM/GAM1)
MPC90=MPC*1-SAM/GAM1)
MPC91=MPC*1-SAM/GAM1)
MPC92=MPC*1-SAM/GAM1)
MPC93=MPC*1-SAM/GAM1)
MPC94=MPC*1-SAM/GAM1)
MPC95=MPC*1-SAM/GAM1)
MPC96=MPC*1-SAM/GAM1)
MPC97=MPC*1-SAM/GAM1)
MPC98=MPC*1-SAM/GAM1)
MPC99=MPC*1-SAM/GAM1)
MPC100=MPC*1-SAM/GAM1)
MPC101=MPC*1-SAM/GAM1)
MPC102=MPC*1-SAM/GAM1)
MPC103=MPC*1-SAM/GAM1)
MPC104=MPC*1-SAM/GAM1)
MPC105=MPC*1-SAM/GAM1)
MPC106=MPC*1-SAM/GAM1)
MPC107=MPC*1-SAM/GAM1)
MPC108=MPC*1-SAM/GAM1)
MPC109=MPC*1-SAM/GAM1)
MPC110=MPC*1-SAM/GAM1)
MPC111=MPC*1-SAM/GAM1)
MPC112=MPC*1-SAM/GAM1)
MPC113=MPC*1-SAM/GAM1)
MPC114=MPC*1-SAM/GAM1)
MPC115=MPC*1-SAM/GAM1)
CONTINUE
300 CONTINUE
31) CONTINUE
* WRITE(6,200)
200 FORMAT(1H,/,93X,22HBLUNT BODY CALCULATION/93X,22(1H)/)
CALL INITIA
C...DETERMINE SIZE
CALL EIGEN
C...INTEGRATE EQUATIONS
DO 1 I=1,ITER
  I=I+1
  CALL SHOCK
  CALL BNORY
  CALL INTEG
  CALL XIETAD(1)
  CONTINUE
1  CONTINUE
C...PRINT DATA
CALL OUTPUT(1)
C
ABMATH 2
COM1 3
COM2 4
COM3 2
COM4 3
COMH2 6
COMH3 7
COMH4 8
COMH5 9
COMH6 10
COMH7 11
COMH8 12
COMH9 13
COMH10 14
COMH11 15
COMH12 16
COMH13 17
COMH14 18
COMH15 19
COMH16 20
COMH17 21
COMH18 22
COMH19 23
COMH20 24
COMH21 25
SUBROUTINE BLUNTB
> COMMON/COM1/JMAX,KMAX,JY,KM,XMACH,ALPHA,GAM,GAMML,CN,DT,SMU,IPRT,
<RINF,GINF,CNF,ICS,IM,CLUS,PT,HUNK,KNODE,NCASE,NPUNCH
COMMON /COM2/ X(25,20),Y(25,20),Z(25,20),XET(25,20),YET(25,20),ZET(25,20)
COMMON /COM3/ J(25,20),I(25,20),K(25,20),L(25,20),M(25,20)
COMMON /COM4/ KVCUN,VCON(20),KRCUN,RCON(20),XC(20,100),YC(20,100),
* VF(20,100),RHO(120,100)
COMMON /BLUNT/ THETA(23),RPI(23,23)
LEVEL 2,VA,VY
COMMON/VCOMP/ VA(20,100),VY(20,100)
COMMON/MINETY/ AMACH,GAM,KRZ,PLINF,RLINE,VLINE,P9(120,3)
* RHOG(120,3),U90(20,3),V90(20,3),W90(20,3),RS90(3),
* RSZ90(3),KSP90(3),HRD,RD
COMMON /SHOCKS/ DRSDX(100),OST(150)
C...INITIALIZE
* WRITE(6,200)
200 FORMAT(1H,/,93X,22HBLUNT BODY CALCULATION/93X,22(1H)/)
CALL INITIA
C...DETERMINE SIZE
CALL EIGEN
C...INTEGRATE EQUATIONS
DO 1 I=1,ITER
  I=I+1
  CALL SHOCK
  CALL BNORY
  CALL INTEG
  CALL XIETAD(1)
  CONTINUE
1  CONTINUE
C...PRINT DATA
CALL OUTPUT(1)
C
ABMATH 2
COM1 3
COM2 4
COM3 2
COM4 3
COMH2 6
COMH3 7
COMH4 8
COMH5 9
COMH6 10
COMH7 11
COMH8 12
COMH9 13
COMH10 14
COMH11 15
COMH12 16
COMH13 17
COMH14 18
COMH15 19
COMH16 20
COMH17 21
COMH18 22
COMH19 23
COMH20 24
COMH21 25

```









```

3 C(1,K2)=C(2,K2)*U0.
4 C(1,K2)=C(2,K2)*U0
RETURN
END

SUBROUTINE INTGR
COMMON /COM1/ XMAX,KMAX,JMAX,KM,XMACH,ALPHA,GAMM1,CN,DT,SMU,IPRT,
<RINF,ANG,NCB,NCC,AA,H,DMEGA,NUN,NI,TAU,ITER,ENT,P,PIF,
COMMON /COM2/ X(25),Y(25),Z(25),A(25),B(4),AB(4,4)
C... COMPUTE BUBBLING FUNCTION AND STORE TEMPORARILY IN 5 ARRAY
CALL BMS
C... ADD FOURTH ORDER DISSIPATION TO SMOOTH SOLUTION
C... SOLVE FOR O-PAR-HAR
DO 1 L=1,4
1 S(1,L)=E(L,L)
C... SOLVE FOR C-PAR
CALL TRIC(2,KM)
C... FILL ELEMENTS OF I-MODEY 3 FOR BLOCK TRIANGULAR INVERSION AT EACH
C... TH LEVEL
CALL TRIC(2,KM)
C... INVERT BLOCK TRIANGULAR MATRIX AT J TH LEVEL AND STORE SOLUTION IN
CALL TRIC(2,KM)
DO 2 L=1,4
2 U(2,L)=E(L,L)*(J,K,L)
RETURN
END

```

```

SUBROUTINE LBLTR(K)
COMMON /COM1/ JMAX,KMAX,JM,KM,XMACH,ALPHA,GAMM1,CN,DT,SMU,IPRT,
> CHOR,NCB,NCC,AA,H,DMEGA,NUN,NI,TAU,ITER,ENT,P,PIF,
<RINF,ANG,NCB,NCC,AA,H,DMEGA,NUN,NI,TAU,ITER,ENT,P,PIF,
COMMON /COM2/ X(25),Y(25),Z(25),A(25),B(4),AB(4,4)
COMMON /COM3/ X(25),Y(25),Z(25),A(25),B(4),AB(4,4)
C... LOAD BLOCK A MATRIX EVALUATED AT N TH LEVEL FOR ALL J INTO HD ARRAY
DO 1 L=1,4
DO 2 J=1,4
CALL ABMAT(J,K,2)
DO 3 I=1,4
DO 4 K=1,4
C... FILL OFF-DIAGONAL AND DIAGONAL ELEMENTS BASED ON A 2-ND ORDER
CENTRAL DIFFERENCE
DO 2 J=2,4
DO 3 I=1,4
DO 4 K=1,4
1 A(J,I,K)=H*(J-I,L,M)*H
2 A(J,I,K)=H*(J-I,L,M)*H
3 C(1,L)=H*(J-I,L,M)*H
C... SET B ON THE DIAGONAL REPRESENTING THE IDENTITY MATRIX TO ONE
2 B(J,M)=1.0
RETURN
END

```

```

SUBROUTINE LBLTR(J)
COMMON /COM1/ JMAX,KMAX,JM,KM,XMACH,ALPHA,GAMM1,CN,DT,SMU,IPRT,
> CHOR,NCB,NCC,AA,H,DMEGA,NUN,NI,TAU,ITER,ENT,P,PIF,
<RINF,ANG,NCB,NCC,AA,H,DMEGA,NUN,NI,TAU,ITER,ENT,P,PIF,
COMMON /COM2/ X(25),Y(25),Z(25),A(25),B(4),AB(4,4)
COMMON /COM3/ X(25),Y(25),Z(25),A(25),B(4),AB(4,4)
C... LOAD BLOCK B MATRIX EVALUATED AT N TH LEVEL FOR ALL K INTO HD ARRAY
DO 1 M=1,4
DO 2 J=1,4
CALL ABMAT(J,K,2)
DO 3 I=1,4
DO 4 K=1,4
C... FILL OFF-DIAGONAL AND DIAGONAL ELEMENTS BASED ON A 2-ND ORDER
CENTRAL DIFFERENCE
DO 2 J=2,4
DO 3 I=1,4
DO 4 K=1,4
1 A(J,I,K)=H*(J-I,L,M)*H
2 A(J,I,K)=H*(J-I,L,M)*H
3 C(1,L)=H*(J-I,L,M)*H
C... SET B ON THE DIAGONAL REPRESENTING THE IDENTITY MATRIX TO ONE
2 B(J,M)=1.0
RETURN
END

```

```

SUBROUTINE LBLTR(J)
COMMON /COM1/ JMAX,KMAX,JM,KM,XMACH,ALPHA,GAMM1,CN,DT,SMU,IPRT,
> CHOR,NCB,NCC,AA,H,DMEGA,NUN,NI,TAU,ITER,ENT,P,PIF,
<RINF,ANG,NCB,NCC,AA,H,DMEGA,NUN,NI,TAU,ITER,ENT,P,PIF,
COMMON /COM2/ X(25),Y(25),Z(25),A(25),B(4),AB(4,4)
COMMON /COM3/ X(25),Y(25),Z(25),A(25),B(4),AB(4,4)
C... LOAD BLOCK B MATRIX EVALUATED AT N TH LEVEL FOR ALL K INTO HD ARRAY
DO 1 M=1,4
DO 2 J=1,4
CALL ABMAT(J,K,2)
DO 3 I=1,4
DO 4 K=1,4
C... FILL OFF-DIAGONAL AND DIAGONAL ELEMENTS BASED ON A 2-ND ORDER
CENTRAL DIFFERENCE
DO 2 J=2,4
DO 3 I=1,4
DO 4 K=1,4
1 A(J,I,K)=H*(J-I,L,M)*H
2 A(J,I,K)=H*(J-I,L,M)*H
3 C(1,L)=H*(J-I,L,M)*H
C... SET B ON THE DIAGONAL REPRESENTING THE IDENTITY MATRIX TO ONE
2 B(J,M)=1.0
RETURN
END

```

```

SUBROUTINE LBLTR(J)
COMMON /COM1/ JMAX,KMAX,JM,KM,XMACH,ALPHA,GAMM1,CN,DT,SMU,IPRT,
> CHOR,NCB,NCC,AA,H,DMEGA,NUN,NI,TAU,ITER,ENT,P,PIF,
<RINF,ANG,NCB,NCC,AA,H,DMEGA,NUN,NI,TAU,ITER,ENT,P,PIF,
COMMON /COM2/ X(25),Y(25),Z(25),A(25),B(4),AB(4,4)
COMMON /COM3/ X(25),Y(25),Z(25),A(25),B(4),AB(4,4)
C... LOAD BLOCK B MATRIX EVALUATED AT N TH LEVEL FOR ALL K INTO HD ARRAY
DO 1 M=1,4
DO 2 J=1,4
CALL ABMAT(J,K,2)
DO 3 I=1,4
DO 4 K=1,4
C... FILL OFF-DIAGONAL AND DIAGONAL ELEMENTS BASED ON A 2-ND ORDER
CENTRAL DIFFERENCE
DO 2 J=2,4
DO 3 I=1,4
DO 4 K=1,4
1 A(J,I,K)=H*(J-I,L,M)*H
2 A(J,I,K)=H*(J-I,L,M)*H
3 C(1,L)=H*(J-I,L,M)*H
C... SET B ON THE DIAGONAL REPRESENTING THE IDENTITY MATRIX TO ONE
2 B(J,M)=1.0
RETURN
END

```

```

SUBROUTINE LBLTR(J)
COMMON /COM1/ JMAX,KMAX,JM,KM,XMACH,ALPHA,GAMM1,CN,DT,SMU,IPRT,
> CHOR,NCB,NCC,AA,H,DMEGA,NUN,NI,TAU,ITER,ENT,P,PIF,
<RINF,ANG,NCB,NCC,AA,H,DMEGA,NUN,NI,TAU,ITER,ENT,P,PIF,
COMMON /COM2/ X(25),Y(25),Z(25),A(25),B(4),AB(4,4)
COMMON /COM3/ X(25),Y(25),Z(25),A(25),B(4),AB(4,4)
C... LOAD BLOCK B MATRIX EVALUATED AT N TH LEVEL FOR ALL K INTO HD ARRAY
DO 1 M=1,4
DO 2 J=1,4
CALL ABMAT(J,K,2)
DO 3 I=1,4
DO 4 K=1,4
C... FILL OFF-DIAGONAL AND DIAGONAL ELEMENTS BASED ON A 2-ND ORDER
CENTRAL DIFFERENCE
DO 2 J=2,4
DO 3 I=1,4
DO 4 K=1,4
1 A(J,I,K)=H*(J-I,L,M)*H
2 A(J,I,K)=H*(J-I,L,M)*H
3 C(1,L)=H*(J-I,L,M)*H
C... SET B ON THE DIAGONAL REPRESENTING THE IDENTITY MATRIX TO ONE
2 B(J,M)=1.0
RETURN
END

```

```

OUTPUT 32  YA=DEL I+SORT((C+.0E10)-I,-XAI)/SORT(I+.0E10)
OUTPUT 33  GO TO 20
OUTPUT 34  12 THE=ATAI(NC(RK(J-1),JK(J-1)))
OUTPUT 55  15 CONTINUE
OUTPUT 56  DLT=(I+.0E10+CBT*THE+2*Q+.1*BT*THE+*.4)*DELTC
OUTPUT 57  XA1=O-(I+C*DELT)*COS(I*THE)
OUTPUT 58  YA=(I+C*D.L11)*SIN(I*THE)
OUTPUT 59  20 CONTINUE
OUTPUT 60  C...BODY SHAP
OUTPUT 61  IF(NBODY) GO TO 30
OUTPUT 62  CALL BODY(YA,XB,RNDSC,MET,MOAN)
OUTPUT 63  GO TO 40
OUTPUT 64  30 XB=I+C*X1(J-1)
OUTPUT 65  YB=PK(J-1)
OUTPUT 66  40 CONTINUE
OUTPUT 67  ZK=XKMAX-1
OUTPUT 68  DX=(XA-XB)/ZK
OUTPUT 69  DY=(YA-YB)/ZK
OUTPUT 70  DL=C+.1,DKMAX
OUTPUT 71  ZK=K-1
OUTPUT 72  XI(J,K)=XB*ZK+DX
OUTPUT 73  YI(J,K)=YB*ZK+DY
OUTPUT 74  CONTINUE
OUTPUT 75  DO 5 K=1,KMAX
OUTPUT 76  XI(K,X)=Z(K,K)
OUTPUT 77  YI(K,X)=Y(Z(K,K)
OUTPUT 78  CONTINUE
OUTPUT 79  RETURN
OUTPUT 80  END
SUBROUTINE OUTPUT(L)
COMMON/COM1/JMAX,KMAX,JK,KX,KH,XMACH,ALPHA,GAM,GAMM1,CN,DT,SMU,IPRT,
C...CHDR,COR,NCB,NCC,AA,HB,DREGA,NU,NI,TAU,ITER,ENT,PTORT,PINF,
C...DINE,LINE,JCS,TN,CLUS,PT,HORN,ROSE,NCASE,APUNCH
COMMON /COM2/ I(25,20),Y(25,20),X(25,20),Z(25,20),
C...XEY(25,20),Z(25,20),
COMMON /COM3/ Q(25,20),EF(25,20),F(4),G(4),AB(4,4)
DIMENSION SL(25),COM(8)
GO TO (1,2,3,4,5)SL
1 CONTINUE
C...OUTPUT FLOWFIELD DATA
PRM=0
INF=GAM/GAMM1*PINF/KH*QINF**2*0.5
WRITE(6,11)
DO 10 K=1,KMAX
DO 6 J=1,JMAX
EN=O(I(J,K)+O(I(J,K)
PH=O(I(J,K)+O(I(J,K)
V=O(I(J,K)+O(I(J,K)
P=GAMMI*EN-RHD*0.5*(U+V*V)
SS=O(I(J,K)+O(I(J,K)
PER=ABS(T-H*INF)+200*O/H*INF
IF(PERR.GT.PERRMX) PERRMX=PERR
RMS=RMS+PERR*2
SL(J)=SORT(U+V*V)/SS
6 CONTINUE
DO 11 J=3,JMAX
IF((SL(J).LE.1.0.AND.SL(J-1).GE.1.0).OR.(SL(J).GT.1.0.AND.SL(J-1)
C...LE.1.0)160 TO 12
12 JSL=J
JSL=JSL-1
CDF=(1.0-SL(JSL))-(SL(JSL)-SL(JSLM)),
XSL=X(JSLM,K)+CDF*(X(JSL,K)-X(JSLM,K))
YSL=Y(JSLM,K)+CDF*(Y(JSL,K)-Y(JSLM,K))
XSL=X(JSL,K)
WRITE(6,10) XSL,YSL
11 CONTINUE
RMS=O
RMS=O
RMS=O
WRITE(6,107) PERRMX,RMS
RETURN
2 CONTINUE
C...OUTPUT E AND F CONSERVATIVE VARIABLES
DO 7 K=1,KMAX
DO 7 J=1,JMAX
CALL EFCON(J,K,1)
DO 8 M=1,4

```

```

SUBROUTINE RMS
COMMON/COM1/JMAX,KMAX,JK,KX,KH,XMACH,ALPHA,GAM,GAMM1,CN,DT,SMU,IPRT,
C...CHDR,COR,NCB,NCC,AA,HB,DREGA,NU,NI,TAU,ITER,ENT,PTORT,PINF,
C...DINE,LINE,JCS,TN,CLUS,PT,HORN,ROSE,NCASE,APUNCH
COMMON /COM2/ I(25,20),Y(25,20),X(25,20),Z(25,20),
C...XEY(25,20),Z(25,20),
COMMON /COM3/ Q(25,20),EF(25,20),F(4),G(4),AB(4,4)
C...EQUATION
C...FORMULAE
DO 1 K=2,KM
DO 2 J=2,JK
CALL EFCON(J,K,1)
DO 2 N=2,N24
2 EF(J,N)=G(N)
C...CENTRAL DIFFERENCE E CONSERVATIVE VARIABLE
DO 1 N=1,4
DO 1 J=2,JK
1 S(F)=F(NH1)+EF(J,N)-EF(J-1,N)11MH
C...ARRAY CONSERVATIVE VARIABLES AND DIFFERENCE. ADD TO PREVIOUS 5
DO 3 J=2,JK
DO 4 K=2,KMAX
CALL EFCON(J,K,2)
DO 4 N=1,COM(2)
4 EF(K,N)=C(N)
C...CENTRAL DIFFERENCE F CONSERVATIVE VARIABLE
DO 3 K=2,KM
S(J,K,N)=S(J,K,N)-((F(K,1,N)-EF(K-1,N))11MH
3 CONTINUE
RETURN
END
SUBROUTINE SHOCK
COMMON/COM1/JMAX,KMAX,JK,KX,KH,XMACH,ALPHA,GAM,GAMM1,CN,DT,SMU,IPRT,
C...CHDR,COR,NCB,NCC,AA,HB,DREGA,NU,NI,TAU,ITER,ENT,PTORT,PINF,
C...DINE,LINE,JCS,TN,CLUS,PT,HORN,ROSE,NCASE,APUNCH
COMMON /COM2/ I(25,20),Y(25,20),X(25,20),Z(25,20),
C...XEY(25,20),Z(25,20),
COMMON /COM3/ Q(25,20),EF(25,20),F(4),G(4),AB(4,4)
DIMENSION PETAL(25),R(25,2),U(25,3),V(25,3),UETA(25),
C...PETAL(25),R(25,2),
PPS=O
C...COMPUTE THE FLOW VARIABLES ONE MESH INTERVAL BELOW SHOCK
QSEM=O
JMH=JMAX-2
ZK=KMAX-1
DO 3 K=1,3
DO 3 J=1,JMAX
KK=KMAX-3*JK
Z1=O/OL(J,K,1)
R(J,K)=O(I(J,K,1)+O(I(J,K,2))+
U(J,K)=O(I(J,K,2))+
V(J,K)=O(I(J,K,2))+

```

```

SUBROUTINE SHOCK
COMMON/COM1/JMAX,KMAX,JK,KX,KH,XMACH,ALPHA,GAM,GAMM1,CN,DT,SMU,IPRT,
C...CHDR,COR,NCB,NCC,AA,HB,DREGA,NU,NI,TAU,ITER,ENT,PTORT,PINF,
C...DINE,LINE,JCS,TN,CLUS,PT,HORN,ROSE,NCASE,APUNCH
COMMON /COM2/ I(25,20),Y(25,20),X(25,20),Z(25,20),
C...XEY(25,20),Z(25,20),
COMMON /COM3/ Q(25,20),EF(25,20),F(4),G(4),AB(4,4)
DIMENSION PETAL(25),R(25,2),U(25,3),V(25,3),UETA(25),
C...PETAL(25),R(25,2),
PPS=O
C...COMPUTE THE FLOW VARIABLES ONE MESH INTERVAL BELOW SHOCK
QSEM=O
JMH=JMAX-2
ZK=KMAX-1
DO 3 K=1,3
DO 3 J=1,JMAX
KK=KMAX-3*JK
Z1=O/OL(J,K,1)
R(J,K)=O(I(J,K,1)+O(I(J,K,2))+
U(J,K)=O(I(J,K,2))+
V(J,K)=O(I(J,K,2))+

```









75 GEOM 76 GEOM 77 GEOM 78 GEOM 79 GEOM 80 GEOM 81 GEOM 82 GEOM 83 GEOM 84 GEOM 85 GEOM 86 GEOM 87 GEOM 88 GEOM 89 GEOM 90 GEOM 91 GEOM 92 GEOM 93 GEOM 94 GEOM 95 GEOM 96 GEOM 97 GEOM 98 GEOM 99 GEOM 100 GEOM 101 GEOM 102 GEOM 103 GEOM 104 GEOM 105 GEOM 106 GEOM 107 GEOM 108 GEOM 109 GEOM 110 GEOM 111 GEOM 112 GEOM 113 GEOM 114 GEOM 115 GEOM 116 GEOM 117 GEOM 118 GEOM 119 GEOM 120 GEOM 121 GEOM 122

THETA=90  
R1=PNDSZ  
C.....PERFORM AN INTEGRATION FROM 90 TO 260 DEGREES  
C  
DO 15 I=1,IMAX  
C.....PREDICTOR  
R=R1+DELTA/RADI\*(GIRL\*XX)  
THETA=THETA+DELTA  
XXX=THETA/RADI  
C.....CORRECTOR  
R=R1+0.5\*DELTA/RADI\*(GIRL\*XX)+G(R,XXX)  
DROTH=GR\*(XXX)  
R1=P  
IF(THETA.LT.190.160 TO 15  
ZSTA(J)=1.\*K\*CDOS(1270.-THETA)/RADI  
PZ(J)=R\*SN(127.-THETA)/RADI  
DPOZ(J)=(-ORDI\*H\*CS(XXX)+R\*SIN(XXX))/(-ORDI\*H\*SIN(XXX))-R\*CDOS(XXX)  
J=J+1  
15 CONTINUE  
RETURN  
C.....BODY SHAPE TABLE SUPPLIED BY USER  
C  
20 CONTINUE  
J=1  
DX2=0.0  
DR2=0.0  
NBOIM=NBOI-1  
DO 25 I=1,NBOIM  
DX1=DX2  
DR1=DR2  
DX2=XRDO(I)+1.-XBD(I)  
DR2=YBOD(I)+1.-YBOD(I)  
IF(XBOD(I).GT.1.0) GO TO 25  
ZSTA(J)=1.-XBD(I)  
RZ(J)=YBOD(I)  
C3=SBRT(DR2\*DR2+DX2\*DX2)  
L2=SBRT(DR2\*DR2+DX2\*DX2)  
DFZ(J)=(-GR1\*DFZ(I)+UR2\*DFZ(I)/DX2)/(L1+DFZ)  
J=J+1  
25 CONTINUE  
ZSTA(J)=1.-XUD(NBOD)  
SZ(J)=YEG(NBOD)  
DROZ(J)=(-DK2\*(1.-0.2\*DI1)/DK2-DR1\*0.2/DX1)/(L1+DK)  
PI=TURN  
END

EIGENM 86 GEOM 2  
EIGENM 87 GEOM 3  
EIGENM 88 GEOM 4  
EIGENM 89 GEOM 5  
EIGENM 90 GEOM 6  
EIGENM 91 GEOM 7  
EIGENM 92 GEOM 8  
EIGENM 93 GEOM 9  
EIGENM 94 GEOM 10  
EIGENM 95 GEOM 11  
GEOM 12  
GEOM 13  
GEOM 14  
GEOM 15  
GEOM 16  
GEOM 17  
GEOM 18  
GEOM 19  
GEOM 20  
GEOM 21  
GEOM 22  
GEOM 23  
GEOM 24  
GEOM 25  
GEOM 26  
GEOM 27  
GEOM 28  
GEOM 29  
GEOM 30  
GEOM 31  
GEOM 32  
GEOM 33  
GEOM 34  
GEOM 35  
GEOM 36  
GEOM 37  
GEOM 38  
GEOM 39  
GEOM 40  
GEOM 41  
GEOM 42  
GEOM 43  
GEOM 44  
GEOM 45  
GEOM 46  
GEOM 47  
GEOM 48  
GEOM 49  
GEOM 50  
GEOM 51  
GEOM 52  
GEOM 53  
GEOM 54  
GEOM 55  
GEOM 56  
GEOM 57  
GEOM 58  
GEOM 59  
GEOM 60  
GEOM 61  
GEOM 62  
GEOM 63  
GEOM 64  
GEOM 65  
GEOM 66  
GEOM 67  
GEOM 68  
GEOM 69  
GEOM 70  
GEOM 71  
GEOM 72  
GEOM 73  
GEOM 74

ORDI=DZ/DI  
ICONST(11)=100\*ICONST(11)  
ICONST(12)=100\*ICONST(12)  
CONTINUE  
RETURN  
103 FORMAT(10,4)NEGATIVE SIGMA-BAR-1 IN EIGENM INDICATES  
104 FORMAT(10,4)NEGATIVE SIGMA-BAR-2 IN EIGENM INDICATES  
END  
SUBROUTINE GEOM(RNDSZ,ANG,RZ,ORDZ,ZSTA,MR,RSD)  
DIMENSION ZSTA(20),ORD(200),RZ(200)  
COMMON /NUEDD/ XBD(100),YBOD(100),NBOD  
C.....FUNCTION DEFINITIONS  
F(A,B)=EXP(-ABS(A-RNDSZ)/H)  
F(A,B)=5\*A\*(1+SIN(12.\*B))-2.\*SQRT(1-(A)-E(A)-SIN(B)\*B)  
E(A,B)=ABS(A\*(1+0.5\*SIN(18)\*COS(B)+SORT(A\*\*2-1.)/((A\*\*2+COS(18)\*B\*\*2-1.)))  
C.....M=EO, J=C, I EQUATORIAL PLANE FOR A MAGNETIC PLANET  
C.....M=EO, J=C, I EQUATORIAL PLANE FOR A MAGNETIC PLANET  
C.....M=EO, J=C, I EQUATORIAL PLANE FOR A MAGNETIC PLANET  
IF(M.EQ.0)GO TO 10  
IF(1+LT.(C)) GO TO 20  
IF (H.LT.0.001) GO TO 30  
C.....THIS DETERMINES THE BODY SHAPE OF A NONMAGNETIC PLANET  
C  
IMAX=200  
PI=3.1415926535898  
FAD(1)=PI  
DELTA=ANG/FLOAT(IMAX)  
THETA=90  
M1=990  
C.....PERFORM AN INTEGRATION FROM 0 TO 170 DEGREES  
C  
ZSTA(1)=0.0  
RZ(1)=0.0  
XX=THETA/RADI  
DADZ(1)=F(I,XX)/R1  
J=2  
IMAXM1=IMAX-1  
DO 5 I=1,IMAXM1  
C.....PREDICTOR  
XX=THETA/RADI  
R=R1+DELTA/RADI\*(FIR,XX)  
THETA=THETA+DELTA  
XXX=THETA/RADI  
R=R1+0.5\*DELTA/RADI\*(FIR,XX)+F(R,XXX)  
DROTH=GR\*(XXX)  
R1=P  
ZSTA(J)=1.+K\*CDOS(110.-THETA)/RADI  
DPOZ(J)=R\*SN(110.-THETA)/RADI  
DROZ(J)=(-ORDI\*H\*CDOS(XXX)+R\*SIN(XXX))/(-ORDI\*H\*SIN(XXX))-R\*CDOS(XXX)  
J=J+1  
5 CONTINUE  
RETURN  
C  
C USE CYLINDRICAL BODY FOR HARD ALT. (0,0,1)  
C  
20 ZSTA(1)=0.0  
ZSTA(2)=0.0  
RZ(1)=0.0  
RZ(2)=0.0  
LPOZ(1)=0.0  
LPOZ(2)=0.0  
LPTURN=0  
LPTURN=0  
30 CONTINUE  
C  
C.....THIS DETERMINES THE BODY SHAPE OF A MAGNETIC PLANET  
C  
J=1  
ANG=ANG\*90.  
IMAX=200  
PI=3.1415926535898  
FAD(1)=PI  
DELTA=ANG/FLOAT(IMAX)

GEOM 2  
GEOM 3  
GEOM 4  
GEOM 5  
GEOM 6  
GEOM 7  
GEOM 8  
GEOM 9  
GEOM 10  
GEOM 11  
GEOM 12  
GEOM 13  
GEOM 14  
GEOM 15  
GEOM 16  
GEOM 17  
GEOM 18  
GEOM 19  
GEOM 20  
GEOM 21  
GEOM 22  
GEOM 23  
GEOM 24  
GEOM 25  
GEOM 26  
GEOM 27  
GEOM 28  
GEOM 29  
GEOM 30  
GEOM 31  
GEOM 32  
GEOM 33  
GEOM 34  
GEOM 35  
GEOM 36  
GEOM 37  
GEOM 38  
GEOM 39  
GEOM 40  
GEOM 41  
GEOM 42  
GEOM 43  
GEOM 44  
GEOM 45  
GEOM 46  
GEOM 47  
GEOM 48  
GEOM 49  
GEOM 50  
GEOM 51  
GEOM 52  
GEOM 53  
GEOM 54  
GEOM 55  
GEOM 56  
GEOM 57  
GEOM 58  
GEOM 59  
GEOM 60  
GEOM 61  
GEOM 62  
GEOM 63  
GEOM 64  
GEOM 65  
GEOM 66  
GEOM 67  
GEOM 68  
GEOM 69  
GEOM 70  
GEOM 71  
GEOM 72  
GEOM 73  
GEOM 74

SUBROUTINE GEOM(RNDSZ,ANG,RZ,ORDZ,ZSTA,MR,RSD)  
DIMENSION ZSTA(20),ORD(200),RZ(200)  
COMMON /NUEDD/ XBD(100),YBOD(100),NBOD  
C.....FUNCTION DEFINITIONS  
F(A,B)=EXP(-ABS(A-RNDSZ)/H)  
F(A,B)=5\*A\*(1+SIN(12.\*B))-2.\*SQRT(1-(A)-E(A)-SIN(B)\*B)  
E(A,B)=ABS(A\*(1+0.5\*SIN(18)\*COS(B)+SORT(A\*\*2-1.)/((A\*\*2+COS(18)\*B\*\*2-1.)))  
C.....M=EO, J=C, I EQUATORIAL PLANE FOR A MAGNETIC PLANET  
C.....M=EO, J=C, I EQUATORIAL PLANE FOR A MAGNETIC PLANET  
C.....M=EO, J=C, I EQUATORIAL PLANE FOR A MAGNETIC PLANET  
IF(M.EQ.0)GO TO 10  
IF(1+LT.(C)) GO TO 20  
IF (H.LT.0.001) GO TO 30  
C.....THIS DETERMINES THE BODY SHAPE OF A NONMAGNETIC PLANET  
C  
IMAX=200  
PI=3.1415926535898  
FAD(1)=PI  
DELTA=ANG/FLOAT(IMAX)  
THETA=90  
M1=990  
C.....PERFORM AN INTEGRATION FROM 0 TO 170 DEGREES  
C  
ZSTA(1)=0.0  
RZ(1)=0.0  
XX=THETA/RADI  
DADZ(1)=F(I,XX)/R1  
J=2  
IMAXM1=IMAX-1  
DO 5 I=1,IMAXM1  
C.....PREDICTOR  
XX=THETA/RADI  
R=R1+DELTA/RADI\*(FIR,XX)  
THETA=THETA+DELTA  
XXX=THETA/RADI  
R=R1+0.5\*DELTA/RADI\*(FIR,XX)+F(R,XXX)  
DROTH=GR\*(XXX)  
R1=P  
ZSTA(J)=1.+K\*CDOS(110.-THETA)/RADI  
DPOZ(J)=R\*SN(110.-THETA)/RADI  
DROZ(J)=(-ORDI\*H\*CDOS(XXX)+R\*SIN(XXX))/(-ORDI\*H\*SIN(XXX))-R\*CDOS(XXX)  
J=J+1  
5 CONTINUE  
RETURN  
C  
C USE CYLINDRICAL BODY FOR HARD ALT. (0,0,1)  
C  
20 ZSTA(1)=0.0  
ZSTA(2)=0.0  
RZ(1)=0.0  
RZ(2)=0.0  
LPOZ(1)=0.0  
LPOZ(2)=0.0  
LPTURN=0  
LPTURN=0  
30 CONTINUE  
C  
C.....THIS DETERMINES THE BODY SHAPE OF A MAGNETIC PLANET  
C  
J=1  
ANG=ANG\*90.  
IMAX=200  
PI=3.1415926535898  
FAD(1)=PI  
DELTA=ANG/FLOAT(IMAX)

GEOM 2  
GEOM 3  
GEOM 4  
GEOM 5  
GEOM 6  
GEOM 7  
GEOM 8  
GEOM 9  
GEOM 10  
GEOM 11  
GEOM 12  
GEOM 13  
GEOM 14  
GEOM 15  
GEOM 16  
GEOM 17  
GEOM 18  
GEOM 19  
GEOM 20  
GEOM 21  
GEOM 22  
GEOM 23  
GEOM 24  
GEOM 25  
GEOM 26  
GEOM 27  
GEOM 28  
GEOM 29  
GEOM 30  
GEOM 31  
GEOM 32  
GEOM 33  
GEOM 34  
GEOM 35  
GEOM 36  
GEOM 37  
GEOM 38  
GEOM 39  
GEOM 40  
GEOM 41  
GEOM 42  
GEOM 43  
GEOM 44  
GEOM 45  
GEOM 46  
GEOM 47  
GEOM 48  
GEOM 49  
GEOM 50  
GEOM 51  
GEOM 52  
GEOM 53  
GEOM 54  
GEOM 55  
GEOM 56  
GEOM 57  
GEOM 58  
GEOM 59  
GEOM 60  
GEOM 61  
GEOM 62  
GEOM 63  
GEOM 64  
GEOM 65  
GEOM 66  
GEOM 67  
GEOM 68  
GEOM 69  
GEOM 70  
GEOM 71  
GEOM 72  
GEOM 73  
GEOM 74

101



```

A=RBZ(K)-T*(R)BPH(K)-RBZ(K)
B=KPB(K)-T*(R)BPH(K)-RBZ(K)
C=KOB(K)-RBZ(K)
D=-(ROBZ(K)-RBZ(K))
E=-(ROBPH(K)-RBZ(K))
DTDZ(J,K)=A/C
DTDPH(J,K)=B/C
ACT(K)=D/C
RCT(K)=E/C
R=C*T*(R)K
X=R*SIN(PHI)
Y=R*CLS(PHI)
CONTINUE
CONTINUE
RETURN
END

SUBROUTINE GEMZ(K3)
LEVEL 2,ET,MP,EO,FO,GO,MO
COMMON/LARGE/ETEMP(4,24,41),EJ(4,24,41),
FO(4,24,41),GO(4,24,41),MO(4,24,41)
LEVEL 2,RHO,P,U,V,W,ROB,ROBZ,VINE,VINE,MINF,ROBPH,Rd,KBZ,
RBPB,DTDP,
* BCT,DTDZ,DTDR,ACT,ICONST,GAM,CONST,NREGDN,RS,RSZ,RSPL,RSZ,RSZT,
COMMON /PVARR/RHO(24,41), P(24,41), U(24,41), V(24,41),
1) ,
ROR(41), ROBZ(41), VINF(41), WINF(41),
* KOBPH(41), RBZ(41), RBZ(41), RBZ(41), RBPH(41),
* DDPH(24,41), BCT(41), DTDZ(24,41), DTDR(41), ACT(41),
* ICONST(50), GAM(23), CONST(50), NREGDN, RS(41),
* RSZ(41), RSPHI(41), RST(41), RST(41), RST(41), RSPHI(41),
COMMON /IDVAR/RK,ETA(41),PHI(41),DTIL(41),DTIL(41),DETA,PI(24)
COMMON/SVAR/RZ,
ZNU, PI, ALPHA, GAMMA, SIGMA, XNACH, XNACH, TAPL2,
TAPL2, DISK1, ALPH, DISK2, SIGM, XNACH, XNACH, TAPL,
DZDPH, ZM, TMU, TML, TML, TML, TML, TML, TML, TML,
* TPL, RZ, BZ, NPH1, NPH1, NPH1, NPH1, NPH1, NPH1, NPH1,
* NPH1, NPH1, NPH1, NPH1, NPH1, NPH1, NPH1, NPH1, NPH1,
* NT, NTL, NT2, NT3, NTL, NTL, NTL, NTL, NTL, NTL, NTL,
* PHF, METHOD, LAG, NBC, PINF, RHOIN, UINF,
* OINF,GASCON,NREAL,NPLNCH
INTEGR,DISK1,DISK2,TAPE1,TAPE2
DC J K=1,NPH12
PHI=PHI(K)
GO TO (3,2),K3
CONTINUE
ROE(K)=RSZ(K)
PORPH(K)=RSPHI(K)
GO TO 4
CONTINUE
RUB(K)=RST(K)
PORB(K)=RSTZ(K)
PORPH(K)=RSPHI(K)
CONTINUE
RETURN
END

SUBROUTINE GEM3(K7,PHE,NPHI,Z,RBZ,RBPB,IPRNT)
COMMON/JOE/ZLL,CFL,CF2,ZLF,ZTRAN,DZTRAN
COMMON /ACCT/NREAL(51)
COMMON /NIN/TV,AMACH,GAMF,KM2,PINF,RIINF,VLINF,P9UI(20,3),
* RSZ90(20,3),V90(20,3),V90(20,3),V90(20,3),RSZ90(3),
LEVEL 2, RB,RBPB,RBZ
DIMENSION RB(41),RBPB(41),RBZ(41),PHIP(41)
DIMENSION ZSTA(200),DRU(200),RZ(200)
C.....CONSTANTS
C
IF(K7.NE.0) GO TO 1
CFZ=1.0
ANG=99.5
NST=J
MHPD
RHOSE=1.
CALL GEUM(HOUSE,ANG,R,Z,DRDE,ZSTA,M,R90)
RETURN
C.....FIND CORRECT Z INTERVAL
C
1 CONTINUE

```

```

37 INITA 37
INITA 38
INITA 39
INITA 40
INITA 41
INITA 42
INITA 43
INITA 44
INITA 45
INITA 46
INITA 47
INITA 48
INITA 49
INITA 50
INITA 51
INITA 52
INITA 53
INITA 54
INITA 55
INITA 56
INITA 57
INITA 58
INITA 59
INITA 60
INITA 61
INITA 62
INITA 63
INITA 64
INITA 65
INITA 66
INITA 67
INITA 68
INITA 69
INITA 70
INITA 71
INITA 72
INITA 73
INITA 74
INITA 75
INITA 76
INITA 77
INITA 78
INITA 79
INITA 80
INITA 81
INITA 82
INITA 83
INITA 84
INITA 85
INITA 86
INITA 87
INITA 88
INITA 89
INITA 90
INITA 91
INITA 92
INITA 93
INITA 94
INITA 95
INITA 96
INITA 97
INITA 98
INITA 99
INITA 100
INITA 101
INITA 102
INITA 103
INITA 104
INITA 105
INITA 106
INITA 107
INITA 108
INITA 109
INITA 110
INITA 111
INITA 112
INITA 113
INITA 114
INITA 115
INITA 116
INITA 117
INITA 118
INITA 119
INITA 120

DETA=PHI/FLOAT(NIPH1)
DPM1=DETA
DT=1.0/DETA
D1=D1*DT
D2=D2*DT
D3=D3*DT
D4=D4*DT
D5=D5*DT
D6=D6*DT
D7=D7*DT
D8=D8*DT
D9=D9*DT
D10=D10*DT
D11=D11*DT
D12=D12*DT
D13=D13*DT
D14=D14*DT
D15=D15*DT
D16=D16*DT
D17=D17*DT
D18=D18*DT
D19=D19*DT
D20=D20*DT
D21=D21*DT
D22=D22*DT
D23=D23*DT
D24=D24*DT
D25=D25*DT
D26=D26*DT
D27=D27*DT
D28=D28*DT
D29=D29*DT
D30=D30*DT
D31=D31*DT
D32=D32*DT
D33=D33*DT
D34=D34*DT
D35=D35*DT
D36=D36*DT
D37=D37*DT
D38=D38*DT
D39=D39*DT
D40=D40*DT
D41=D41*DT
D42=D42*DT
D43=D43*DT
D44=D44*DT
D45=D45*DT
D46=D46*DT
D47=D47*DT
D48=D48*DT
D49=D49*DT
D50=D50*DT
D51=D51*DT
D52=D52*DT
D53=D53*DT
D54=D54*DT
D55=D55*DT
D56=D56*DT
D57=D57*DT
D58=D58*DT
D59=D59*DT
D60=D60*DT
D61=D61*DT
D62=D62*DT
D63=D63*DT
D64=D64*DT
D65=D65*DT
D66=D66*DT
D67=D67*DT
D68=D68*DT
D69=D69*DT
D70=D70*DT
D71=D71*DT
D72=D72*DT
D73=D73*DT
D74=D74*DT
D75=D75*DT
D76=D76*DT
D77=D77*DT
D78=D78*DT
D79=D79*DT
D80=D80*DT
D81=D81*DT
D82=D82*DT
D83=D83*DT
D84=D84*DT
D85=D85*DT
D86=D86*DT
D87=D87*DT
D88=D88*DT
D89=D89*DT
D90=D90*DT
D91=D91*DT
D92=D92*DT
D93=D93*DT
D94=D94*DT
D95=D95*DT
D96=D96*DT
D97=D97*DT
D98=D98*DT
D99=D99*DT
D100=D100*DT
D101=D101*DT
D102=D102*DT
D103=D103*DT
D104=D104*DT
D105=D105*DT
D106=D106*DT
D107=D107*DT
D108=D108*DT
D109=D109*DT
D110=D110*DT
D111=D111*DT
D112=D112*DT
D113=D113*DT
D114=D114*DT
D115=D115*DT
D116=D116*DT
D117=D117*DT
D118=D118*DT
D119=D119*DT
D120=D120*DT

38 CONST(2)=COS(ALPH)
39 UINF=QINF*CONST(2)
40 DD 3 K=2,NPH1
41 PHI=PHI*(K)
42 VINF(K)=QINF*CONST(1)*COS(PHI)
43 WINF(K)=QINF*CONST(1)*SIN(PHI)
44 CONTINUE
45 DD 26 J=3,NTZ
46 P(J,K)=P0(J-2,K-2)
47 RHO(J,K)=RH0(J-2,K-2)
48 U(J,K)=U0(J-2,K-2)
49 V(J,K)=V0(J-2,K-2)
50 W(J,K)=W0(J-2,K-2)
51 CONTINUE
52 DD 29 K=3,NPH1
53 PS(K)=P50(K-2)
54 RSZ(K)=RSZ0(K-2)
55 RSPHI(K)=RSPHI0(K-2)
56 ZINT=ZC
57 DD 25 K=3,2
58 M=6-K
59 I=NPH1+K
60 N=NPH1-K
61 PS(K)=RSZ(K)
62 RSZ(K)=RSZ(K)
63 RSPHI(K)=RSPHI(K)
64 RSZ(I)=RSZ(I)
65 RSPHI(I)=RSPHI(I)
66 RSPHI(I)=RSPHI(I)
67 RSPHI(I)=RSPHI(I)
68 CONTINUE
69 WRITE TAPE - INITIAL DATA AND BODY SHAPE
70 ZM=P(3,3)/ABS(RHO(3,3))*GAMMA
71 ZM=ABS(ZM)
72 DD 3P K=3,NPH1
73 SE(K)=P(3,K)/ABS(RHO(3,K))*SAMMA
74 SE(K)=ABS(SE(K))
75 CONTINUE
76 S(2)=S(4)/(S(1)+S(3))
77 S(NPH1)=S(NPH1)
78 CALL GEOM(1,P,HP,NPH1,Z,RP,RBZ,KBPH,IPRNT)
79 RETURN
80
81
82
83
84
85
86
87
88
89
90
91
92
93
94
95
96
97
98
99
100
101
102
103
104
105
106
107
108
109
110
111
112
113
114
115
116
117
118
119
120

SUBROUTINE UCUNT(K1)
LEVEL=2,ITL=AP,3,2,2,GO,HO
COMLEN=1,ARG=1,7,RP(4,2,6,41),E2(4,2,4,43),
* FC(4,2,4,41)
LEVEL=2, RHO=2,4,5, V=2,8,8,9, VINF=1,8,8,9, V, DTDPH,
* BCT, DTDP, DTOR, ACT, ICNST, GAM, CUNST, RRCOND, RS, RZ, RZ, PH, RZ, RZ,
* RSPHI
COMMON /VARS/ RHO(2,4,41), P(2,4,41), U(2,4,41), W(2,4,41),
* RSPHI(41), KOSZ(41), VINF(41), WINF(41),
* KOPPH(41), RBZ(41), RBZ(41), RBP(41),
* OTDPH(2,4,41), BCT(41), OTDP(2,4,41), DTOR(41), ACT(41),
* ICNST(2,4), RRCOND,
* RSZ(41), RSPHI(41), RSPHI(41), RSPHI(41), RSPHI(41),
* COPMUN/IDVARS/RK, ZTA(41), PHIP(41), DTIL(41), DTIL(41), DTIL(41),
* COMMUN/SVARS/TAPE, ZENCL, PI, ALPHA, GAMMA, SIGMA, KMACH, LABEL,
* ZM=ABS(ZM), ZM=ABS(ZM), ZM=ABS(ZM), ZM=ABS(ZM), ZM=ABS(ZM),
* DTDPH, ZM, TM=U, TM=U, TM=U, TM=U, TM=U, TM=U,
* TIMH, RZ, RZ, RZ, RZ, RZ, RZ, RZ, RZ, RZ, RZ, RZ, RZ, RZ, RZ, RZ,
* NPH1, NPH1, NPH1, NPH1, NPH1, NPH1, NPH1, NPH1, NPH1, NPH1,
* NT, NT, NT, NT, NT, NT, NT, NT, NT, NT, NT, NT, NT, NT,
* PHIP, METHO, LAG, RBC, PINF, RMDIN, UINF,
* QINF, GASCUN, NK, CAL, NPLANCH
* INI, GEL, DISK, DISK, TAPE,
* COMMUN/REKOD/WR, RBC, CUM, OR, CUM, WR, MK, P, P, PH, WR, WR, WR, WR, NTAL
* COMMUN/REKOD/WR, RBC, CUM, OR, CUM, WR, MK, P, P, PH, WR, WR, WR, WR, NTAL
* COMMUN/ALCONT/NFECA(1)
* COMMUN/CELLSTR/RJAX(1,2,4), TIK(2,4), ITIL(2,4)
* DIMENSION I(4), J(4), K(4), L(4)
* CLUMPON /LUCON/NTEST(1), NCRITA, NOSTAY(4), NCRITB(1,3), NSWCH(1,3), IN(1,3,2)
* IN(1,3,4)
* GO TO (4, 5, 6) II
CONTINUE
DD 3 K=2,NPH1
DD 3 J=3,NTZ
WRITE TAPE, I, J, K, L
C...CUDJ, CONS, M, Z, TIVE, VARI, LABELS, I, J, K, L, M, N, O

INITA 121
INITA 122
INITA 123
INITA 124
INITA 125
INITA 126
INITA 127
INITA 128
INITA 129
INITA 130
INITA 131
INITA 132
INITA 133
INITA 134
INITA 135
INITA 136
INITA 137
INITA 138
INITA 139
INITA 140
INITA 141
INITA 142
INITA 143
INITA 144
INITA 145
INITA 146
INITA 147
INITA 148
INITA 149
INITA 150
INITA 151
INITA 152
INITA 153
INITA 154
INITA 155
INITA 156
INITA 157
INITA 158
INITA 159
INITA 160
INITA 161
INITA 162
INITA 163
INITA 164
INITA 165

CONST(1)=COS(ALPH)
CONST(2)=SIN(ALPH)
CONST(3)=COS(ALPH)
CONST(4)=SIN(ALPH)
CONST(5)=COS(ALPH)
CONST(6)=SIN(ALPH)
CONST(7)=COS(ALPH)
CONST(8)=SIN(ALPH)
CONST(9)=COS(ALPH)
CONST(10)=SIN(ALPH)
CONST(11)=COS(ALPH)
CONST(12)=SIN(ALPH)
CONST(13)=COS(ALPH)
CONST(14)=SIN(ALPH)
CONST(15)=COS(ALPH)
CONST(16)=SIN(ALPH)
CONST(17)=COS(ALPH)
CONST(18)=SIN(ALPH)
CONST(19)=COS(ALPH)
CONST(20)=SIN(ALPH)
CONST(21)=COS(ALPH)
CONST(22)=SIN(ALPH)
CONST(23)=COS(ALPH)
CONST(24)=SIN(ALPH)
CONST(25)=COS(ALPH)
CONST(26)=SIN(ALPH)
CONST(27)=COS(ALPH)
CONST(28)=SIN(ALPH)
CONST(29)=COS(ALPH)
CONST(30)=SIN(ALPH)
CONST(31)=COS(ALPH)
CONST(32)=SIN(ALPH)
CONST(33)=COS(ALPH)
CONST(34)=SIN(ALPH)
CONST(35)=COS(ALPH)
CONST(36)=SIN(ALPH)
CONST(37)=COS(ALPH)
CONST(38)=SIN(ALPH)
CONST(39)=COS(ALPH)
CONST(40)=SIN(ALPH)
CONST(41)=COS(ALPH)
CONST(42)=SIN(ALPH)
CONST(43)=COS(ALPH)
CONST(44)=SIN(ALPH)
CONST(45)=COS(ALPH)
CONST(46)=SIN(ALPH)
CONST(47)=COS(ALPH)
CONST(48)=SIN(ALPH)
CONST(49)=COS(ALPH)
CONST(50)=SIN(ALPH)
CONST(51)=COS(ALPH)
CONST(52)=SIN(ALPH)
CONST(53)=COS(ALPH)
CONST(54)=SIN(ALPH)
CONST(55)=COS(ALPH)
CONST(56)=SIN(ALPH)
CONST(57)=COS(ALPH)
CONST(58)=SIN(ALPH)
CONST(59)=COS(ALPH)
CONST(60)=SIN(ALPH)
CONST(61)=COS(ALPH)
CONST(62)=SIN(ALPH)
CONST(63)=COS(ALPH)
CONST(64)=SIN(ALPH)
CONST(65)=COS(ALPH)
CONST(66)=SIN(ALPH)
CONST(67)=COS(ALPH)
CONST(68)=SIN(ALPH)
CONST(69)=COS(ALPH)
CONST(70)=SIN(ALPH)
CONST(71)=COS(ALPH)
CONST(72)=SIN(ALPH)
CONST(73)=COS(ALPH)
CONST(74)=SIN(ALPH)
CONST(75)=COS(ALPH)
CONST(76)=SIN(ALPH)
CONST(77)=COS(ALPH)
CONST(78)=SIN(ALPH)
CONST(79)=COS(ALPH)
CONST(80)=SIN(ALPH)
CONST(81)=COS(ALPH)
CONST(82)=SIN(ALPH)
CONST(83)=COS(ALPH)
CONST(84)=SIN(ALPH)
CONST(85)=COS(ALPH)
CONST(86)=SIN(ALPH)
CONST(87)=COS(ALPH)
CONST(88)=SIN(ALPH)
CONST(89)=COS(ALPH)
CONST(90)=SIN(ALPH)
CONST(91)=COS(ALPH)
CONST(92)=SIN(ALPH)
CONST(93)=COS(ALPH)
CONST(94)=SIN(ALPH)
CONST(95)=COS(ALPH)
CONST(96)=SIN(ALPH)
CONST(97)=COS(ALPH)
CONST(98)=SIN(ALPH)
CONST(99)=COS(ALPH)
CONST(100)=SIN(ALPH)
CONST(101)=COS(ALPH)
CONST(102)=SIN(ALPH)
CONST(103)=COS(ALPH)
CONST(104)=SIN(ALPH)
CONST(105)=COS(ALPH)
CONST(106)=SIN(ALPH)
CONST(107)=COS(ALPH)
CONST(108)=SIN(ALPH)
CONST(109)=COS(ALPH)
CONST(110)=SIN(ALPH)
CONST(111)=COS(ALPH)
CONST(112)=SIN(ALPH)
CONST(113)=COS(ALPH)
CONST(114)=SIN(ALPH)
CONST(115)=COS(ALPH)
CONST(116)=SIN(ALPH)
CONST(117)=COS(ALPH)
CONST(118)=SIN(ALPH)
CONST(119)=COS(ALPH)
CONST(120)=SIN(ALPH)

30 CONTINUE
31 WRITE TAPE, I, J, K, L
32 GAMMA=1.0/(GAMMA+1.0)
33 AA=1.0+GAMMA/(1.0+GAMMA**2)
34 BB=AA-1.0
35 PINF=1.0/AA**CAR(3)
36 HCIN=1.0/(1.0+AA**GAM(4))
37 UINF=SQRT(PB/AA)
38 CONST(1)=SIN(ALPH)

```

```

DO 20 N=1,4
  O=(N+J,K)=F(N)
  F=(N+J,K)=F(N)
  G=(N+J,K)=G(N)
  H=(N+J,K)=H(N)
  CONTINUE
  GO TO 3
3
  CONTINUE
  DO 5 N=1,4
  IF(J+Q=NT2) GO TO 30
  GO TO 31
30
  ETEMP(J,K)=(N)
  F(J,K)=F(N)
  G(J,K)=G(N)
  H(J,K)=H(N)
  CONTINUE
  RETUR
2
  CONTINUE
  DO 5 N=1,4
  C=CC-CCS; CONSERVATIVE VARIABLES AT N+1 TILDE
  IF(J+Q=NT2) GO TO 30
  GO TO 31
30
  ETEMP AT BODY AND SHOCK
  32
  CONTINUE
  F(J,K)=F(N)
  G(J,K)=G(N)
  H(J,K)=H(N)
  CONTINUE
  5
  CONTINUE
  2
  CONTINUE
  C=CC-CCS; CONSERVATIVE VARIABLES--PERFECT GAS
  DO 1 K=1,NPHI
  DD 1 J=1,NT2
  A=ETEMP(J,K)
  B=LTEMP(J,K)
  C=LTEMP(J,K)
  D=ETEMP(J,K)
  PE=9/A
  VIJ,K)=C/A
  VIJ,K)=D/A
  PL=B5+2*4.0*AA*CC
  IF(ED) 7,8,9
  7
  CONTINUE
  8
  CONTINUE
  VIJ,K)=(-RB*SRRT(DD))/(Z*G*AA)
  PHD(J,K)=A/VIJ,K)
  FIJ,K)=H(J,K)+(1.0-VIJ,K)**2-VIJ,K)**2
  CONTINUE
  1
  RETURN
  END
SUPROUTINE OUTPIM
  LEVEL 2, ETAP, S, F, G, H
  CEMP, JN, LARG, ETEMP(4,24,41), ED(4,24,41),
  F(4,24,41), G(4,24,41), H(4,24,41)
  LEVEL 2, KH0, P, U, V, W, RO, ROZ, RVIN, F, W, IN, F, R, U, B, P, R, B, KBZ, R, B, P, M, D, T, D, P,
  BCT, DT, D, D, ACT, ICUNST, GA, CUNST, NRECON, RS, MSZ, A, S, P, H, I, K, S, T, R, S, Z, I,
  KSPHIT
  COMMON /PVAR3/ R=DDI(2,41), P(2,4,41), U(2,4,41), V(2,4,41), W(2,4,41)
  RDB(41), ROBZ(41), VINF(41), WINF(41)
  RDBP(41), RBZ(41), RBZ(41), RBZ(41), RBPH(41)
  GTPD(2,4,41), PCT(41), DD(2,4,41), DTDK(41), ACT(41)
  ICUNST(20), GAM(20), CONST(53), ANLEGON, NS(41)
  KST(41), KSPHIT(41), RST(41), RSZT(41), RSPHIT(41)
  COMMON /IDVAB/ KK, ETA(41), PHIP(41), DTIL(41), DTILE(41), DTI(41), DTI(24)
  COMMON /SVAB/ T, Z, PHI, DT, Z, JPHI, Z, ZINT
  ZENG, PI, ALPHA, GAMMA, SIGMA, AMACH, TAPEL
  TAPE2, DISKA, ALPH, DISK2, SIGM, NPKN, DZOT
  GZUPH, ZR, TMU, TMLD, TM, TML, TTM
  TML, ZR, BZ, NPHI, NIT, KPHI, NITER
  NPHI, NP41, NPHI2, NPHI3, NPHI4, NPHI5, NPHI6
  NT, NTL, NIT2, NIT3, PHIF, NCDME, RADJ
  PHF, METHUD, LAG, NMC, PINF, KNOIN, VINF
  GINT, GASCON, NRE4, NPNUNCH
  JN1, G, D, S, D, I, S, K, E, TAPE2
  COMMON /NTRD/ ST(41,2,41), ZFLD, ITPRIB, ITPRFF, NCA3, NTDSDS
  COMMON /CLSTR/ N(41,2,41), TXI(24), TXIT(24)
  COMMON /ORST/ ZFLD, NRECON, ZEN, NRECON, ZADU
  COMMON /CONTR/ KYCON, YCON(20), KCON, RCON(20), XC(2,4), XOC(2), YC(20,10),
  YI(20), ZI(4), XJ(20,100)
  COMMON /BLCNT/ THETA(20), RP(20,25)
  COMMON /VCOMP/ V(12,2,100), VY(2,2), VJ(2)
  COMMON /VCOMP/ V(12,2,100), VY(2,2), VJ(2)
  COMMON /SHOCKS/ ORSDX(100), ADST(150)
  IF (NEN) GO TO C) WRITE(6,61)
  NZEN=NZENE+1

```



SHOCKM 58  
SHOCKM 59  
SHOCKM 60  
SHOCKM 61  
SHOCKM 62  
SHOCKM 63  
SHOCKM 64  
SHOCKM 65  
SHOCKM 66  
SHOCKM 67  
SHOCKM 68  
SHOCKM 69  
SHOCKM 70  
SHOCKM 71  
SHOCKM 72  
SHOCKM 73  
SHOCKM 74  
SHOCKM 75  
SHOCKM 76  
SHOCKM 77  
SHOCKM 78  
SHOCKM 79  
SHOCKM 80  
SHOCKM 81  
SHOCKM 82  
SHOCKM 83  
SHOCKM 84  
SHOCKM 85  
SHOCKM 86  
SHOCKM 87  
SHOCKM 88  
SHOCKM 89  
SHOCKM 90  
SHOCKM 91  
SHOCKM 92  
SHOCKM 93  
SHOCKM 94  
SHOCKM 95  
SHOCKM 96  
SHOCKM 97  
SHOCKM 98  
SHOCKM 99  
SHOCKM 100  
SHOCKM 101  
SHOCKM 102  
SHOCKM 103  
SHOCKM 104  
SHOCKM 105  
SHOCKM 106  
SHOCKM 107  
SHOCKM 108  
SHOCKM 109  
SHOCKM 110  
SHOCKM 111  
SHOCKM 112

```
M=C-K  
I=NPPI*K  
N=NPPI-K  
RSZ(K)=PSZT(M)  
RSZ(L)=RSZT(N)  
RSPH(K)=RSPH(M)  
RSPH(L)=RSPH(N)  
CONTINUE  
RETURN  
2 CONTINUE  
C..SHOCK CORR=LCIOR  
DU F K=3,NFHL  
RS(K)=RS(K)*.5*(RSZ(K)+RSZT(K))*DZ  
DU 9 K=1,2  
M=C-K  
I=NPPI*K  
N=NPPI-K  
RS(K)=PSZ(M)  
RS(L)=RSZ(N)  
CONTINUE  
DU 10 K=3,NFHL  
RSPH(K)=RSPH(M)  
RSPH(L)=RSPH(N)  
PS=PS/2*ZK  
FSPAT=PS/PI*NF  
UIT=UIT/LLD(PSRAT)  
PHRAT=PHR/PSRAT  
PSI=PSI(K)  
RSPH=RSRPH(K)  
FSPH=RSRPH(K)  
FACIL=VINF(K)-WINF(K)*RSPH  
FACIZ=UINF+UINF-UIT*UIT  
IF(FACTZ.LT.5)UIT=UIT  
RSZL=DRSDZ(ULT,RSPH,FACIL,FACIZ)  
RSZ(K)=RSZL  
ABART=ABAR(VINF(K),WINF(K),PSZL,RSPH,RHRAT)  
USF=USOINF,ABART,RSZL  
WSF=WS(VINF(K),ABART)  
WSP=WS(VINF(K),ABART,RSPH)  
PHO(INL,EO,3) RSPH=PHRAT*PHOIN  
PHO(INZ,K)=ROSE  
UINZ,K)=RUSF  
VINZ,K)=VSF  
W(INZ,K)=WSF  
CONTINUE  
DU 11 K=1,2  
M=C-K  
I=NPPI*K  
N=NPPI-K  
RSZ(K)=PSZ(M)  
RSZ(L)=RSZ(N)  
RSPH(K)=RSPH(M)  
RSPH(L)=RSPH(N)  
CONTINUE  
RETURN  
END
```

SETDAT 98  
SETDAT 99  
SETDAT 100  
SETDAT 101  
SETDAT 102  
SETDAT 103

```
SHOCKM 2  
SHOCKM 3  
SHOCKM 4  
SHOCKM 5  
SHOCKM 6  
SHOCKM 7  
SHOCKM 8  
SHOCKM 9  
SHOCKM 10  
SHOCKM 11  
SHOCKM 12  
SHOCKM 13  
SHOCKM 14  
SHOCKM 15  
SHOCKM 16  
SHOCKM 17  
SHOCKM 18  
SHOCKM 19  
SHOCKM 20  
SHOCKM 21  
SHOCKM 22  
SHOCKM 23  
SHOCKM 24  
SHOCKM 25  
SHOCKM 26  
SHOCKM 27  
SHOCKM 28  
SHOCKM 29  
SHOCKM 30  
SHOCKM 31  
SHOCKM 32  
SHOCKM 33  
SHOCKM 34  
SHOCKM 35  
SHOCKM 36  
SHOCKM 37  
SHOCKM 38  
SHOCKM 39  
SHOCKM 40  
SHOCKM 41  
SHOCKM 42  
SHOCKM 43  
SHOCKM 44  
SHOCKM 45  
SHOCKM 46  
SHOCKM 47  
SHOCKM 48  
SHOCKM 49  
SHOCKM 50  
SHOCKM 51  
SHOCKM 52  
SHOCKM 53  
SHOCKM 54  
SHOCKM 55  
SHOCKM 56  
SHOCKM 57
```

11 CONTINUE  
RETURN  
END

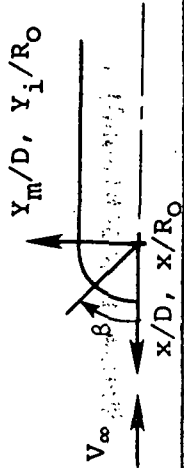
## REFERENCES

1. Spreiter, J. R. and Jones, W. P.: On the Effect of a Weak Interplanetary Magnetic Field on the Interaction Between the Solar Wind and the Geomagnetic Field. *Jour. Geophys. Res.*, vol. 68, 1963, pp. 3555-3564.
2. Spreiter, J. R., Alksne, A. Y., and Summers, A. L.: Hydromagnetic Flow Around the Magnetopause. *Plan. & Space Sci.*, vol. 14, 1966, pp. 223-253.
3. Spreiter, J. R., Alksne, A. Y., and Summers, A. L.: External Aerodynamics of the Magnetosphere. Physics of the Magnetosphere (Ed. R. L. Carovillano, J. F. McClay, and H. R. Radoski), D. Reidel Pub. Co., 1968, pp. 304-378 (also NASA TN 4482, 1968).
4. Spreiter, J. R. and Alksne, A. Y.: Plasma Flow Around the Magnetosphere. *Rev. Geophys.*, vol. 7, 1969, pp. 11-50.
5. Spreiter, J. R., Summers, A. L., and Rizzi, A. W.: Solar Wind Flow Past Nonmagnetic Planets - Venus and Mars. *Plan. & Space Sci.*, vol. 18, 1970, pp. 1281-1289.
6. Spreiter, J. R. and Alksne, A. Y.: Solar Wind Flow Past Objects in the Solar System. *Ann. Rev. Fluid Mech.*, vol. 2, pp. 313-354 (Ed. W. R. Sears, M. D. Van Dyke, and W. G. Vincenti), Annual Review, Inc., Palo Alto, CA, 1970.
7. Spreiter, J. R., March, C. M., Summers, A.: Hydromagnetic Aspects of Solar Wind Flow Past the Moon. *Cosmic Electrodynamics*, vol. 1, no. 1, 1970, pp. 5-50.
8. Spreiter, J. R. and Rizzi, A. W.: Aligned Magneto-hydrodynamics Solution for Solar Wind Flow Past the Earth's Magnetosphere. *Acta Astronautica*, vol. 1, 1974, pp. 15-35.
9. Briggs, B. R. and Spreiter, J. R.: Theoretical Determination of the Boundary and Distortion of the Geomagnetic Field in a Steady Solar Wind. NASA TR R-178, 1963.
10. Chapman, S. and Ferraro, V. C. A.: An Outline of a Theory of Magnetic Storms. *Terrest. Magnetism Atmospheric Elec.*, vol. 36, 1931, pp. 77-97, 171-186.
11. Midgley, J. E. and Davis, Jr., L.: Calculation by a Moment Technique of the Perturbation of the Geomagnetic Field by the Solar Wind. *Jour. Geophys. Res.*, vol. 68, 1963, pp. 5111-5123.
12. Mead, G. D. and Beard, D. B.: Shape of the Geomagnetic Field Solar Wind Boundary. *Jour. Geophys. Res.*, vol. 69, 1964, pp. 1169-1179.
13. Olsen, W. P.: The Shape of the Titled Magnetopause. *Jour. Geophys. Res.*, Vol. 74, 1969, pp. 5642-5651.

14. Beard, D. B.: The Interaction of the Terrestrial Magnetic Field with the Solar Corpuscular Radiation. Jour. Geophy. Res., vol. 65, 1960, pp. 3559-3568.
15. Spreiter, J. R. and Briggs, B. R.: Theoretical Determination of the Form of the Hollow Produced in the Solar Corpuscular Stream by Interaction with the Magnetic Dipole Field of the Earth. NASA TR R-120, 1961.
16. Spreiter, J. R. and Briggs, B. R.: Theoretical Determination of the Form of the Boundary of the Solar Corpuscular Stream Produced by Interaction with the Magnetic Dipole Field of the Earth. Jour. Geophys. Res., vol. 67, no. 1, Jan. 1962, pp. 37-51.
17. Spreiter, J. R. and Briggs, B. R.: On the Choice of Condition to Apply at the Boundary of the Geomagnetic Field in the Steady-State Chapman-Ferraro Problem. Jour. Geophys. Res., vol. 67, no. 7, Jul. 1962, pp. 2983-2985.
18. Davis, Jr., L. and Beard, D. B.: A Correction to the Approximate Condition for Locating the Boundary Between a Magnetic Field and a Plasma. Jour. Geophys. Res., vol. 67, 1962, pp. 4505-4507.
19. Spreiter, J. R. and Summers, A. L.: On Conditions Near the Neutral Points on the Magnetosphere Boundary. Plan. & Space Sci., vol. 15, 1967, pp. 787-798.
20. Kuhn, G. D., Goodwin, F. K., and Perkins, Jr., S. C.: User's Manual for Space-Shuttle Computer Programs. NEAR TR 110, Apr. 1976.
21. Chaussee, D. S., Stahara, S. S., and Spreiter, J. R.: Application of an Axisymmetric Implicit Blunt Body Procedure: Computation of Solar Wind Flows Past Terrestrial Planets. AIAA Paper No. 77-700, Jun. 1977.
22. Beam, R. M. and Warming, R. F.: An Implicit Finite-Difference Algorithm for Hyperbolic Systems in Conservation-Law Form. J. Comp. Phys., vol. 22, no. 1, Sep. 1976.
23. Kutler, P., Reinhardt, W. A., and Warming, R. F.: Multi-Shocked, Three-Dimensional Supersonic Flow Fields with Real Gas Effects. AIAA Journal, vol. 11, May 1973, pp. 657-664.
24. Kutler, P., Reinhardt, W. A., and Warming, R. F.: Numerical Computations of Multi-Shocked Three-Dimensional Supersonic Flow Fields with Real Gas Effects. AIAA Paper No. 72-702, Jun. 1972.
25. Chaussee, D. S., Holtz, T., and Kutler, P.: Inviscid Supersonic/Hypersonic Body Flow Fields and Aerodynamics from Shock-Capturing Technique Calculations. AIAA Paper No. 75-837, Jun. 1975.
26. MacCormack, R. W.: The Effect of Viscosity in Hypervelocity Impact Cratering. AIAA Paper No. 69-354, 1969.
27. Alksne, A. Y. and Webster, D. L.: Magnetic and Electric Fields in the Magnetosheath. Plan. & Space Sci., vol. 18, 1970, pp. 1203-1212.

28. Grad, H.: Reducible Problems in Magneto-Fluid Dynamics Steady Flows. Rev. Mod. Phys., vol. 32, 1960, pp. 830-847.
29. Imai, I.: On Flows of Conducting Fluids Past Bodies. Rev. Mod. Phys., vol. 32, 1960, pp. 992-999.
30. Inouye, M. and Lomax, H.: Comparison of Experimental and Numerical Results for the Flow of a Perfect Gas About Blunt-Nosed Bodies. NASA TD-1426, Sep. 1962.





$\beta$	MAGNETOPOUSE		IONOPOAUSE		IONOPOAUSE		IONOPOAUSE	
	$x/D$	$Y_m/D$	$H/R_0 = 0.01$	$H/R_0 = 0.1$	$H/R_0 = 0.2$	$H/R_0 = 0.5$	$x/R_0$	$Y_i/R_0$
$0^\circ$	1.0	0.0	1.0	1.0	1.0	1.0	1.0	0.0
$2^\circ$	0.9995	0.0349	0.9994	0.9995	0.9995	0.9995	0.9996	0.0349
$6^\circ$	0.9957	0.1046	0.9946	0.9954	0.9958	0.9966	0.9966	0.1047
$10^\circ$	0.9879	0.1742	0.9851	0.9870	0.9883	0.9906	0.9906	0.1747
$14^\circ$	0.9764	0.2434	0.9709	0.9745	0.9771	0.9814	0.9814	0.2447
$18^\circ$	0.9610	0.3122	0.9520	0.9580	0.9621	0.9692	0.9692	0.3149
$22^\circ$	0.9417	0.3805	0.9285	0.9373	0.9434	0.9537	0.9537	0.3853
$26^\circ$	0.9185	0.4480	0.9006	0.9125	0.9209	0.9349	0.9349	0.4560
$30^\circ$	0.8915	0.5147	0.8684	0.8838	0.8945	0.9127	0.9127	0.5269
$34^\circ$	0.8607	0.5805	0.8320	0.8510	0.8643	0.8869	0.8869	0.5982
$38^\circ$	0.8260	0.6453	0.7916	0.8143	0.8302	0.8573	0.8573	0.6698
$42^\circ$	0.7874	0.7089	0.7473	0.7738	0.7921	0.8238	0.8238	0.7418
$46^\circ$	0.7448	0.7713	0.6995	0.7293	0.7501	0.7862	0.7862	0.8141
$50^\circ$	0.6984	0.8323	0.6481	0.6811	0.7040	0.7441	0.7441	0.8868
$54^\circ$	0.6480	0.8919	0.5936	0.6292	0.6538	0.6974	0.6974	0.9598
$58^\circ$	0.5935	0.9499	0.5362	0.5736	0.5995	0.6456	0.6456	1.0332
$62^\circ$	0.5350	1.0062	0.4760	0.5144	0.5408	0.5885	0.5885	1.1068
$66^\circ$	0.4723	1.0609	0.4134	0.4516	0.4778	0.5256	0.5256	1.1806
$70^\circ$	0.4054	1.1137	0.3486	0.3852	0.4104	0.4566	0.4566	1.2546
$74^\circ$	0.3340	1.1648	0.2819	0.3154	0.3383	0.3809	0.3809	1.3285

Table 1.- Ordinates of Various Magneto/Ionopause Shapes

$\beta$	MAGNETOPAUSE		IONOPAUSE $H/R_0 = 0.01$		IONOPAUSE $H/R_0 = 0.1$		IONOPAUSE $H/R_0 = 0.2$		IONOPAUSE $H/R_0 = 0.5$	
	$x/D$	$Y_m/D$	$x/R_0$	$Y_1/R_0$	$x/R_0$	$Y_1/R_0$	$x/R_0$	$Y_1/R_0$	$x/R_0$	$Y_1/R_0$
78°	0.2580	1.2138	0.2134	1.0041	0.2419	1.1382	0.2614	1.2298	0.2981	1.4024
82°	0.1772	1.2610	0.1435	1.0212	0.1650	1.1737	0.1796	1.2777	0.2074	1.4759
86°	0.0913	1.3060	0.0723	1.0345	0.0843	1.2062	0.0925	1.3232	0.1083	1.5491
90°	0.0	1.3491	0.0	1.0442	0.0	1.2356	0.0	1.3661	0.0	1.6216
94°	-0.0972	1.3900	-0.0735	1.0507	-0.0882	1.2620	-0.0983	1.4065	-0.1184	1.6932
98°	-0.2008	1.4289	-0.1482	1.0547	-0.1806	1.2854	-0.2029	1.4441	-0.2479	1.7636
102°	-0.3115	1.4656	-0.2246	1.0568	-0.2776	1.3058	-0.3143	1.4788	-0.3895	1.8325
106°	-0.4302	1.5002	-0.3033	1.0577	-0.3795	1.3233	-0.4332	1.5106	-0.5447	1.8997
110°	-0.5578	1.5327	-0.3851	1.0580	-0.4870	1.3380	-0.5603	1.5394	-0.7150	1.9646
114°	-0.6959	1.5630	-0.4711	1.0581	-0.6011	1.3501	-0.6968	1.5651	-0.9024	2.0269
118°	-0.8461	1.5913	-0.5626	1.0581	-0.7230	1.3598	-0.8442	1.5877	-1.1092	2.0861
122°	-0.0107	1.6175	-0.6612	1.0581	-0.8543	1.3672	-1.0043	1.6072	-1.3384	2.1419
126°	-1.1927	1.6416	-0.7688	1.0581	-0.9973	1.3727	-1.1797	1.6237	-1.5938	2.1936
130°	-1.3961	1.6638	-0.8879	1.0581	-1.1550	1.3765	-1.3737	1.6371	-1.8803	2.2409
134°	-1.6262	1.6840	-1.0218	1.0581	-1.3317	1.3790	-1.5911	1.6476	-2.2048	2.2832
138°	-1.8905	1.7022	-1.1752	1.0581	-1.5332	1.3805	-1.8387	1.6555	-2.5767	2.3200
142°	-2.1997	1.7186	-1.3544	1.0581	-1.7679	1.3812	-2.1261	1.6611	-3.0093	2.3511
146°	-2.5696	1.7332	-1.5688	1.0581	-2.0483	1.3816	-2.4679	1.6646	-3.5226	2.3761
150°	-3.0242	1.7460	-1.8328	1.0581	-2.3932	1.3817	-2.8866	1.6666	-4.1480	2.3948
154°	-3.6026	1.7571	-2.1695	1.0581	-2.8330	1.3817	-3.4189	1.6675	-4.9365	2.4077

Table 1 (Continued)

$\beta$	MAGNETOPAUSE		IONOPAUSE		IONOPAUSE		IONOPAUSE			
	$x/D$	$y_m/D$	$x/R_0$	$y_i/R_0$	$x/R_0$	$y_i/R_0$	$x/R_0$	$y_i/R_0$		
	Equatorial Trace		$H/R_0 = 0.01$		$H/R_0 = 0.1$		$H/R_0 = 0.2$		$H/R_0 = 0.5$	
$158^\circ$	-4.3723	1.7665	-2.6190	1.0581	-3.4199	1.3817	-4.1281	1.6678	-5.9779	2.4152
$162^\circ$	-5.4608	1.7743	-3.2567	1.0582	-4.2526	1.3817	-5.1333	1.6679	-7.4439	2.4187
$166^\circ$	-7.1412	1.7805	-4.2440	1.0582	-5.5419	1.3817	-6.6897	1.6679	-9.7048	2.4197
$170^\circ$	-10.1239	1.7851	-6.0011	1.0582	-7.8363	1.3818	-9.4594	1.6679	-13.7235	2.4198
$174^\circ$	-17.0135	1.7882	-10.0678	1.0582	-13.1466	1.3818	-15.8695	1.6680	-23.0232	2.4198

Table 1 (Concluded)

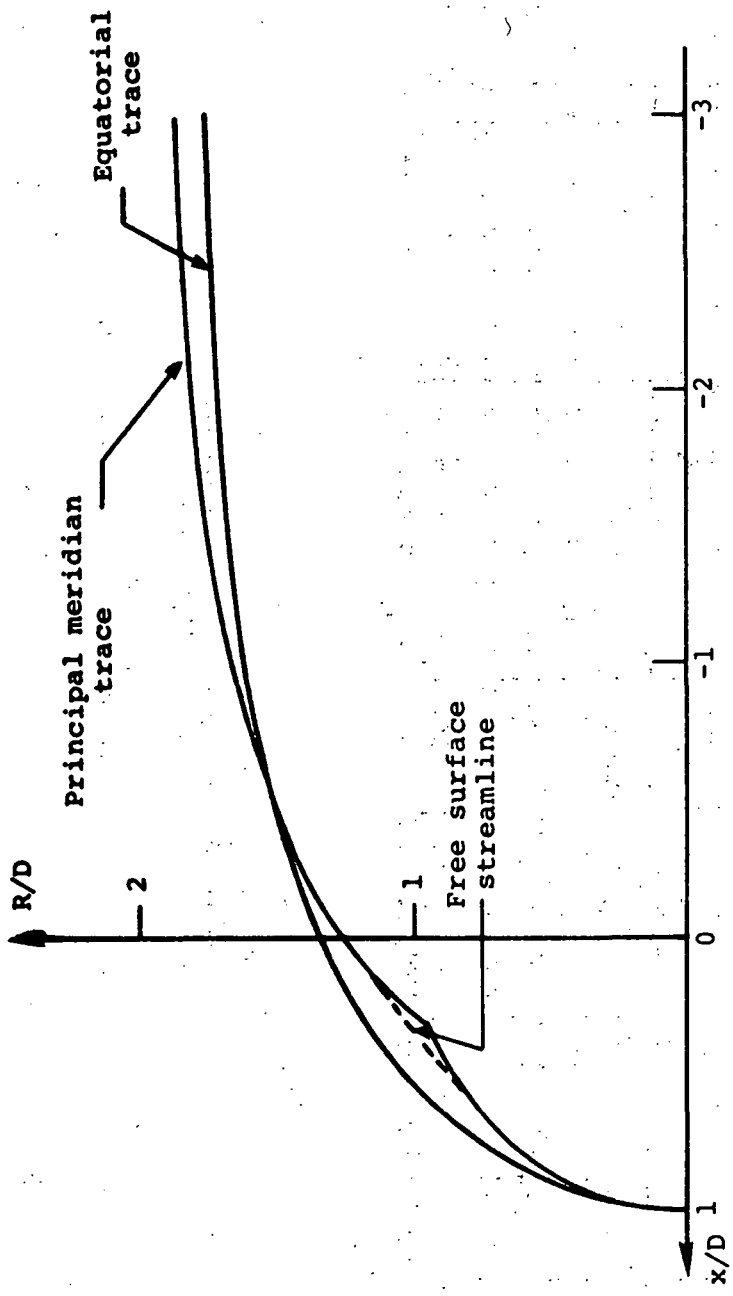


Figure 1. - Comparison of the equatorial and principal meridian traces of the magnetosphere boundary as provided by the simplified theory of equation 16.

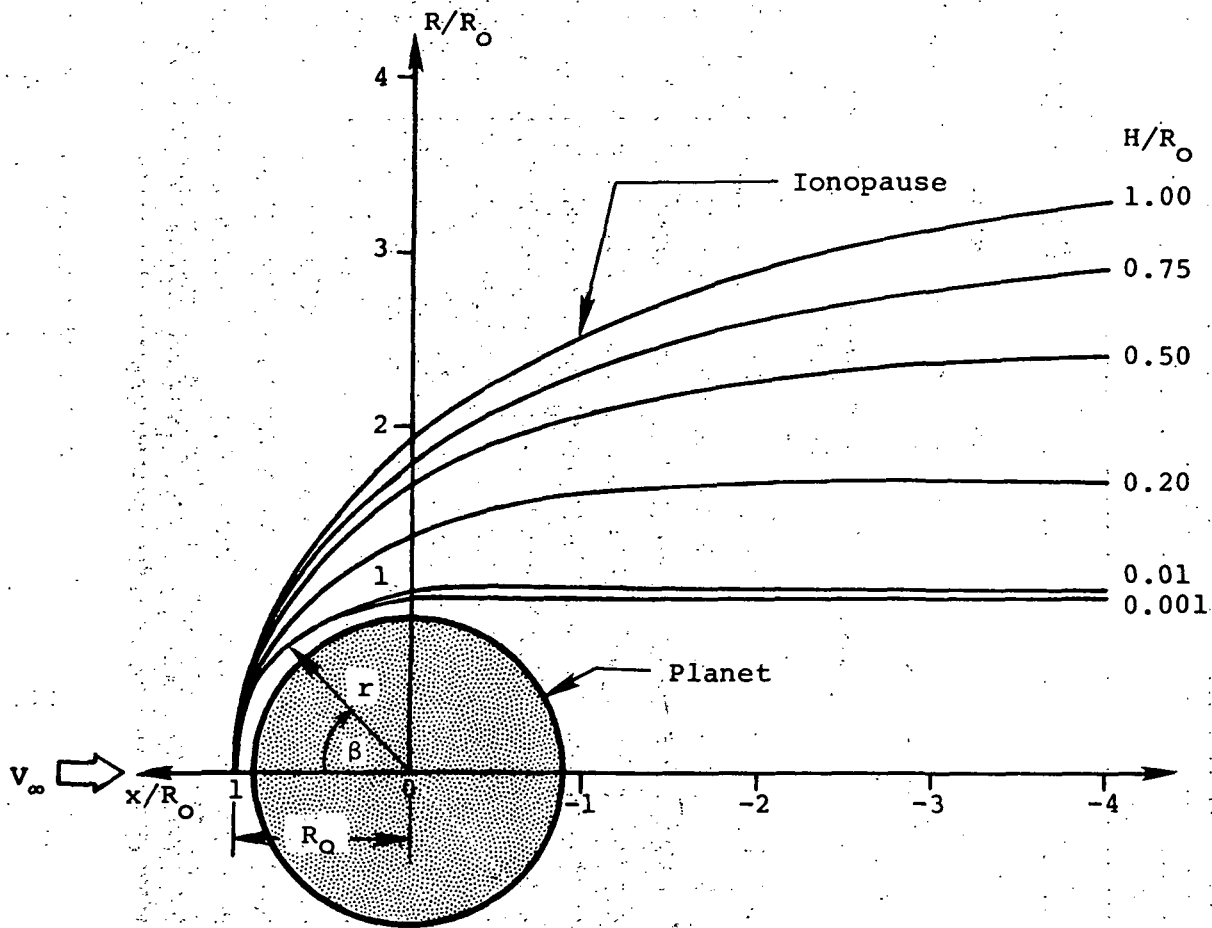


Figure 2. - Illustration of ionopause shapes for various values of the ionosphere scale height to shock standoff distance ratio  $H/R_0$ .

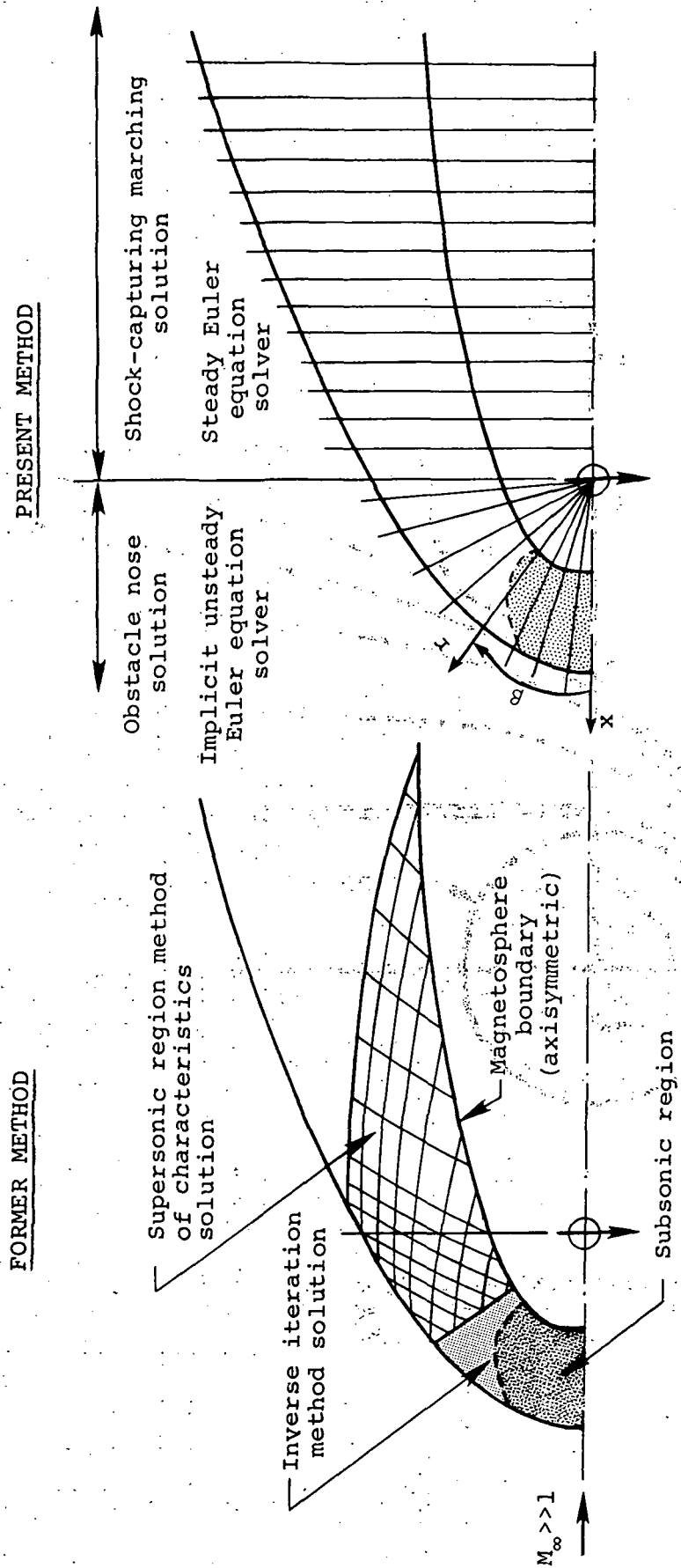


Figure 3 - Comparison of former and present computational procedures for determining the gasdynamic flow properties of solar wind-magneto/ionopause interactions.

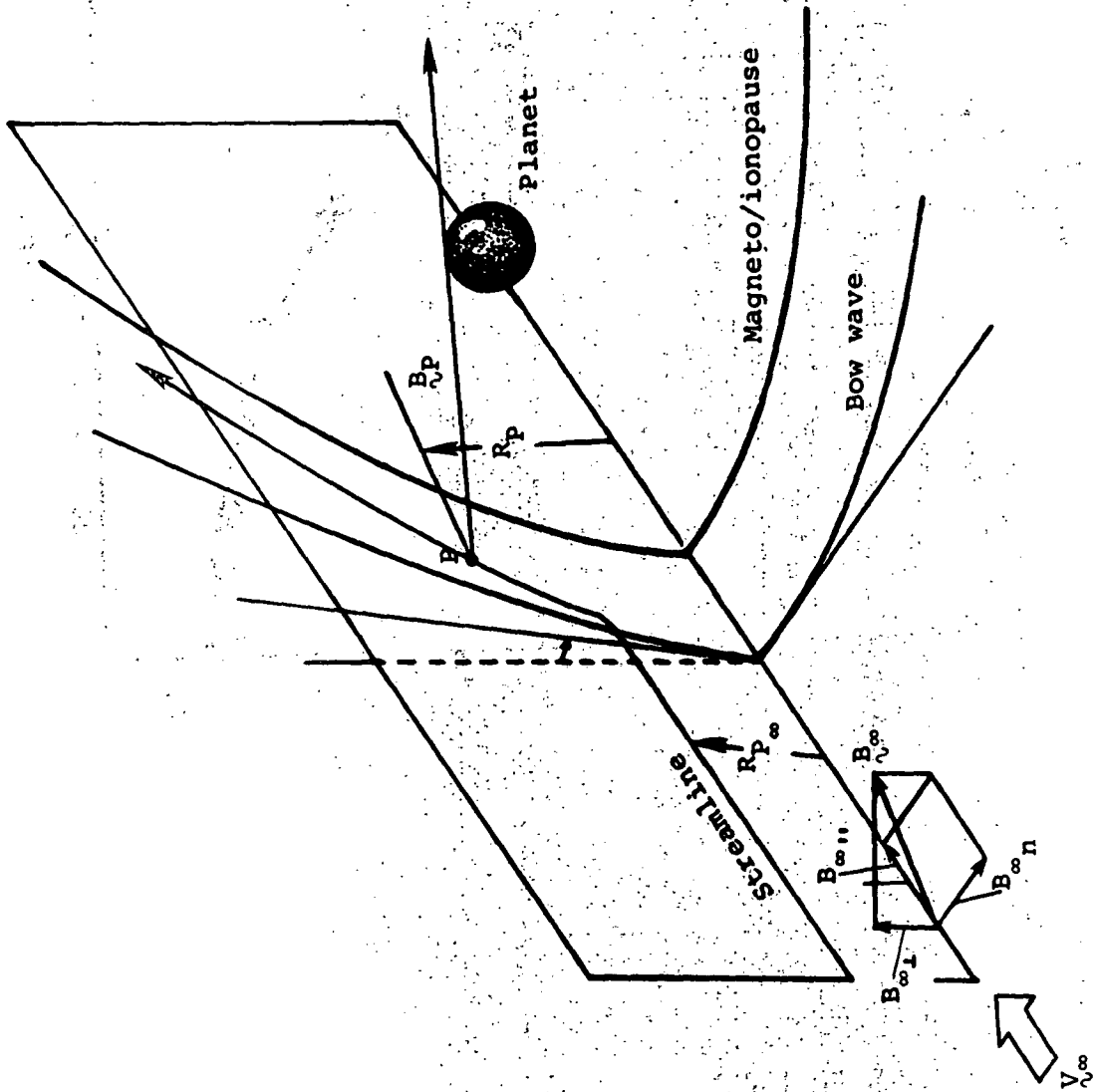
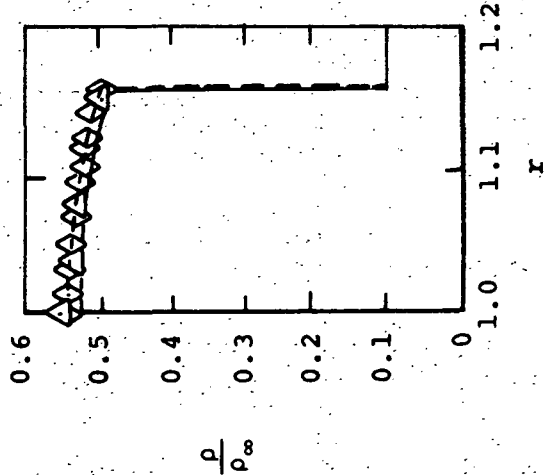
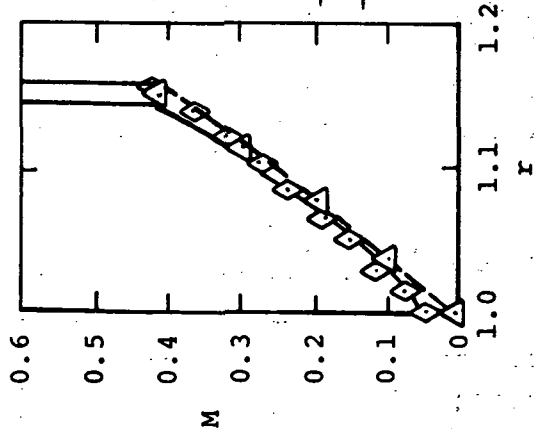


Figure 4. - Illustration of the components of the three-dimensional magnetic field.



$\gamma = 1.4$   $M_\infty = 4.926$

SPHERE

- ◇ Implicit
- Experiment (Xerikos & Anderson)
- Finite volume
- Explicit (Moretti)
- △ Explicit (Barnwell)
- Explicit (Chaussee)

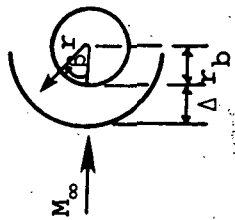
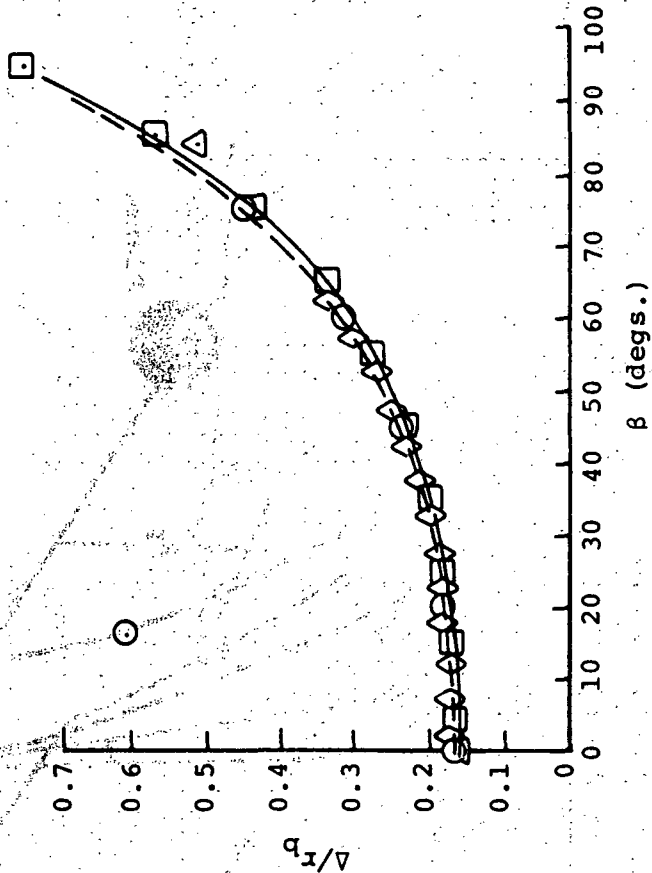
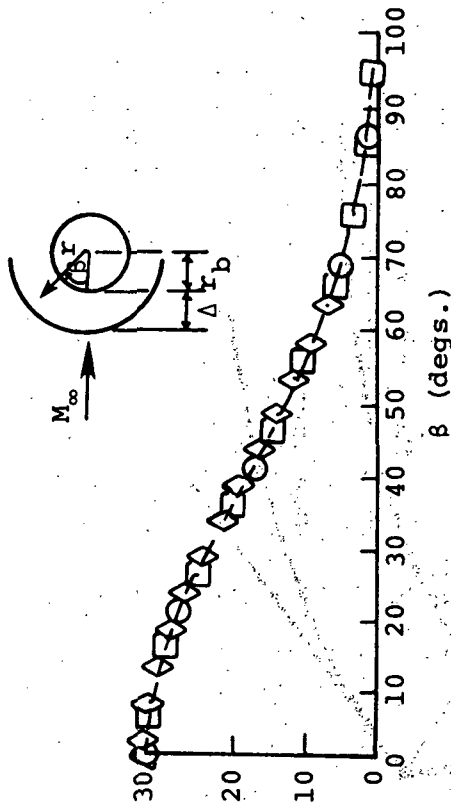
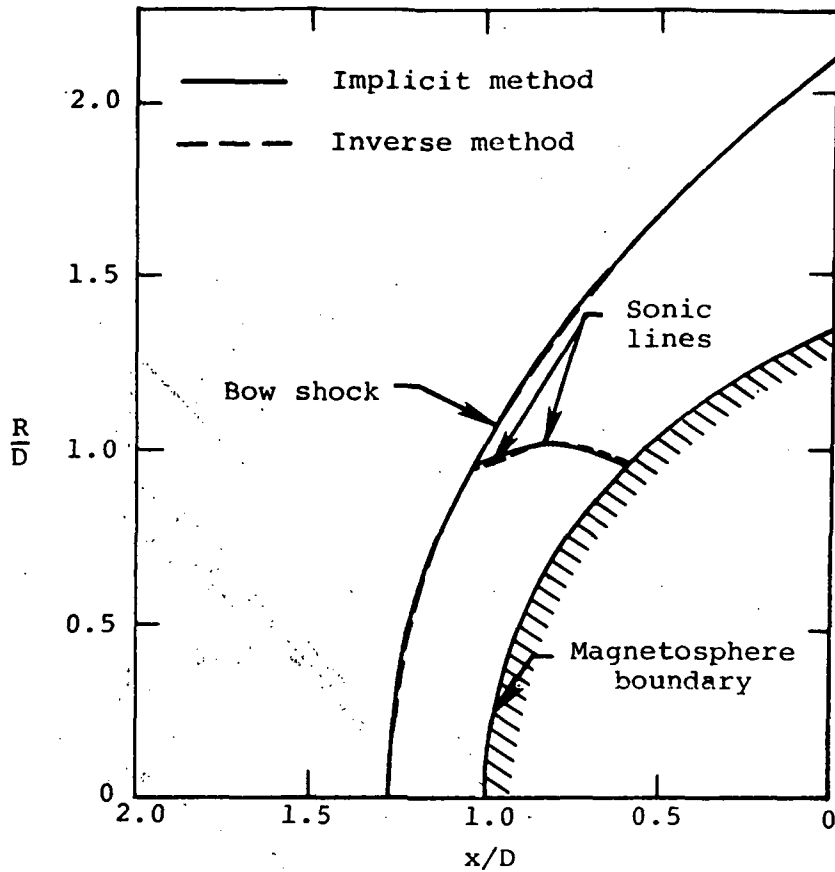
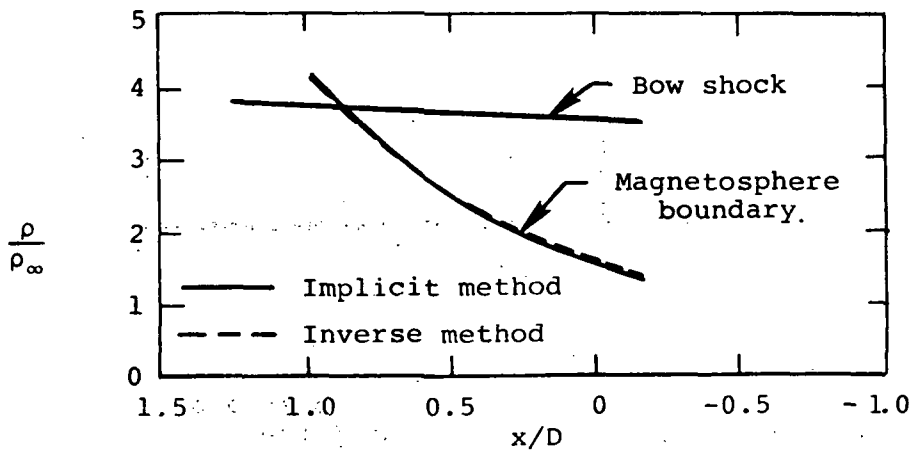


Figure 5. - Comparison of flow properties predicted by the present implicit method with other techniques and experiment for supersonic flow past a sphere;  $M_\infty = 4.926$ ,  $\gamma = 1.4$ .





(a) Shock shape and sonic line location.



(b) Density distribution.

Figure 6. - Comparison of implicit and inverse methods for shock shape and sonic line location, and density distribution along bow shock and magnetosphere boundary for  $M_\infty = 8$ ,  $\gamma = 5/3$  flow past the rotated equatorial trace of the magnetopause.

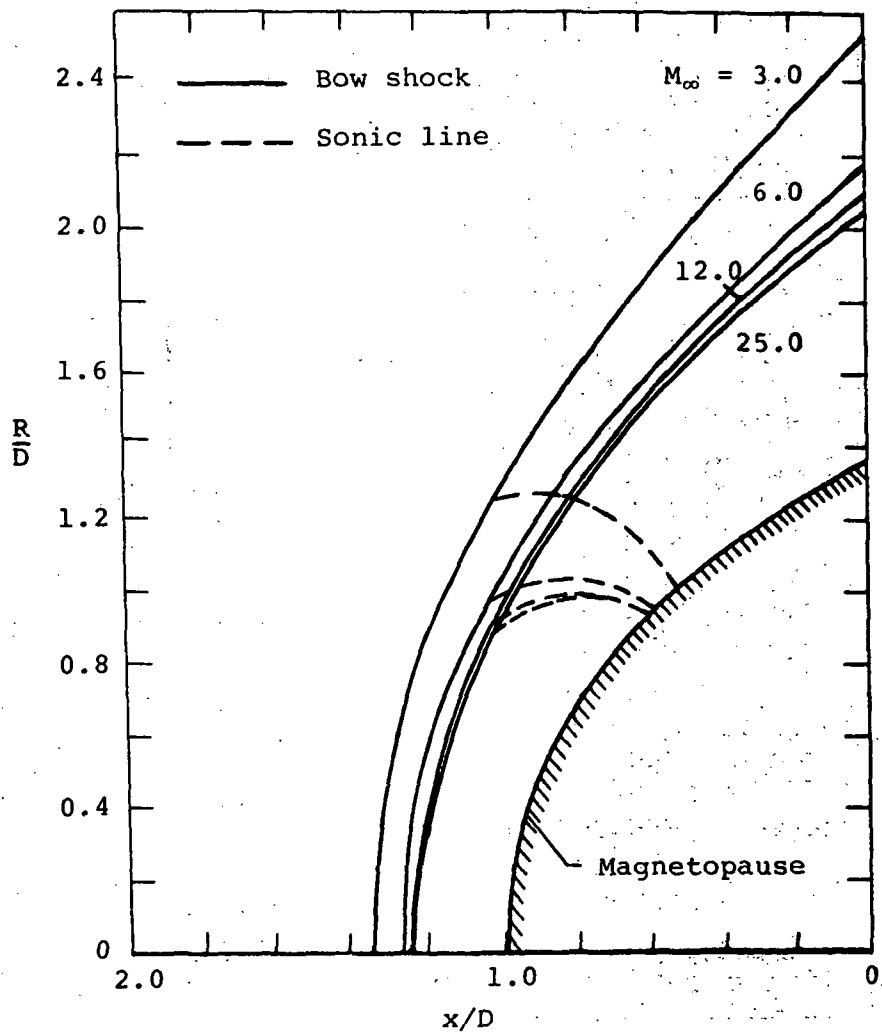


Figure 7. - Bow wave and sonic line locations for various supersonic flows past the rotated equatorial trace of the magnetopause with  $\gamma = 5/3$ .

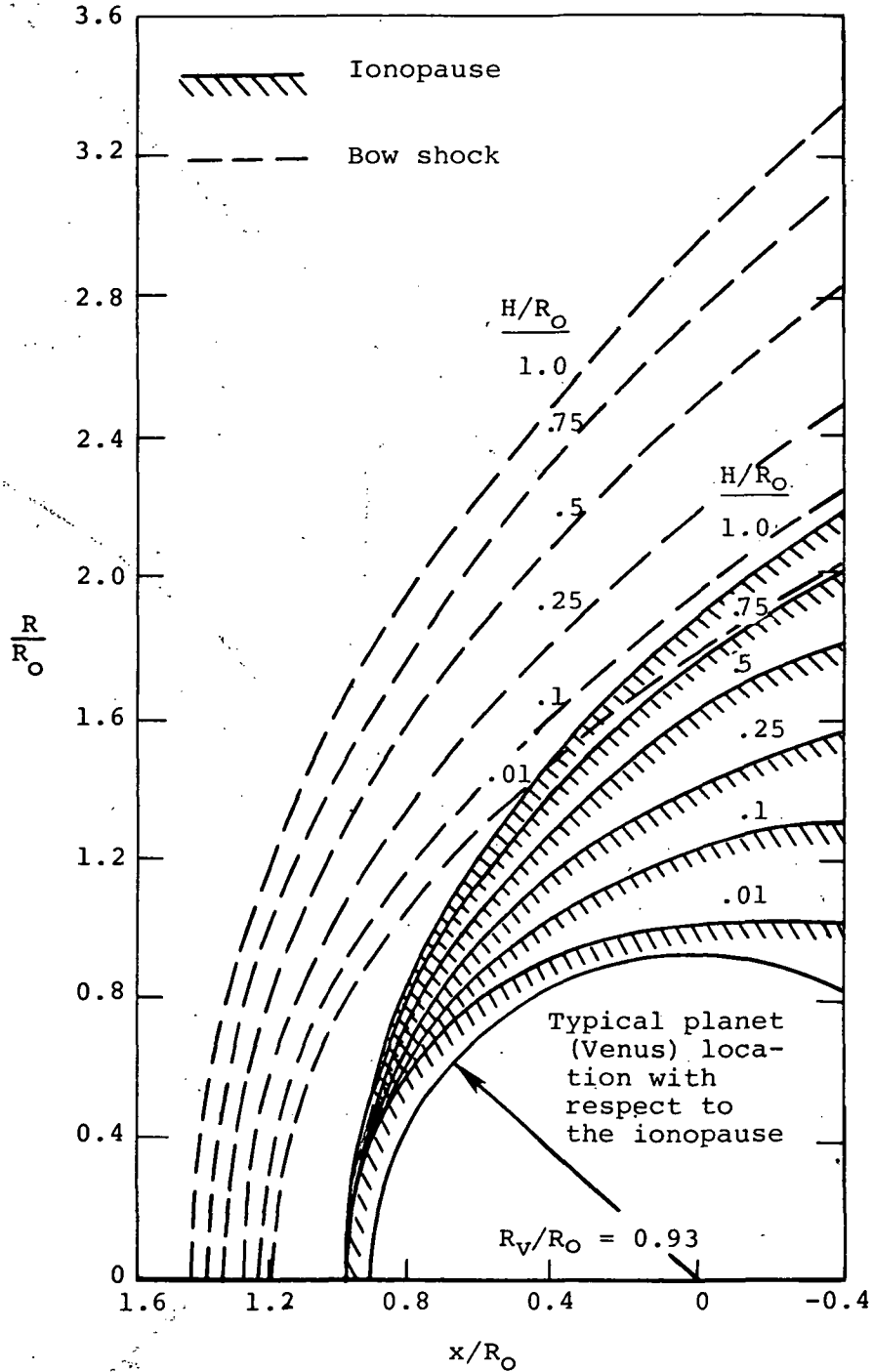


Figure 8. - Bow shock location for solar wind flow with  $M_\infty = 8$ ,  $\gamma = 5/3$  past various ionopause shapes.

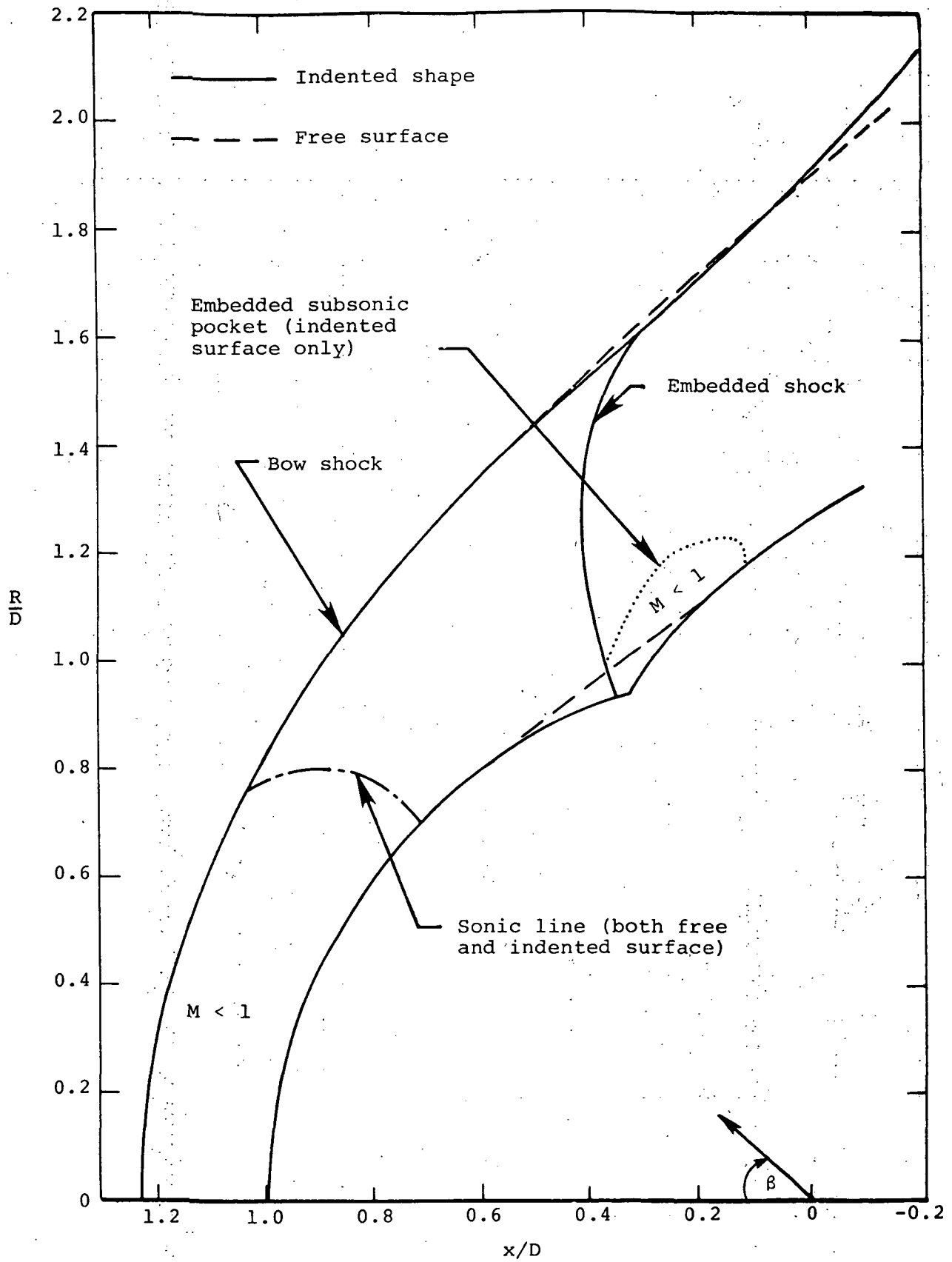


Figure 9. - Bow shock and embedded shock locations for solar wind flow with  $M_\infty = 5$ ,  $\gamma = 5/3$  past the rotated principal meridian of the magnetosphere.

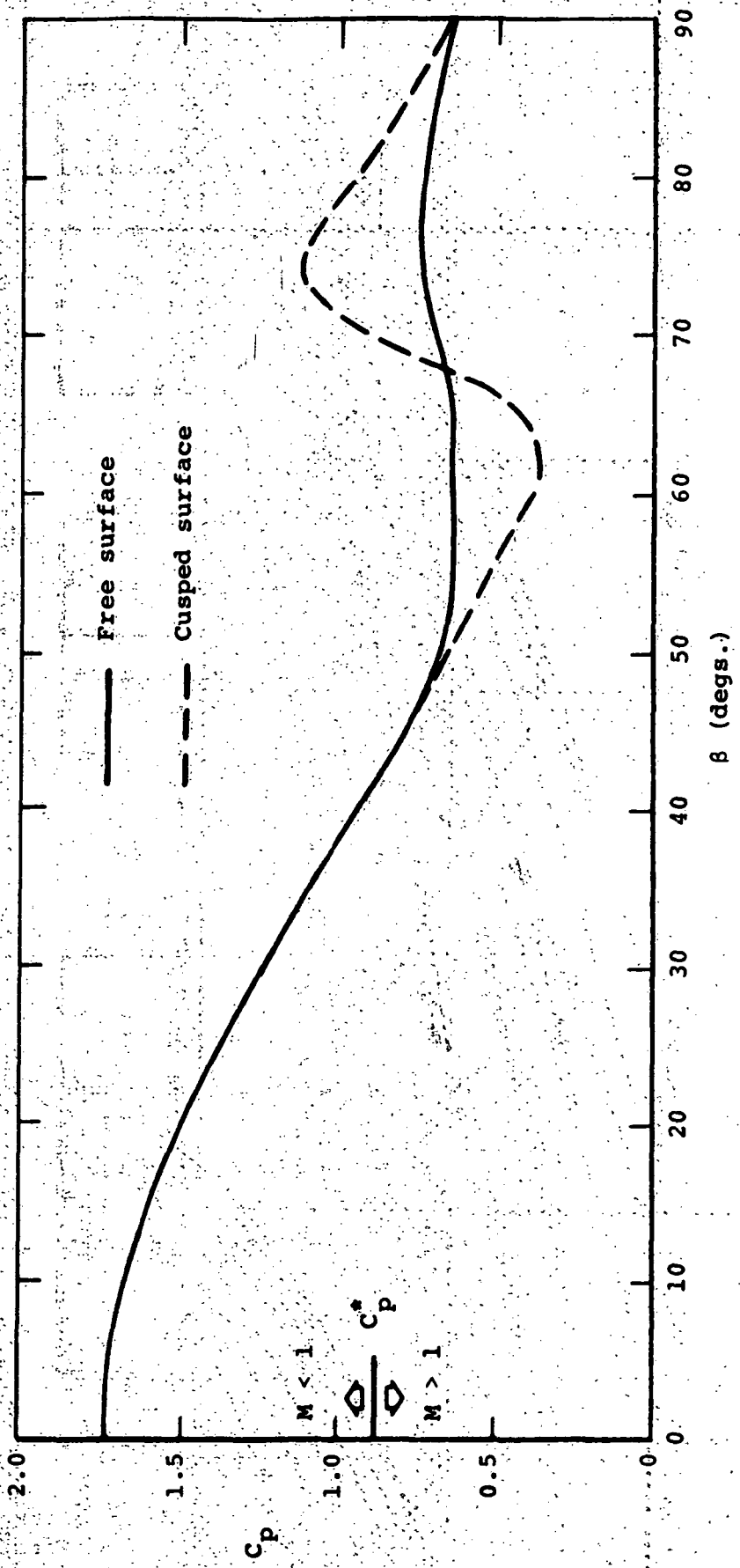
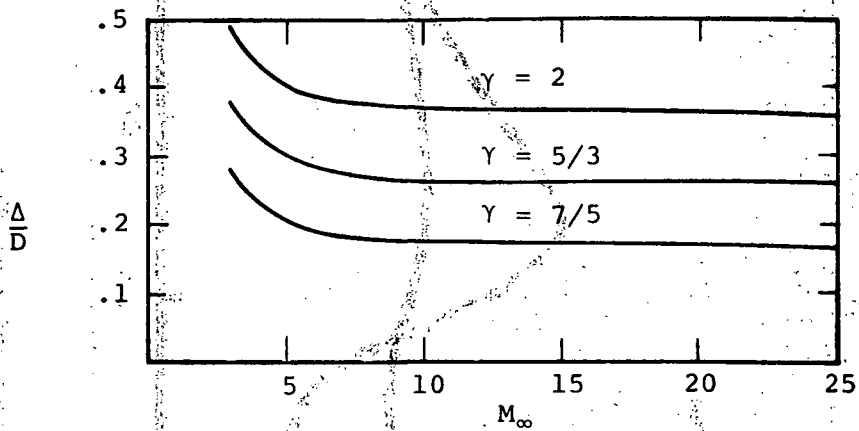
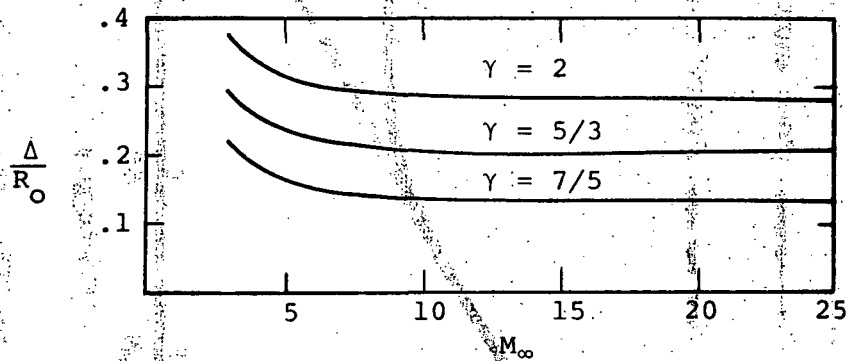


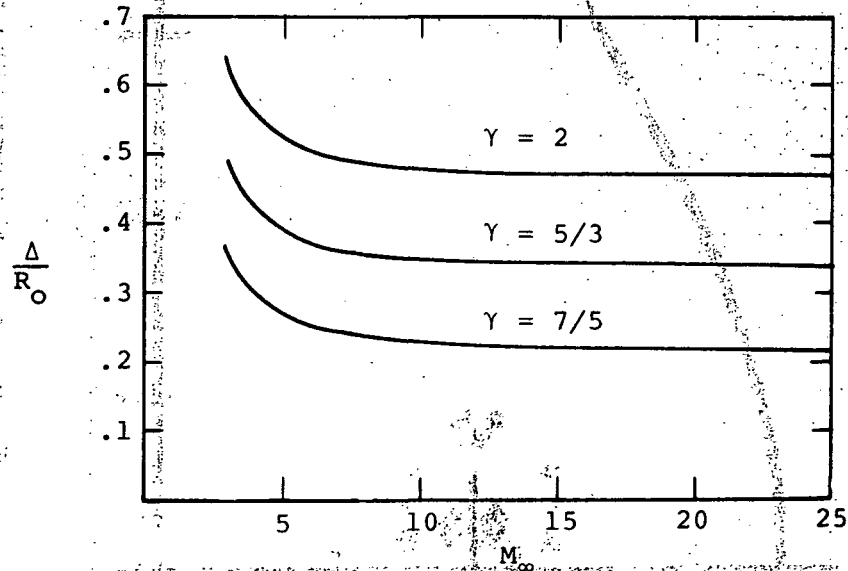
Figure 10. - Magnetopause pressure coefficients for the principal meridian magnetopause shapes shown in figure 9.



(a) Magnetopause equatorial trace



(b) Ionopause trace -  $H/R_0 = .01$



(c) Ionopause trace -  $H/R_0 = .5$

Figure 11. - Variation of shock stand-off distance with oncoming Mach number and ratio of specific heats for various magneto/ionopause traces as determined by the present implicit procedure.

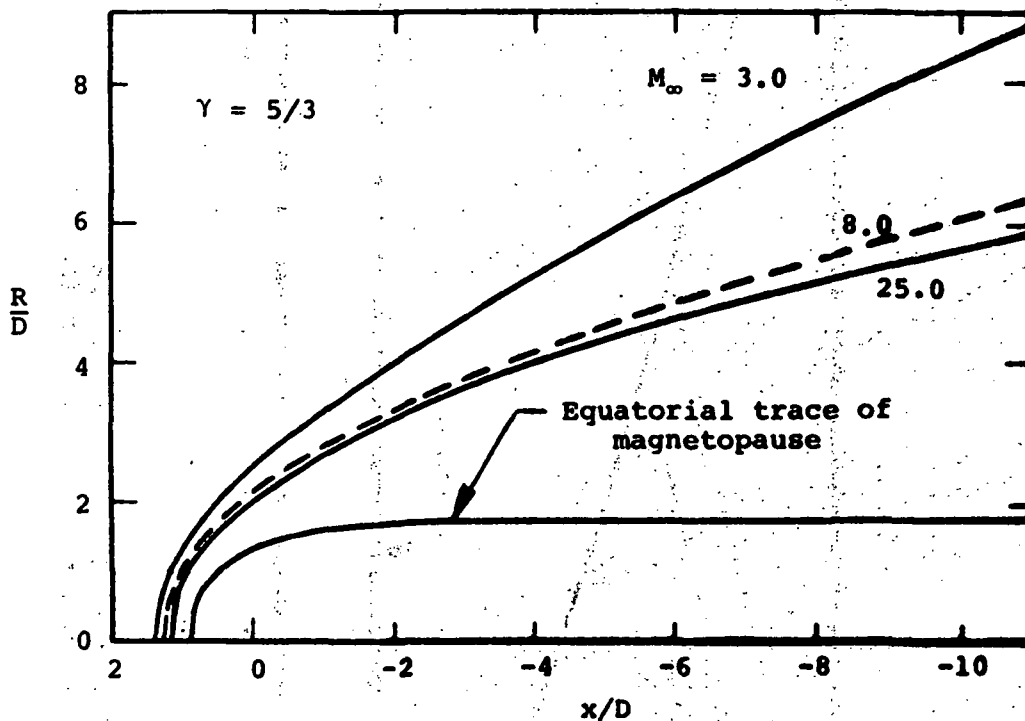


Figure 12. - Shock shapes for various supersonic flows past the rotated equatorial trace of the magnetopause; combined near (blunt body) and far (marching) solutions.

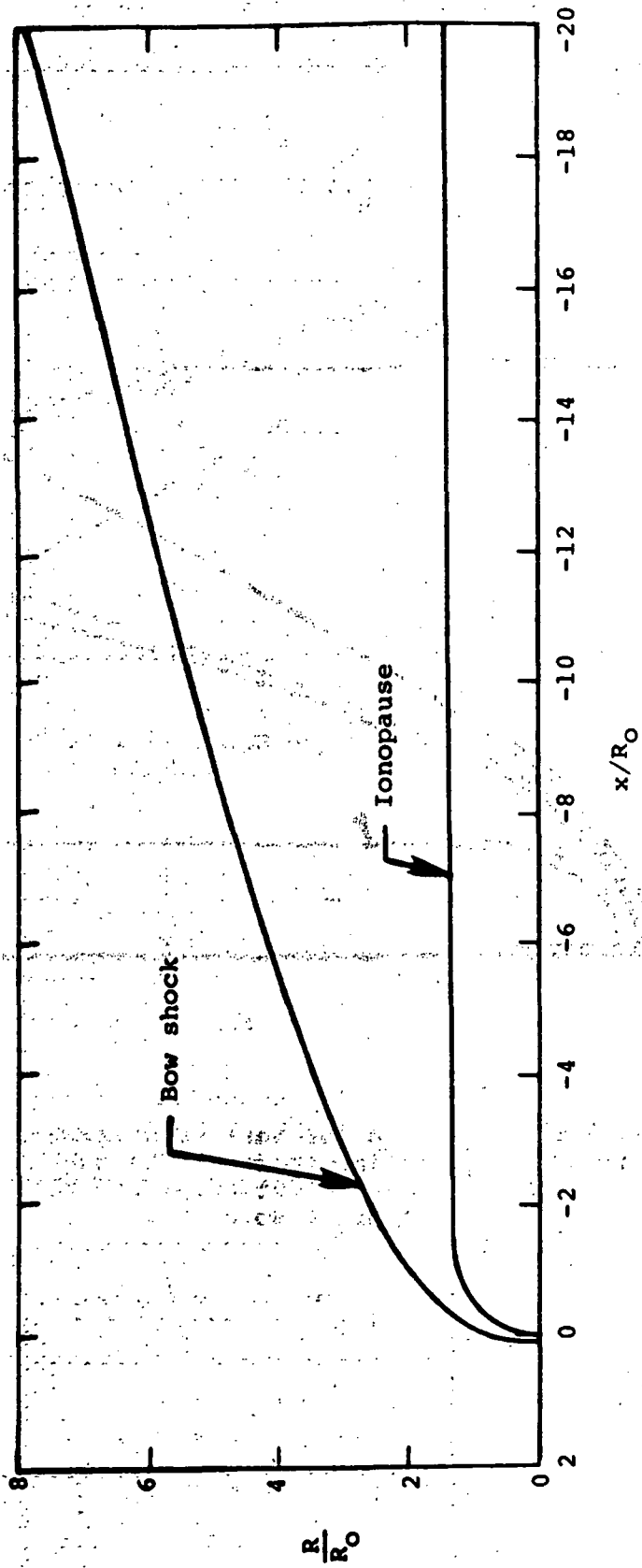
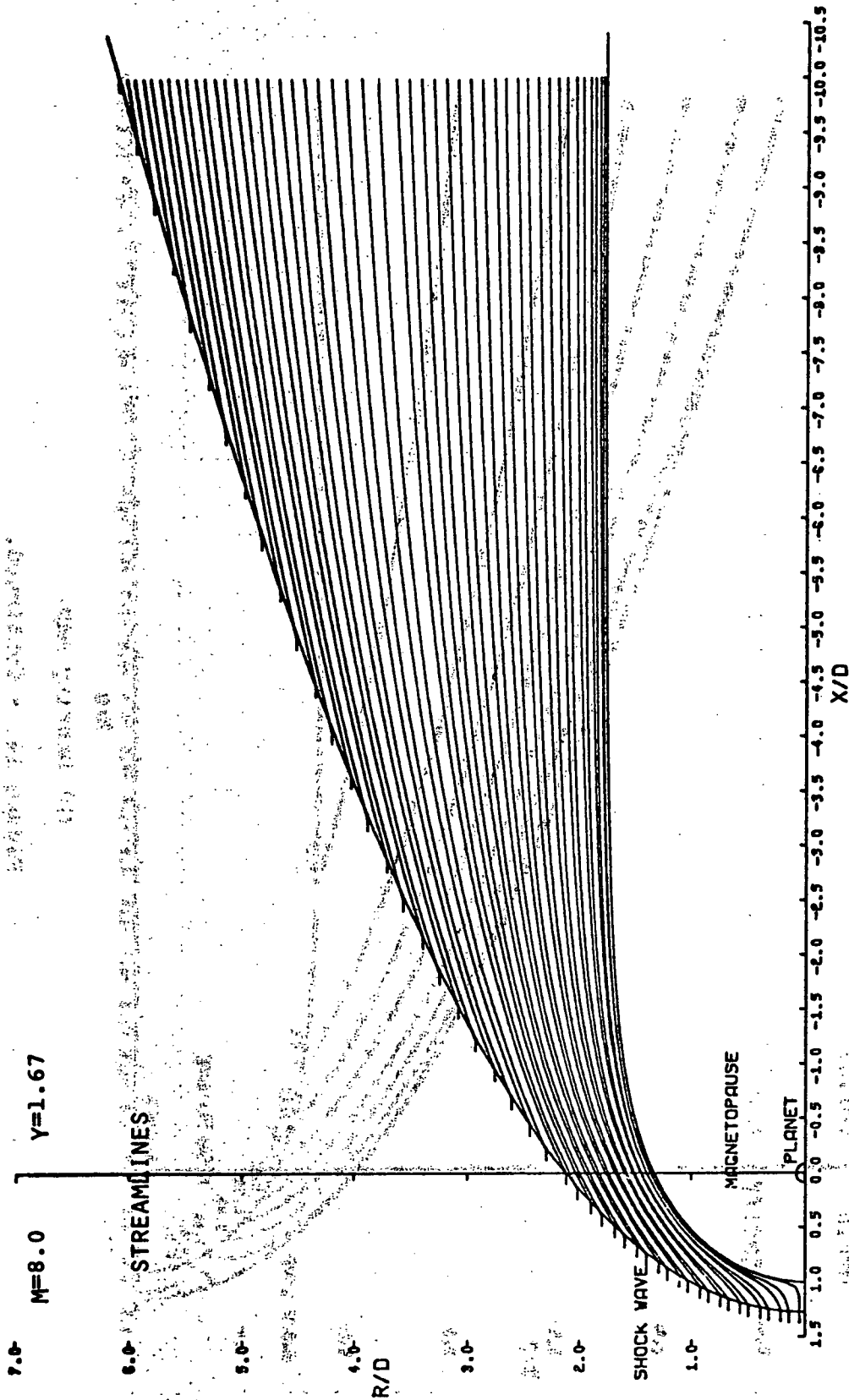


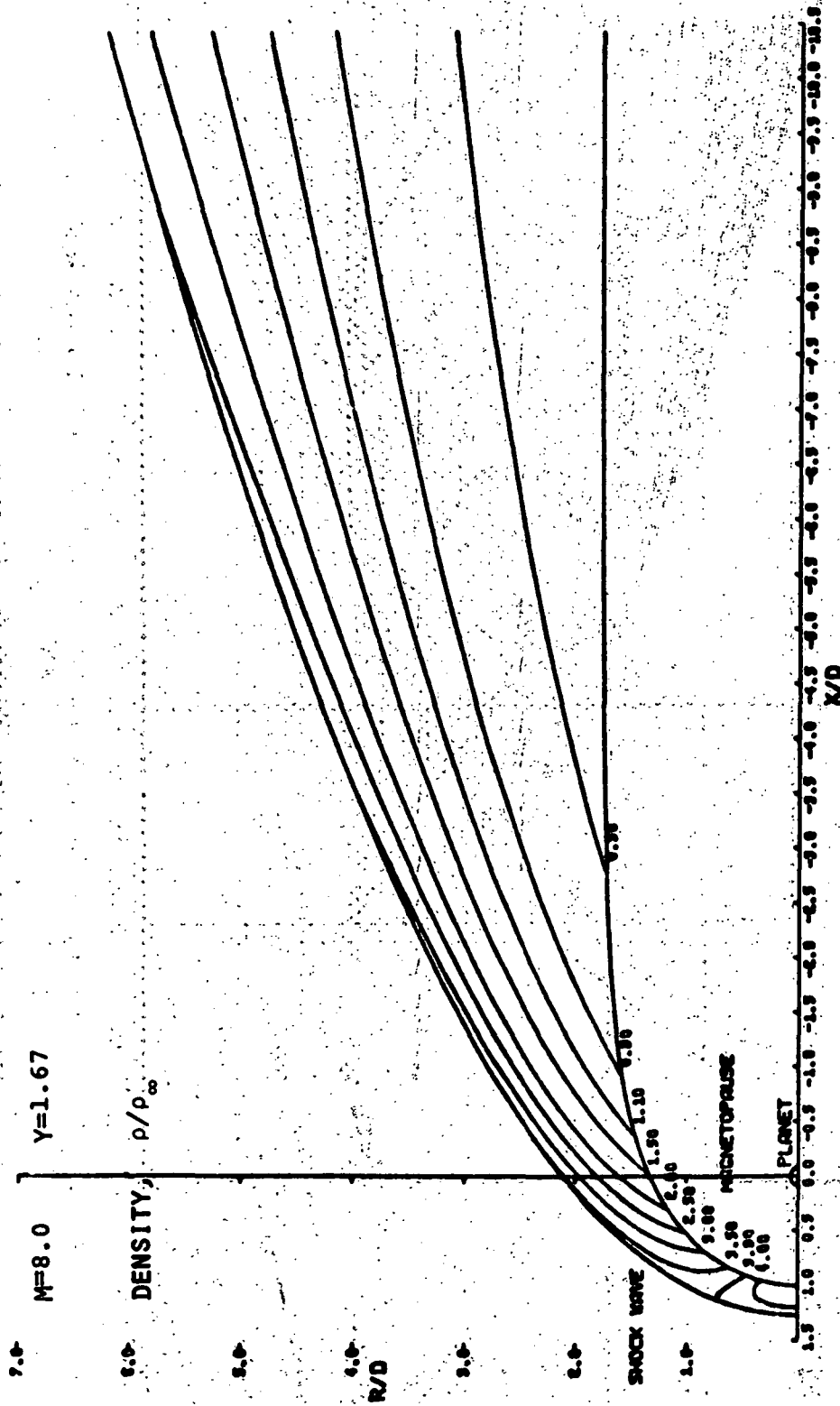
Figure 13. - Shock shape for  $M_{\infty} = 8$ ,  $\gamma = 5/3$  flow past an ionopause shape with  $H/R_0 = 0.1$ ; combined near (blunt body) and far (marching) field solutions.





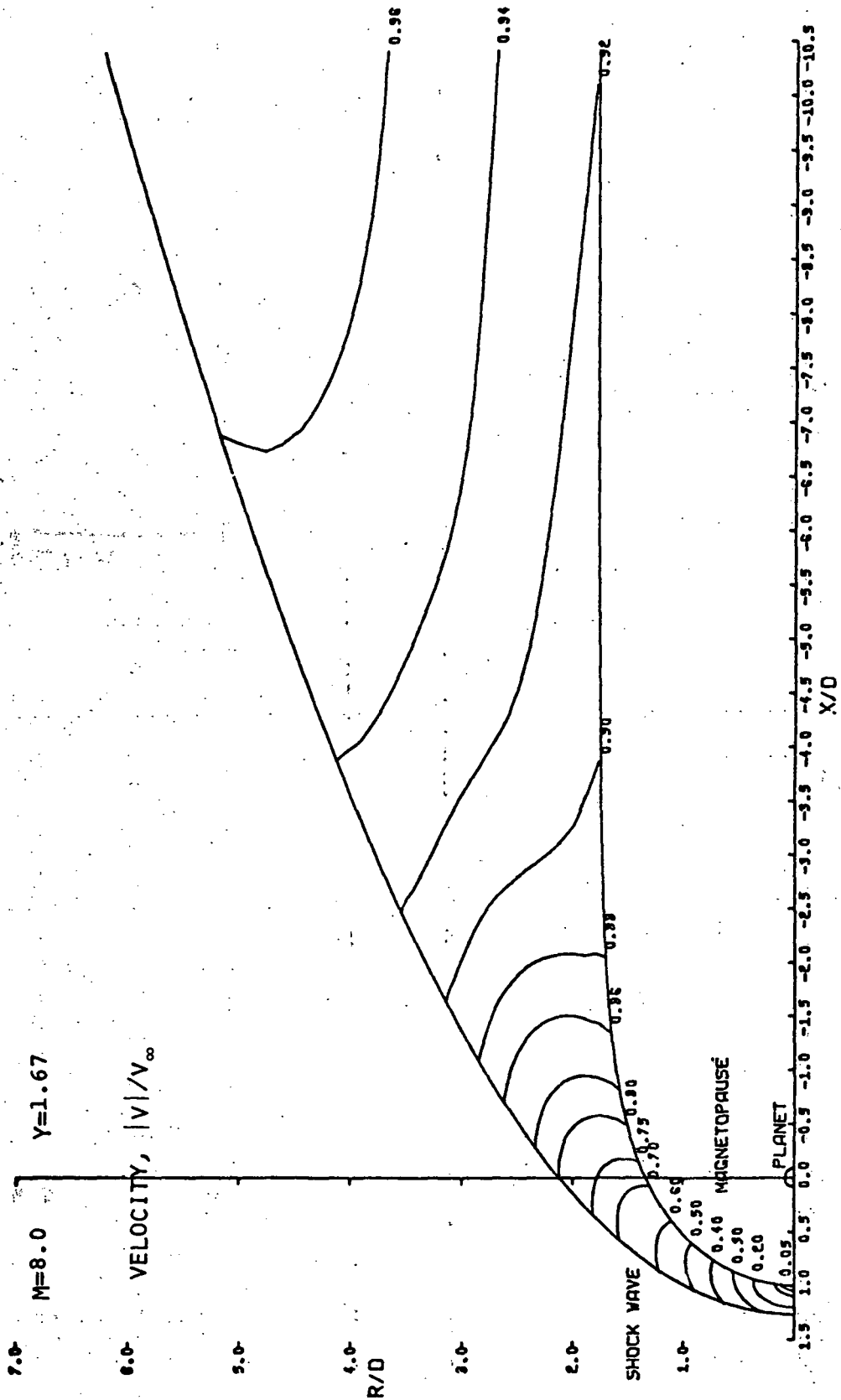
(a) Streamline Map.

Figure 14. - Streamline, density, and velocity maps for  $M_\infty = 8.0$ ,  $\gamma = 5/3$  flow past the rotated equatorial trace of the magnetopause; combined blunt body and marching flow field.



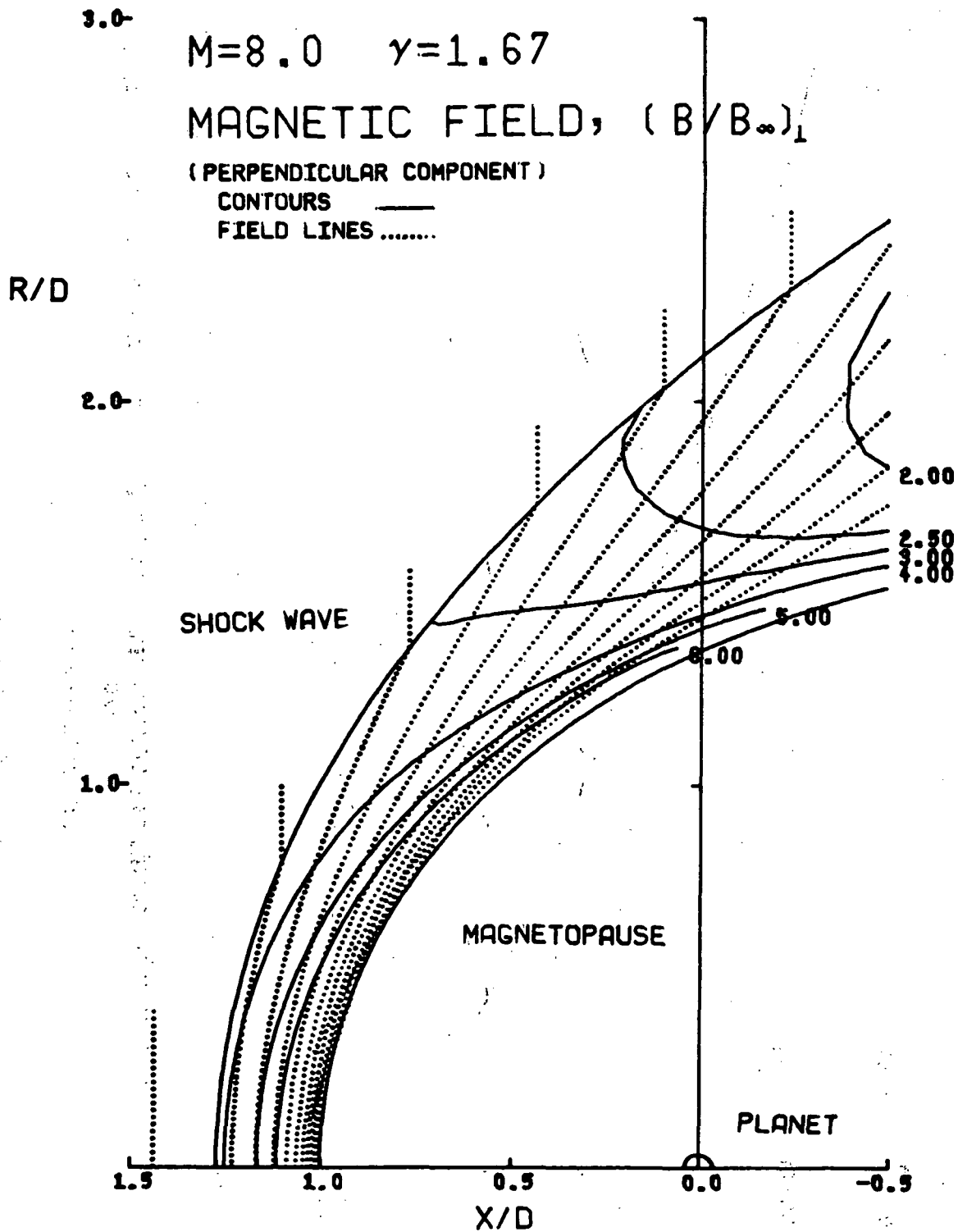
(b) Density map.

Figure 14. - Continued.



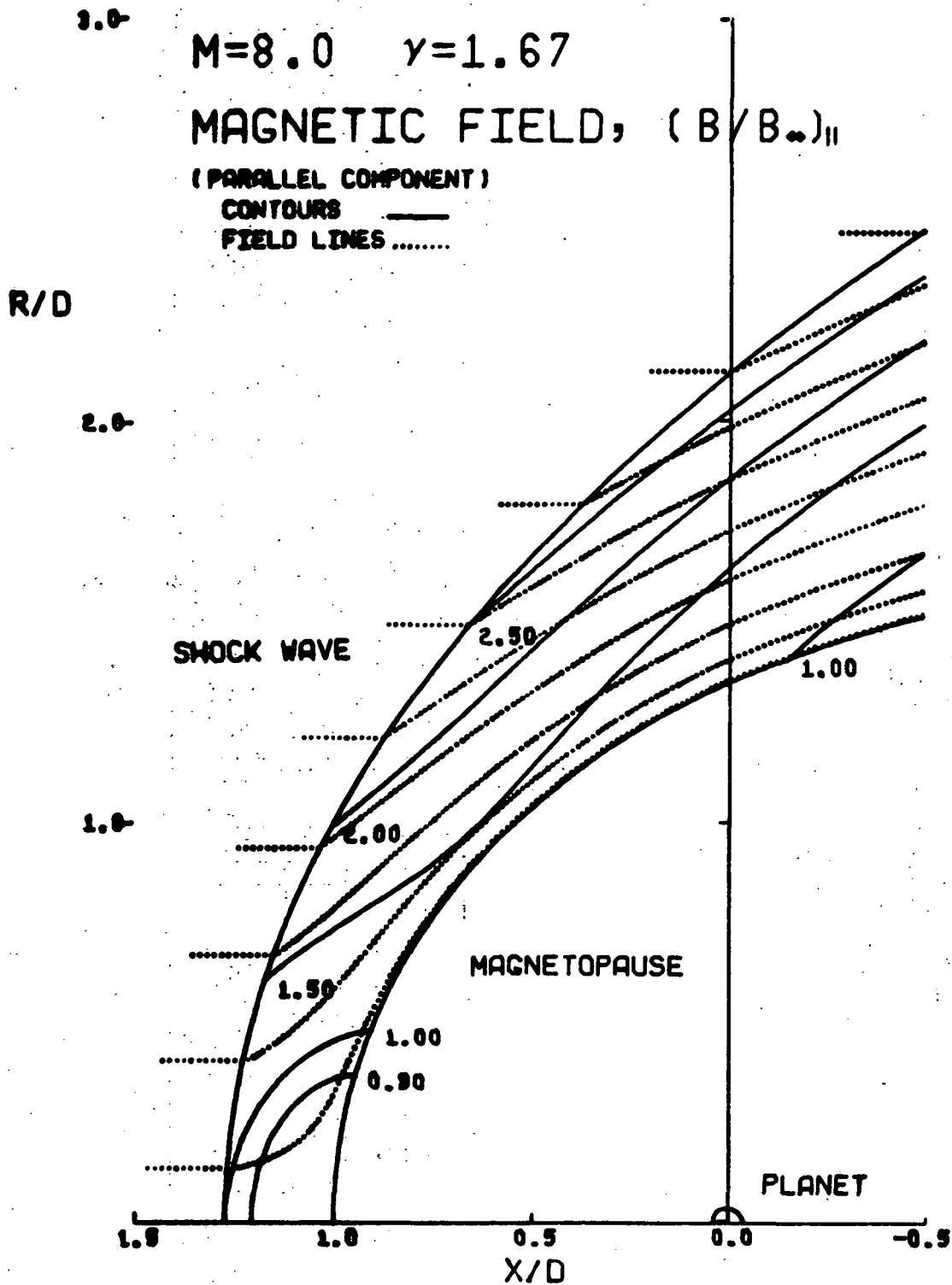
(c) Velocity map.

Figure 14. - Concluded.



(a) Perpendicular component  $(B/B_\infty)_\perp$

Figure 15. - Contours and field line locations of the in-plane magnetic field components  $(B/B_\infty)_\perp$  and  $(B/B_\infty)_\parallel$  for  $M_\infty = 8$  and  $\gamma = 5/3$  flow past the rotated equatorial trace of the magnetopause.



(b) Parallel component  $(B/B_\infty)_\parallel$

Figure 15. - Concluded.

National Aeronautics and  
Space Administration

Washington, D.C.  
20546

Official Business

Penalty for Private Use, \$300

THIRD-CLASS BULK RATE

Postage and Fees Paid  
National Aeronautics and  
Space Administration  
NASA-451



**NASA**

POSTMASTER: If Undeliverable (Section 158  
Postal Manual) Do Not Return

---